PhD Thesis
Imperial College London

On the detectability of latitudinal biodiversity gradients in deep time

Lewis Alan Jones
Department of Earth Science and Engineering, Imperial College London

Supervised by:

Professor Peter A. Allison
Imperial College London

Dr Philip D. Mannion
University College London

Submitted for the degree of Doctor of Philosophy at Imperial College London

September 2020

–This page is intentionally left blank–

"It is a curious situation that the sea, from which life first arose should now be threatened by the activities of one form of that life. But the sea, though changed in a sinister way, will continue to exist; the threat is rather to life itself."

— Rachel Carson, The Sea Around Us

Declaration of Originality

I, Lewis Alan Jones, hereby declare that the work presented in this thesis is my own, unless otherwise stated. Any supporting material or collaboration has been cited and disclosed accordingly.

Lewis A. Jones

20 September 2020

Copyright Declaration

The copyright of this thesis rests with the author. Unless otherwise indicated, its contents are licensed under a Creative Commons Attribution-Non Commercial 4.0 International Licence (CCBY-NC). Under this licence, you may copy and redistribute the material in any medium or format. You may also create and distribute modified versions of the work. This is on the condition that: you credit the author and do not use it, or any derivative works, for a commercial purpose. When reusing or sharing this work, ensure you make the licence terms clear to others by naming the licence and linking to the licence text. Where a work has been adapted, you should indicate that the work has been changed and describe those changes. Please seek permission from the copyright holder for uses of this work that are not included in this licence or permitted under UK Copyright Law.

Lewis A. Jones

20 September 2020

Acknowledgements

Throughout school I was never particularly good or bad at anything, except perhaps French... I was pretty bad at that. Nevertheless, after somehow making it to university, I started to find my academic groove. I believe I owe this to the dedicated lecturers at the University of Hull (2011–2015). I would like to particularly thank Dr Lucy Clarke and Professor David Bond. Lucy provided early guidance and encouragement for my pursuit of a PhD, including settling any of my self-doubt. David was my supervisor for my master's thesis, and inspired me to pursue research in palaeontology with his exciting field work to remote places such as Svalbard. Whilst the fieldwork for my master's project was less glamorous, with knee-deep mud and clay in a soggy quarry in Newark, he fostered an excellent first experience of independent research.

I must also thank my PhD supervisors Dr Philip Mannion (University College London) and Professor Peter Allison (Imperial College London) for their support over these past four years. Without them, I have no doubt that the work presented here would be a lesser version of itself. Phil deserves particularly recognition for his efforts in providing critical feedback in all aspects of my work. It is fair to say that I was dumped on him as an additional student for the sake of following departmental regulations. I do not think I have ever been more grateful for bureaucracy. My gratitude is also owed to Peter for providing a resourceful environment and fostering fruitful collaborations with other institutions and industry. I am particularly grateful to Peter for enabling me to attend all the conferences and workshops I have. My PhD experience, and self-development, would surely be a shadow of itself without this. At this point, I would also like to thank the donors who provide Imperial College London with the funds for the President's PhD scholarship. This scholarship allowed me to undertake the research presented here, and expand my knowledge.

There is a long list of colleagues who have my gratitude for their support throughout my PhD. In particular, Dr Neftalí Sillero (University of Porto) has my thanks for his

teachings on ecological niche modelling. He is truly an exceptional educator. Additional gratitude is extended to the climate modelling group at the University of Bristol for providing data that facilitated the research presented within this thesis. Particularly, Dr Alexander Farnsworth has my thanks for his support, and always providing a light-hearted take on the most negative of reviews. Gratitude is also paid to Drs Sarah-Jane Kelland and Andy Quallington (Getech Group PLC) who made data available for my research.

It is fair to say I have picked up a number of friends on my PhD journey. Dr Christopher Dean was a huge support since day one of my time at Imperial — from showing me around the campus and making me feel welcome, to making me split a shed load of shale in the Mesa Verde National Park. Dr Alessandro Chiarenza deserves a special mention. We have had a somewhat symbiotic relationship through the development and application of our respective research, with many laughs and the occasional shared grievance along the way. And while I don't share your obsession, I guess dinosaurs are OK. My time at Imperial would not have been nearly as fun as it was without Ernesto, Jonny, Nan, Graham and Aaron. From barbeques and board-games, to someone (undisclosed) obtaining the nickname 'Shimmy' for their tabletop dancing, and energetic use of a tambourine in a medieval pub in Prague. Thank you for the good times. My dear friends Iuliana, Claire, Simon, Paul, Sofia, and many others have undeniably made my time in the 'Big Smoke' more pleasant, whether by escaping to the outdoors or enjoying a pint down the pub. I thank you all for that.

Many thanks are also owed to the past and current members of the extended lab group I find myself part of: Philip Mannion, Christopher Dean, Alessandro Chiarenza, Jonathan Rio, Cecily Nicholl and Miranda Kouvari. You have all enriched my experience and knowledge while at Imperial, including adventures to 'Popworld'.

Words will never convey my appreciation for my family. They have supported me throughout my growth as an individual, and for that I thank them. Finally, one individual in particular deserves my lasting gratitude: Paloma, thank you for all the support and sacrifices you have made over the years. Eres un buen huevo.

Abstract

The latitudinal biodiversity gradient (LBG), in which species richness increases from the poles to tropical regions, is one of the most pervasive biodiversity patterns today. However, deep-time studies suggest that the LBG has varied in the geological past, with a range of taxonomic groups characterised by flattened or even bimodal gradients. Moreover, these studies suggest that tropical peaks and poleward declines in biodiversity are restricted to intervals of the Palaeozoic, and the last 30 million years (Myr), when cool icehouse climatic regimes persisted. Yet, the reconstruction of macroecological patterns in deep time is hampered by inherent geological and anthropogenic biases. In particular, spatial sampling heterogeneity has the potential to hinder the reconstruction of LBGs due to the ubiquitous scaling of species richness with area. In this thesis, a series of case studies that attempt to quantify the impact of spatial sampling heterogeneity on the reconstruction of LBGs are presented. Earth System and ecological niche modelling are applied to test whether observed biodiversity trends are the result of spatial sampling heterogeneity, or a genuine biological signal. In addition, a novel subsampling protocol is implemented to provide sampling-standardised estimates of biodiversity. Collectively, this work suggests spatial sampling heterogeneity often prevents the recovery of genuine LBGs in deep time. Estimates of zooxanthellate coral richness over the past 250 Myr demonstrate that the modern LBG got markedly steeper during the last 20 Myr, and a unimodal-type LBG likely persisted during the Early Cretaceous, coinciding with a geologically long-lived 'cold-snap'. These findings are supported by ecological niche modelling, which suggest a tropical increase, and temperate decline in suitable habitat area during these intervals. Overall, these studies highlight the significance of correcting for spatial sampling heterogeneity when reconstructing biodiversity patterns from the fossil record, as well as the value of inferential methods in understanding past macroecological patterns.

Thesis Contents

Declaration of Originality 3

Copyright Declaration 4

Acknowledgements 5

Abstract 7

Thesis Contents 8

List of Figures 12

List of Tables 16

1 Introduction 17

1.1 Introduction to the thesis 19

1.2 The Latitudinal biodiversity gradient 21

1.2.1 Overview 21

1.2.2 The drivers of the latitudinal biodiversity gradient 22

1.2.3 Deep time perspective 26

1.3 Corals, reefs, and global climatic change 27

1.4 Estimating biodiversity in deep time 30

1.4.1 Historical context 30

1.4.2 Taphonomic biases 32

1.4.3 Sampling bias 34

1.4.4 Mitigating sampling bias 38

1.5 Thesis objectives and layout 43

2 Materials: Earth System Modelling and occurrence datasets 45

2.1 Palaeogeography and digital elevation models 47

2.1.1 Overview 47

2.1.2 Palaeobathymetric data 47

2.2 Climate and palaeoclimate models 50

2.2.1 Overview 50

2.2.2 HadCM3 51
2.2.3 HadCM3L 52
2.3 Occurrence datasets 53
2.3.1 Overview 53
2.3.2 Modern 54
2.3.3 Fossil 56
3 Identifying spatial sampling bias in the fossil record using ecological niche modelling 57
3.1 Introduction 60
3.2 Materials and methods 62
3.2.1 Biogeographic data 62
3.2.2 Diversity analyses 64
3.2.3 Environmental data 65
3.2.4 Ecological niche modelling 68
3.2.5 Range comparisons 69
3.2.6 Model validation 70
3.3 Results 70
3.3.1 Diversity analyses 70
3.3.2 Ecological niche modelling 72
3.3.3 Range dynamics 79
3.3.4 Clamping masks 83
3.4 Discussion 85
3.5 Summary 90
4 The impact of spatial sampling heterogeneity on reconstructing latitudinal biodiversity gradients in deep time 91
4.1 Introduction 94
4.2 Materials and methods 96
4.2.1 Simulations 96
4.2.2 Spatial sampling coverage 101
4.2.3 Latitudinal biodiversity gradient analyses 103
4.3 Results 107

4.3.1 Spatial sampling coverage....107
4.3.2 Simulated latitudinal biodiversity gradients....111
4.3.3 Sampled latitudinal biodiversity gradients....112
4.3.4 Sampling-standardisation latitudinal biodiversity gradients....122
4.4 Discussion....124
4.5 Summary....130
5 The evolution of the latitudinal biodiversity gradient in zooxanthellate corals....131
5.1 Introduction....134
5.2 Methods....136
5.2.1 Fossil occurrence data....136
5.2.2 Binning protocol....136
5.2.3 Latitudinal sampling and diversity....139
5.2.4 Sampling-standardisation protocol....139
5.3 Results....141
5.3.1 Palaeolatitudinal sampling and biodiversity patterns....141
5.3.2 Sampling-standardised richness estimates....145
5.4 Discussion....151
5.5 Summary....154
6 Modelling the latitudinal distribution of reef habitat....155
6.1 Introduction....158
6.2 Methods....160
6.2.1 Occurrence data....160
6.2.2 Environmental data....162
6.2.3 Ecological niche modelling algorithm....164
6.2.4 Model verification....165
6.2.5 Post-modelling analyses....166
6.3 Results....167
6.3.1 Model verification....167
6.3.2 Model predictions....170
6.3.3 Model clamping and MESS analyses....176

6.4 Discussion 177
6.5 Summary 182
7 Conclusions and future work 183
7.1 Key findings 185
7.2 Future work 189
References 193
Appendices 219
Appendix A 219
Appendix B 221
Appendix C 242

List of Figures

Figure 1.1. Graphical representation of different types of latitudinal biodiversity gradients 22

Figure 1.2. The first Phanerozoic diversity curve based on data from the British fossil record 30

Figure 1.3. Raup and Sepkoski's diversity curve (Raup and Sepkoski, 1982) 31

Figure 1.4. Palaeolatitudinal distribution of Phanerozoic marine sedimentary rock outcrop in Europe and North America 35

Figure 1.5. Illustrative example of shareholder quorum subsampling for two different time bins 41

Figure 2.1. Albian (Lower Cretaceous) example of palaeogeography and palaeobathymetry 48

Figure 2.2. Palaeogeographic mapping workflow schematic 49

Figure 2.3. Maastrichtian (Upper Cretaceous) example of mean seasonal (June–August) sea surface temperature 53

Figure 3.1. Global distribution of modern and Last Interglacial zooxanthellate coral occurrences 64

Figure 3.2. Global maps of annual sea surface temperature for the Last Interglacial, modern and Representative Concentration Pathways 4.5 and 8.5 66

Figure 3.3. Latitudinal distribution of zooxanthellate coral occurrences and species richness in 5° latitudinal bins. 71

Figure 3.4. Receiver operating characteristic curves from the modern-trained ensemble model. 73

Figure 3.5. Receiver operating characteristic curves from the LIG-trained ensemble model. 74

Figure 3.6. Combined binary suitability maps from modern- and LIG-trained ecological niche models. 75

Figure 3.7. Cropped binary suitability maps for the Indo-Australian Archipelago, under four climatic scenarios: Last Interglacial, modern, Representative Concentration Pathways 4.5 and 8.5. 76

Figure 3.8. Cropped binary suitability maps for the Caribbean and the Gulf of Mexico, under four climatic scenarios: Last Interglacial, modern, Representative Concentration Pathways 4.5 and 8.5. 77

Figure 3.9. Cropped binary suitability maps for the Red Sea, under four climatic scenarios: Last Interglacial, modern, Representative Concentration Pathways 4.5 and 8.5..... 78

Figure 3.10. Cropped binary suitability maps of the Mediterranean, under four climatic scenarios: Last Interglacial, modern, Representative Concentration Pathways 4.5 and 8.5..... 79

Figure 3.11. Latitudinal plots of predicted habitability from ecological niche modelling under four climatic scenarios: Last Interglacial, modern, Representative Concentration Pathways 4.5 and 8.5. 81

Figure 3.12. Clamping masks for model projections trained on the Last Interglacial climatic conditions and occurrences. 83

Figure 3.13. Clamping masks for model projections trained on modern climatic conditions and occurrences. 84

Figure 4.1. Graphical representation of the different types of latitudinal biodiversity gradients simulated in this study. 97

Figure 4.2. Diagram showing the simulation workflow of this study. 98

Figure 4.3. Range size frequency distributions of species within the marine invertebrate groups..... 100

Figure 4.4. Example of range size frequency distributions from a unimodal-type latitudinal biodiversity gradient simulation. 101

Figure 4.5. Occurrence frequency distributions for the five major marine invertebrate groups..... 101

Figure 4.6. Diagram depicting how the sum of proportional latitudinal richness differences are calculated. 105

Figure 4.7. A palaeolatitudinal plot (15° bins) of spatial sampling coverage for all stratigraphic stages from Asselian to Piacenzian. 108

Figure 4.8. Palaeolatitudinal skewness of spatial sampling coverage from the Asselian to Piacenzian. 109

Figure 4.9. Palaeogeographic distribution of fossil collections housed in the Paleobiology Database. 110

Figure 4.10. Heat maps of mean simulated, sampled, and sampling-standardised richness from the Asselian to Piacenzian at stage-level, and within 15° latitudinal bins. 112

Figure 4.11. Heat maps of the change in proportional latitudinal richness between simulated and sampled/sampling-standardised latitudinal biodiversity gradients. ..113

Figure 4.12. Sum of proportional latitudinal richness differences (Asselian to Piacenzian) between unimodal- and bimodal-type latitudinal biodiversity gradients. 114

Figure 4.13. Asselian to Piacenzian plot of the latitudinal bin with peak diversity for simulated flat-, unimodal-, and bimodal-type latitudinal biodiversity gradients.....116

Figure 4.14. Sum of proportional latitudinal richness differences between simulated and sampled, and simulated and sampling-standardised latitudinal biodiversity gradients 117

Figure 4.15. Relationship between the sum of proportional latitudinal richness differences and the skewness of palaeolatitudinal spatial sampling coverage. 118

Figure 4.16. Relationship between the sum of proportional latitudinal richness differences and palaeolatitudinal data absence. 119

Figure 4.17. Slope estimates of simulated, sampled, and sampling-standardised latitudinal biodiversity gradients. 121

Figure 4.18. Global raw counts of sampled diversity from simulations of species' distributions and richness, conforming to a flat-, unimodal-, and bimodal-type latitudinal biodiversity gradient. 122

Figure 5.1. The present-day latitudinal biodiversity gradient of zooxanthellate corals at varying bin protocols.....138

Figure 5.2. Absolute palaeolatitudinal distribution of fossil zooxanthellate coral bearing collections (Anisian to Piacenzian). 142

Figure 5.3. Raw counts of genera, collections, formations, and occupied equal-area grid cells (250 km spacings), within palaeolatitudinal and ~10 million-year time bins. ..143

Figure 5.4. Summed minimum-spanning tree length between occupied equal-area grid cells (250 km spacings) within palaeolatitudinal, and ~10 million-year time bins. ..144

Figure 5.5. Relationship between uncorrected genus richness and sampling per palaeolatitudinal and temporal bin. 144

Figure 5.6. Coverage-standardised richness estimates implemented with a fixed grid cell rarefaction procedure.....146

Figure 5.7. Coverage-standardised richness estimates implemented with a minimum grid cell rarefaction procedure 148

Figure 5.8. Comparison plot of uncorrected and corrected tropical (0–30°N) and temperate (30–60°N) diversity. 149

Figure 5.9. Relationship between sampling and coverage-standardised genus richness estimates, implemented with a grid cell rarefaction procedure per palaeolatitudinal and temporal bin. 150

Figure 6.1. Global distribution of warm-water coral reefs during the present day...161

Figure 6.2. Global distribution of fossil (Anisian–Piacenzian) warm-water coral reefs occurrences used in this study. 162

Figure 6.3. Predictive performance of model projections for binary thresholds MaxSSS and LTP 170

Figure 6.4. Binary habitat suitability map and species/genus-richness-area curves. 171

Figure 6.5. Relationship between estimated suitable habitat area and zooxanthellate coral species richness within variable latitudinal bin sizes. 172

Figure 6.6. Relationship between estimated suitable habitat area and zooxanthellate coral species richness within variable latitudinal bin sizes. 172

Figure 6.7. Relationship between estimated suitable habitat area and zooxanthellate coral genus richness within variable latitudinal bin sizes. 173

Figure 6.8. Relationship between estimated suitable habitat area and zooxanthellate coral genus richness within variable latitudinal bin sizes. 173

Figure 6.9. Palaeolatitudinal plots of estimated suitable habitat area for warm-water coral reefs under binary thresholds LTP and MaxSSS. 175

Figure 6.10. Palaeolatitudinal shifts in the centroid of suitable habitat area from the Anisian to Piacenzian for warm-water coral reefs. 176

Figure A.1. Difference maps of estimated habitat suitability for the Last Interglacial for different sea levels 219

Figure A.2. Difference map of estimated habitat suitability for modern projections from the modern-trained ecological niche model with and without aragonite saturation state variable included 219

Figure B.1. Stage-level (Piacenzian–Asselian) latitudinal plots (15° bins) of simulated, sampled, and sampling-standardised latitudinal biodiversity gradients for three different types of gradient (flat, unimodal and bimodal). 223

Figure C.1. Palaeolatitudinal plots of estimated unclamped suitable habitat area for warm-water coral reefs under binary thresholds LTP and MaxSSS. 242

Figure C.2. Bartonian–Piacenzian mean stage-level August sea surface temperature from the HadCM3L. 243

Figure C.3. Bartonian–Piacenzian mean stage-level February sea surface temperature from the HadCM3L. 244

Figure C.4. Bartonian–Piacenzian palaeobathymetry reconstructions from the Getech PLC digital elevation models. 245

List of Tables

Table 1.1. Mechanisms proposed to explain the latitudinal biodiversity gradient. ... 23

Table 3.1. Latitudinal habitability from binary predictions..... 82

Table 4.1. Summary statistics of palaeolatitudinal spatial sampling coverage.....108

Table 5.1. Composite time bins used in this study. 137

Table 5.2. Latitudinal binning protocol used in this study 138

Table 6.1. Palaeolatitudinal binning protocol used in this study 167

Table 6.2. The predictive performance of model projections.....169

Table A.1. Mean biomod2 variable importance test scores for modern-trained ecological niche model with aragonite saturation state variable included 220

Table A.2. Mean biomod2 variable importance test scores for ecological niche models trained on both modern and Last Interglacial training datasets 220

Table B.1. Kolmogorov-Smirnov two-sample test results from empirical range size frequency distributions and those simulated. 221

Table B.2. Kolmogorov-Smirnov two-sample test results from empirical occurrence frequency distributions and those simulated. 222

–This page is intentionally left blank–

1 Introduction

1.1 Introduction to the thesis

Human activity continues to decimate the planet. Although geologically short-lived, our species has profoundly influenced the global environment through land surface transformation and altering the Earth's oceans and atmosphere (Bellard et al., 2012; Lewis and Maslin, 2015). These global environmental changes have encouraged some to endorse the recognition of a new human-dominated geological epoch, the Anthropocene (Ruddiman, 2013; Lewis and Maslin, 2015). Moreover, the ongoing global biodiversity crisis has led some researchers to suggest we may be entering, or already in the midst of the 'sixth mass extinction' (Dirzo and Raven, 2003; Wake and Vredenburg, 2008; Barnosky et al., 2011; Dirzo et al., 2014; McCallum, 2015). Whilst extinction rates have historically been magnified by anthropogenically-driven habitat loss, hunting and invasive species (Dirzo and Raven, 2003; Dirzo et al., 2014), projected global warming of 1.8–5.6°C (O'Neill et al., 2016) will likely soon compete with habitat loss as the most important driver of biodiversity loss (Dirzo et al., 2014). Rising sea surface temperatures have already generated ecological disturbances and substantial range shifts of marine organisms (Poloczanska et al., 2013, 2016; García Molinos et al., 2016). Coral reefs—one of the most biologically diverse and economically valuable ecosystems in the marine realm (Moberg and Folke, 1999)—now face collapse in their current tropical distribution as a direct result of thermal anomalies (Pandolfi et al., 2003; Heron et al., 2016; Hughes et al., 2017b; Kim et al., 2019). However, constraining the long-term response of organisms to projected global warming is challenging. Conservation biology has traditionally relied almost exclusively on modern (or recent historical) data about populations and ecosystems, providing limited temporal perspective (Turvey and Saupe, 2019). Today, the International Union for Conservation of Nature (IUCN) Red List provides the world's most comprehensive inventory of the conservation status of species. However, the 'long-term' ecological datasets that it depends on are generally restricted to the last 30–40 years (Vié et al., 2009), when population decline was largely driven by habitat loss (Dirzo et al., 2014). Disentangling the impacts of global warming from other anthropogenic impacts is

therefore difficult. Furthermore, such narrow temporal scales limit our ability to understand 'natural' baseline patterns of species diversity, as well as the long-term recovery or loss of ecosystems in response to secular climate change (Dietl et al., 2015; Turvey and Saupe, 2019).

The fossil record provides an archive of the evolution of life on Earth. It documents biotic responses to instantaneous events, such as asteroid impacts (Brusatte et al., 2015), and those sustained over geological time scales, such as plate tectonic shifts (Crame and Rosen, 2002; Renema et al., 2008). Significantly, the fossil record can also help define ecosystem baselines, and improve our understanding of the long-term biotic response to global climatic change. This insight has significant value for conservation efforts as anthropogenic pressures continue to disrupt ecosystems, and drive further global change (Dietl et al., 2015; Barnosky et al., 2017; Turvey and Saupe, 2019). However, just beneath the surface of this wealth of empirical data, an inherent and universally recognised problem exists: the fossil record is incomplete and severely biased. Geological and anthropogenic processes have generated pervasive and non-uniform biases in the fossil record, resulting in an archive that is unevenly distributed through time and space (Holland, 1995; Smith and McGowan, 2007; Upchurch et al., 2011; Close et al., 2020b). The impact of these biases on the reconstruction of biotic patterns and processes has been described and documented for almost half a century (Raup, 1972; Sheehan, 1977; Raup and Sepkoski, 1982; Allison and Briggs, 1993; Cherns and Wright, 2000). However, palaeobiologists continue to dispute the extent of these issues, and how best to correct for them (Smith and McGowan, 2007; Alroy, 2010a; Benson and Butler, 2011; Smith and McGowan, 2011; Vilhena and Smith, 2013; Close et al., 2018, 2020b). Understanding the nature of these biases, and developing the mitigating strategies for managing them, is paramount to unlocking the full potential of the fossil record.

In this thesis, a range of interdisciplinary tools are used to evaluate whether macroecological patterns observed in the fossil record are a genuine biological signal, or the result of sampling bias. The focus of this work is one of Earth's most pervasive

macroecological patterns, the latitudinal biodiversity gradient. Though the aim of this thesis is not to focus on any particular taxonomic group, Scleractinia (stony corals) and coral reefs are used to test hypotheses proposed in three of the four results chapters, while the whole marine fossil record of animals is used in the other. This introductory chapter provides an overview of the themes addressed in this thesis, providing fundamental context for subsequent chapters. However, background specific to the work presented in each research chapter (3–6) is provided therein.

1.2 The Latitudinal biodiversity gradient

1.2.1 Overview

One of the most prominent macroecological patterns on Earth today is the latitudinal biodiversity gradient (LBG), in which species richness decreases from tropical to polar regions (Rosenzweig, 1995; Willig et al., 2003; Hillebrand, 2004). The majority of extant fauna and flora (e.g. corals, fish, foraminiferans, mammals, reptiles, and vascular plants) conform to this unimodal gradient (Willig et al., 2003; Hillebrand, 2004; Field et al., 2009; Kiessling et al., 2012; Willig and Presley, 2018), and it has been described as Earth's first-order biodiversity pattern (Krug et al., 2009). In fact, one meta-analysis with nearly 600 LBGs assembled from the literature corroborated the high generality of this gradient (Hillebrand, 2004). However, whilst the LBG is a pervasive pattern across most taxa today, not all groups conform to this gradient. It is noteworthy that the diversity peaks of some groups (e.g. parasites, aquatic flora, marine birds and mammals) is at higher latitudes (Chown et al., 1998; Procheş, 2001; Willig et al., 2003; Wiens, 2007; Tittensor et al., 2010; Willig and Presley, 2018). Reconstructions from fossil occurrence data have also questioned the permanence of the LBG, with a range of taxonomic groups characterised by flattened or even bimodal gradients in deep time (Figure 1.1) (e.g. Mannion et al., 2012; Yasuhara et al., 2012; Powell et al., 2015; Marcot et al., 2016; Nicholson et al., 2016; Brocklehurst et al., 2017; Kröger, 2018).

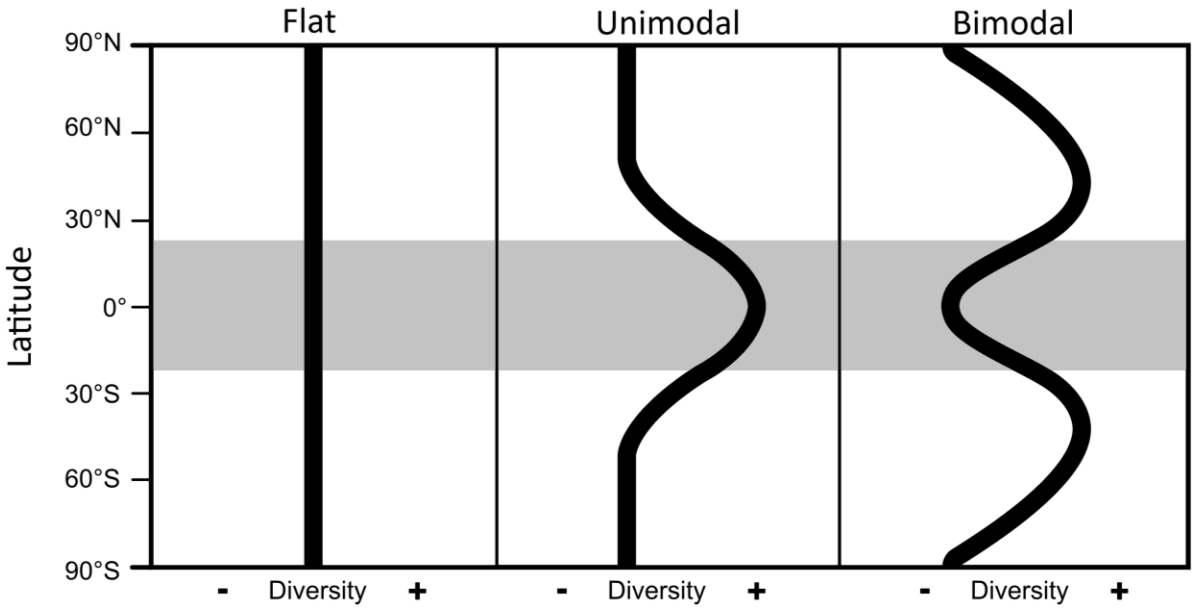


Figure 1.1. Graphical representation of different types of latitudinal biodiversity gradients. A flat latitudinal biodiversity gradient has no prominent latitudinal peak in diversity; a unimodal (modern type) gradient has a tropical peak in diversity, with taxonomic richness declining poleward; a bimodal gradient has twin temperate peaks in diversity, with taxonomic richness declining towards the equator and the poles. Grey shaded area illustrates the extent of the tropics today (23.4°N–23.4°S), as defined as the areas of Earth's surface that receive direct overhead solar radiation at some point during the year. Note that this is the classical definition of the tropics, but variability in definition exist (see Feeley and Stroud, 2018).

1.2.2 The drivers of the latitudinal biodiversity gradient

The LBG is recognised as one of ecology's oldest patterns, and has been studied and debated for more than two centuries (Humboldt, 1808; Hawkins, 2001; Jablonski et al., 2017). However, considerable debate continues regarding the relative importance of individual drivers of the LBG, with stochastic, historical, ecological and evolutionary processes advocated by macroecologists (Jablonski et al., 2017; Willig and Presley, 2018). To date, over 25 hypotheses have been proposed to explain the presence of the LBG (Table 1.1) (Rohde, 1992; Mittelbach et al., 2007; Brown, 2013; Fine, 2015; Jablonski et al., 2017; Willig and Presley, 2018). However, the majority of these hypotheses can be rejected for being circular, interlinked, or too specific to explain the pervasiveness of this gradient (Willig et al., 2003; Willig and Presley, 2018). Herein, several of the most heavily debated mechanisms are expanded upon. However, as will become evident, not all are mutually exclusive.

Table 1.1. Mechanisms proposed to explain the latitudinal biodiversity gradient. Table compiled from Willig and Presley (2018).

Circular	Empirically unsubstantiated
Competition	Environmental stability
Mutualism	Environmental predictability (contingency)
Predation	Productivity
Epidemics	Abiotic rarefaction
Biotic spatial heterogeneity	Physical heterogeneity
Population size	Angle of the sun above the horizon
Niche width	Area
Population growth rate	Aridity
Patchiness	Seasonality
Epiphyte load	Number of habitats
Host diversity	Rapoport's rule
Harshness	Ecological time
	Evolutionary time
	Temperature dependence of chemical reactions
	Solar energy
	Evolutionary speed
	Stochastic placement of species ranges

Net diversification rates. The modern-type LBG can be explained by greater net diversification rates (i.e. origination rate minus extinction rate) in the tropics than other regions. Subsequently, the tropics have often been regarded as either a 'cradle', with higher origination rates than temperate or polar regions, or a 'museum', with lower tropical extinction rates than in temperate or polar regions (Gaston and Blackburn, 1996; Chown and Gaston, 2000; Mittelbach et al., 2007; Arita and Vázquez-Domínguez, 2008; Krug et al., 2009; Rull, 2011). However, studies have also found evidence of higher origination rates and lower extinction rates in the tropics, suggesting this region may serve as both a cradle and a museum of diversity (Allen and Gillooly, 2006; Jablonski et al., 2006, 2017; McKenna and Farrell, 2006; Mittelbach et al., 2007; Weir and Schluter, 2007; Jablonski, 2008). Many of the drivers proposed to explain the modern LBG can directly or indirectly affect rates of origination and/or extinction. However, the relative contribution of origination and extinction rates in the tropics is uncertain, and further complicated by dispersal into and out of the tropics (Gaston and Blackburn, 1996; Chown and Gaston, 2000; Jablonski et al., 2006; Roy and Goldberg, 2007; Arita and Vázquez-Domínguez, 2008; Saupe et al., 2019c).

Furthermore, a number of studies have found evidence for contrarian patterns, such as faster rates of speciation in marine fishes at polar latitudes (Rabosky et al., 2018), and similar diversification rates of mammals across all latitudes (though see Soria-Carrasco and Castresana, 2012; Rolland et al., 2014). One school of thought is that net diversification rates are primarily driven by temperature (Rohde, 1992). As physiological processes are faster at higher temperatures, and warmer environments support shorter generation times and increased mutation rates, the tropics ought to favour greater origination rates (Rohde, 1992; Willig and Presley, 2018). Greater net diversification rates may also be the result of low seasonality in the tropics. Low seasonality might encourage the origination of species with narrow ecological niches, which may result in limited dispersal capacity across environmental gradients, as well as population fragmentation and speciation (Archibald et al., 2010). Indirect climatic factors have also been postulated as a potential driver of the LBG. Due to the angle of incidence of insolation, lower latitudes receive greater solar radiation than higher latitudes, promoting increased productivity in the tropics (Waide et al., 1999). However, whilst it is generally accepted that higher productivity levels result in larger viable population sizes and species richness, there are instances where this relationship is not emulated (Waide et al., 1999; Archibald et al., 2010). Nevertheless, seasonality is often considered the most important driver of the LBG by some authors (Archibald et al., 2010, 2013; Valentine and Jablonski, 2015).

Geographic Area Hypothesis. The greater availability of geographic area in the tropics has been proposed as a potential mechanism that contributes to the LBG (Terborgh, 1973; Rosenzweig, 1995; Jetz and Fine, 2012). Whilst the tropics contains a single contiguous geographic area with similar climatic conditions, temperate and polar regions are separated by a substantial geographic distance and strong environmental barriers. Larger geographic areas of similar environmental conditions could promote lower extinction rates as they enable larger range and population sizes, reducing risk from stochastic extinction (Willig and Presley, 2018). In addition, the formation of geographic barriers due to sea level changes, or other geological events,

should occur more frequently in larger geographic areas, resulting in allopatric speciation (i.e. greater origination rates). In combination, these factors might explain higher net diversification rates in the tropics today via lower extinction rates and higher origination rates.

Mid-domain hypotheses. Whilst species richness gradients may arise through environmental and/or historical gradients, simple geometric constraints on species range boundaries can also produce gradients in taxonomic richness (Colwell and Lees, 2000). The random placement of species geographic range boundaries, within a geographic framework, produces peaks in species richness near the centre, which could explain tropical peaks in species richness (Colwell and Lees, 2000; Colwell et al., 2004). This is known as the mid-domain effect, and has been proposed as one mechanism that contributes to the LBG (Colwell and Hurtt, 1994; Colwell and Lees, 2000; Colwell et al., 2004). However, the validity of the mid-domain effect at global scale has been the subject of serious debate (Colwell et al., 2004; Fieldsend, 2020). Perhaps most significant is the misrepresentation of the Earth's surface. For the mid-domain effect to arise at global scale, the Earth needs to be considered as a bounded geographical domain, with the poles as the boundaries. However, the surface of the Earth is (roughly) a sphere, and the arbitrary placement of the boundaries at the Poles is misleading in a geometric sense (Fieldsend, 2020). Whilst from a human perspective we envisage the tropics as the mid-domain of Earth, the Poles are no more the boundary conditions than any other point on the surface of the planet.

Rapoport's rule. The Rapoport effect, or Rapoport's rule, describes the relationship between species geographic range size and latitude. Specifically, it postulates that species geographic range size decreases from high to low latitudes, and is potentially a result of seasonality (Stevens, 1989). Seasonality increases poleward, suggesting temperate species must tolerate greater variations in climate than tropical species. This seasonal variability in climate could predispose temperate species to have wider abiotic niches and larger geographic range sizes, while tropical species should have narrower abiotic niches and smaller geographic range sizes. In theory, smaller geographic range

sizes at low latitudes could enable more species to coexist than at higher latitudes, producing tropical peaks in diversity (Stevens, 1989). However, it is unclear how a lack of seasonality within a single large contiguous geographic area (~50°) would limit the range size of species in the tropics (Willig and Presley, 2018). Nevertheless, whilst Rapoport's rule has been demonstrated in a range of groups including mammals, reptiles, amphibians, fish, and trees (Rapoport, 1975, 1982; Stevens, 1989), its generality is not supported in all taxonomic groups (e.g. mollusks, eucalypts, marsupials and bats) (Roy et al., 1994; Hughes et al., 1996; Willig and Lyons, 1998).

1.2.3 Deep time perspective

The fossil record offers a unique perspective into the drivers and evolution of the LBG, including responses to continental reconfiguration and major climatic perturbations (Powell, 2009; Mannion et al., 2012; Nicholson et al., 2016; Brocklehurst et al., 2017). Studies focused solely on the present day are limited to the final page of an archive spanning hundreds of millions of years. Whilst climatic and geographic conditions are broadly static today, they have fluctuated substantially since the evolution of complex life. Furthermore, as the LBG is ultimately a function of latitudinal differences in net diversification rates, in which complex combinations of origination and extinction persist, fossil data are needed to understand its evolution (Jablonski et al., 2013).

Early reconstructions of the LBG suggested that a unimodal gradient, with tropical peaks in diversity, was present throughout the Phanerozoic (the last 540 million years (myr) (Crame, 2001; Powell, 2007, 2009; Alroy et al., 2008; Krug et al., 2009; Powell et al., 2012), though evidently shallower at certain intervals (Crame, 2001; Mittelbach et al., 2007). Several authors also recognised that the LBG did not particularly strengthen to form the present-day steep gradient until 30 million years ago (Ma) (Thomas and Gooday, 1996; Crame, 2001; Powell, 2009; Archibald et al., 2013). However, the strength of these conclusions has been questioned due to failures to correct for sampling biases, which might produce artefactual diversity peaks or gradients (Note to the reader: discussion on the different types of sampling biases is

reserved for a later section of this chapter). Recent analyses, which have mitigated for varying levels of sampling intensity, have suggested that tropical peaks and poleward declines in taxonomic richness were not universal throughout the Phanerozoic, with a range of taxonomic groups characterised by flattened or even bimodal gradients (e.g. Mannion et al., 2012; Yasuhara et al., 2012; Powell et al., 2015; Marcot et al., 2016; Nicholson et al., 2016; Brocklehurst et al., 2017; Kröger, 2018). In fact, tropical peaks and poleward declines in taxonomic richness appear to be largely restricted to intervals of the Palaeozoic, and the past 30 myr, when cold icehouse climatic regimes have persisted (Jablonski et al., 2006; Powell, 2009; Archibald et al., 2010; Yasuhara et al., 2012; Mannion et al., 2014; Marcot et al., 2016; Fenton et al., 2016).

Whilst recent studies have tended to correct for sampling intensity, they do not address the spatiotemporal heterogeneity in sampled geographic area (Vilhena and Smith, 2013; Benson et al., 2016; Close et al., 2017, 2020a). As inherently spatial patterns, reconstructions of LBGs in deep time have the capacity to be particularly impacted by variation in the geographic sampling universe (area available to sample by palaeontologists), which can result in drastically different sizes of underlying taxon pools (Close et al., 2017, 2020b). Correcting for the spatial structure of the fossil record and inherent data absence remains a fundamental issue for palaeobiologists.

1.3 Corals, reefs, and global climatic change

Scleractinia, or more colloquially stony corals, are an order of polypoidal marine invertebrates belonging to the taxonomic class Anthozoa of the Cnidaria phylum. Their origin is considered to be deeply rooted in the Palaeozoic, with evidence of 'scleractiniamorphs' as early as 450 Ma during the Ordovician (Stolarski et al., 2011). However, prior to the Triassic, scleractiniamorphs are sparsely represented in the fossil record, and it is only from the Anisian (247.2 Ma) that Scleractinia have a continuous fossil record (Stolarski et al., 2011; Kiessling and Kocsis, 2015). Nevertheless, this 247.2 myr presence in the geological record makes them ideal candidates for assessing the veracity of biodiversity patterns in deep time.

Today, scleractinians maintain a global distribution, and are responsible for the formation of modern coral reef systems. Zooxanthellate, azooxanthellate, and apozooxantehllate corals are found within the taxonomic order, and strongly differ in their ecological requirements and environmental occupancy. Zooxanthellate corals have a photosymbiotic relationship with single-celled dinoflagellates called zooxanthellae. This relationship can contribute up to 90% of the nutritional needs of the coral (Muscatine and Porter, 1977; Lipps and Stanley, 2016). Conversely, azooxanthellate corals lack a photosymbiotic relationship and principally gather their nutritional needs from filtration feeding. Uniquely, apozooxanthellate maintain a facultative symbiosis with zooxanthellae, and have the capacity to switch back and forth depending on their environmental occupancy (Stanley, 2003). Whilst zooxanthellate and azooxanthellate corals are equally as diverse today (Cairns, 1999, 2007; Kiessling and Kocsis, 2015), apozooxantehllate are exceptionally rare.

The dependence of zooxanthellate corals on photosymbiosis limits them to well-lit, warm, and shallow waters, resulting in a predominantly tropical distribution (Kleypas et al., 1999; Couce et al., 2012; Muir et al., 2015). However, whilst ecologically limiting, photosymbiosis provides zooxanthellate corals with the metabolic advantages required for rapid calcification, and prolific reef building (Muscatine and Porter, 1977; Lipps and Stanley, 2016). Though azooxanthellate corals also occupy tropical environments, they preferentially inhabit deep and cold waters in the aphotic zone (Cairns, 2007). If nutrient levels are high enough, azooxanthellate corals may also build reefs. However, deep-water coral reef building is typically restricted to a few azooxanthellate taxa, and reefs at any given location are typically constructed by one species (Freiwald et al., 2004). For example, the Røst Reef off the coast of Norway is constructed by *Lophelia pertusa*, and occupies an area of 100 km^2, making it the world's largest (known) deep-water coral reef complex (Freiwald et al., 2004). Though capable of forming large habitats, deep-water coral reefs are incomparable to their shallow marine tropical counterparts. The Great Barrier Reef—the largest warm-water coral reef complex—is more than 30,000 km^2 in total area.

Warm-water coral reefs are one of the most biologically diverse and economically valuable ecosystems in the marine realm (Moberg and Folke, 1999; Cesar, 2000; Knowlton, 2001). They provide a range of services including habitat structure, coastal protection, food security, recreational opportunities, and raw materials (Moberg and Folke, 1999; Cesar, 2000; Hughes et al., 2017a). However, rising sea surface temperatures increasingly trigger mass bleaching events of zooxanthellate corals, including three pan-tropical events in the last two decades (Pandolfi et al., 2003; Heron et al., 2016; Hughes et al., 2017b). Thermal stress during marine heatwaves disrupts the photosymbiotic relationship between coral and algal symbiont, resulting in the loss of the corals' colour (hence 'bleaching') (Spalding and Brown, 2015). Bleached corals are physiologically damaged, and prolonged bleaching tends to lead to high levels of mortality (Glynn, 1984; Berkelmans et al., 2004; Hughes et al., 2017b). As bleaching events become increasingly frequent, declines in coral cover and reef structural complexity will impact all marine species who depend on coral reefs (estimated at ~35% of all described marine species) (Reaka-Kudla, 2005; Knowlton et al., 2010). As such, understanding the long-term response of corals, and coral reefs, to global warming is of paramount importance for conserving global biodiversity.

Today, zooxanthellate corals have a steep unimodal-type LBG (Veron, 2000; Kiessling et al., 2012; Spano et al., 2016), with high diversity confined to tropical regions and absolute latitudinal limits of 45° either side of the equator (Kiessling et al., 2012; Muir et al., 2015). However, several zooxanthellate coral species have already expanded their ranges poleward in response to increasing sea surface temperatures (Precht and Aronson, 2004; Yamano et al., 2011; Baird et al., 2012). As global warming continues to intensify, it is likely that equatorial range retractions will follow these poleward range expansions (Kiessling et al., 2012). Throughout their evolutionary history, many zooxanthellate corals (and coral reefs) have occupied palaeolatitudes higher than 45° (Kiessling and Kocsis, 2015). However, the evolution of the LBG in zooxanthellate corals remains unresolved.

1.4 Estimating biodiversity in deep time

1.4.1 Historical context

One of the earliest reconstructions of diversity over geological timescales was by Heinrich Georg Bronn, in which he compiled an inventory of the known fossil record to produce spindle diagrams, and identify patterns of dynamic succession (Bronn, 1848). However, it was not until 1860 that geologist John Phillips produced the first Phanerozoic 'diversity curve', on the basis of the British fossil record (Phillips, 1860). Even during the 1800s, geologists recognised that the fossil record was imperfect (Darwin, 1859; Phillips, 1860). Philips (1860) himself expressed concerns about sampling bias in the fossil record, and attempted to correct his Phanerozoic diversity curve by stratigraphic interval thickness. However, it was not until the 1950s when interest in eon-scale diversity patterns started to flourish, energised by Norman Newell who proposed that cyclic changes in sea level drove variation in marine diversity (Newell, 1952).

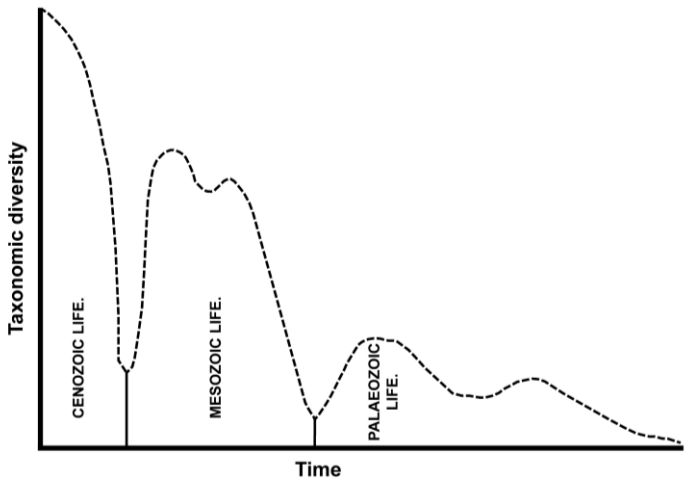


Figure 1.2. The first Phanerozoic diversity curve based on data from the British fossil record. Figure is redrawn from Phillips (1860).

Whilst this early work—which required collating data by hand—was seminal to the study of past diversity, it was the advent of general-purpose computing in the 1970s that enabled a burst of eon-scale biodiversity studies. General-purpose computing allowed the construction of digital databases, which improved efficiency in data curation, sharing, and analyses. Appropriately referred to as the 'palaeobiological

revolution', the 1970s and 1980s were witness to some of the first palaeobiological studies conducted using digital databases (Raup, 1976a, 1976b; Valentine et al., 1978; Raup and Sepkoski, 1982). Significantly, this revolution resulted in the publication that identified the 'Big Five' mass extinctions (Raup and Sepkoski, 1982). However, early work by David Raup highlighted the ties between species diversity and the volume of sedimentary outcrop, casting doubts on raw counts of diversity (Raup, 1976b). Peter Sheehan raised similar concerns, and demonstrated a strong relationship between the number of described species within an interval, and so called 'Palaeontological Interest Units' (the number of palaeontologists working in an interval) (Sheehan, 1977). However, despite these concerns the impact of biases on estimates of past diversity were largely neglected until the turn of the century (e.g. Allison and Briggs, 1993; Miller and Foote, 1996; Markwick, 1998; Alroy et al., 2001). Nevertheless, by the early 2000s, studies began to indicate systematic bias in outcrop area (Peters and Foote, 2001), geographic representation (Jackson and Johnson, 2001), habitat representation (Smith, 2001; Allison and Wells, 2006), and fossil collections (Alroy et al., 2001). Socioeconomic factors, such as population and gross domestic product, were also identified as influencing the known fossil record (Kiessling, 2005).

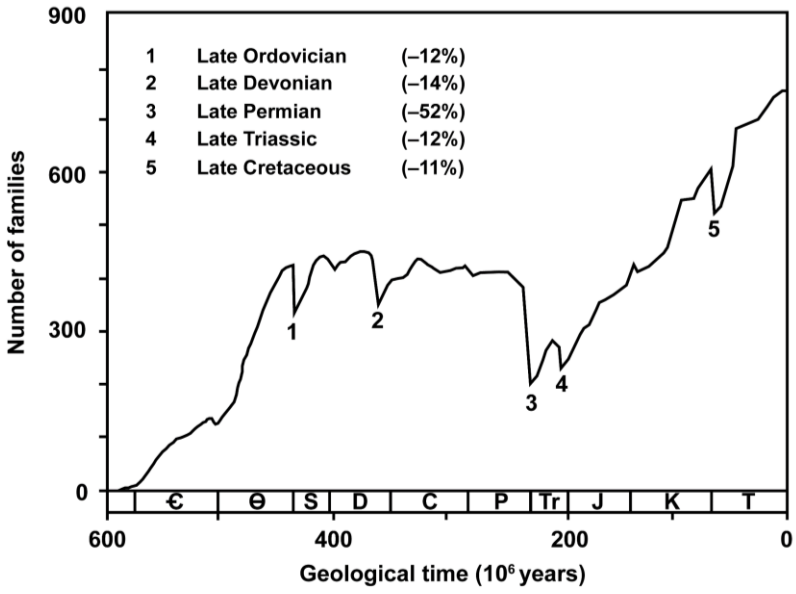


Figure 1.3. Raup and Sepkoski's diversity curve (Raup and Sepkoski, 1982). Figure shows the standing diversity through time for marine vertebrates and invertebrate families, and identifies five mass extinction events. The relative magnitude of each extinction event is given in the parentheses in the upper left corner. Figure is redrawn from Raup and Sepkoski (1982).

Despite the advocation of sampling-standardisation procedures decades before (Raup, 1975), it was not until this century that their implementation became widespread in palaeobiological studies. This was likely a result of the increasing familiarity and accessibility to computers, as well as the previously described flourish of studies investigating the impacts of bias on estimates of palaeodiversity (e.g. Jackson and Johnson, 2001; Peters and Foote, 2001; Smith, 2001; Alroy et al., 2001). Nevertheless, in the past two decades, the development and application of a number of sampling-standardisation strategies have been implemented to correct for sampling bias in the fossil record, and provide fairer estimates of past biodiversity (e.g. Alroy, 2000; Smith and McGowan, 2007; Alroy, 2010a; Mannion et al., 2012; Lloyd et al., 2012; Smith et al., 2012; Lloyd and Friedman, 2013; Alroy, 2014; Mannion et al., 2015; Benson et al., 2016; Starrfelt and Liow, 2016; Close et al., 2017; Cleary et al., 2018; Close et al., 2018; Dunne et al., 2018; Dean et al., 2019; Close et al., 2020a, 2020b; De Celis et al., 2020). In subsequent sections, further details on these approaches are provided. However, it is first pertinent to review the biases that influence the fossil record.

1.4.2 Taphonomic biases

A suite of biological characteristics and taphonomic processes influence the information available from the fossil record. In 1940, Ivan Efremov officially introduced the subdiscipline of 'taphonomy', defining it at as "the study of the transition of animal remains from the biosphere into the lithosphere" (Efremov, 1940). However, it should be noted that earlier work by German researchers had already laid the foundations for taphonomy (Abel, 1912; Wasmund, 1926; Weigelt, 1927; Richter, 1928). Today, taphonomy has a broader definition, and is defined as "the study of processes of preservation, and how they affect information in the fossil record" (Behrensmeyer and Kidwell, 1985). Taphonomic bias refers to the systematic preservation or removal of an organism as a result of some internal or external control. Herein, a general overview of some of the key taphonomic biases in the fossil record are provided. However, for an exhaustive review, the reader is referred to key texts such as Allison and Briggs (1991), Lyman and Lyman (1994), Martin (1999), and Allison and Bottjer (2010).

Taphonomic bias may be introduced into the fossil record by an organism's body composition, morphology and ecology. For example, hard biomineralized remains of organisms—teeth, shells and bones—have a high preservation potential, whereas soft tissues are rarely preserved (Briggs, 2003; Allison and Bottjer, 2010). Modern marine communities may be composed of up to 67% soft-bodied species (Lawrence, 1968), suggesting potential for significant information loss from body composition alone. This mechanism undoubtedly results in a large underrepresentation of soft-bodied taxa across the Phanerozoic, especially for taxonomic groups such as Scyphozoa ('true jellyfish'). However, biomineralized remains may also be impacted by preservation biases. For example, the preferential dissolution of the biogenic carbonate polymorph aragonite, relative to its more stable calcitic form, has the capacity to influence estimates of past biodiversity and community structure (Cherns and Wright, 2000; Dean et al., 2019). The body size of an organism also influences preservation potential, with larger organisms more readily preserved in the fossil record (Kidwell, 1997; Cooper et al., 2006). The environment an organism inhabits also impacts upon preservation potential (Behrensmeyer et al., 2000). For example, reduced erosion and enhanced sediment supply in the marine realm promotes a more complete fossil record than the terrestrial environment (Kidwell and Holland, 2002). In fact, sediment accumulation rate has been advocated as the primary control on the nature of the fossil record, with strong correlations between various evolutionary trends and changes in sedimentation rates (Kidwell, 1986). Intuitively, biota from environments of high sediment accumulation rates might therefore be disproportionately represented in the fossil record. Post-burial processes, such as bioturbation, microbial decay, chemical alteration, reworking and exhumation may also lead to variability in the preservation potential and quality of remains (Behrensmeyer et al., 2000). The final fate of an organisms' preservation potential will often depend upon processes such as compaction and burial depth after entering the lithosphere. Each sedimentary package, and the remains they contain, have their own unique and complex geological histories. These histories play a significant role in determining the survival or loss of fossil remains.

1.4.3 Sampling bias

Sampling attempts to estimate the patterns and processes of a whole population based on a subset of individuals. To remain representative, a sample should meet a predetermined number of observations, and not be subject to a biased sampling methodology. For centuries, palaeontologists have used the known fossil record—a sample of life in the geological past—to gain understanding of macroevolutionary patterns and processes. However, the quality and quantity of this data is influenced by geological and anthropogenic factors that generate an uneven temporal and spatial structure in the fossil record. Failure to correct for this uneven structure results in a biased sampling of life in the past, and fundamentally contradicts the characterisation of a sample. Herein, some of the main geological and anthropogenic factors that influence the fossil record are discussed in further detail.

The spatiotemporal variability of Earth system processes results in a heterogeneous distribution of rock volume, and a non-uniform sampling window of geographic regions, time periods and environments. Early work by Raup (1972) was amongst the first to identify the potential impacts of sampling biases on estimates of diversity, in which he outlined seven "sources of error". One of these sources of errors (= sampling biases), came from the strong relationship between sedimentary rock volume and species richness (Raup, 1972). Raup (1972) suggested that the number of taxa within a given time bin must be a function of the volume of sedimentary rock available for sampling. Since this early work, a suite of studies has demonstrated the impacts of variable sedimentary rock volume and surface exposure on estimates of taxonomic richness (Wall et al., 2009; Smith and McGowan, 2011; Upchurch et al., 2011; Vilhena and Smith, 2013; Dunhill et al., 2014; Dean et al., 2016). Unsurprisingly, these studies unequivocally confirm that a greater surface area of exposed sedimentary rock leads to a greater volume in collected species. At temporal scales, this relationship has the potential to drive observed trends in biodiversity patterns, including extinction and speciation events (Signor and Lipps, 1982; Miller and Foote, 1996; Sepkoski, 1998; Alroy et al., 2001). However, this relationship also has the potential to influence our

understanding of past macroecological patterns, such as the latitudinal biodiversity gradient. A key example of this is how the palaeolatitudinal distribution of sedimentary rock volume has shifted throughout the Phanerozoic (Figure 1.4), tracked by palaeolatitudinal biodiversity estimates (Allison and Briggs, 1993; Vilhena and Smith, 2013). Such changes in the spatiotemporal distribution of sampling could lead to erroneous conclusions about the shape of the latitudinal biodiversity gradient in deep time. However, correlation between variables such as the surface area of exposed sedimentary rock and diversity does not necessarily equal causation. An alternative view is the 'common-cause' hypotheses, in which both sampling and diversity are driven by some common factor such as sea level fluctuations (Peters, 2005; Butler et al., 2010; Dunhill et al., 2014).

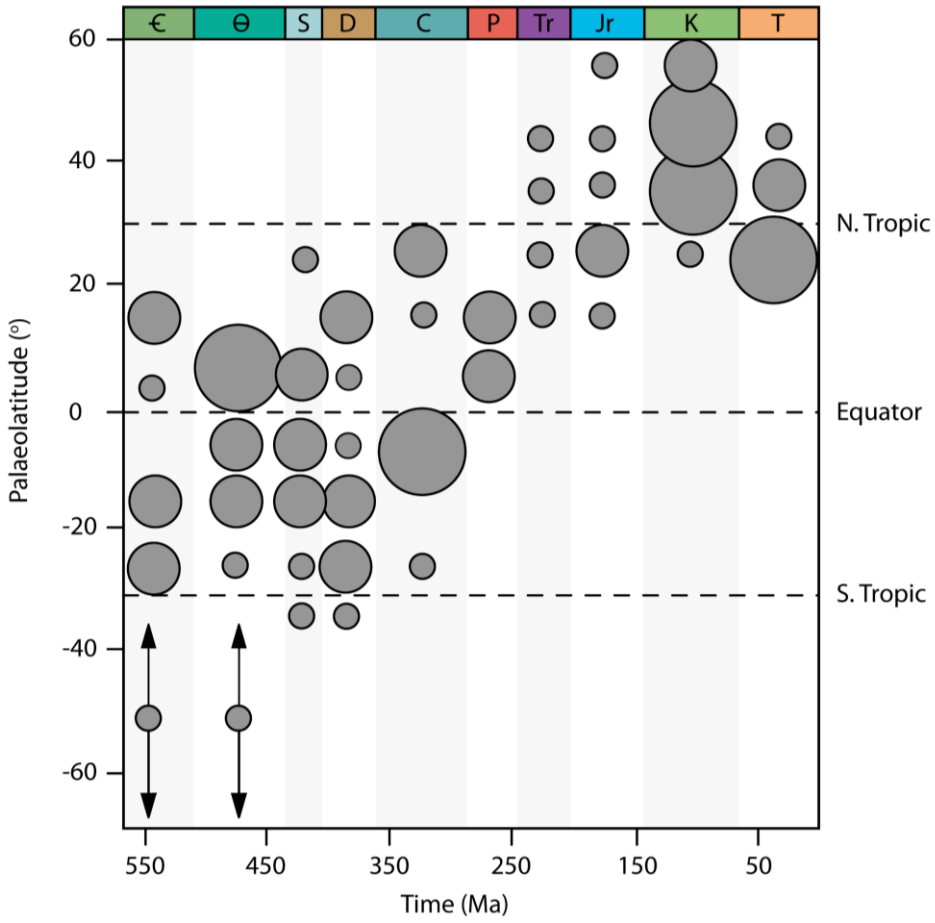


Figure 1.4. Palaeolatitudinal distribution of Phanerozoic marine sedimentary rock outcrop in Europe and North America. Circles indicate the areas of outcrop: small—<100,000 km^2; medium—100,000 to 500,000 km^2; large—>500,000 km^2. Arrows indicate potential variation in depositional latitude for areas of rapidly drifting continental masses. Figure is redrawn from Dean (2018), and based on original figure from Allison and Briggs (1993).

Another source of error in the fossil record is the general increasing quality of the sedimentary record with proximity to the recent. Younger parts of the geological record tend to be represented by larger volumes of rock and are less covered by overlying strata (increasing accessibility for collectors). Significantly, the amount of erosion, metamorphism and deformation also tends to be less in younger sedimentary packages (Raup, 1972). In general, these processes produce an increasing degradation of data quality and quantity with time, which subsequently impacts upon our understanding of past biotic patterns and processes.

Time bins employed in diversity studies tend to use geological units (i.e. stages) which have variable temporal durations. It has been argued that this is problematic as longer time intervals have the opportunity to preserve higher levels of taxonomic richness (Raup, 1972; Foote, 1994). In theory, the total amount of sedimentation should also be higher in longer time intervals, leading to an increase in the preservation potential of organisms (Miller and Foote, 1996). However, as Earth system processes vary over time, with fluctuating depositional and erosional rates, this relationship is not universal. In fact, many studies have failed to find any correlation between biodiversity and time bin duration (e.g. Fastovsky et al., 2004; Butler et al., 2010). Nevertheless, recent studies have frequently attempted to correct for the impact of unequal duration by using 'near-equal' time bins, in which intervals are clumped together to form more similar bin lengths (Alroy, 2010c; Mannion et al., 2015; Close et al., 2020a). However, it is important to note that geological time units are primarily defined based on biostratigraphy. Therefore, the lengths of these units are not necessarily independent of species turnover through time.

The level of interest in a particular taxonomic group, geographic region or time period has also been advocated as a potential bias on estimates of palaeodiversity (Raup, 1972; Sheehan, 1977). This was first referred to as the 'monographic effect' by Raup (1972). As an example of this, Raup cited a single monograph that shifted a previously established temporal diversity peak from the Devonian to the Ordovician (Cooper, 1958). However, it is important to note that these monographic effects continue to

influence data collection and analyses today. For example, there is a substantial bias towards studying certain taxonomic groups. This is largely a result of their value in reconstructions of past climate and biostratigraphy (e.g. foraminifera, ammonites), or their charismatic nature (e.g. mammals and dinosaurs). Moreover, there is a well-documented sampling bias towards certain geographic regions, with the majority of reported fossil occurrences collected in the Northern Hemisphere, specifically Asia, Europe and North America (Kiessling, 2005; Upchurch et al., 2011; Dean et al., 2016; Mannion et al., 2019). It has also been proposed that such geographic sampling biases are more controlled by socioeconomic factors, such as gross domestic product, than any geological processes (Kiessling, 2005).

Areas of exceptional preservation, such as the Cambrian Burgess Shale in Canada and the Eocene Messel Pit in Germany, provide invaluable evidence in understanding the evolution of Phanerozoic life. These deposits are generally referred to as Lagerstätten (Seilacher, 1970; Raup, 1972; Dean et al., 2016; Mannion et al., 2019), or Konservat-Lagerstätten in the case of soft-tissue preservation (Allison, 1988). The presence or absence of Lagerstätten can have a strong impact on reconstructions of palaeodiversity. For example, Raup (1972) postulated that the low diversity of insects during the Cretaceous was an artefact arising from the lack of unique conditions required for good insect preservation. Furthermore, recent work has quantitatively demonstrated a strong relationship between the presence of Lagerstätten and high concentrations of fossils (Friedman and Sallan, 2012; Cleary et al., 2015; Dean et al., 2016). Whilst Raup (1972) noted that Lagerstätten are more likely to be present in younger rocks, new Lagerstätten continue to be discovered—including from the early Cambrian—providing novel insights into the evolution of life on Earth (Fu et al., 2019).

Species geographic distributions are limited by barriers to their dispersal. Consequently, when a previously overlooked geographic area is explored, there is a high chance of discovering undescribed taxa (Raup, 1972). In part, this is related to increased sampling, but also the universal scaling of taxonomic richness with area (Connor and McCoy, 1979; Rosenzweig, 1995; Lagomarcino and Miller, 2012).

Accordingly, time intervals that have broader spatial sampling patterns should recover higher levels of diversity. In fact, recent work has shown this to be true for both the marine and terrestrial fossil records (Close et al., 2020a, 2020b), with spatial sampling accounting for up to 67% of the temporal variation in counts of fossil species (Close et al., 2020a).

1.4.4 Mitigating sampling bias

Whilst a plethora of sampling biases clearly plague the fossil record, palaeobiologists have not forsaken the reconstruction of macroevolutionary and macroecological patterns. Since Raup (1972), several approaches have been developed to correct for sampling biases, providing fairer comparisons of relative richness ratios between temporal and spatial bins. One approach previously used is the 'residual diversity method'. This method uses the residuals from a modelled relationship between palaeodiversity and sampling proxies (e.g. number of formations) in an attempt to remove the signal of sampling (Smith and McGowan, 2007; Lloyd, 2012). The residual diversity method assumes that diversity is driven purely by sampling in the fossil record, and any deviations from the modelled relationship represent a genuine biological signal. However, whilst the residual diversity method was initially widely utilised in palaeobiology (Benson et al., 2010; Benson and Mannion, 2011; Mannion et al., 2012; Lloyd and Friedman, 2013), recent studies have demonstrated that residual diversity curves do not necessarily represent genuine biological signals (Brocklehurst, 2015; Dunhill et al., 2018). Their application in deep time studies has therefore been cautioned (Dunhill et al., 2018), and largely abandoned.

Rarefaction (or 'subsampling'), in which occurrence datasets are randomly sampled to a given threshold (Sanders, 1968; Raup, 1975), is the most common approach used to mitigate for the impacts of sampling biases on palaeodiversity estimates. The focus of subsampling approaches has been to retrieve an 'equal' or 'fair' representation of diversity, without examining potential driving factors such as outcrop availability. Numerous variants of subsampling approaches have been developed over recent

decades, including 'sampling-based rarefaction' (Sanders, 1968), 'by-list unweight sampling' (Alroy, 1996), 'by-list sampling weighted by occurrences' (Alroy, 2000), and 'coverage-based rarefaction' (Alroy, 2010c). Herein, the two most widely applied of these is discussed: sampling-based rarefaction and coverage-based rarefaction.

Sampling-based rarefaction (synonyms: classical rarefaction, by-occurrence subsampling) was the earliest developed subsampling approach, and has been implemented in a wide range of ecological and palaeobiological studies (Sanders, 1968; Raup, 1975; Foote, 1992; Alroy et al., 2008; Kiessling et al., 2012; Rasmussen et al., 2019). Broadly speaking, this approach standardises samples by size, randomly drawing samples to equal numbers of specimens, individuals or localities from the entire available sampling pool (Sanders, 1968; Close et al., 2018). Despite its continued use today (e.g. Reddin et al., 2019; Rasmussen et al., 2019), it has been heavily criticised on several fronts. For example, item-quota standardisation methods tend to under-sample more diverse assemblages, compressing relative richness ratios and artificially flattening diversity curves (Chao and Jost, 2012; Close et al., 2018). Furthermore, sampling-based rarefaction assumes that uniform sampling equates to fair sampling (Alroy, 2010a), and that organism abundances are fixed through time and/or space. This is contrary to what is observed in both modern and fossil collections (Cotgreave and Harvey, 1994; Alroy, 2010b; Benson and Butler, 2011). The rarity of species within samples inherently influences the relative diversity estimated between samples when fixed thresholds are applied. For instance, if 95% of the individuals within a sample are represented by a single species, with the remaining 5% comprised of 49 species, it is unlikely sampling-based rarefaction will capture many of these rare species, if any at all. Conversely, if a bin contained 50 species, with each contributing 2% of the total occurrences, a significantly higher richness estimate would be generated via sampling-based rarefaction than the former scenario. The similarity between species abundances is termed evenness, with the latter example representative of a bin with high evenness, while the former would be considered to have low evenness. The examples above demonstrate the potential of sampling-based rarefaction to influence relative richness

ratios in samples varying in evenness, and may artificially flatten diversity curves when low subsampling thresholds are applied (Alroy, 2010a; Chao and Jost, 2012).

Coverage-based rarefaction (Alroy, 2010c; Chao and Jost, 2012) was an approach developed to help overcome the issue of varying levels of evenness (Figure 1.5). In palaeobiology, coverage-based rarefaction is more commonly referred to as shareholder quorum subsampling (SQS), while the former name is generally reserved for the ecological literature. Uniquely, SQS standardises samples to equal levels of completeness (or 'coverage') of the species' (or other taxonomic levels) underlying frequency distribution (Alroy, 2010a; Chao and Jost, 2012), and has been shown to reconstruct relative richness ratios with high accuracy, providing abundance distributions that do not vary substantially between assemblages (Alroy, 2010a, 2010b; Chao and Jost, 2012; Close et al., 2018). Coverage is considered an objective measure of diversity-sample completeness, which is estimated from the frequencies of rare species (Esty, 1986; Close et al., 2018). In both ecology and palaeobiology, coverage is most commonly estimated using Good's u (Good, 1953), and is calculated using:

$$u = 1 - \frac{n_1}{O}$$

Where O is the total number of observations (occurrences), and n_1 is the number of singletons (species represented by one occurrence). To obtain relative richness ratios between assemblages, Good's u is calculated for each assemblage (or bin) and divided into q. In this instance, q denotes the 'quorum level', which is a specific amount of coverage, or proportion of the entire frequency distribution represented by the observed species. Significantly, SQS differs from item-quota standardisation methods in that it allows proportional sampling, opposed to equal sampling. Uniquely, it also provides some indication of sampling quality. Coverage values of zero indicate that there are no sampled occurrences in an assemblage, or that all taxa in the pool are singletons. Conversely, higher coverage estimates indicate that there is a more even distribution of sampled taxa.

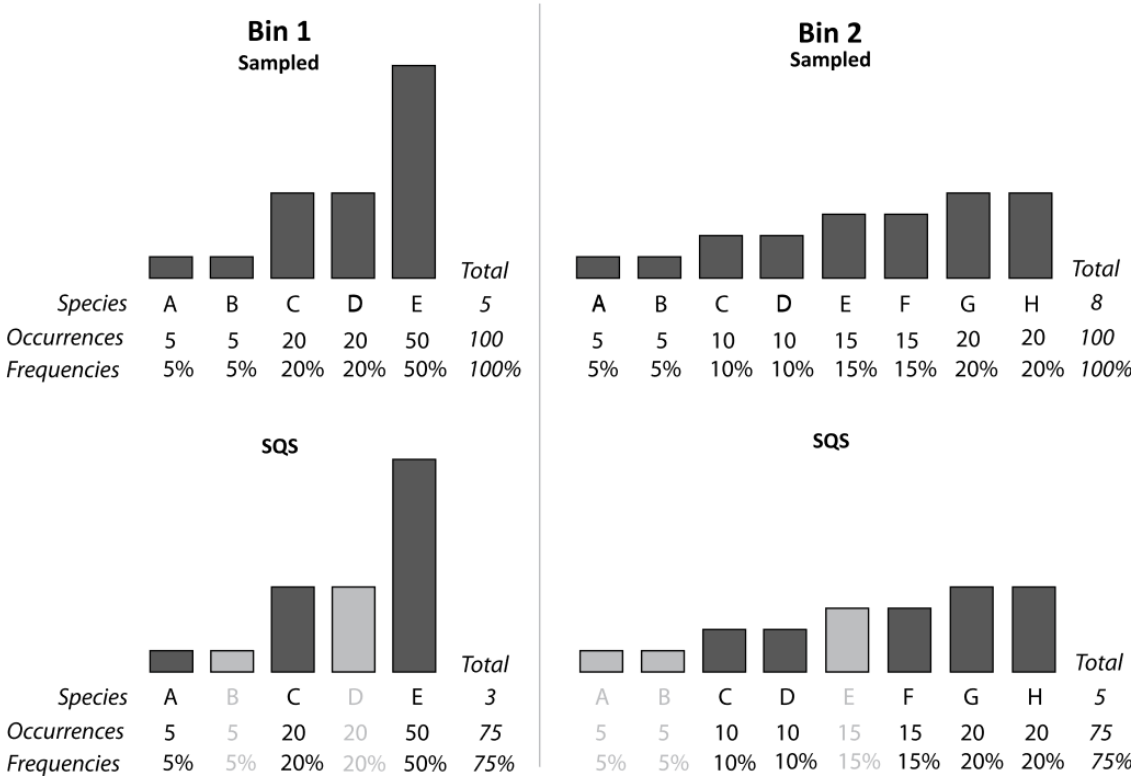


Figure 1.5. Illustrative example of shareholder quorum subsampling (SQS) for two different time bins. Top row shows the number of occurrences and frequency distributions of a raw data set, i.e. sampled fossil occurrences. Bottom row indicates the taxa randomly drawn for a single subsampling trial for a quorum level of 0.75. Randomly drawn taxa are in dark grey.

Despite its favoured use in palaeobiology, SQS is not without its own limitations. Whilst early work suggested that a quorum level of 0.4 was sufficient to accurately capture relative richness ratios between assemblages (Alroy, 2010b), more recent studies have demonstrated the impact of quorum selection on the amplitude of relative richness ratios (Dunne et al., 2018). Specifically, it is often the case that low quorum levels are needed to provide diversity estimates (e.g. 0.4) along the entire time series due to variability in sampling levels. However, this can cause SQS to diminish the relative richness of highly diverse bins. Nevertheless, perhaps one of the most severe limitations of SQS that has not previously been considered is the varying level of geographic extent that samples are drawn from (though see Close et al., 2017, 2020a, 2020b). This has the potential to artificially inflate diversity estimates when one temporal or spatial bin has sampled a broader geographic area than another. Similarly, diversity estimates could be further biased when one bin contains a range of sampled environments (e.g. lacustrine, reef, and deep water), and another contains little variety

(e.g. only estuarine). Intuitively, the former should result in the recovery of more taxa due to inherently different ecological tolerances required for each environment. Whilst such biases may be introduced anthropogenically by selective sampling procedures, they are also caused by geological processes such as erosion and burial. Consequently, SQS in its current widespread use has the potential to be significantly impacted by variable spatial sampling and data absence when estimating palaeodiversity.

Whilst it is beyond the scope of this thesis to review all subsampling methods, TRiPS (True Richness estimation using Poisson Sampling) was recently proposed as an alternative approach to estimating palaeodiversity (Starrfelt and Liow, 2016). TRiPS is a parametric approach to sampling-standardisation that models sampling as a Poisson process to calculate the maximum-likelihood estimates of 'true' underlying richness (Starrfelt and Liow, 2016). Unfortunately, TRiPS is also prone to the influence of very common taxa as it fits a single sampling rate for all taxa in a bin (Starrfelt and Liow, 2016). The presence of common taxa in a bin can cause an over inflation of the binomial sampling probability for a bin, causing it to saturate prematurely. This has the potential to cause TRiPS to underestimate palaeodiversity as it ceases to extrapolate richness while many taxa remain undiscovered. Despite its recent development, a review of the best performing method, found SQS to outperform comparable subsampling approaches, including TRiPS (Close et al., 2018).

New subsampling methods, variants of old techniques, and other approaches (e.g. likelihood frameworks such as PyRate (Silvestro et al., 2014)) will continue to emerge in palaeobiology, invigorating further debate about the best approach to estimate palaeodiversity. However, subsampling approaches are inherently bound to a naturally incomplete dataset which is irreparable, and severely biased. Changes to the questions palaeobiologists ask, and the way that they are asked, are timely. As a field, palaeontology has traditionally relied solely on empirical evidence to test various hypotheses. However, a suite of novel tools, including Earth System modelling and ecological niche modelling, are now available for palaeobiologists to exploit in order to bring palaeontology into the field of experimental science.

1.5 Thesis objectives and layout

The following chapters of this thesis use a combination of modelling and analytical tools to evaluate whether macroecological patterns observed in the fossil record are a genuine biological signal, or a result of spatial bias in the fossil record. The focus of this work is one of Earth's most pervasive macroecological patterns, the latitudinal biodiversity gradient.

Chapter 2 of this thesis outlines the materials and data utilised in subsequent chapters, including details on the sources of modern and fossil occurrence datasets, the construction of palaeogeographies, (palaeo-) digital elevation models, and palaeoclimatic simulations.

In Chapter 3, ecological niche modelling is applied to test whether a previously observed shift in coral latitudinal diversity during the Last Interglacial, 125,000 years ago (Kiessling et al., 2012) is the result of fossil bias, or a genuine loss in habitat suitability. The value of using fossil data to improve model predictions under varied climate states is also demonstrated.

Chapter 4 investigates whether we can identify different types of latitudinal biodiversity gradients from the fossil record. Three different types of latitudinal biodiversity gradient are simulated from the Permian to Neogene and degraded based on the known sampling window. Building upon these simulations, sampling-standardisation protocols are applied to test whether simulated latitudinal biodiversity gradients can be reconstructed from sampled or sampling-standardised counterparts.

Chapter 5 examines the palaeolatitudinal trends in zooxanthellate coral biodiversity, and assesses the impact of sampling on observed diversity patterns. A novel sampling-standardisation protocol—which accounts for heterogeneity in spatial sampling—is implemented to provide fairer estimates of latitudinal diversity trends.

In Chapter 6, ecological niche modelling is applied to model the palaeolatitudinal distribution of suitable habitats for coral reefs from the Triassic to the Neogene. Assuming conservation of abiotic tolerances, and accurate reconstructions of past

climate, the capacity of ecological niche models to predict the presence of coral reefs in the geological past is assessed. In addition, inferences are made about the potential palaeolatitudinal distribution of biodiversity based on available reef habitat.

Finally, the main conclusions of this thesis and directions for future research are discussed in Chapter 7.

–This page is intentionally left blank–

2 Materials: Earth System modelling and occurrence datasets

2.1 Palaeogeography and digital elevation models

2.1.1 Overview

Palaeogeographic reconstructions are central to addressing key questions in geospatial studies. The term 'palaeogeography' was first coined in 1873, by petroleum geologist Thomas Hunt in his paper on the geographic history of North America (Hunt, 1873). Since this early work, palaeogeographic reconstructions have improved significantly, with the ever-expanding archive of information gathered from the geological record (see Markwick, 2019 for a review). For the most part, this improvement has been motivated by the potential value offered to hydrocarbon exploration efforts by palaeogeographic reconstructions (e.g. Zuber, 1934; Weeks, 1947; Ziegler, 1982, 1990, 1999). Some of the first palaeobiogeographic work was undertaken by Arldt in the early 20th century (Arldt, 1919; Ebach and Dowding, 2017), building upon ideas proposed by Humboldt and Bonpland over a century before (Humboldt and Bonpland, 1807). Nevertheless, it was the advent of general-purpose computing in the late 20th century that enabled reconstructions of palaeogeography, palaeotopography and palaeobathymetry based on 'big data' (Markwick, 2019). This work was primarily developed by Fred Ziegler's 'Paleogeographic Atlas Project' (e.g. Ziegler et al., 1979, 1983), and set the stage for the use of palaeogeographic reconstructions in downstream analyses, such as boundary conditions for palaeoclimate modelling and lithofacies retrodiction (Markwick and Valdes, 2004; Markwick, 2019). Today, reconstructions of past topography and bathymetry are collectively termed palaeo-digital elevation models, and are used in studies ranging from hydrocarbon exploration, dinosaur habitat reconstructions, and predicting rates of sediment discharge and erosion in deep time (Markwick, 2019; Chiarenza et al., 2019; Lyster et al., 2020).

2.1.2 Palaeobathymetric data

In Chapters 3, 4 and 6 of this compilation of work, stratigraphic stage-level palaeobathymetric data extracted from global digital elevation models (DEMs) are used, provided by Getech PLC (Figure 2.1). These DEMs have a horizontal resolution

of 0.1°x 0.1° and are modelled on the basis of a global syntheses of sedimentological, stratigraphic, biostratigraphic and palaeogeographic data (Markwick and Valdes, 2004; Markwick, 2007). Crucially, they provide an explicit definition of depth and altitude in metres. For each time slice (i.e. stratigraphic stage), estimated palaeobathymetry is based on available seismic, lithological and palaeontological data between the shoreline and the shelf break. Beyond the shelf break (i.e. continental slope, continental rise, and abyssal plain), palaeobathymetry of the oceanic crust is estimated using age-depth equations (Stein and Stein, 1992), while also correcting for sea-level changes, sediment cover and intrusions from seamounts. Whilst these estimates are based on empirical data, the quality of these reconstructions is dependent on the availability of the data that underpins it. Consequently, the accuracy of these DEMs attenuates in deeper time due to information loss brought about by recycling of the Earth's lithosphere. Nevertheless, the reconstruction of palaeogeography and palaeo-elevation is an iterative process, with models continuously improving with the ever-expanding archive of information collected from the geological record (Figure 2.2). These DEMs are state-of-the-art, and represent the sum of current understanding of palaeogeography and palaeo-elevation in deep time.

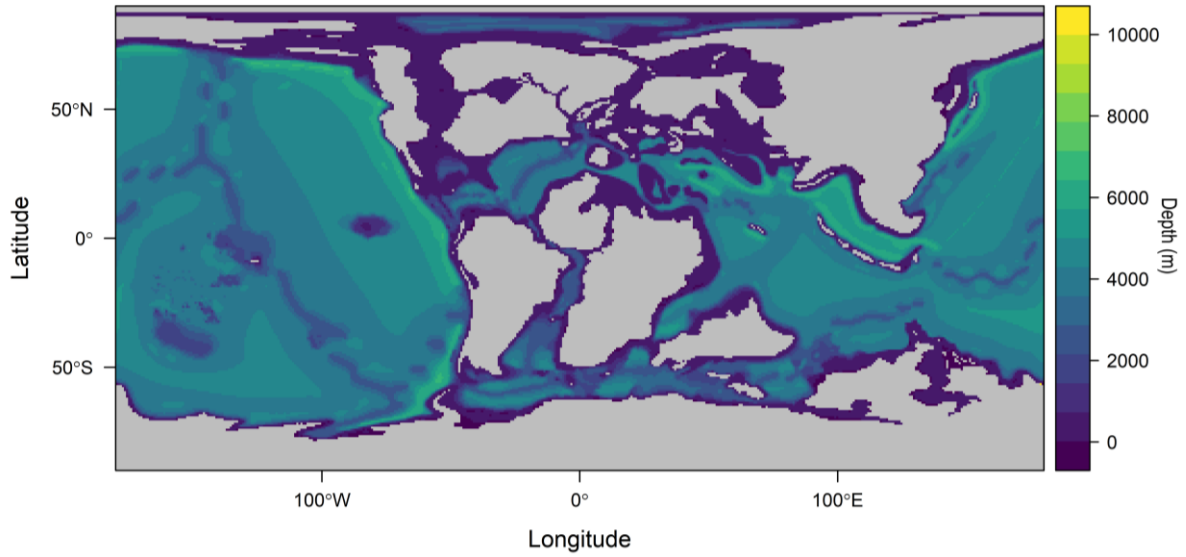


Figure 2.1. Albian (Lower Cretaceous) example of palaeogeography and palaeobathymetry from Getech's global digital elevation model. Colour key indicates depth in metres. Data is projected in the coordinate reference system: World Geodetic System 1984 (WGS84).

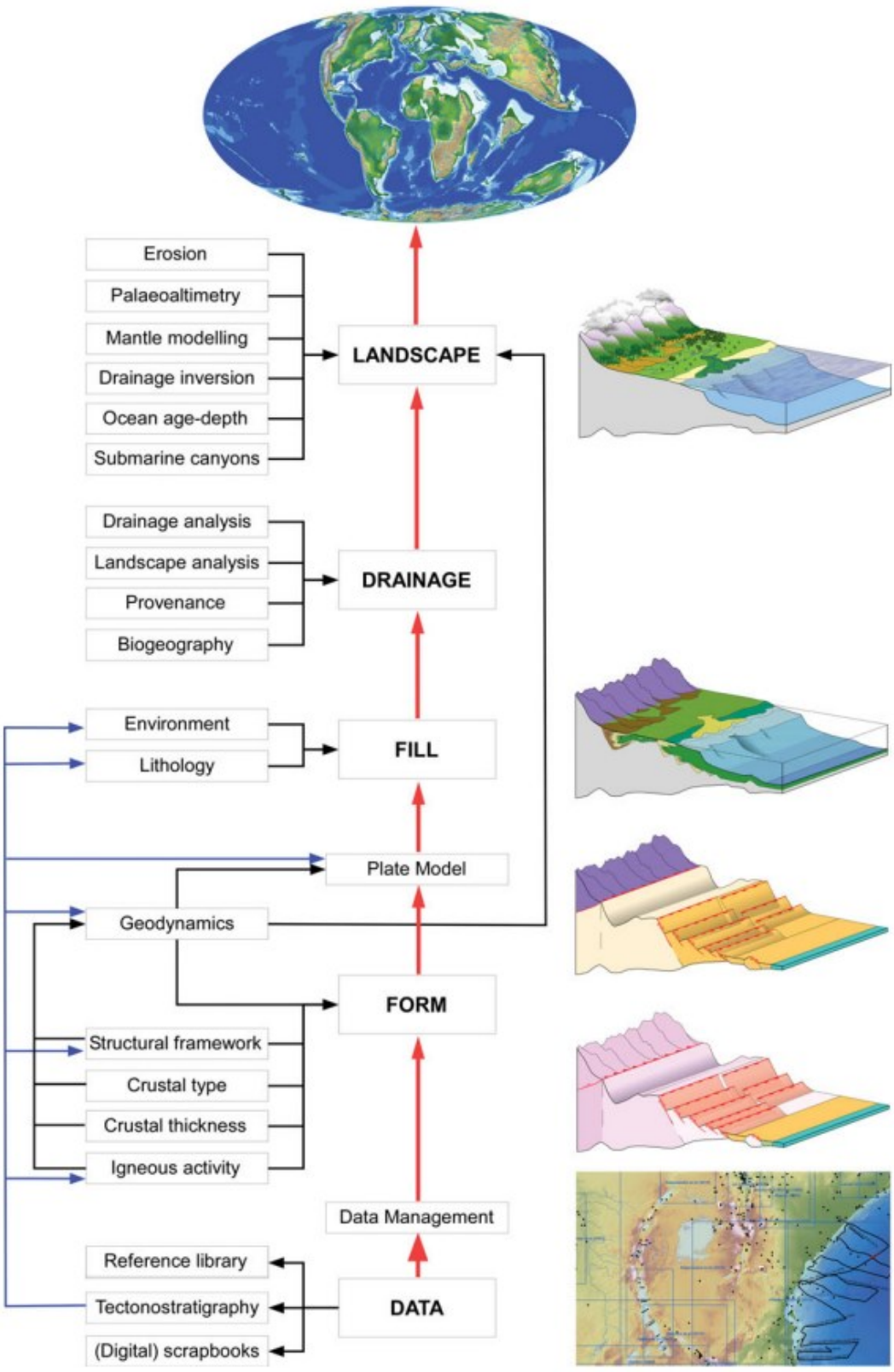


Figure 2.2. Palaeogeographic mapping workflow schematic (Markwick, 2019). This workflow follows the structure of the Earth, progressing from the crustal architecture through the basin fill to drainage and landscape. Significantly, this is an iterative process with improved models developing with the ever-expanding archive of information observed from the geological record. This image has been used with permission from Cambridge University Press.

The palaeo-positions of tectonic plates in these DEMs are reconstructed using Getech's in-house global geodynamic plate model. This plate model is rigid (i.e. the shape of continental plates does not change over time) and uses the present-day global distribution of tectonic plates, and a set of finite rotations, to describe the relative motion between each plate. During a given time interval, the motion of one plate relative to another can be described as the angle of rotation about a fixed semi-axis (Euler Pole) on Earth's surface. This is what is known as a finite rotation. To calculate the absolute palaeo-position of a given plate, relative to Earth's spin axis, finite rotations are added within a plate hierarchy. The tectonic plate boundaries in Getech's plate model are defined based on empirical data (i.e. field data), and relative plate motions constrained by data sources such as oceanic magnetic anomalies, palaeomagnetic poles, geological relationships, and fracture zone orientations. The methods used to build both DEMs and palaeogeographic reconstructions are thoroughly discussed in Markwick and Valdes (2004) and Markwick (2007, 2019), with additional information provided at https://www.getech.com/.

2.2 Climate and palaeoclimate models

2.2.1 Overview

The history of climate modelling offers an account of the emergence of conceptual models (e.g. Eratosthenes in the 3rd century BC, who described and mapped five climate zones), to the realisation of mathematical models capable of predicting climatic patterns at global scale (reviewed in Edwards, 2011). Today, these mathematical models are referred to as general circulation models (GCMs), and continue to increase in complexity by incorporating additional physical processes and fine-tuning parameters (Le Treut et al., 2007). Coupled atmosphere-ocean general circulation models (AOGCMs) are now routinely used to model global climate for historical periods, the present-day and future climate scenarios (Le Treut et al., 2007; Edwards, 2011; IPCC, 2013). However, these models have also been used to understand the evolution of climate on Earth, in what is now commonly referred to as palaeoclimate

modelling (Haywood et al., 2019). One of the first applications of palaeoclimate modelling was published in the 1970s, and provided estimates of Earth's climate during the Last Glacial Maximum (Gates, 1976). Since these early simulations, the application of these models have matured significantly (Haywood et al., 2019), with studies now investigating the impacts of climate change on matters such as the evolution of the East Asian monsoon (Farnsworth et al., 2019a), avian latitudinal distribution shifts (Saupe et al., 2019a), and sediment discharges in deep time (Lyster et al., 2020).

In this compilation of work, two AOGCMs (HadCM3; HadCM3L) in conjunction with other methods, are used to test several hypotheses. Explicit details on these AOGCMs are provided in the following sections. However, specific details regarding data preparation for each chapter is provided therein.

2.2.2 HadCM3

For Chapter 3 of this thesis, climate data for the modern (pre-industrial), Last Interglacial (LIG; 125,000 years ago), and two future (2100 AD) climate scenario simulations were derived from HadCM3M2.1N, a version of UK Met Office HadCM3 (Valdes et al., 2017). HadCM3 has been heavily used as part of the Intergovernmental Panel on Climate Change (IPCC) 4th and 5th assessment reports (IPCC, 2013), and successfully applied to studies of both present-day and past climate and biodiversity (Sheppard, 2003; Singarayer and Valdes, 2010; Stone et al., 2013; Capron et al., 2014; Saupe et al., 2014; Holloway et al., 2016). Specifically, HadCM3 is a three-dimensional, fully dynamic AOGCM without flux adjustment. The atmospheric component of HadCM3 has a horizontal resolution of 3.75° longitude x 2.5° latitude, and a vertical resolution of 19 levels. A sub-grid scale of orographic features based on topography are calculated within the model, enabling finer scale features to have an impact on the climate signal. The horizontal resolution of the oceanic component has a higher resolution of 1.25° x 1.25°, with a vertical resolution of 20 levels to a depth of 5500 m. This version of the HadCM3 has a time step of 30 minutes. A full technical description of HadCM3 is available in Gordon et al (2000) and Valdes et al (2017).

For LIG palaeoclimate simulations, HadCM3 was run for 300 model years, with a CO_2 concentration of 266 ppmv. Climate simulations of the modern (pre-industrial) were run for 200 model years, with a CO_2 concentration of 280 ppmv. IPCC representative concentration pathways (RCP) 4.5 and 8.5 were used to represent two future climate change scenarios. RCP4.5 is a climate scenario simulation which stabilizes radiative forcing at 4.5 W m^{-2} (approximately equivalent to 650 ppmv CO_2) by the end of the century, without ever surpassing that value, whereas RCP8.5 has a radiative forcing of 8.5 W m^{-2} (approximately equivalent to 936 ppmv CO_2) by 2100 (Riahi et al., 2011; Thomson et al., 2011). The RCP4.5 scenario assumes that climate policies are put into practise to curb global greenhouse emissions, resulting in the stabilization of emissions (Thomson et al., 2011). Conversely, the RCP8.5 scenario assumes a global population of 12 billion by 2100, slow income growth, meek energy efficiency development, and little progress in curbing emissions (Riahi et al., 2011). All (palaeo-) climate simulations were run by the Bristol Research Initiative for the Dynamic Global Environment (BRIDGE) group at the University of Bristol, and are available at: http://www.bridge.bris.ac.uk/resources/simulations.

2.2.3 HadCM3L

For Chapter 6 of this thesis, stage-level (Anisian–Piacenzian) climate data (Figure 2.3) were derived from the HadCM3BL-M2.1aE, a version of the HadCM3L (Valdes et al., 2017). The HadCM3L is equivalent to the heavily utilised HadCM3 (Sheppard, 2003; Singarayer and Valdes, 2010; Stone et al., 2013; Capron et al., 2014; Saupe et al., 2014; Holloway et al., 2016), but with a lower resolution ocean (3.75° longitude x 2.5° latitude). HadCM3L has recently been used in a number of deep-time studies (Loptson et al., 2014; Marzocchi et al., 2015; Kennedy et al., 2015; Waterson et al., 2016; Chiarenza et al., 2019; Saupe et al., 2019a; Lyster et al., 2020), and is favoured for deep time palaeoclimate modelling due to the substantial spin-up time (thousands of years) required under radically different climates (Valdes et al., 2017; Haywood et al., 2019). Significantly, this version of the HadCM3L utilises Getech DEMs as boundary conditions during simulations, providing spatially explicit data for when continent-

configuration, topography, and bathymetry were different from today. The CO_2 concentration is held constant through all simulations at 1,120 ppmv, until the Oligocene when it decreases to 560 ppmv, 400 ppmv during the Neogene and early Pliocene, and finally 280 ppmv during the late Pliocene and Pre-Industrial. The solar constant in palaeoclimate simulations varies according to Gough (1981). Each simulation was run for 1,422 model years, which has been shown to provide an accurate representation of ocean circulation (Farnsworth et al., 2019b). This version of the HadCM3L has a time step of 30 minutes. A full technical description of HadCM3L is available in Valdes et al (2017) and Farnsworth et al (2019a). All palaeoclimate simulations were run by the BRIDGE group at the University of Bristol, and are available at: http://www.bridge.bris.ac.uk/resources/simulations.

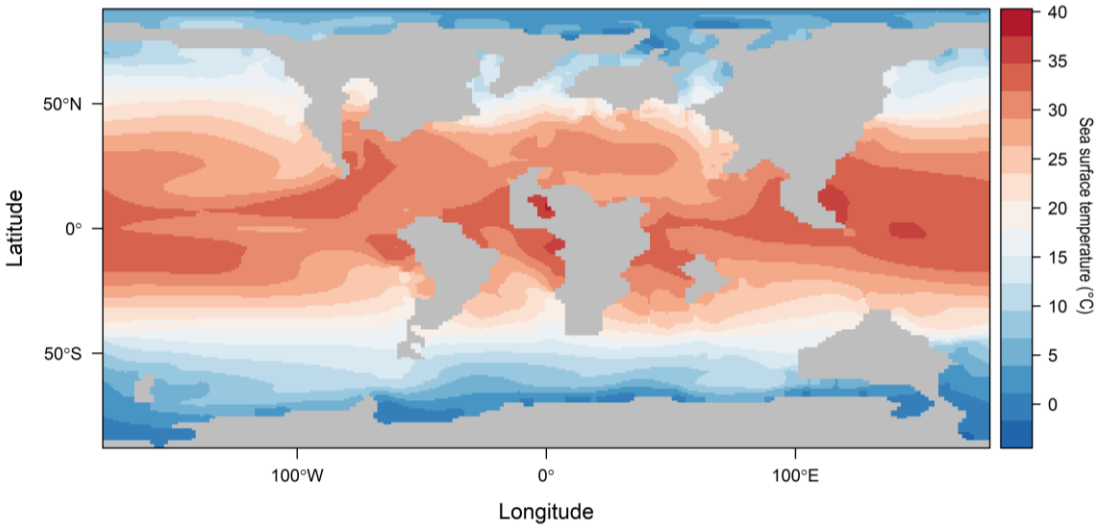


Figure 2.3. Maastrichtian (Upper Cretaceous) example of mean seasonal (June–August) sea surface temperature from the HadCM3L atmosphere-ocean general circulation model. Colour key indicates sea surface temperature (°C). Data is projected in the coordinate reference system: World Geodetic System 1984 (WGS84).

2.3 Occurrence datasets

2.3.1 Overview

Occurrence datasets are the foundation of ecological and palaeontological research. Historically, these datasets were painstakingly compiled by hand to answer key questions about the distribution of life in time and space. However, the advent of general-purpose computing in the 1970s allowed the construction of digital databases,

which improved efficiency in data curation, sharing, and analyses. Since the dawn of the Information Age (also known as the Digital Age), web-based data and information systems have accumulated immense quantities of biological (e.g. Global Biodiversity Information Facility) and palaeontological data (e.g. Paleobiology Database and Neotoma) enabling vast amounts of research. For example, over 4,500 peer-reviewed papers have been published using data from the Global Biodiversity Information Facility (https://www.gbif.org/), and over 375 from the Paleobiology Database (https://www.paleobiodb.org/).

In this thesis, data is drawn from several large online databases. An overview of this data is provided below. However, specific details regarding data preparation for each dataset is provided in the relevant chapter.

2.3.2 Modern

Modern occurrences of marine organisms used in this thesis were gathered from the Ocean Biogeographic Information System (OBIS; www.iobis.org). OBIS itself is a global open-access database on marine organisms, housing 59,048,550 occurrences for 127,973 species at time of writing (07/02/2019). The database contains information on various groups ranging from Bacteria to Cetaceans, and has contributions from over 500 institutions across 56 countries. In addition, the OBIS database offers three-dimensional occurrence data, sourced from all geographic regions, and from the ocean surface to oceanic trenches. Significantly, this data is routinely vetted and has several data control and quality protocols for all entered data. Whilst the main function of the database is to provide occurrence data, extensive metadata is also housed within OBIS, including information regarding the type of dataset (e.g. rapid ecological assessments), year recorded, depth of occurrence, and environmental setting (e.g. temperature) the occurrence was recorded in.

In this thesis, a coral occurrence dataset was used in several chapters (Chapters 3, 5 and 6). As such, specific details regarding this dataset are stated here to provide overview. Modern coral occurrences were downloaded from OBIS on the 5th July 2017,

using the search criteria 'Scleractinia'. This resulted in the recovery of 589,817 occurrences. Subsequently, this dataset was filtered to exclude data not identified to species level, as well as further quality control checks (e.g. synonymizations). As the work presented in this thesis focused on zooxanthellate corals, azooxanthellate and apozooxanthellate corals were removed from the dataset. Classification of symbiotic mode was based on information housed in the World Register of Marine Species (http://www.marinespecies.org/), as well as the Coral Trait Database (https://www.coraltraits.org/). Further quality control was performed on the OBIS dataset, whereby occurrences found to occur on land or at depths greater than 100 m were removed under the assumption that there were errors in their geographic coordinates, species identification or are in fact fossil occurrences. In addition, data collected from rapid ecological assessments were omitted to improve the credibility of species-level identification, as well as those from coral transplant studies. Duplicate occurrence records of the same species from exactly the same coordinates were also removed. The resultant modern occurrence dataset contained 700 zooxanthellate species, comprising 48,577 occurrences with 3,553 unique coordinates. This dataset was the focus of the work presented in Chapter 3, but was also used in Chapter 5 and 6 for additional analyses.

For the work presented in Chapter 4 of this thesis, occurrence data for five major marine invertebrate groups (anthozoans [= 'Anthozoa'], bivalves [= 'Bivalvia'], brachiopods [= 'Brachiopoda'], echinoids [= 'Echinoidea'], and sponges [= 'Porifera']) were downloaded from OBIS. These data were used to assess the empirical range size and occurrence frequency distributions of marine organisms for comparison with the simulations used in this chapter. As the aim of using these data were to provide only an overview of range size and occurrence frequency distributions, no specific data preparation was conducted.

In Chapter 6 of this thesis, a dataset of the global distribution of warm-water coral reefs was used. These data were downloaded from the United Nations Environment Programme (UNEP): World Conservation Monitoring Centre (http://data.unep-

wcmc.org/datasets/1) on the 6th May 2020 (UNEP-WCMC et al., 2018). This dataset is currently the most comprehensive of its kind, and is compiled from multiple sources including the Millennium Coral Reef Mapping Project (approximately 85% of the dataset), as well as the World Atlas of Coral Reefs (Spalding, 2001; IMaRS-USF and IRD, 2005; UNEP-WCMC et al., 2018). Notably, this dataset has been extensively validated by the UNEP World Conservation Monitoring Centre via field surveys and remote sensing (UNEP-WCMC et al., 2018).

2.3.3 Fossil

Fossil occurrence data used in this body work were sourced from the Paleobiology Database (PBDB; https://www.paleobiodb.org/). The PBDB is a non-governmental, non-profit, and publicly available (Creative Commons BY 4.0 International License) palaeontological database. The PBDB contains fossil occurrence and collection records throughout earth history, with 1,457,966 occurrences and 207,576 collections at time of writing (07/02/2019). The database itself is maintained by the global palaeobiology research community (410 contributors at time of writing), who continue to enter the metadata (e.g. taxonomy, stratigraphy, location) from the peer reviewed published literature, and evaluate the data for any inaccuracies. Whilst the PBDB may not contain all known fossil data (e.g. Marshall et al., 2018), the PBDB has been the foundation of over 375 palaeobiology studies over the past two decades.

For Chapter 3 of this work, fossil coral occurrence data were downloaded from the PBDB on the 19th July 2017. The PBDB returned 8,021 occurrences for Pleistocene Scleractinia. This dataset was filtered to exclude data not identified to species level, as well as further quality control checks (e.g. synonymizations). As the work in Chapter 3 focused on zooxanthellate corals, azooxanthellate and apozooxanthellate corals were removed from the dataset. Assignment to zooxanthellate class focused on the principle of uniformitarianism for fossil coral taxa. The dataset was further filtered to exclude occurrences which cannot be reliably assigned to the LIG (130–115 ka). Duplicate occurrence records of the same species from exactly the same coordinates were also

removed. The resultant dataset contained 190 zooxanthellate species, comprising 1,337 occurrences (from 301 collections) with 166 unique coordinates.

For Chapter 5 of this work, Scleractinia fossil occurrences from the Anisian (247.1 Ma) to Piacenzian (2.58 Ma) were downloaded from the PBDB on the 13th March 2020, yielding 27,233 occurrences. To improve data quality, this dataset was filtered to exclude data not identified to genus level, as well as taxonomically unresolved genera, based on expert opinions in Corallosphere (http://www.corallosphere.org/). Analyses were centred on zooxanthellate corals, and therefore azooxanthellate and apozooxanthellate corals were removed from the dataset. For this dataset, the inferred symbiotic states of coral genera from previous work were followed (Kiessling and Kocsis, 2015), retaining only those with high levels of confidence. This designation of photosymbiotic mode for genera was based on three lines of evidence: morphological, geochemical, and uniformitarian. Based solely on morphology, 96% of extant corals would have their symbiotic mode correctly classified, and this approach is therefore likely robust when applied to fossil data (Kiessling and Kocsis, 2015). The final dataset contains 15,324 fossil occurrences, from 3,121 unique collections.

For Chapter 6 of this work, fossil coral reef occurrence data were downloaded from the PaleoReef Database (accessible via: https://www.paleo-reefs.pal.uni-erlangen.de/) (Kiessling and Flügel, 2002). This database provides a range of data on fossil reef systems across the Phanerozoic, and currently contains geographical, geological and palaeontological information on more than 4,000 fossil reef sites. For Chapter 6, data on fossil coral reef systems from the Anisian (247.1 Ma) to Piacenzian (2.58 Ma) were extracted from the PaleoReef Database. Fossil reefs identified as cold-water coral reefs were removed from the dataset as these develop in fundamentally different environments to warm-water coral reefs. To increase data quality, fossil reef occurrence data not constrained to stratigraphic stage level were removed from the dataset. The final dataset contains 375 occurrences across the Anisian–Piacenzian, though data quality is variable with some stages containing no reported fossil warm-water coral reefs.

3 Identifying spatial sampling bias in the fossil record using ecological niche modelling

Disclosure: Some of the content reported in this chapter has already been published (Jones et al., 2019). While the primary author wrote most of this text, contribution by the co-authors of this study, particularly the two supervisors (Prof. Peter A. Allison and Dr Philip D. Mannion), are contained in this chapter, as well as the input received from the peer review process. The relevant text, revised below, can be found in: Jones, L.A., Mannion, P.D., Farnsworth, A., Valdes, P.J., Kelland, S.-J., and Allison, P.A., 2019, Coupling of palaeontological and neontological reef coral data improves forecasts of biodiversity responses under global climatic change: Royal Society Open Science, v. 6, p. 182111, doi:10.1098/rsos.182111.

OVERVIEW

Zooxanthellate corals are currently undergoing climatically driven poleward range expansions, with some evidence for equatorial range retractions. Predicting their response to future climate change scenarios is critical to their conservation, but ecological models are based only on short-term observations. The fossil record provides the only empirical evidence for the long-term response of organisms under perturbed climate states. The palaeontological record from the Last Interglacial (LIG; 125 000 years ago), a time of global warming, suggests that zooxanthellate corals experienced poleward range shifts and an equatorial decline relative to their modern distribution. However, this record is spatiotemporally biased, and existing methods cannot account for data absence. Here, sampling-standardisation methods are implemented to demonstrate the impact of data absence. Building upon these analyses, ecological niche modelling is applied to estimate the geographic distribution of zooxanthellate corals during the LIG, present day and under two future climate change scenarios. Results from ecological niche modelling suggest zooxanthellate corals' ranges during the LIG were likely comparable to the present, with no prominent equatorial decrease in habitability. However, under projected global warming, zooxanthellate corals are likely to experience poleward range expansion and large equatorial declines. Nevertheless, this range expansion is likely optimistic in the face of anthropogenic climate change due to the apparent rate of global warming.

3.1 Introduction

Anthropogenic climate change, with a projected global warming of 2–4.8°C by 2100 (representative concentration pathway scenarios), is the principal challenge of the twenty-first century (IPCC, 2014). Rising sea-surface temperatures (SSTs), associated with global warming, have already generated ecological disturbances and substantial range shifts of marine organisms (Poloczanska et al., 2013, 2016; García Molinos et al., 2016). Today, zooxanthellate corals provide one of the most biologically diverse and economically valuable ecosystems in the marine realm, the coral reef (Moberg and Folke, 1999). Already, thermal stress associated with global warming, has generated unprecedented mass bleaching of zooxanthellate corals, with three pan-tropical events recorded in the last two decades, leading to a decline in abundance, diversity and habitat structure (Pandolfi et al., 2003; Heron et al., 2016; Hughes et al., 2017b). Global warming has also led to clear poleward range expansion of some zooxanthellate corals (Precht and Aronson, 2004; Yamano et al., 2011; Baird et al., 2012; Muir et al., 2015; Grupstra et al., 2017). However, the evidence for equatorial range retractions is debatable (Yamano et al., 2011; Kiessling et al., 2012). Ecological studies tend to be based on short-term observations, during which time a taxon might never have occupied its full geographical or environmental space. This issue makes it difficult to predict whether this expansion/retraction trend is a function of global warming, or simply reflects the ongoing response of a species to a pre-existing forcing already applied to the system. Greater understanding of the range dynamics of zooxanthellate corals is, therefore, critical to their conservation.

Several studies have used ecological niche modelling (ENM) to evaluate the environmental controls on coral reefs, and predict their global distribution under future climate change scenarios (Couce et al., 2012, 2013; Freeman et al., 2013; Freeman, 2015). However, the fossil record provides the only empirical evidence for the long-term responses of organisms to environmental perturbations (e.g. Dietl et al., 2015; Barnosky et al., 2017), offering a ground truth for model projections under varying climate scenarios. In addition, this life history data potentially enables additional

insights into the niche hypervolume (the full multi-dimensional abiotic space which a taxon might occupy indefinitely), commonly referred to as the fundamental niche (Hutchinson, 1957). Furthermore, it has been demonstrated that the integration of both palaeontological and neontological data improves biodiversity risk assessments (Lima-Ribeiro et al., 2017). Future projections trained solely on modern occurrences might therefore underestimate habitat suitability due to a restricted present-day range in climatic variation. Through incorporation of the fossil record, more of this variation is captured. Thus, palaeontological data from warmer intervals should improve projections to future climate scenarios that are closer analogues than the present day.

Apparent range shifts have been observed in the Quaternary (2.58–0 Ma) fossil record of zooxanthellate corals (Muhs et al., 2002; Precht and Aronson, 2004; Greenstein and Pandolfi, 2008; Kiessling et al., 2012), with Kiessling et al. (2012) demonstrating poleward range shifts and an equatorial decline in zooxanthellate corals during the Last Interglacial (LIG), ~125,000 years ago. Several authors have provided approximations on global SSTs for the LIG, with estimates ranging from no significant difference to as much as 2°C warmer than today (Clark and Huybers, 2009; McKay et al., 2011; Hoffman et al., 2017). Kiessling et al. (2012) proposed that this temperature rise was the driver of the dramatic range shifts observed in LIG zooxanthellate corals. Consequently, these authors suggested that anthropogenic global warming today means that an equatorial decline of zooxanthellate corals is likely to follow their current poleward expansion. This has important implications for conservation, such as which geographical regions should be prioritized. However, the fossil record is spatially and temporally biased, impacted by incomplete sampling, variable fossil preservation, erosion and burial. Although existing subsampling methods, such as those applied by Kiessling et al. (2012) can ameliorate problems associated with uneven 'raw' occurrence data (e.g. Alroy, 2010b), they cannot account for the absence of data. ENM offers the prospect of mitigating for biases caused by the uneven distribution of known occurrences (i.e. raw data) by estimating habitat suitability, providing insights into

the potential geographical distribution of organisms through consideration of their observed realized niche.

Here, ENM is used to: (i) evaluate the extent to which the LIG equatorial decline of zooxanthellate corals is the result of fossil bias or a genuine loss in habitat suitability; (ii) quantify the variation in geographical range of zooxanthellate corals during the LIG and under future climate scenarios, with implications for understanding the evolution of the zooxanthellate coral latitudinal biodiversity gradient; and (iii) demonstrate the value of using fossil zooxanthellate coral data to improve model predictions through consideration of the realized niche under varied climate states.

3.2 Materials and methods

3.2.1 Biogeographic data

Modern coral occurrences were downloaded on the 5th July 2017 from the Ocean Biogeographic Information System (OBIS; www.iobis.org) using the search criteria 'Scleractinia', yielding 589,817 occurrences. Fossil coral occurrence data were accessed on the 19th July 2017 through the Paleobiology Database (PBDB; www.paleobiodb.org). The PBDB returned 8,021 occurrences for Pleistocene Scleractinia. These datasets were then filtered to exclude data not identified to species level, as well as further quality control checks (e.g. synonymizations). Analyses were based on zooxanthellate corals, herein referred to as Z-corals, which host unicellular organisms known as zooxanthellae in their tissue, forming a photosymbiotic relationship (Veron, 2000). Assignment to zooxanthellate class focused on the principle of uniformitarianism for fossil coral taxa. Azooxanthellate (those without a photosymbiotic relationship) and apozooxanthellate (those which may or may not sustain a photosymbiotic relationship) corals were removed from both databases. Classification of symbiotic mode was based on information housed in the World Register of Marine Species (http://www.marinespecies.org/), as well as the Coral Trait Database (https://www.coraltraits.org/). Further, quality control was performed on the OBIS dataset, whereby occurrences found to occur on land or at depths greater

than 100 m were removed under the assumption that there were errors in their geographical coordinates, species identification or are in fact fossil occurrences. In addition, data collected from rapid ecological assessments were omitted to improve the credibility of species-level identification, as well as those from coral transplant studies. The PBDB data were filtered to exclude occurrences which cannot be reliably assigned to the LIG. Duplicate occurrence records of the same species from exactly the same coordinates were also removed from both datasets.

The resultant modern occurrence dataset contains 700 zooxanthellate species, comprising 48,577 occurrences with 3,553 unique coordinates, while the LIG dataset contains 190 zooxanthellate species, comprising 1,337 occurrences (from 301 collections) with 166 unique coordinates (Figure 3.1). When implementing ENM, most studies have focused on analyses of individual species (Guinan et al., 2009; Davis et al., 2014, 2014; Saupe et al., 2014; Lima-Ribeiro et al., 2017). However, due to the relative rarity of fossil occurrence data at global scale, occurrence data were used at ecotype level (i.e. a group which shares specific environmental preferences), in accordance with previous studies (e.g. Waterson et al., 2016). The environmental limits of modern coral reefs to ecological variables are broadly similar at a global level, recognized as being limited to warm, clear and shallow water habitats (Kleypas et al., 1999). In preparation of ecological niche modelling, all occurrences were clipped by environmental layers to correspond with the environmental data. To account for species that have become extinct since the LIG, or that lack modern occurrence records in the OBIS, species which do not occur in both the clipped fossil and modern datasets were excluded. The final modern and fossil datasets comprise 157 shared species, composed of 22,726 modern Z-coral occurrences and 1,022 LIG Z-coral fossil occurrences. Finally, point occurrences were spatially subsampled at a raster resolution of 1.25° × 1.25° to account for spatial sampling bias. Spatial subsampling resulted in the retention of 295 presence sites for modern Z-corals and 56 for LIG Z-corals (note that this does not affect the overall distribution, but prevents multiple records being excessively weighted during model calibration) (Figure 3.1).

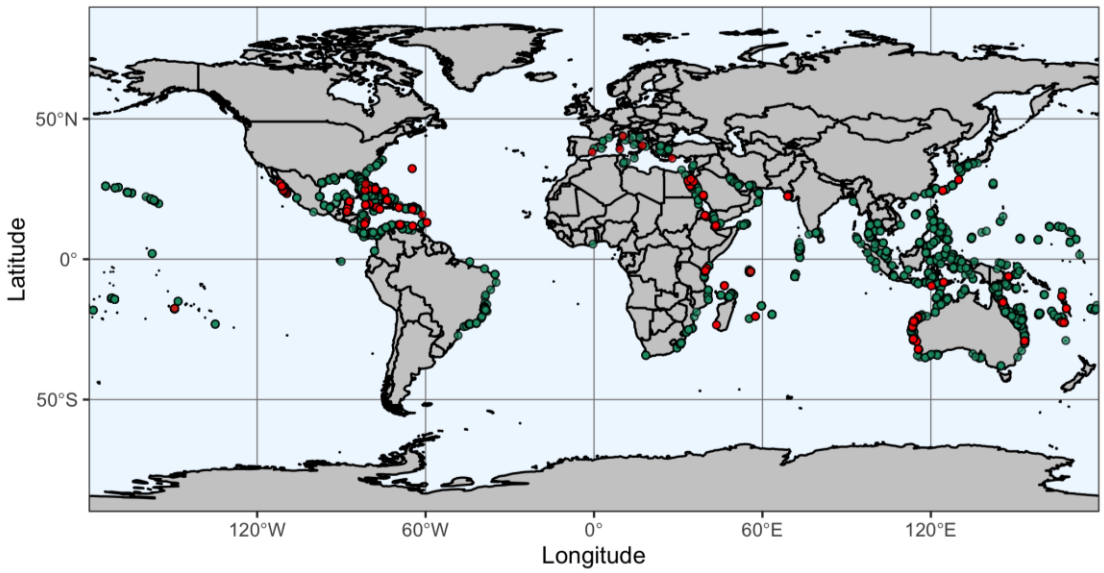


Figure 3.1. Global distribution of modern (green circles) and Last Interglacial (red circles) zooxanthellate coral occurrences. Data is projected in the coordinate reference system: World Geodetic System 1984 (WGS84).

3.2.2 Diversity analyses

Raw counts

To enable this study to be directly comparable to previous work (i.e. Kiessling et al., 2012), 'raw' (= uncorrected) counts of species richness were computed within 5° latitudinal bins for both the modern and LIG. To provide an indication of sampling effort, counts of reported occurrences and sampling localities were also computed. Localities were counted as the number of unique coordinates reported in the modern and LIG dataset.

Sampling-standardisation

To enable further comparison with previous work (i.e. Kiessling et al., 2012), sampling-based rarefaction (classical rarefaction; CR) was applied with a constant 75 occurrences sampled for each latitudinal band, for 1,000 subsampling trials. CR is a commonly applied sampling-standardisation approach which accounts for large differences in sampling between latitudinal bands and temporal windows (Sanders, 1968; Raup, 1975; Mannion et al., 2012; Kiessling et al., 2012). It does so by repeatedly drawing a fixed number of random occurrences from designated latitudinal and/or temporal bins to provide a fairer estimate of species richness. All results from CR are reported as the

arithmetic mean from the 1,000 trials, along with one standard deviation. As CR has the potential to be particularly impacted by the evenness of the underlying sample, species evenness for each latitudinal bin was also calculated using *Pielou's evenness index*:

$$J' = \frac{H'}{\ln S}$$

Where H' is the value derived from the *Shannon diversity index*, and S is the total number of species within a sample. The *Shannon diversity index* is calculated as:

$$H' = -\sum_{i=1}^{S} p_i \ln(p_i)$$

Where P is the proportion of individuals of one particular species, divided by the total number of individuals found, and S is the total number of species.

3.2.3 Environmental data

Climate variables for the modern (pre-industrial), LIG and two future (2100 AD) climate scenario simulations were derived from HadCM3M2.1N (Valdes et al., 2017). The HadCM3M2.1N is a version of UK Met Office HadCM3, a coupled atmosphere–ocean General Circulation Model (AOGCM). The atmospheric component of HadCM3 has a horizontal resolution of 3.75° longitude x 2.5° latitude and a vertical resolution of 19 levels, with a time step of 30 min. The horizontal resolution of the oceanic component has a higher resolution of 1.25° x 1.25°, with a vertical resolution of 20 levels to a depth of 5500 m. In this study, irradiance (atmospheric component) was bilinearly interpolated to 1.25° x 1.25° to match the resolution of the corresponding oceanic variables. HadCM3 is relatively low in resolution compared with more local-scale models, but it performs well, particularly in regard to mean climate state (Flato et al., 2013). Although the resolution of environmental data might represent an aggregated value of the true value at occurrence localities, this is likely insignificant for parameters such as irradiance and SST (Figure 3.2), whereas salinity and bathymetry might vary quite considerably over small geographical distances (Wiens et

al., 2009). However, previous work has shown salinity to be considerably less significant than both SST and irradiance at a global scale for coral reefs, with little contribution to model construction (Couce et al., 2012). Nevertheless, at localised scales salinity and bathymetry are likely to have an impact upon the persistence of Z-corals, and it should be borne in mind that it will not be captured within this study's ecological niche models (ENMs).

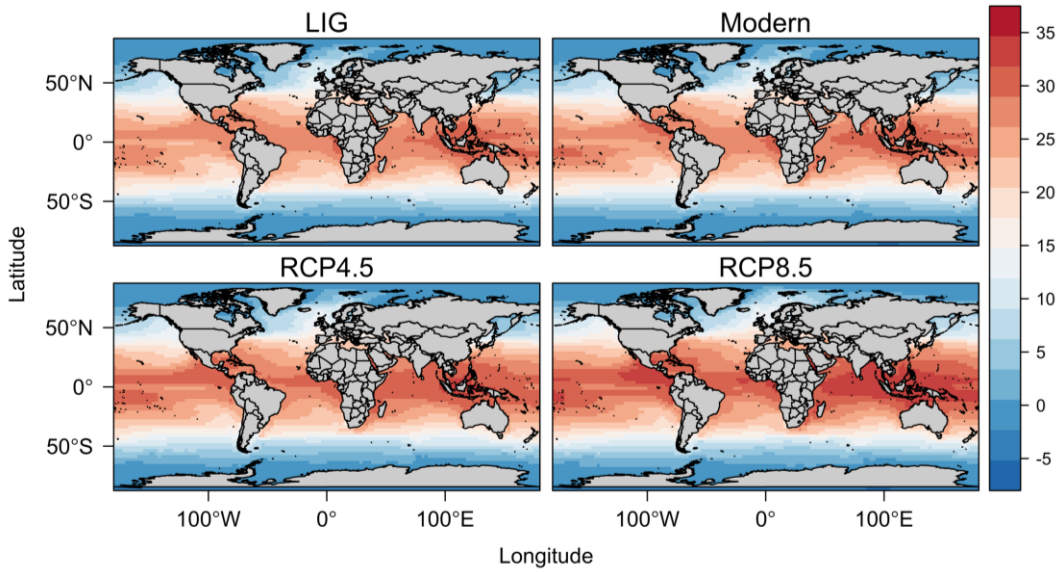


Figure 3.2. Global maps of annual sea surface temperature (°C) for the Last Interglacial (LIG), modern and Representative Concentration Pathways (RCP) 4.5 and 8.5. Sea surface temperature values are from the HadCM3 climate model. Data is projected in the coordinate reference system: World Geodetic System 1984 (WGS84).

HadCM3 has previously been used as part of the Intergovernmental Panel on Climate Change (IPCC) 4th and 5th assessment reports (Stocker et al., 2013). It has also been successfully applied to studies of both present-day and LIG climate and biodiversity (Singarayer and Valdes, 2010; Stone et al., 2013; Capron et al., 2014; Saupe et al., 2014; Holloway et al., 2016; Valdes et al., 2017). Here, IPCC Representative Concentration Pathways (RCP) 4.5 and 8.5 were used for future climate scenario simulations (Riahi et al., 2011; Thomson et al., 2011). RCP4.5 is a climate scenario simulation which stabilizes radiative forcing at 4.5 W m^{-2} (approximately equivalent to 650 ppmv CO_2) by the end of the century, without ever surpassing that value (Thomson et al., 2011), whereas RCP8.5 has a radiative forcing of 8.5 W m^{-2} (approximately equivalent to 936 ppmv CO_2) by 2100 (Riahi et al., 2011). The RCP4.5

scenario assumes that climate policies are put into practise to curb global greenhouse emissions, resulting in the stabilization of emissions (Thomson et al., 2011). Conversely, the RCP8.5 scenario assumes a global population of 12 billion by 2100, slow income growth, meek energy efficiency development, and little progress in curbing emissions (Riahi et al., 2011).

To further improve ENMs, bathymetric data were extracted from Getech's present-day digital elevation model (DEM). This DEM provides a gridded representation of both the Earth's topography and bathymetry, and has a resolution of 0.1° x 0.1°. In this study, bathymetric data were aggregated to 1.25° x 1.25° to be consistent with the resolution of the climate variables for ENM. To prevent the loss of shallow water areas surrounding small oceanic islands, a minimum-value aggregating technique was used, assigning the minimum depth within the aggregated area as the cell value. Preferably, a Last Interglacial (LIG) DEM would be used for constructing LIG ENMs and projections; however, DEMs for this time period were not available. Generally, the LIG eustatic sea level is thought to have been between 4 and 9 m higher than the present day (Veeh, 1966; Stirling et al., 1998; Clark and Huybers, 2009; McKay et al., 2011; Dutton and Lambeck, 2012). Sensitivity analyses were conducted to evaluate the impact of a heightened sea level at such large spatial scales, running models with sea level increased by 10 m (Appendix A: Figure A.1). No considerable difference in model output was found; as such, a modern DEM was used in both modern and LIG ENM constructs.

Environmental variables known to be ecologically limiting for modern corals (i.e. SST, salinity, irradiance and bathymetry) (Kleypas et al., 1999; Veron, 2000; Couce et al., 2012), and that can be viably determined for the fossil record from AOGCM outputs, were chosen to reflect abiotic niche characteristics. Initially, these variables were considered at several temporal levels: annual, seasonal and monthly. However, to reduce co-linearity between variables and prevent over-fitting, only combinations of climate variables with a Pearson's pairwise correlation coefficient of less than 0.7 were retained. After enquiry, five environmental variables were used for final niche

modelling: (i) mean annual SST; (ii) mean December–February irradiance; (iii) mean June–August irradiance; (iv) mean annual salinity; and (v) bathymetry.

While additional variables (e.g. aragonite saturation state) might be valuable for estimating Z-coral distribution, not all variables can be viably approximated for the geological past. Despite this, several biophysical studies have shown that the fundamental niche of an organism can be reasonably approximated by a limited set of biologically important variables (e.g. Kearney et al., 2010). In addition, Couce et al. (2012) demonstrated that SST was the primary control on coral reef distribution, with high light availability, salinity, aragonite saturation state and low nutrient concentrations being of secondary significance. Nevertheless, sensitivity analyses were conducted to compare modern projections from modern-trained models with and without aragonite saturation state to gauge the potential impact upon results (Appendix A: Figure A.2). As aragonite saturation state data were not available from AOGCM outputs, global gridded data from Jiang et al. (2015) were used, calculated from a number of in situ measurements via a Matlab version of CO2SYS. These data were resampled and clipped in accordance to the environmental data used for ENM analyses. No considerable differences were found in global model projections for the modern (Appendix A: Figure A.2), with the exception of a few isolated regions (Timor Sea, South China Sea, and to a lesser extent, northern Andaman Sea [Myanmar], eastern Mediterranean Sea, and south-eastern Atlantic Ocean [Angola/Namibia]). Variable contribution analysis (Appendix A: Table A.1) confirms that aragonite saturation state is of secondary importance for global scale ENM. However, its contribution to ENM is not insignificant, with similar scores to seasonal irradiance (June–August), and should therefore be considered within this context for the interpretation of ENM results.

3.2.4 Ecological niche modelling

To map the potential distribution of Z-corals in the modern, LIG and under future climate change scenarios (RCP4.5 and RCP8.5), three ENM methods were

implemented: BIOCLIM (Booth et al., 2014), randomForest (Liaw and Wiener, 2002) and MaxEnt v. 3.4.1 (Phillips et al., 2017). In particular, MaxEnt has been shown to perform well in previous studies on coral reefs, as well as those using the fossil record for other taxonomic groups (Couce et al., 2012; Freeman et al., 2013; Saupe et al., 2014; Soto-Centeno and Steadman, 2015; Freeman, 2015; Waterson et al., 2016; Chiarenza et al., 2019). ENMs were generated using the R-package 'biomod2' v. 3.3-7 (Thuiller et al., 2009, 2016), running 100 subsample replicates with 75% of occurrences for model training, while 25% were reserved (randomly seeded) for model testing. To provide insights into the occupied niche and distribution of Z-corals under two diverse climate states, two model classes were generated, training the ENM with LIG and modern Z-coral occurrences. Using the three ENM algorithms, an ensemble model was produced, with each model weighted proportional to their true skill statistic scores (Allouche et al., 2006; Thuiller et al., 2016). In addition, to identify geographical areas which indicate environmental variable values outside of the training range, Multivariate Environmental Similarity Surface (MESS) (Elith et al., 2010) analyses was conducted, and clamping masks built.

3.2.5 Range comparisons

In order to measure distribution dynamics, continuous model outputs were transformed into binary predictions. For binary conversion, a threshold that maximises the sum of sensitivity and specificity (MaxSSS) was implemented. As short-term observations are intrinsically biased and perhaps incomplete in both environmental and geographical space, binary predictions generated from both LIG- and modern-trained models were combined. This was done for each time-slice/climate scenario to establish a multi-temporal approach, estimating the wider geographical localities Z-corals may occupy. Whether this approach improved the models' capacity to predict the occurrence of both LIG and modern localities was then assessed, which would have implications for forecasting under future climate scenarios. The latitudinal range and habitability of Z-corals for past, present and future climatic scenarios were computed as a function of

the sum of suitable cells, within 5° latitudinal bins, for each model class' projections (LIG, modern and coupled).

3.2.6 Model validation

Model performance was assessed using the area under the curve (AUC) statistic (Peterson et al., 2008), derived from receiver operating characteristic (ROC) analyses, and the true skill statistic (TSS) (Allouche et al., 2006). In general, evaluation criteria for AUC values have been interpreted as good (0.90–1.00), moderate (0.7–0.9), and poor (0.5–0.7), whereas a score of less than 0.5 is worse than one would expect from a random model (Swets, 1988; Franklin, 2010). Evaluation scores for TSS range from −1 to 1, where a score of 1 demonstrates perfect model performance, while less than 0 is considered worse than a random model (Allouche et al., 2006). As two ENM constructs were used (LIG- and modern-trained), with respective forecasting and hindcasting (backtesting) projections generated, AUC scores were calculated using LIG occurrence cells and modern occurrence cells as an evaluation dataset for model projections to other climate scenarios (i.e. modern-trained and LIG projection; LIG-trained and modern projection).

3.3 Results

3.3.1 Diversity analyses

Latitudinal diversity analyses corroborate previous work (i.e. Kiessling et al., 2012). Unsurprisingly, sampling of LIG Z-corals is far less comprehensive than those of the modern, particularly within tropical latitudinal bins which exhibit one order of magnitude less occurrences and localities than in the modern (Figure 3.3). Latitudinal species richness tends to track the number of reported occurrences, with a high correlation between the two variables in both the modern (Spearman rho = 0.809, $P = < 0.001$) and LIG (Spearman rho = 0.984, $P = < 0.001$).

The modern 'raw' latitudinal biodiversity gradient of Z-corals suggests a tropical peak in diversity, declining poleward (Figure 3.3A). However, there is also a small decline

in species richness proximal to the equator, coinciding with a substantial decrease in the number of reported occurrences and localities. The most poleward latitudinal bins occupied by modern Z-corals are 40–45° in the Northern Hemisphere, and 35–40° in the Southern Hemisphere. Results from CR on modern Z-corals suggest similar latitudinal trends in diversity to those indicated by the uncorrected data (Figure 3.3B). However, there is a prominent decline in species richness between 15–20°N. This is a consequence of the low evenness (*Pielou's evenness index* = 0.670) of the occurrence data within this bin, with 14/136 (~10%) species comprising 3,264/4,261 (~75%) of the occurrences.

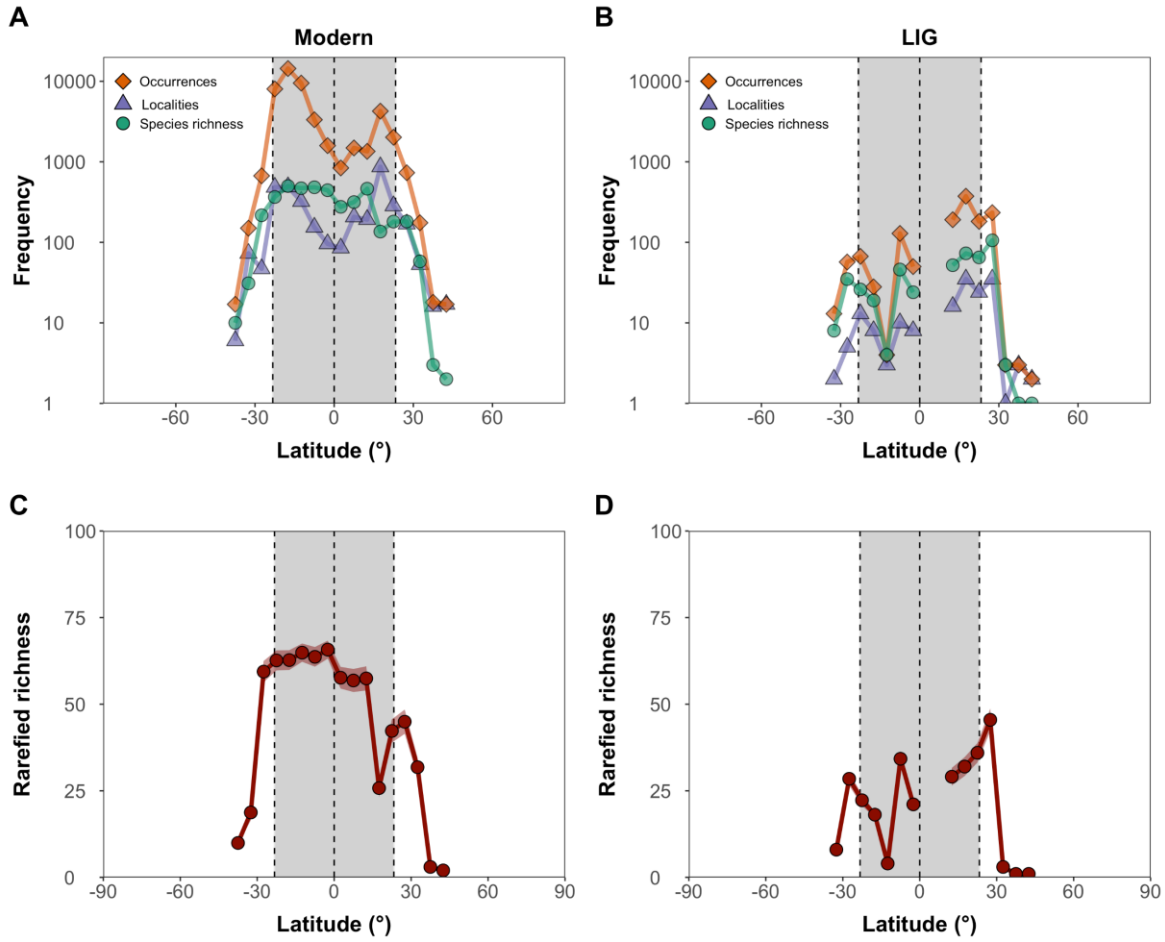


Figure 3.3. Latitudinal distribution of zooxanthellate coral occurrences and species richness in 5° latitudinal bins. (A, B) Orange diamonds indicate the number of occurrences for the modern (A) and Last Interglacial (LIG) (B), purple triangles depict the number of localities, defined as unique coordinates, and green circles illustrate the species richness. (C, D) Mean rarefied richness of zooxanthellate corals for the modern (C) and LIG (D), based on a subsampling quota of 75 occurrences across 1,000 trials. The red ribbon represents the error bars (one standard deviation) from the 1,000 trials. Shaded grey area highlight the latitudinal extent of the tropics. Black dashed lines indicate the Equator, Northern Tropic and Southern Tropic.

The LIG raw latitudinal biodiversity gradient of Z-corals suggests a subtropical peak in biodiversity (25–30°N: 106 species), declining both poleward and equatorward (Figure 3.3B). The lack of reported LIG occurrences within bins 0–5°N and 5–10°N prevents assessment of species richness within these latitudinal bands. However, adjacent latitudinal bins suggest an equatorial decline in LIG species richness, analogous to the modern Z-coral latitudinal biodiversity gradient. Interestingly, the Southern Hemisphere exhibits latitudinal biodiversity peaks in the tropics (5–10°S) and subtropics (25–30°S), separated by a diversity trough (10–15°S). The most poleward latitudinal bins occupied by LIG Z-corals are 40–45° in the Northern Hemisphere, and 30–45° in the Southern Hemisphere. Results from CR on LIG Z-corals suggest similar latitudinal trends in diversity to those indicated by the uncorrected data (Figure 3.3C). However, the low evenness of the occurrence data in tropical bins may influence richness estimates. For example, for latitudinal bin 15–20°N, 15/73 (~20%) species contribute 250/374 (~67%) of the occurrences (*Pielou's evenness index* = 0.851). Conversely, for latitudinal bin 25–30°N (estimated to be most diverse) 18/106 (~20%) species contribute only 115/234 (~50%) of the occurrences (*Pielou's evenness index* = 0.927).

3.3.2 Ecological niche modelling

Model performance

On the basis of the mean AUC scores, the MaxEnt models performed best for both modern-trained (MaxEnt: 0.974, randomForest: 0.963, BIOCLIM: 0.843) and LIG-trained (MaxEnt: 0.976, randomForest: 0.950, BIOCLIM: 0.807) models, across individual projections. Conferring to AUC evaluation criteria (Swets, 1988; Franklin, 2010), all models performed well with the exception of the BIOCLIM models, which can still be considered as fair. TSS scores reflect similar results in terms of model performance for modern-trained (MaxEnt: 0.899, randomForest: 0.866, BIOCLIM: 0.685) and LIG-trained ENMs (MaxEnt: 0.924, randomForest: 0.832, BIOCLIM: 0.615), with all models performing well, except BIOCLIM. The modern-trained

ensemble model had mean AUC scores of 0.879, 0.874 and 0.754 (Figure 3.4) for the full occurrence dataset, test dataset and evaluation dataset, respectively. The LIG-trained model had AUC scores of 0.840, 0.838 and 0.690 (Figure 3.5). In addition, combined modern binary projections were able to predict 83.95% of modern occurrence cells, while LIG-trained-only projections were able to predict 40.61%. Similarly, combined LIG binary projections were able to predict 87.50% of LIG fossil occurrence cells, whereas modern-trained-only projections were able to predict 57.14%.

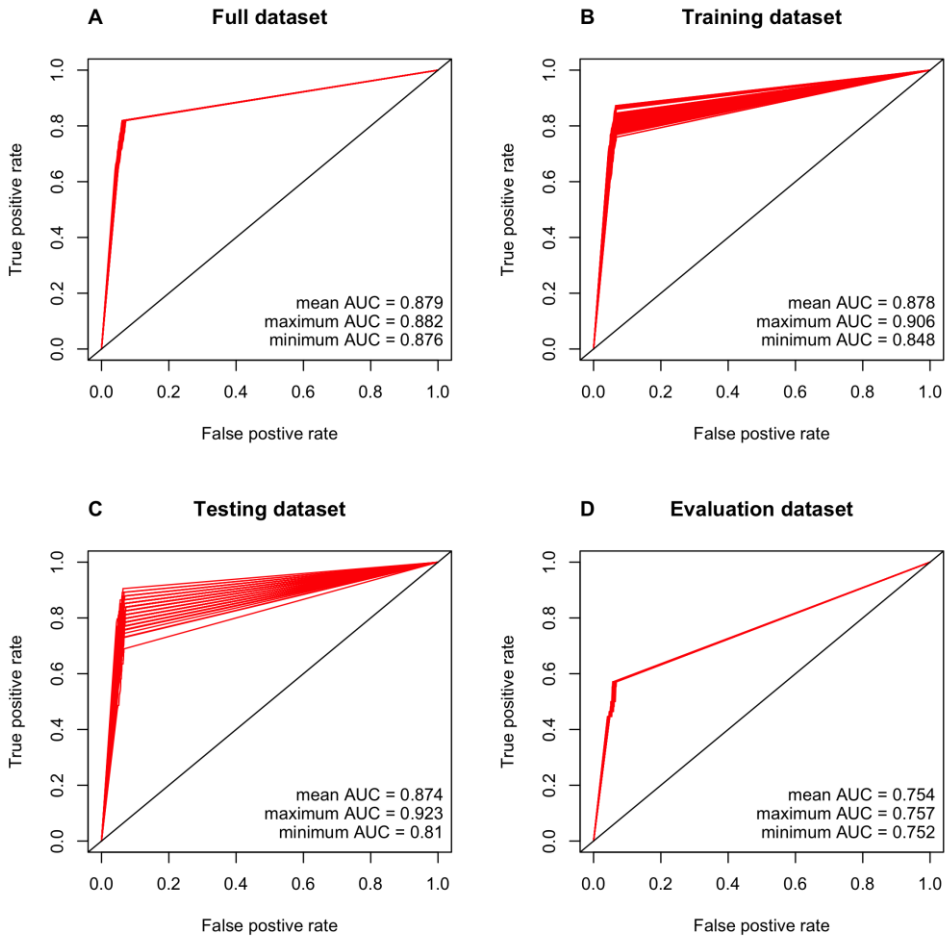


Figure 3.4. Receiver operating characteristic (ROC) curves from the modern-trained ensemble model. (A) ROC curves and area under the curve (AUC) values generated using the complete modern occurrence dataset and modern projection. (B) ROC curves and AUC values generated using the modern training dataset and modern projection. (C) ROC curves and AUC values generated using the modern testing dataset and modern projection. (D) ROC curves and AUC values generated using LIG occurrences as an evaluation dataset with the modern-trained LIG projection. Each plot curve represents one of the one hundred training/testing/background occurrence datasets. The black diagonal line indicates an AUC of 0.5, which is the AUC of a null expectation curve.

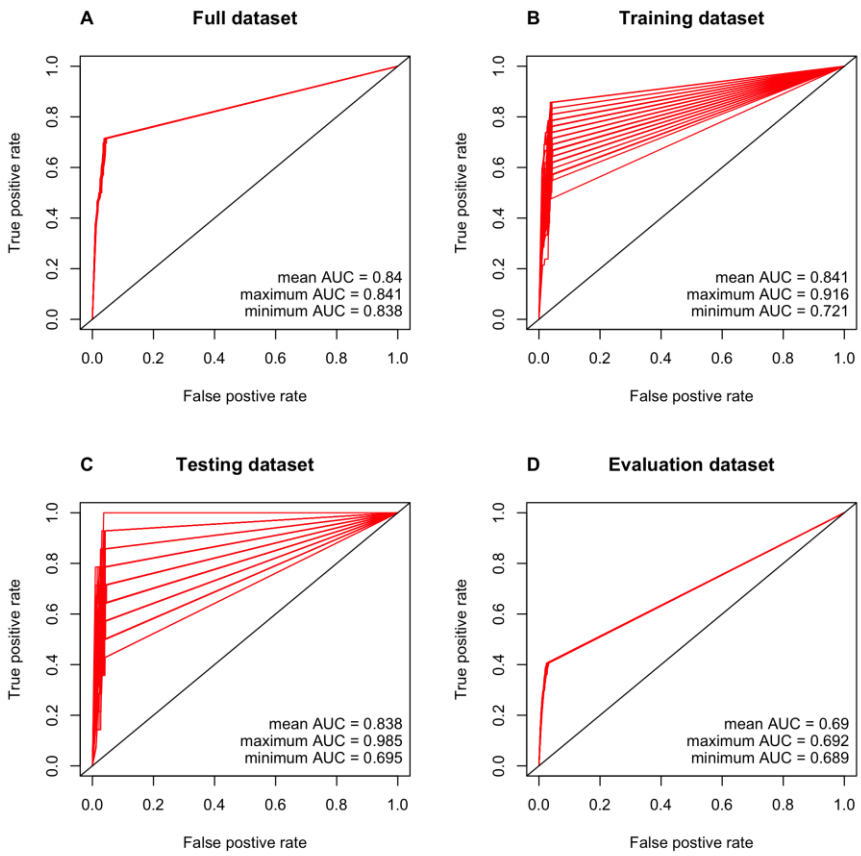


Figure 3.5. Receiver operating characteristic (ROC) curves from the LIG-trained ensemble model. (A) ROC curves and area under the curve (AUC) values generated using the complete LIG occurrence dataset and modern projection. (B) ROC curves and AUC values generated using the LIG training dataset and LIG projection. (C) ROC curves and AUC values generated using the LIG testing dataset and LIG projection. (D) ROC curves and AUC values generated using modern occurrences as an evaluation dataset with the LIG-trained modern projection. Each plot curve represents one of the one hundred training/testing/background occurrence datasets. The black diagonal line indicates an AUC of 0.5, which is the AUC of a null expectation curve.

Geographic predictions

Global modern-trained binary suitability maps predict more suitable cells than the LIG-trained ENM for all climate scenarios (Figure 3.6). The LIG-trained ENM estimates a smaller sum of suitable cells within the tropics than the modern-trained ENM. Combining model outputs from both ENMs shows an increase in suitable cells for the Northern Hemisphere during the LIG (10–40°N; Table 3.1). In addition, there is a small increase in the number of suitable cells for the modern, RCP4.5, and RCP8.5. Notably, for RCP4.5 and RCP8.5, the combined projections predict additional suitability at higher latitudes in the Northern Hemisphere, yet provide no such significant results for lower latitudes, or in the Southern Hemisphere.

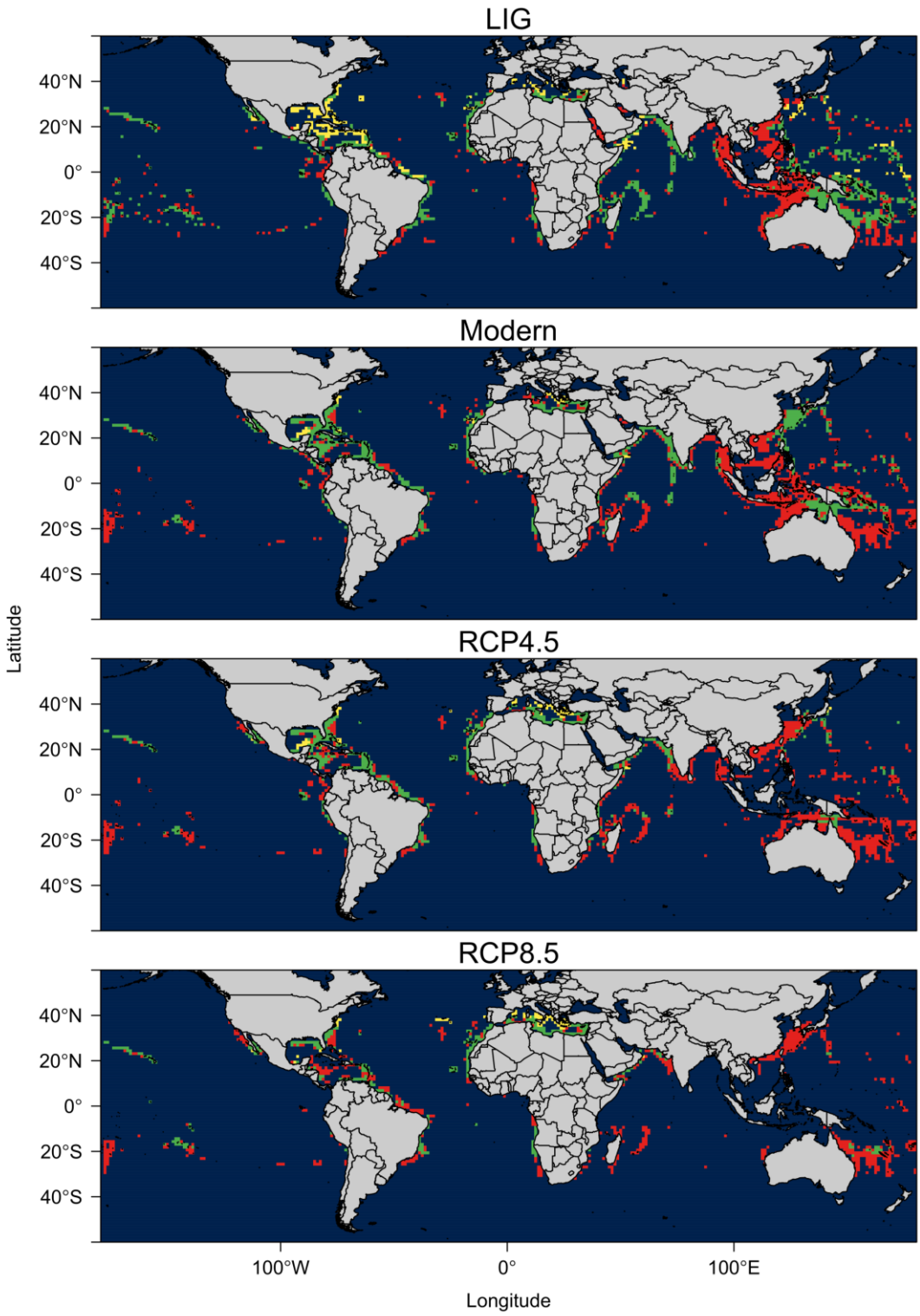


Figure 3.6. Combined binary suitability maps from modern- and LIG-trained ecological niche models (ENM). Suitability maps are for zooxanthellate corals under four climatic scenarios: Last Interglacial (LIG), modern, Representative Concentration Pathways (RCP) 4.5 and 8.5. Binary conversion was implemented using the MaxSSS threshold, which maximises the sum of sensitivity and specificity of the model. Red cells indicate suitable localities from the modern-trained ENM; yellow cells indicate suitable localities from the LIG-trained ENM; green cells indicate suitable localities from the modern- and LIG-trained ENM (i.e. model agreement). Data is projected in the coordinate reference system: World Geodetic System 1984 (WGS84).

Indo-Australian Archipelago. Combined binary suitability maps for the Indo-Australian Archipelago (IAA) indicate a small decrease in the number of suitable cells between the LIG and the modern (Figure 3.7). However, under projected climate change scenarios RCP4.5 and RCP8.5, a large decrease in the number of suitable cells is estimated for the IAA region. Specifically, this decrease in suitable cells is centred around the equator in RCP4.5, expanding to higher latitudes under RCP8.5. Notably, no significant decrease in equatorial suitability is estimated from combined binary projections for the LIG. However, there is also little agreement between modern- and LIG-trained projections within equatorial latitudes, with the modern-trained model suggesting suitable cells for the LIG, while the LIG-trained model suggests unsuitable cells. The stronger agreement between LIG fossil occurrences and the modern-trained LIG projection, provides additional support for the modern-trained projection. Furthermore, the LIG-trained modern projection shows strong disagreement with the modern occurrence data, resulting in a high number of false negatives.

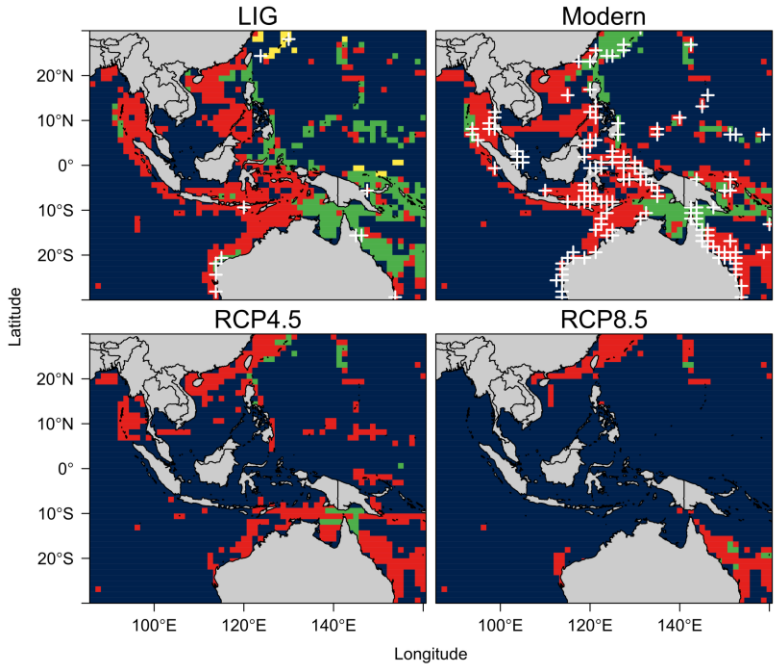


Figure 3.7. Cropped binary suitability maps for the Indo-Australian Archipelago, under four climatic scenarios: Last Interglacial (LIG), modern, Representative Concentration Pathways (RCP) 4.5 and 8.5. Binary conversion was implemented using the MaxSSS conversion method, which maximises the sum of sensitivity and specificity of the model. Red cells indicate suitable localities from the modern-trained ENM; yellow cells indicate suitable localities from the LIG-trained ENM; green cells indicate suitable localities from the modern- and LIG-trained ENM (i.e. model agreement). White crosshairs indicate LIG (top-left) and modern (top-right) zooxanthellate coral occurrences.

Caribbean and Gulf of Mexico. Combined binary suitability maps for the Caribbean and Gulf of Mexico indicate a small increase in the number of suitable cells between the LIG and the modern (Figure 3.8). Under projected climate change scenario RCP4.5, no significant change in the number of suitable cells is estimated for the region. However, under RCP8.5 a large decrease in the region's suitable localities is estimated. Binary suitability maps suggest a high-level of agreement between modern- and LIG trained projections for the modern and RCP4.5. Conversely, LIG projections show significant disagreement between the two models' binary predictions. The LIG-trained ENM suggests that during the LIG, the Caribbean and the Gulf of Mexico was comparably suitable for Z-corals as the modern, whereas the modern-trained model suggests the region was largely unsuitable. However, the disagreement between LIG fossil occurrences and the modern-trained LIG projection, provides stronger support for the LIG-trained projection.

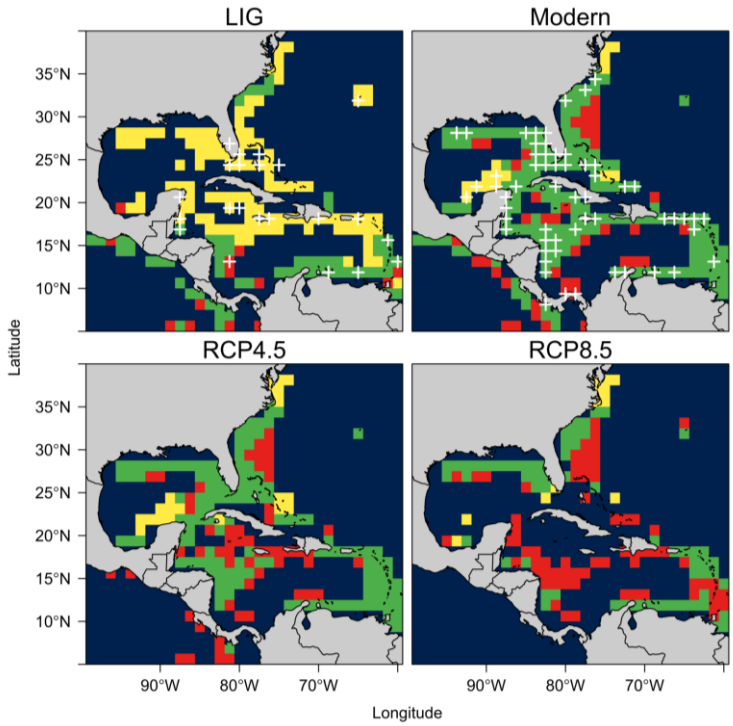


Figure 3.8. Cropped binary suitability maps for the Caribbean and the Gulf of Mexico, under four climatic scenarios: Last Interglacial (LIG), modern, Representative Concentration Pathways (RCP) 4.5 and 8.5. Binary conversion was implemented using the MaxSSS conversion method, which maximises the sum of sensitivity and specificity of the model. Red cells indicate suitable localities from the modern-trained ENM; yellow cells indicate suitable localities from the LIG-trained ENM; green cells indicate suitable localities from the modern- and LIG-trained ENM (i.e. model agreement). White crosshairs indicate LIG (top-left) and modern (top-right) zooxanthellate coral occurrences.

Red Sea. Combined binary suitability maps for the Red Sea indicate no suitable habitats during the modern and under future climate scenarios RCP4.5 and RCP8.5 (Figure 3.9). The presence of Z-corals in the Red Sea today indicates that neither ENM class (modern- or LIG-trained) is performing well for the region, with clear false negatives for the modern. This is a direct result of the binary threshold selection, which maximises the sum of both sensitivity (true positive rate) and specificity (true negative rate) at global scale, resulting in false negatives for the region. Nevertheless, combined predictions suggest the presence of suitable habitats during the LIG, with both model classes in agreement, along with the fossil data.

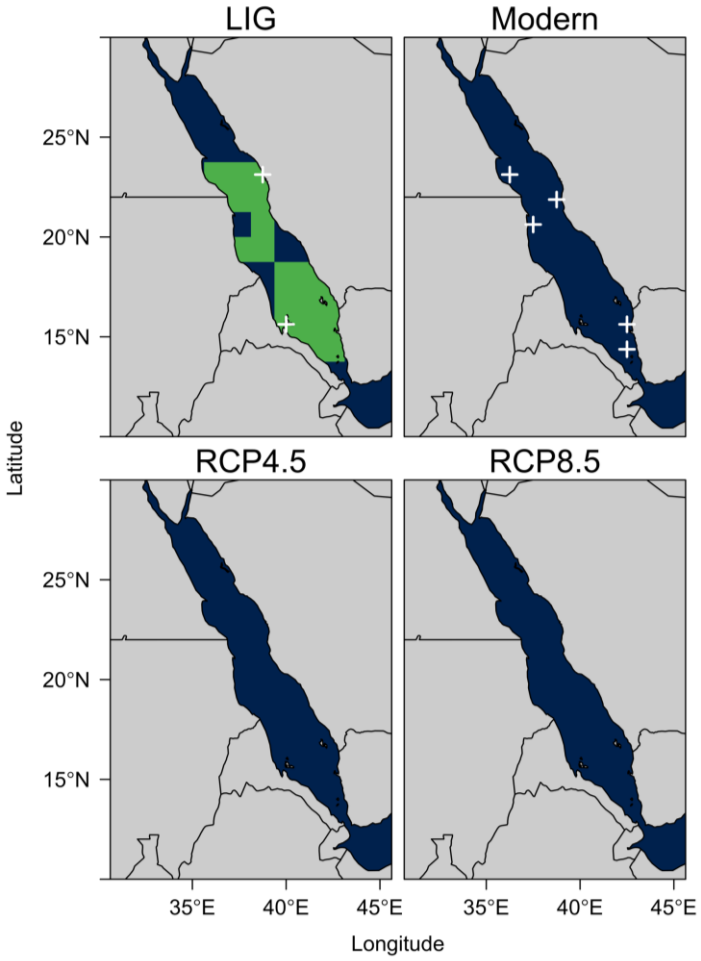


Figure 3.9. Cropped binary suitability maps for the Red Sea, under four climatic scenarios: Last Interglacial (LIG), modern, Representative Concentration Pathways (RCP) 4.5 and 8.5. Binary conversion was implemented using the MaxSSS conversion method, which maximises the sum of sensitivity and specificity of the model. Red cells indicate suitable localities from the modern-trained ENM; yellow cells indicate suitable localities from the LIG-trained ENM; green cells indicate suitable localities from the modern- and LIG-trained ENM (i.e. model agreement). White crosshairs indicate LIG (top-left) and modern (top-right) zooxanthellate coral occurrences.

Mediterranean. Combined binary suitability maps for the Mediterranean show a relatively small increase in the number of suitable cells from the LIG to the modern (Figure 3.10). Under projected climate change scenarios RCP4.5 and RCP8.5, there is a significant increase in the number of cells predicted to be suitable cells for the Mediterranean. Binary suitability maps do not suggest a high-level of agreement between modern- and LIG-trained projections for all climatic regimes. Notably, disagreement between model projections is highest for future climate scenario projections RCP4.5 and RCP8.5. Modern and LIG projections indicate a poor discriminatory capacity for the Mediterranean, with only 36% of occurrence localities correctly predicted in the Modern, and 25% for the LIG. Parallel to the Red Sea, this is a direct result of the elected binary threshold, leading to an increase in false negatives for some regions.

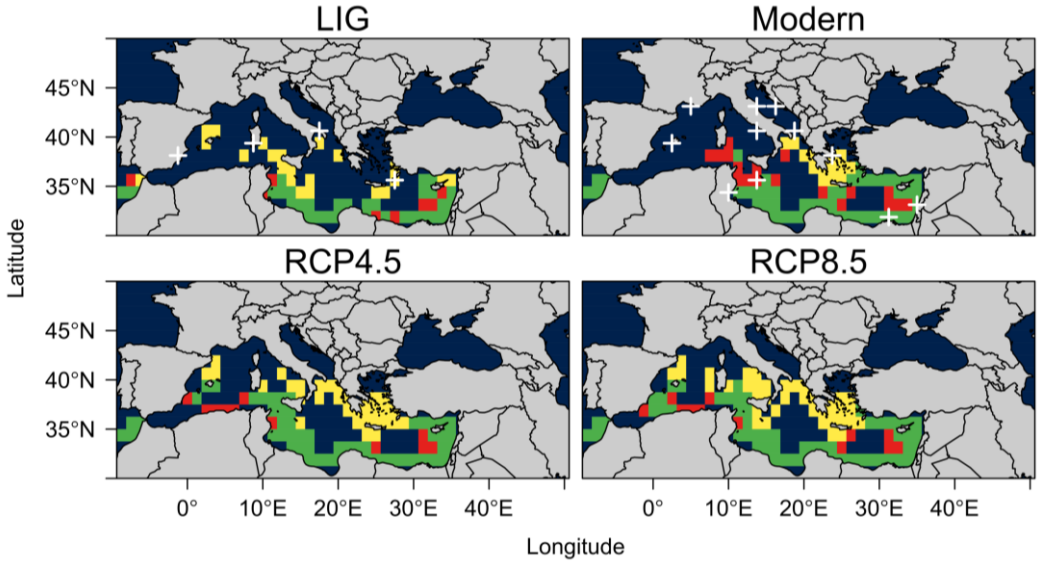


Figure 3.10. Cropped binary suitability maps of the Mediterranean, under four climatic scenarios: Last Interglacial (LIG), modern, Representative Concentration Pathways (RCP) 4.5 and 8.5. Binary conversion was implemented using the MaxSSS conversion method, which maximises the sum of sensitivity and specificity of the model. Red cells indicate suitable localities from the modern-trained ENM; yellow cells indicate suitable localities from the LIG-trained ENM; green cells indicate suitable localities from the modern- and LIG-trained ENM (i.e. model agreement). White crosshairs indicate LIG (top-left) and modern (top-right) zooxanthellate coral occurrences.

3.3.3 Range dynamics

The LIG binary maps indicate habitat suitability at equatorial latitudes for both modern- and LIG-trained models (Figure 3.11). For latitudinal bin 0–5°N, LIG binary

maps predict 49, 85, and 95 suitable cells for the LIG-trained, modern-trained and coupled ENM projections, respectively (Table 3.1). South of the equator, LIG binary maps predict 66, 124, and 138 suitable cells for the LIG-trained, modern-trained and coupled ENM projections for 0–5°S. Modern binary maps for latitudinal bin 0–5°N suggest 27, 89, and 89 suitable cells for the LIG-trained, modern-trained and coupled ENM projections, respectively. In the southern hemisphere, modern binary maps predict 32, 125, and 125 suitable cells for the LIG-trained, modern-trained and coupled ENM projections for 0–5°S. Overall, ENM results suggests that equatorial latitudes during the LIG were more suitable for Z-corals than today. In addition, habitability was generally greater within the tropics (25°N to 25°S) during the LIG than in the modern (Figure 3.11), with 8%, 4%, and 62% more suitable cells predicted from the combined, modern-trained and LIG-trained projections, respectively.

Combined binary maps indicate suitable cells at more poleward latitudes during the LIG (40–45°N; 35–40°S), than in the modern (35–40°N; 30–35°S). However, 48 cells were predicted to be suitable for the modern binary map at 35–40°N, while only 29 cells were predicted to be suitable for the LIG in the same latitudinal bin. Conversely, in the southern hemisphere, only one cell was predicted to be suitable for the modern binary map at 30–35°S, and 53 cells for the LIG.

Under future climate change scenarios, the combined binary maps suggest a considerable decrease in habitability within the tropics (25°S to 25°N), with a 24% (RCP4.5) and 60% (RCP8.5) decrease in the number of suitable cells relative to the modern. Notably, a large proportion of this tropical decrease is in the centre of the hyper-diverse Coral Triangle (Indo-Australian Archipelago). By contrast, habitability increases at higher latitudes (25–45°N) in the Northern Hemisphere (Figure 3.11; Table 3.1), with a 11% and 20% increase in the number of suitable cells under RCP4.5 and RCP8.5, respectively. South of the equator, there is a similar gain at higher latitudes (25–40°S), with a 17% and 33% increase in the number of suitable cells under RCP4.5 and RCP8.5.

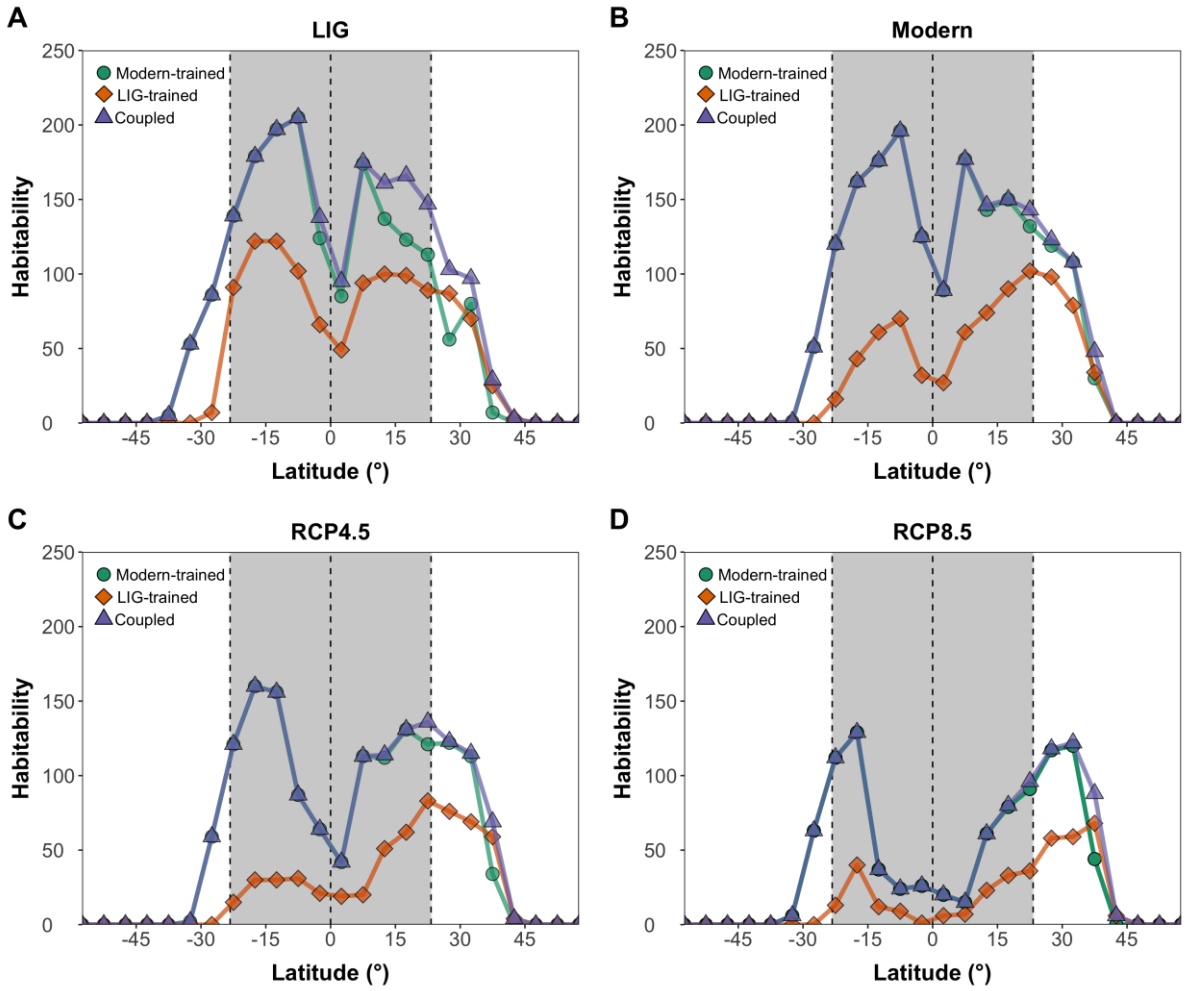


Figure 3.11. Latitudinal plots of predicted habitability from ecological niche modelling under four climatic scenarios: Last Interglacial (LIG), modern, Representative Concentration Pathways (RCP) 4.5 and 8.5. In this instance, habitability is the sum of cells designated as habitable after binary conversion, within 5° latitudinal bins. Binary conversion was implemented using the MaxSSS conversion method, which maximises the sum of sensitivity and specificity of the model. Green points indicate results from modern-trained ecological niche model projections; orange diamonds depict results from LIG-trained ecological niche model projections; purple triangles illustrate the results from the coupled projections (modern- and LIG-trained ecological niche models); grey shading highlights the extent of the tropics; black dashed-line indicates the Equator, Northern Tropic and Southern Tropic.

Table 3.1. Latitudinal habitability from binary predictions made by ecological niche models trained on modern (M) and Last Interglacial (LIG) zooxanthellate coral occurrence datasets. In this instance, habitability is the sum of cells designated as habitable after binary conversion, within 5° latitudinal bins. Binary conversion was implemented using the MaxSSS conversion method, which maximises the sum of sensitivity and specificity of the model. Coupled predictions represent the combined suitability predictions of modern- and LIG-trained ecological niche models.

Latitude (°)	Modern-trained				LIG-trained				Coupled			
	LIG	M	RCP 4.5	RCP 8.5	LIG	M	RCP 4.5	RCP 8.5	LIG	M	RCP 4.5	RCP 8.5
60–55	0	0	0	0	0	0	0	0	0	0	0	0
55–50	0	0	0	0	0	0	0	0	0	0	0	0
50–45	0	0	0	0	0	0	0	0	0	0	0	0
45–40	0	0	0	0	3	0	4	6	3	0	4	6
40–35	7	30	34	44	25	34	59	68	29	48	69	88
35–30	80	108	113	120	70	79	69	59	97	108	115	122
30–25	56	119	122	117	87	98	76	58	103	123	123	118
25–20	113	132	121	91	89	102	83	36	147	143	136	96
20–15	123	150	131	79	99	90	62	33	166	150	131	80
15–10	137	143	112	61	100	74	51	23	161	146	114	61
10–5	174	177	113	15	94	61	20	7	175	177	113	15
5–0	85	89	42	20	49	27	19	6	95	89	42	20
0–5	124	125	64	26	66	32	21	1	138	125	64	26
5–10	205	196	87	24	102	70	31	9	205	196	87	24
10–15	197	176	156	37	122	61	30	12	197	176	156	37
15–20	179	162	160	129	122	43	30	40	179	162	160	129
20–25	139	120	121	112	91	16	15	13	139	120	121	112
25–30	86	51	59	63	7	0	0	0	86	51	59	63
30–35	53	1	2	6	0	0	0	0	53	1	2	6
35–40	5	0	0	0	0	0	0	0	5	0	0	0
40–45	0	0	0	0	0	0	0	0	0	0	0	0
45–50	0	0	0	0	0	0	0	0	0	0	0	0
50–55	0	0	0	0	0	0	0	0	0	0	0	0
55–60	0	0	0	0	0	0	0	0	0	0	0	0
Total	1763	1779	1437	944	1126	787	570	371	1978	1815	1496	1003

3.3.4 Clamping masks

Last Interglacial calibration

Clamping masks for the LIG-trained ENM show comparatively little uncertainty in model projections for the modern (Figure 3.12). However, the modern Red Sea and Western coast of Australia appear to be outside of the calibration range of the LIG-trained model, explaining the lack of predicted suitable cells within these regions and the disagreement with empirical evidence (modern occurrence data). RCP4.5 clamping masks identify similar regions to those of the modern, with the addition of equatorial localities in the IAA. However, under RCP8.5 this uncertainty expands across the tropics, and most notably within the IAA. MESS analyses indicate this uncertainty at equatorial and tropical localities is driven by novel sea surface temperatures under RCP4.5 and RCP8.5 climate scenarios.

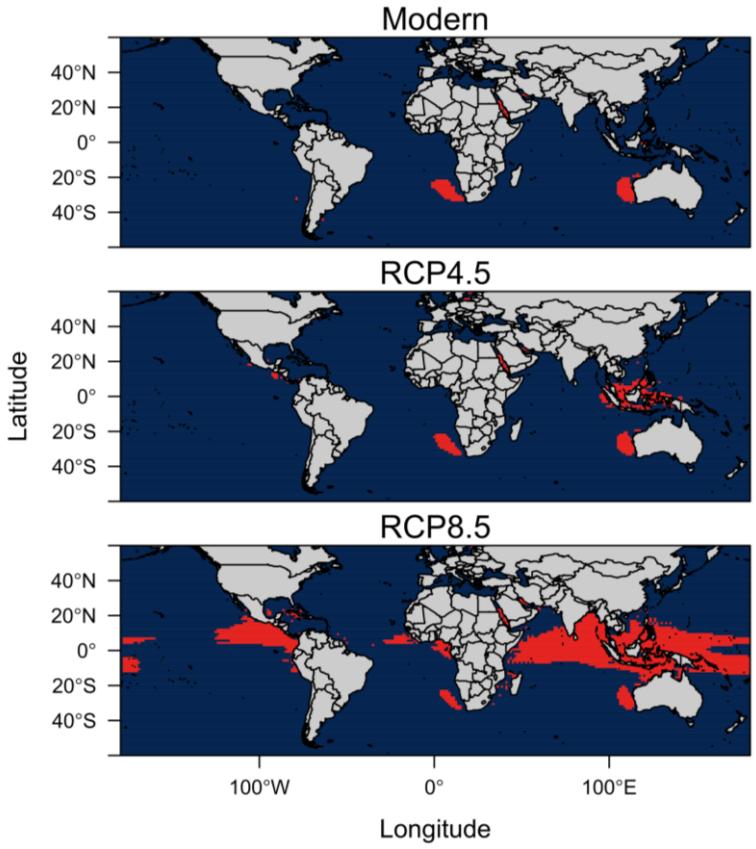


Figure 3.12. Clamping masks for model projections trained on the Last Interglacial climatic conditions and occurrences. These masks identify locations where predictions are uncertain as the values of the variables are outside the range of those used to calibrate the model. Red cells highlight areas where one variable is outside of the model calibration range. Data is projected in the coordinate reference system: World Geodetic System 1984 (WGS84).

Modern calibration

Clamping masks for the modern-trained ENM generally show little uncertainty in model projections for the LIG at global scale (Figure 3.13). However, in large areas of the Caribbean, LIG climatic conditions are outside of the calibration range of the modern-trained ENM. MESS analyses indicate this is a result of novel summer (June–August) irradiance values. RCP4.5 clamping masks identify uncertainty in equatorial regions of the IAA. However, under RCP8.5 this uncertainty expands across the tropics, and most notably within the IAA. Corresponding to the LIG-calibrated model, MESS analyses indicate that this uncertainty at equatorial and tropical localities is driven by novel sea surface temperatures under RCP4.5 and RCP8.5 climate scenarios.

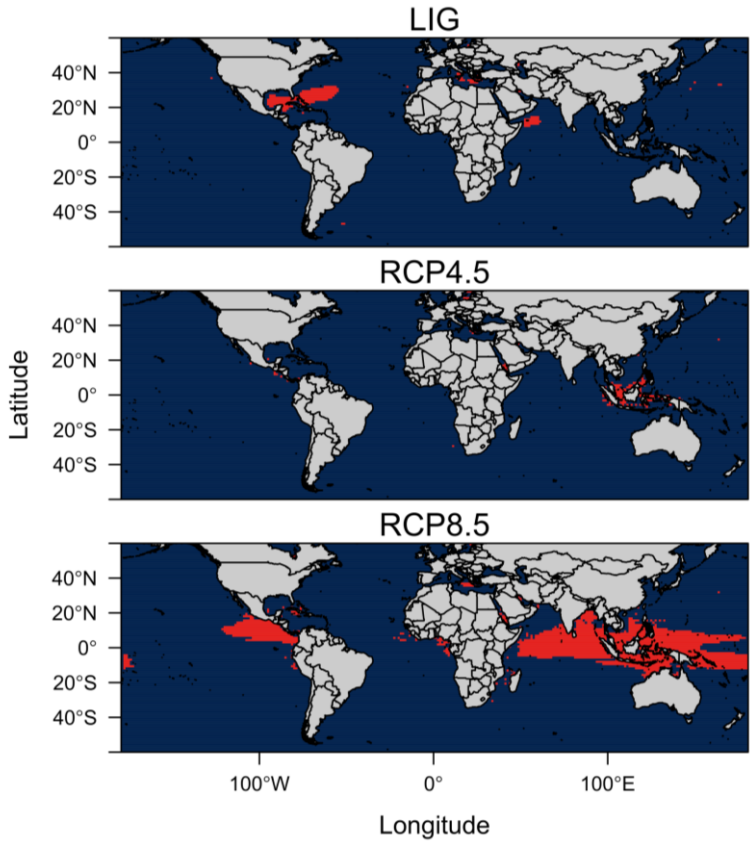


Figure 3.13. Clamping masks for model projections trained on modern climatic conditions and occurrences. These masks identify locations where predictions are uncertain as the values of the variables are outside the range of those used to calibrate the model. Red cells highlight areas where one variable is outside of the model calibration range. Data is projected in the coordinate reference system: World Geodetic System 1984 (WGS84).

3.4 Discussion

The Last Interglacial (LIG) has occasionally been considered as an analogue for the impacts of global warming on species' distribution (Tyrberg, 2010; Kiessling et al., 2012; Jeffers and Willis, 2014). At face value, the LIG fossil record of zooxanthellate corals (Z-corals) depicts a global biogeographic pattern that is considerably dissimilar to that observed in the present day (Figure 3.3). Whereas today, both species abundance and diversity are highest within the tropics, with an equatorial dip, the LIG record shows a poleward shift in occurrence records and species diversity, with both increasing at higher latitudes in the Northern Hemisphere, and a prominent equatorial decline (Kiessling et al., 2012). Support for this observed pattern is also provided when subsampling methods are applied to ameliorate biases pertaining to uneven latitudinal sampling (Kiessling et al., 2012). However, using ecological niche modelling (ENM), this study's findings provide little support for an equatorial decline in habitability for Z-corals during the LIG. Instead, LIG Z-corals likely occupied similar, though not equivalent, geographic distributions to those of modern Z-corals. This study's results suggest that during the LIG, global habitability was generally greater than the modern, particularly at equatorial latitudes. In addition, modelled habitability is more pronounced at high latitudes in both hemispheres, with a more poleward distribution. These results support a poleward range expansion of Z-corals during the LIG, as suggested by previous studies (Greenstein and Pandolfi, 2008; Kiessling et al., 2012), but not an equatorial decline (Kiessling et al., 2012). This suggests that the observed equatorial decline in the fossil record might be a result of sampling bias within equatorial regions.

Under climate scenarios RCP4.5 and RCP8.5, ENM results indicate that high latitude habitability should increase (i.e. range expansion), while equatorial latitudes will see a large decrease in favourable habitats (i.e. range retraction) compared to the modern. Most notably, this includes the centre of the Coral Triangle, in the Indo-Pacific Ocean, the 'heart' of modern-day coral biodiversity, with 605 Z-coral species, representing over three-quarters of global Z-coral diversity (Veron et al., 2009). In addition to the direct

risk to biodiversity (including the multitude of species that live in coral reef environments), the economic, social and cultural benefits that coral reefs provide are of crucial importance to island communities within this region (Spalding et al., 2001; Hoegh-Guldberg, 2011). However, model clamping masks also suggest that under RCP4.5 and RCP8.5, both modern- and LIG-trained ENMs are outside of their calibration range, adding uncertainty to these predictions and a 'worst-case scenario'. Nevertheless, it should also be borne in mind that Z-corals, and coral reef ecosystems, are far less likely to survive other stressors, such as overfishing and pollution, when exposed to heat stress. Furthermore, as ENM projections do not include aragonite saturation state, they may be relatively optimistic in the face of anthropogenic climate change as they do not account for the impacts of ocean acidification.

Implications for the evolution of the latitudinal biodiversity gradient

Attempts to reconstruct latitudinal biodiversity gradients in geological time have historically been achieved using direct reading of occurrence records (Crame, 2001), potentially leading to circumscribed results (Mannion et al., 2014). Although subsampling approaches have been applied in more recent studies, and provide more useful insights than uncorrected 'raw' diversity data (Kiessling et al., 2012), they ultimately cannot predict which data we might be missing, i.e. fossils and/or palaeoenvironments that we have not sampled, or that never entered the fossil record (Kiessling, 2005; Vilhena and Smith, 2013). ENM results suggest that the LIG Z-coral record is geographically biased through the amount of predicted habitable area within latitudinal bins, herein referred to as the latitudinal habitability gradient. Thus, given suitable preservational conditions, one should expect to find additional LIG Z-coral occurrence data from equatorial latitudes. Whether new LIG fossil collections within tropical and equatorial regions will result in higher observed richness remains to be seen. However, assuming the ubiquitous scaling of species richness with habitat size (species-area relationship) holds for Z-corals (Connor and McCoy, 1979; Rosenzweig, 1995), equatorial and tropical diversity during the LIG was likely similar to today.

Unimodal-type ('Modern-type') latitudinal biodiversity gradients, with tropical peaks in diversity, have been suggested to form under cold icehouse climate regimes, whereas flattened gradients or temperate peaks are restricted to warmer greenhouse regimes (Mannion et al., 2014). Additionally, it has been proposed that non-modern-type latitudinal biodiversity gradients might also form during interglacials (Yasuhara et al., 2012; Mannion et al., 2014). However, based on modelled habitability, ENMs imply a contrarian result for the LIG, and suggest that interglacials might not be warm enough to produce latitudinal biodiversity gradients similar to those observed in greenhouse climate regimes.

Utility of the fossil record in forecasting

Variable contribution analyses computed within biomod2 (Thuiller et al., 2016) clearly demonstrate that bathymetry and SST are the principal parameters controlling the distribution of both modern and LIG Z-corals (Appendix A: Table A.2). It is to be expected that bathymetry has the largest explanative power as the very nature of zooxanthellate corals restricts them to shallow marine settings. While LIG bathymetry is generally similar to that of the modern at a global scale, several areas have experienced localized tectonic uplift (e.g. Huon Peninsula, Barbados, Sumba and Vanuatu (McCulloch and Esat, 2000)). However, this is not likely to impact this study's results, based on sea-level sensitivity tests (Appendix A: Figure A.1). As both models used the same DEM, SST might be considered the dominant factor in determining any difference between ENM and projected distributions. In fact, ENM results are in line with those suggested by palaeoclimatic proxy and modelling data, which propose that annual mean SST and seasonality at low latitudes for the LIG were similar to those of the modern (McCulloch and Esat, 2000; McKay et al., 2011; Hoffman et al., 2017). Data from uplifted LIG coral reefs from the Huon Peninsula of New Guinea and western Australia also indicate mean annual temperatures and seasonal ranges comparable to present-day SST (McCulloch and Esat, 2000; Dalbeck et al., 2011). However, it has also been suggested that seasonality was greater at higher latitudes, with increased SST and insolation modelled in the Northern Hemisphere

(McKay et al., 2011; Brocas et al., 2016, 2018). This might have permitted Z-corals to reside at greater depths at higher latitudes, as well as at more poleward localities due to higher insolation and SST in the LIG, as supported by habitability modelling results.

To avoid environmentally driven extinction, taxa need to be able to adapt to changing environments, either through distributional shifts (i.e. habitat tracking) or by altering their abiotic preferences (Greenstein and Pandolfi, 2008; Warren et al., 2013; Saupe et al., 2014). The thermal limits of organisms are widely acknowledged as shaping diversity gradients on geological time scales (e.g. Yasuhara et al., 2012; Sunday et al., 2012; Jablonski et al., 2013). Although the latitudinal habitability gradient remained fairly stable between the LIG and modern climatic regimes, we might expect to see a greater reshaping of the latitudinal habitability and biodiversity gradients under future scenarios. While Z-corals might be able to adapt over geological time intervals, it is unlikely that they will be able to keep pace with the rapid rate of climatic change predicted under RCP4.5 or RCP8.5 scenarios. Studies based solely on modern occurrences (Freeman et al., 2013; Hooidonk et al., 2014) propose a much more drastic decline in coral reefs under RCP4.5 and RCP8.5 scenarios than this study's results indicate for Z-corals. This is likely the consequence of differences in methodological approach, selection of environmental variables, AOGCMs and differences in training datasets for modelling. Perhaps of particular note is the lack of aragonite saturation state and cumulative thermal stress variables applied in this study, whereas bathymetry was not directly considered in others (e.g. Freeman et al., 2013). The inclusion of environmental variables such as aragonite saturation state would likely improve this study's model predictions; however, such data are not available for the geological record. With this in mind, model outputs are likely optimistic in the face of anthropogenic climate change, particularly for Z-corals in high latitude regions, as the aragonite saturation state is generally lower than at tropical latitudes (Jiang et al., 2015). In relation to other environmental variables, best practice requires the construction of generalized models when projecting to other time slices. An ENM focused on one spatial or temporal extent may perform very well with a large number

of explanatory variables. However, an ENM might also find causal relationships that are non-existent, resulting in over-fitting, hindering the applicability and any projections of the model under different spatial/temporal extents. Sensitivity analyses comparing modern projections from modern-trained ENMs with and without aragonite saturation state suggest little difference between predictions at global scale. However, some noticeable variations are observable at local scale (Appendix A: Figure A.1). Variable contribution analyses indicate aragonite saturation state is of secondary importance in the construction of global ENMs (Appendix A: Table A.1). However, under continued acidification of the world's oceans, aragonite saturation state may become more of a limiting factor for Z-corals than what is observed in the modern. Therefore, RCP4.5 and RCP8.5 projections should be considered as relatively optimistic in the face of continued CO_2 emissions. However, this is conditional on Z-corals being able to acclimatize to heightened temperatures or shift distributions to suitable temperature localities in the first place. Integrating palaeontological data into ENM promotes two clear advantages to aid model projections: (i) the opportunity to test models with empirical evidence across temporal windows and climate regimes and (ii) the ability to combine palaeontological and neontological data to consider the full ecological limits of a particular taxon, rather than just the occupied niche in its current biogeographic pattern.

Although the LIG fossil record is biased, the inclusion of fossil Z-coral data provides additional insight into the niche hypervolume and potential distribution of Z-corals under future climate change. As with previous studies (Lima-Ribeiro et al., 2017), predictions including fossil data suggest significantly more habitability at wider geographical ranges than those based solely on modern occurrences. ENM predictions which only include modern occurrences run the risk of modelling the occupied niche, whereas fossil occurrences can provide additional understanding into the fundamental niche of a species (Soberón and Nakamura, 2009; Peterson et al., 2011). Indeed, this particular study still might provide limited insights into the fundamental niche due to the incompleteness of the LIG Z-coral record. However, the inclusion of fossil

occurrences enables us to test which models perform best across temporal boundaries, as well as the importance of establishing the fundamental niche using true positive fraction. It is clear from ENM results that a multi-temporal approach improves predictive performance, providing support for projected habitat suitability under future climate scenarios.

3.5 Summary

The results from this study suggest that LIG Z-corals might have expanded their poleward ranges during the LIG, but that they did not experience an equatorial decline. Instead, the apparent equatorial decline appears to reflect an aspect of bias (i.e. absence of reported fossil collections/occurrences) that cannot currently be ameliorated by existing subsampling approaches. Findings are in agreement with the results from multiple modelling and palaeoclimatic studies, which suggest that annual mean SST and seasonal ranges at equatorial latitudes in the LIG were comparable to today (McCulloch and Esat, 2000; McKay et al., 2011; Hoffman et al., 2017). Under the future (2100 AD) climate scenarios RCP4.5 and RCP8.5, ENM results suggest a relatively large decrease in habitat suitability at equatorial latitudes, and an increase at higher latitudes, particularly within the Northern Hemisphere. However, these conclusions are likely somewhat optimistic in the face of anthropogenic climate change as they do not account for ocean acidification, destructive fishing practices or other anthropogenic environmental impacts, and yet they make alarming predictions. Finally, the fossil record provides additional insights into the niche hypervolume of Z-corals, and improves predictive performance. Consequently, the fossil record might improve biodiversity risk assessments under future climate change, and it should therefore play an important role in focusing conservation efforts.

–This page is intentionally left blank–

4 The impact of spatial sampling heterogeneity on reconstructing latitudinal biodiversity gradients in deep time

Disclosure: Some of the content reported in this chapter is in review at *Nature Ecology and Evolution*. While the primary author wrote most of this text, contribution by the co-authors of this study are contained in this chapter, as well as the input received from the peer review process. The relevant text, revised below, is from: Jones, L. A., Dean, C.D., Mannion, P.D. Farnsworth, A., Allison, P.A. (in review). Spatial sampling heterogeneity limits the detectability of deep time latitudinal biodiversity gradients. *Nature Ecology and Evolution*.

OVERVIEW

The latitudinal biodiversity gradient (LBG), in which species richness decreases from tropical to polar regions, is a pervasive pattern of the modern biosphere. However, fossil occurrence data suggest that this pattern has potentially varied in the geological past, with either flattened or bimodal gradients being proposed for some groups. Nevertheless, the reconstruction of palaeobiogeographic patterns is hampered by geological and anthropogenic biases. In particular, spatial sampling heterogeneity has the capacity to impact upon the reconstruction of latitudinal biodiversity gradients in deep time. Here, a simulation framework is used to test the detectability of three different types of latitudinal biodiversity gradient (flat, unimodal, and bimodal) over the last ~300 million years. To do so, biodiversity gradients were simulated on stage-level palaeogeographies, and sampled according to the global geographic sampling window of fossil collections for each respective stage. Results indicate that heterogeneity in spatial sampling significantly impacts upon the detectability of genuine LBGs, with known biodiversity patterns often indistinguishable after applying the spatial sampling window. Sampling-standardisation aids the reconstruction of relative richness ratios, but cannot account for artefactual absences introduced by geological and anthropogenic biases. These issues also have the potential to bias global estimates of past biodiversity, and obscure the recognition of extinction and radiation events. Previous studies might have failed to recover the 'true' LBG type because of incomplete sampling and the heterogeneous distribution of the available sedimentary record. Therefore, caution should be taken when reconstructing LBGs in deep time.

4.1 Introduction

The fossil record is a spatial and temporal archive of past biodiversity, evolution, extinction, and biological recovery through deep time. It also provides critical context for understanding the impact of climate change on global ecosystems, and offers potentially vital information for current conservation efforts (Barnosky et al., 2017; Turvey and Saupe, 2019). However, this archive is impacted by preservational and sampling biases that render it incomplete, and potentially shroud the true nature of evolutionary events (Raup, 1972; Allison and Briggs, 1993; Cherns and Wright, 2000; Bush and Bambach, 2004; Smith and McGowan, 2011; Benson et al., 2016). Despite a growing number of mitigating techniques (e.g. Close et al., 2018), understanding the degree to which these biases control our perception of spatial biodiversity patterns in deep time is still particularly challenging (Benson et al., 2016; Close et al., 2017). What questions can palaeobiologists truly ask of the fossil record given the quality of data? Is it possible to evaluate macroecological patterns throughout Earth's history (e.g. Powell, 2009; Mannion et al., 2012; Nicholson et al., 2016), or is there a limit to the grain of the questions that can be asked of a biased dataset?

The latitudinal biodiversity gradient (LBG), in which species richness decreases from tropical to polar regions, is one of the most recognisable global macroecological patterns today. Although the present-day LBG has been extensively documented and its causes debated for over two centuries (Willig et al., 2003; Hillebrand, 2004; Kinlock et al., 2018), it is only in recent decades that the LBG has been considered within a deep time context (Jablonski et al., 2006, 2017; Archibald et al., 2010; Mannion et al., 2014). Fossil occurrence data suggest that the 'modern-type' (unimodal) LBG is not a permanent feature of past ecosystems, with a range of taxonomic groups characterised by flattened or even bimodal gradients in deep time (e.g. Rose et al., 2011; Mannion et al., 2012; Yasuhara et al., 2012; Kiessling et al., 2012; Fraser et al., 2014; Powell et al., 2015; Marcot et al., 2016; Nicholson et al., 2016; Brocklehurst et al., 2017; Kröger, 2018; Allen et al., 2020). However, the extent to which these latitudinal patterns are the result of inherent biases (such as variable fossil preservation, stratigraphic

completeness and geographic sampling bias), as opposed to biological processes, remains uncertain (e.g. Raup, 1972; Allison and Briggs, 1993; Cherns and Wright, 2000; Johnson, 2003; Bush and Bambach, 2004; Smith and McGowan, 2011; Vilhena and Smith, 2013; Benson et al., 2016; Fraser, 2017).

Several methodologies have been developed to standardise sampling and mitigate problems associated with uneven 'raw' occurrence data (Sanders, 1968; Raup, 1975; Alroy, 2010a; Chao and Jost, 2012). These approaches have most commonly been applied to allow comparisons between temporal bins (Alroy, 2010a, 2010c, 2010b; Kiessling and Kocsis, 2015; Benson et al., 2016; Close et al., 2018; Dunne et al., 2018; De Celis et al., 2020). However, it is also recognised that spatial bias in sampling (e.g. preferential sampling in Europe and North America) also skews observed palaeobiogeographic patterns (Raup, 1972; Allison and Briggs, 1993; Cherns and Wright, 2000; Johnson, 2003; Bush and Bambach, 2004; Smith and McGowan, 2011; Benson et al., 2016; Close et al., 2017). Although sampling-standardisation approaches have been implemented between palaeolatitudinal bins in a small number of studies (e.g. Mannion et al., 2012; Kiessling et al., 2012; Nicholson et al., 2016; Allen et al., 2020), these methods do not explicitly address the spatiotemporal heterogeneity in sampled geographic area (Vilhena and Smith, 2013; Benson et al., 2016; Close et al., 2017). As inherently spatial patterns, estimations of LBGs in deep time have the capacity to be particularly impacted by this bias: variation in the geographic sampling universe (area sampled by palaeontologists) between different palaeolatitudinal bands can result in radically different sizes of underlying taxon pools (Vilhena and Smith, 2013; Close et al., 2017). Consequently, despite the critical information contained within the fossil record, it is possible that limited and heterogeneous spatial sampling has prevented the reconstruction of genuine LBGs in deep time.

Recent studies have implemented simulation-based approaches to test the impact of climate on biogeographic patterns in the geological past, circumventing the issues of sampling heterogeneity and data absence within the fossil record (e.g. Saupe et al., 2019c). Here, a similar framework is used to test the impact of spatial sampling bias

on deep time palaeobiogeographic patterns within shallow marine environments (0–200 m depth). Occurrence data conforming to three different types of LBG (flat, unimodal, and bimodal) were simulated for 56 stratigraphic stages, spanning the beginning of the Permian (Asselian) to the end of the Neogene (Piacenizan) (298.9–2.58 Ma). These data were then spatially filtered using the global palaeogeographic sampling window of fossil collections for each stage. Simulated and sampled latitudinal biodiversity curves were constructed using this filtered data, and were compared to explore the data lost between the 'known' and sampled fossil record. The utility of sampling-standardisation methods in reconstructing different types of LBGs, in the light of variable spatial sampling through time, was also evaluated. Finally, the palaeogeographic evolution of latitudinal sampling through time, and its impact on our understanding of the LBG in deep time is evaluated. The approach used here emulates how the true distribution of biodiversity might be masked by the 'known' spatial sampling window, and tests whether genuine LBGs can be reconstructed from the fossil record.

4.2 Materials and methods

4.2.1 Simulations

Life occurrence data were simulated to represent three different types of diversity gradients: (1) a LBG, with no specified peak in biodiversity (flat-type); (2) a tropical peak in biodiversity with a sharp decline towards the poles (unimodal-type, or 'modern-type'); and (3) temperate peaks in biodiversity that decline towards the poles and equator (bimodal-type) (Figure 4.1).

To generate realistic LBGs, the distribution of 1,000 species were simulated on stage-level palaeogeographies (1° x 1°), with weighted probability grids equating to each LBG-type to 'force' the occurrences to fit the elected LBG (Figure 4.2). This level of diversity is similar to what is observed in some extant groups today, such as zooxanthellate corals (Kiessling et al., 2012). LBGs were produced for each stratigraphic stage for the last ~300 million years (Asselian to Piacenzian), with

probability grids generated in the R package NLMR ver. 0.4.2 (Sciaini et al., 2018). Probability grids were used to define an initial point (source population) for each 'virtual' species (for example, this point would be more likely to be allocated in the tropics than the poles in a unimodal-type LBG). This initial point was subsequently used to construct a radial distance probability grid on which the occurrences of each species were generated, effectively simulating range size and species' distribution (Figure 4.2).

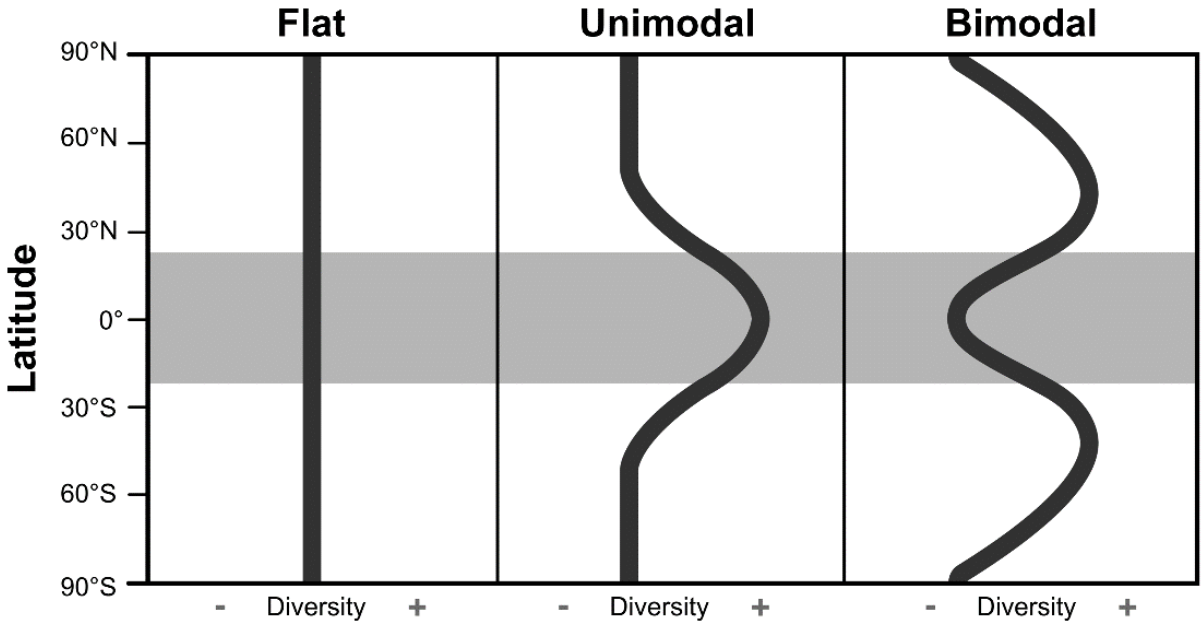


Figure 4.1. Graphical representation of the different types of latitudinal biodiversity gradients simulated in this study. A flat latitudinal biodiversity gradient has no prominent latitudinal peak in diversity; a unimodal gradient has a tropical peak in diversity, with taxonomic richness declining poleward; a bimodal gradient has twin temperate peaks in diversity, with taxonomic richness declining towards the equator and the poles. Grey shaded area illustrates the extent of the tropics today (23.4°N–23.4°S).

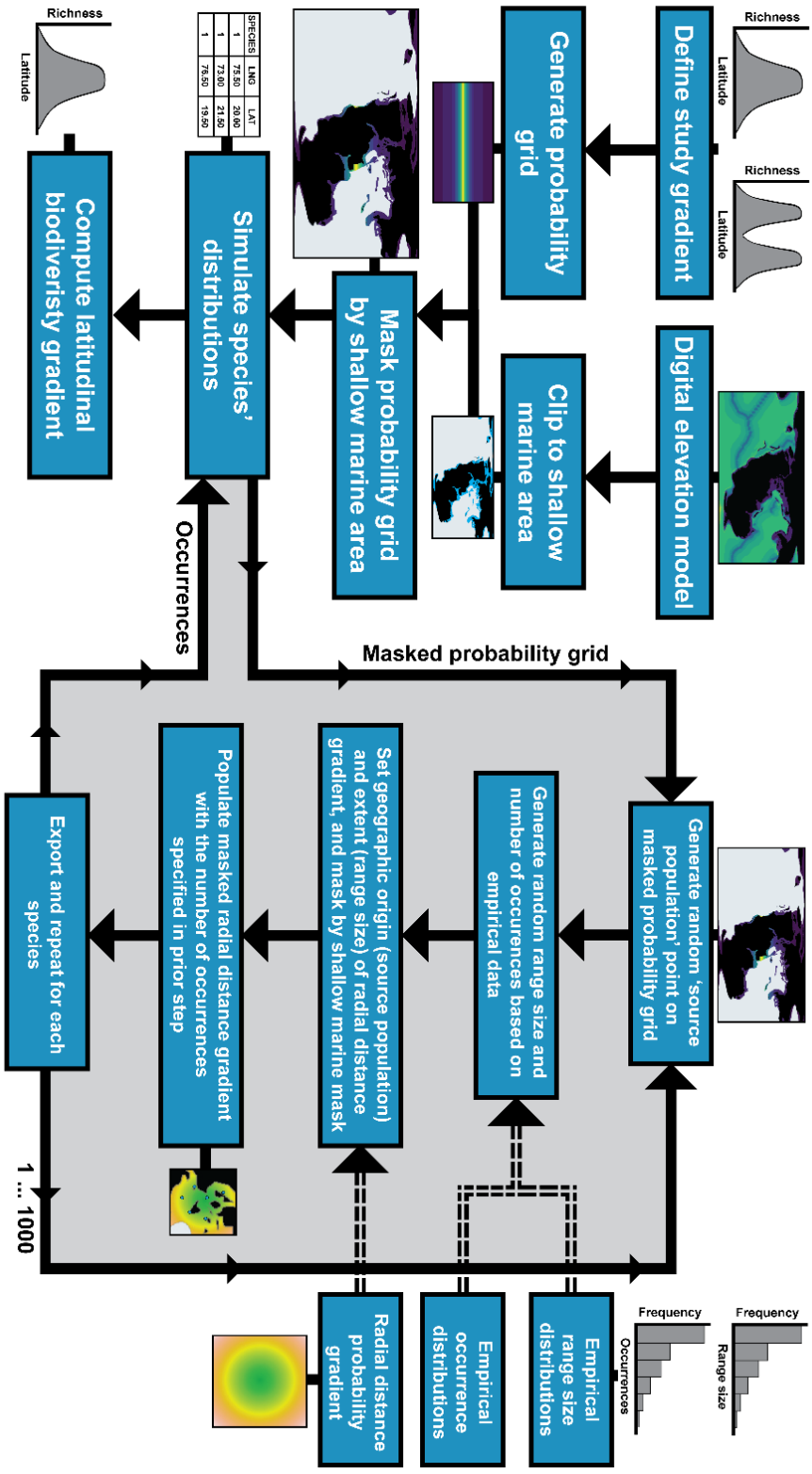


Figure 4.2. Diagram showing the simulation workflow of this study. Simulations are not intended to reconstruct genuine latitudinal biodiversity gradients in deep time. The purpose of these simulations is to emulate the distribution of biodiversity given three different types of gradient (flat, unimodal and bimodal). Diagram depicts only one simulation run. However, simulations were run 100 times for each latitudinal biodiversity gradient (= 3) and stratigraphic stage (= 56) (100 x 3 x 56 = 16,800 simulation runs). In this study, 1,000 species were generated for each simulation run. Shallow marine area was defined as 0–200 m depth in this study.

In order to produce realistic distributions of species, the empirical range size and occurrence frequency distributions of present-day species within five major marine invertebrate groups (anthozoans [= 'Anthozoa'], bivalves [= 'Bivalvia'], brachiopods [= 'Brachiopoda'], echinoids [= 'Echinoidea'], and sponges [= 'Porifera']) were assessed, based on data housed within the Ocean Biogeographic Information System (OBIS; https://www.obis.org/) (Figure 4.3–Figure 4.5). Using these data, the extent (range size) of the distance probability grid and the number of occurrences for each species (between 1 and 150) were randomly generated, following a geometric probability distribution (Figure 4.3–Figure 4.5). For simulations of 'virtual species', a broad ecological niche was opted for, constraining distributions to shallow marine environments. Therefore, probability grids were clipped prior to point generation to include only shallow marine area (≤ 200 m depth, approximating the photic zone), using digital elevation models (DEMs) provided by Getech PLC (Figure 4.2). These DEMs provide global gridded data (0.1° x 0.1°) on topography and bathymetry at stratigraphic stage level (Markwick and Valdes, 2004; Markwick, 2019). For this analysis, DEMs were aggregated to a spatial resolution of 1° x 1°, retaining the minimum depth within each cell, and hence shallow marine environments. The entire simulation procedure was repeated 100 times to get an average representation of each LBG-type for every stratigraphic stage (Figure 4.2). Kolmogorov–Smirnov two-sample tests were used to assess the similarity of simulated species' geographic range sizes and occurrence frequency distributions to those of empirical groups (anthozoans, bivalves, brachiopods, echinoids, and sponges). This was done to test the validity of simulated occurrences, and frame subsequent analyses. These tests indicate both statistically significant ($P < 0.05$) and insignificant ($P > 0.05$) differences depending on the pair-wise combination of simulated and empirical groups (Appendix B: Table B.1–Table B.2). However, similar results were found for tests between empirical groups.

Finally, although simulations are set up to emulate different LBG-types, the steepness of these gradients is also reliant on the distribution of available shallow marine area for populating with occurrences, producing more realistic distributions for each time

interval (i.e. species-area relationship (MacArthur and Wilson, 1967; Rosenzweig, 1995; Whittaker and Fernández-Palacios, 2007)). For example, if a latitudinal band has twice as many cells as another latitudinal band, but the cells between bands have the same weighted probability, the former is likely to be much more diverse than the latter. All analyses were performed in R ver. 3.6.2 (R Core Team, 2019).

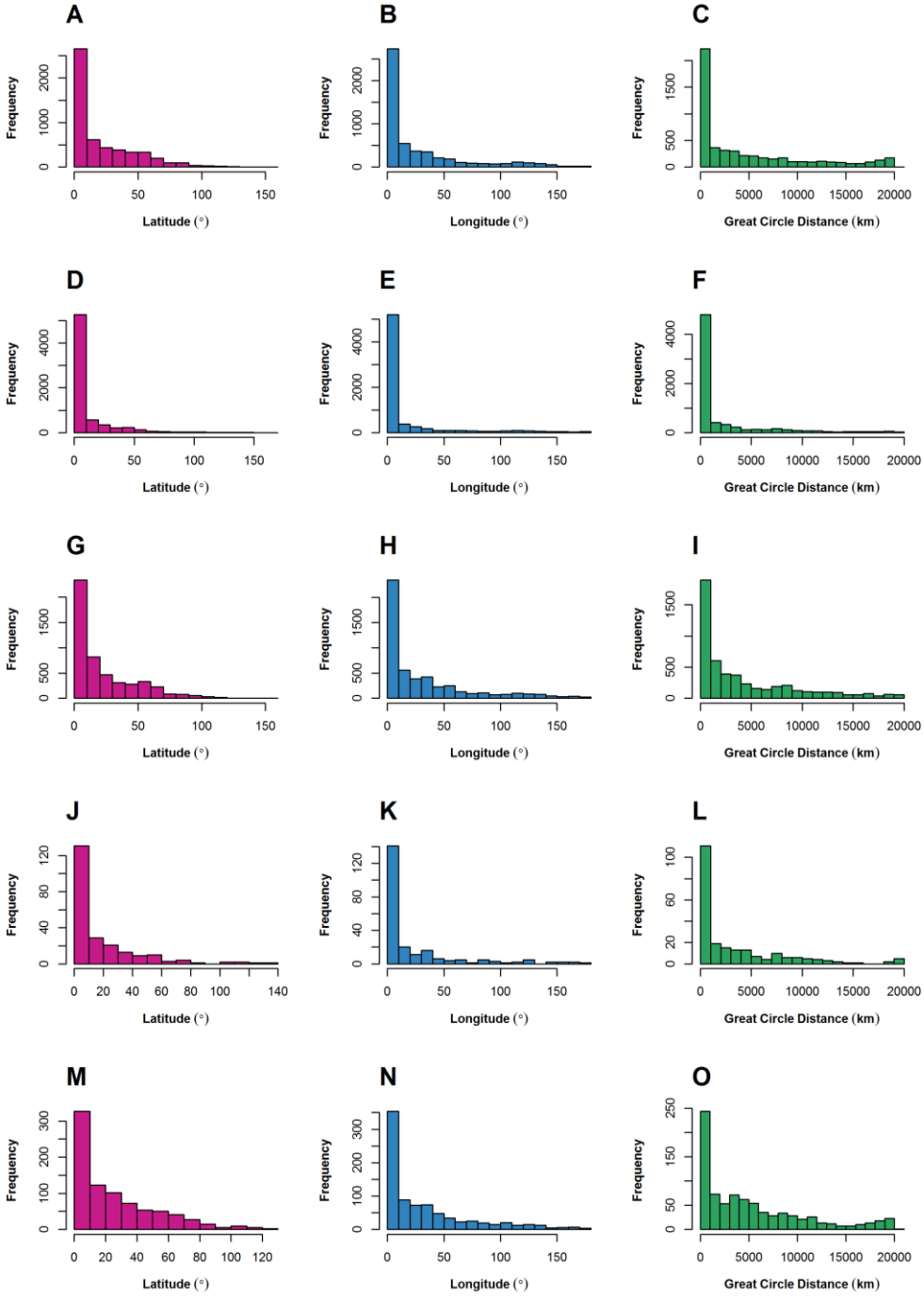


Figure 4.3. Range size frequency distributions of species within the marine invertebrate groups: Anthozoa (A, B, C); Porifera (D, E, F); Bivalvia (G, H, I); Brachiopoda (J, K, L); and Echinoidea (M, N, O). (A, D, G, J, M) Latitude; (B, E, H, K, N) longitude; (C, F, I, L, O) Great Circle Distance.

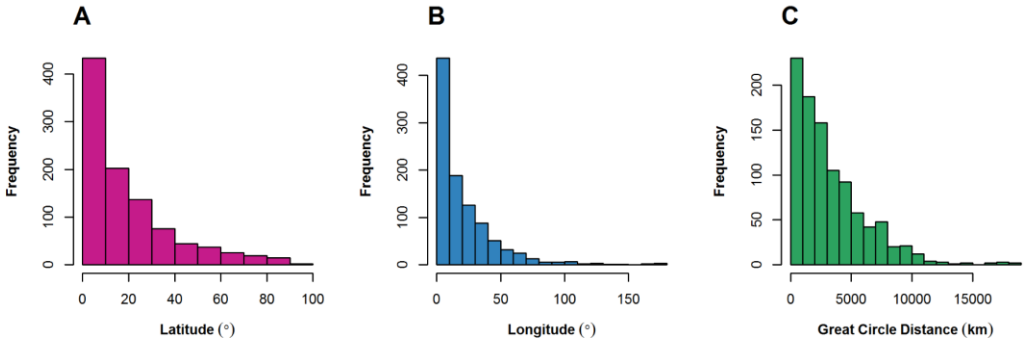


Figure 4.4. Example of range size frequency distributions from a unimodal-type latitudinal biodiversity gradient simulation. (A) Latitude; (B) longitude; (C) Great Circle Distance.

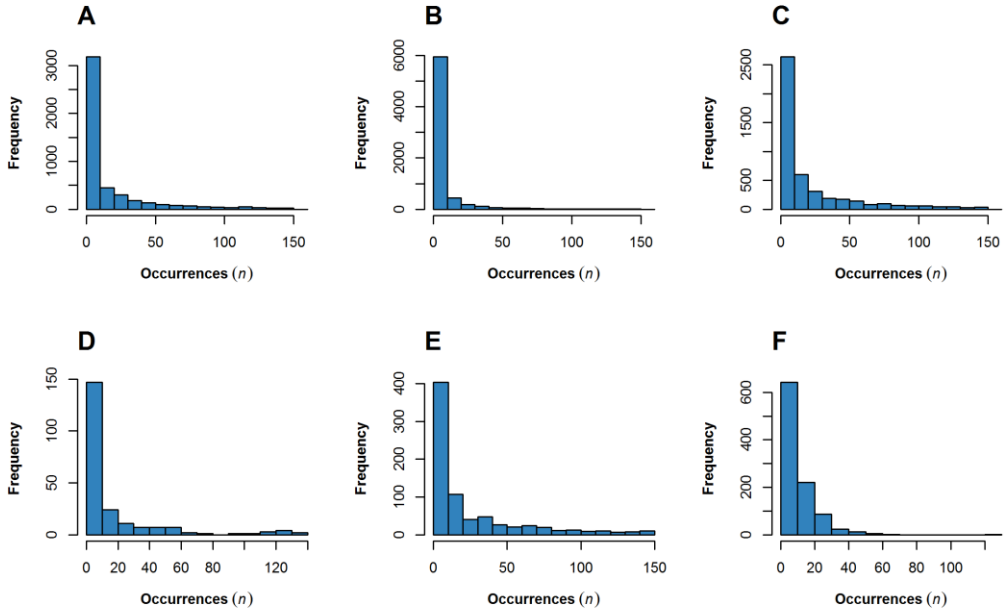


Figure 4.5. Occurrence frequency distributions for the five major marine invertebrate groups (A–E) with a maximum bin size of 150 occurrences for comparison with simulated distributions. (A) Anthozoa; (B) Bivalvia; (C) Brachiopoda; (D) Echinoidea; (E) Porifera; and (F) simulated. (F) Occurrence frequency distribution example for a unimodal-type latitudinal biodiversity gradient simulation.

4.2.2 Spatial sampling coverage

Biogeographic patterns recovered from the fossil record are heavily dependent on available sampling area, which is intrinsically linked to sedimentary rock outcrop (Raup, 1972, 1976b, 1976a; Sheehan, 1977; Peters and Foote, 2001; Wall et al., 2009; Vilhena and Smith, 2013). To test how spatial sampling availability potentially influences our understanding of the LBG through time, simulated occurrence data were filtered using the palaeogeographic sampling window of fossil collections for each stratigraphic stage. This enabled estimation of what the 'known' simulated LBG would

look like when restricted to available sampled area, and demonstrate how observed biogeographic patterns from the fossil record might deviate from their actual state. Whilst this approach ignores the potential impact of differences in preservation between sites, true sampling rates are enigmatic for the fossil record (Foote and Raup, 1996; Kidwell and Flessa, 1996; Kidwell and Holland, 2002; Fraser, 2017). Sampling all occurrences within sampled cells prevented confounding the interpretation of this study's results, and enabled focus upon the impact of spatial sampling bias. However, it should also be noted that this presents the 'best-case' scenario for preservation, and simulation results should be considered within this context. To generate per-stage sampling windows, all available Asselian–Piacenzian fossil collection data were downloaded from the Paleobiology Database (PBDB; www.paleobiodb.org) on the 17th January 2020, yielding 139,831 fossil collections. Using the palaeo-coordinates (rotated from modern coordinates via GPlates (https://www.gplates.org/) (Wright et al., 2013)) of collections, global stage-level 1° x 1° grids were produced. These grids represent sampled area at the same extent of the DEMs, with a grid cell deemed to have been sampled if at least one collection appeared within it. Subsequently, sampled grids were filtered to include only cells falling within shallow marine area grids (i.e. excluding terrestrial sampled cells, and marine sampled cells inferred to be deeper than 200 m). Although these data are only a proxy for available outcrop area and are therefore likely incomplete in terms of representing all known and sampled outcrop, the data within the PBDB are extremely rich and have been the foundation of numerous palaeobiogeographic studies over the past two decades. They therefore represent a meaningful approximation of the known fossil record.

For the purpose of this study, a new metric was established to assess whether sampled area controls biodiversity estimates between stages and palaeolatitudinal bins: Spatial Sampling Coverage (SSC). Here, SSC is defined as the percentage of sampled cells within a chosen set of available cells, where the latter refers to the total number of cells within shallow marine grids, and sampled cells refers to cells containing collections. This metric is comparable to the traditional 'occupancy' metric used in

ecology and palaeontology (e.g. Kunin, 1998; Foote et al., 2007). However, SSC is distinguished from occupancy as the latter is reserved for describing biological patterns, and this study's focus is on sampling. For the SSC metric, it should be kept in mind that available cells do not reflect the total sampling opportunities available to collectors; sampled cells are a subset of preserved outcrop, which is itself a subset of total available cells. Whilst SSC values are influenced by the resolution of the study (e.g. the percentage of sampled cells relative to available cells will generally be lower at higher resolutions), this issue was avoided by keeping the resolution of this study constant. SSC was calculated for each stage at both a global scale, and within 15° palaeolatitudinal bins for comparison with biodiversity estimates. In addition, the palaeolatitudinal skewness of SSC was calculated for each stratigraphic stage, using the skewness() function from the R package 'e1071' ver. 1.7–3 (Dimitriadou et al., 2008). As a general rule of thumb, skewness is typically considered high if the value is less than -1 or greater than 1, moderate when between -1 and -0.5 or 0.5 and 1, and approximately symmetrical when between -0.5 and 0.5 (Hair Jr et al., 2016). Using these data, the coefficient of determination (R^2) between time and skewness was calculated to determine whether there was a long-term temporal shift in the skewness of palaeolatitudinal SSC. To examine whether the spatial sampling window evolved in the study period, the geographic and palaeogeographic centroids of PBDB collections contained within shallow marine mask was calculated (≤ 200 m depth).

4.2.3 Latitudinal biodiversity gradient analyses

To test the extent to which relative latitudinal biodiversity patterns can be recovered from degraded samples, the mean richness for simulated, sampled (via sampling window), and sampling-standardised LBGs for each simulation was calculated. All LBGs were computed within 15° latitudinal bins, a common bin size used in deep time studies (e.g. Nicholson et al., 2016; Kröger, 2018). As this study was principally focused on the relative shape of LBGs, all (simulated, sampled, and sampling-standardised) LBGs were normalised within their respective stages on a scale from 0 to 1, providing proportional latitudinal richness curves. This was achieved by dividing the richness of

each latitudinal bin by the total richness for latitudinal bins within each respective stage. All subsequent latitudinal analyses were conducted using these proportional richness curves.

For sampling-standardisation, classical rarefaction (by-occurrence subsampling) was applied to the sampled occurrence data to account for large differences in sampling between palaeolatitudinal bins (Raup, 1975; Close et al., 2018). The number of occurrences drawn from each latitudinal bin and stage were kept at 50 occurrences, a similar threshold to fossil palaeolatitudinal biodiversity studies (Mannion et al., 2012; Kiessling et al., 2012). Subsampling was implemented with 1,000 bootstrap replicates for each LBG simulation replication/type (100 x 3), with the mean biodiversity recorded for each latitudinal bin. The mean of means for each LBG-type, and stage were then calculated. Coverage-based rarefaction was purposely not used as it is typically implemented with sampling units (e.g. collections and formations) (Alroy, 2010c; Mannion et al., 2015; Cleary et al., 2018; De Celis et al., 2020). Whilst simulating sampling units for occurrence data would not be impossible, the underlying structure of collections and formations is complex (Plotnick, 2017). In addition, collections themselves are not standardised and may be influenced by anthropogenic (e.g. variable sampling effort and intensity) and/or geological (e.g. variable fossil preservation and outcrop accessibility) factors. As this study was principally focused on the influence of spatial sampling, simulations were intentionally kept simple. For each LBG-type, the sampled global richness (total number of virtual species sampled per stage) was also calculated to assess whether variation in the 'known' spatial sampling window impacted upon sampled global biodiversity for different types of LBGs. This was examined by calculating the coefficient of determination (R^2) between global sampled richness and global SSC for each LBG type.

To quantify the similarity between simulated LBGs and their sampled/sampling-standardised counterparts, the difference between all pair-wise combinations of latitudinal bins (e.g. simulated 15–30°N with sampled 15–30°N) was computed for each stage (Figure 4.6). To examine temporal shifts in the difference between simulated and

sampled/sampling-standardised LBGs, the difference from all pair-wise combinations of latitudinal bins for each stage were totalled (Figure 4.6). For the purpose of this study, this metric is referred to as the sum of proportional latitudinal richness differences (SLD) (Figure 4.6). The SLD for pair-wise combinations of simulated unimodal- and bimodal-type LBGs, as well as sampled/sampling-standardised LBGs was also calculated to quantify the difference between types of LBG. SLD scores for proportional LBGs can range between 0 and 2, with 0 representing no difference between pair-wise combinations of curves, and 2 indicating maximum possible difference. However, as different types of LBG might have inherent overlap due to the distribution of simulated biodiversity, comparisons of simulated unimodal- and bimodal-type LBGs provide a null expectation of the difference between LBG-types, against which sampled and sampling-standardised LBGs can be evaluated. Whilst Fréchet distances (Alt and Godau, 1995) have been used in previous studies to compare similarity between LBGs (Saupe et al., 2019c), it does not explicitly measure the total difference between all latitudinal bins, and therefore is not implemented in this study.

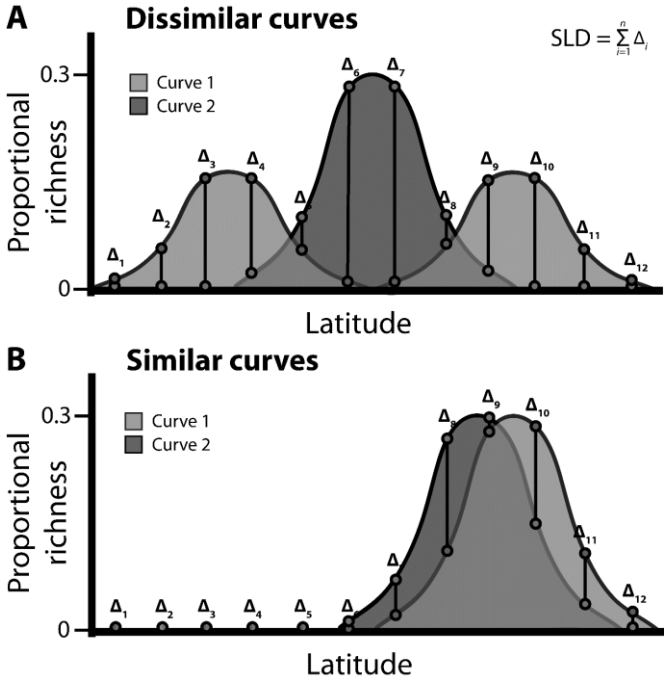


Figure 4.6. Diagram depicting how the sum of proportional latitudinal richness differences (SLD) are calculated. SLD provides a measure of curve similarity, in which high SLD represents low similarity (A), and low SLD represents high similarity (B). Equation for SLD is provided in top-right corner of figure. Delta (Δ) represents the difference between the proportional richness of paired latitudinal bins for the two curves (e.g. curve 1: 15–30°N and curve 2: 15–30°N).

To evaluate how simulated LBGs changed after applying the spatial sampling window and sampling-standardisation techniques, the slope of each simulated, sampled, and sampling-standardised LBG was determined. This approach is in accordance with previous studies (e.g. Marcot et al., 2016), and provides insight into how the overall gradient varies between curves. To estimate the slope, latitudinal bins were split into Northern and Southern Hemispheres, and proportional latitudinal richness was regressed on the midpoint latitudes of latitudinal bins. To ensure a fair estimation of the slope, only hemispheres with three or more latitudinal bins with richness values had their slope computed.

To test statistically whether different types of LBG can be identified from the fossil record, Wilcoxon signed-rank tests were applied to determine whether there was a significant ($a = 0.05$) difference between pair-wise combinations of: (1) LBG types before and after sampling/sampling-standardisation (e.g. sampled unimodal-type and sampled bimodal-type) to establish whether sampling/sampling-standardisation influences the ability to distinguish between LBG variants; (2) simulated and sampled LBGs (e.g. simulated unimodal-type and sampled unimodal-type) to evaluate whether the original known biodiversity signal is retained after sampling; (3) simulated and sampling-standardised LBGs (e.g. simulated bimodal-type and sampling-standardised bimodal-type) to evaluate whether sampling-standardisation improves (via increased differences) the capacity to reconstruct genuine LBGs. To compare results across time and space, latitudinal bins from all stages were pooled for Wilcoxon signed-rank tests. This ensured an appropriate sample size for analyses, and enabled high confidence in results.

To provide insight into the impact of heterogeneous SSC, the Pearson product-moment correlation coefficient and coefficient of determination (R^2) between the SLD, and the skewness of palaeolatitudinal SSC was calculated for pair-wise combinations of: (1) simulated and respective sampled LBGs; and (2) simulated and respective sampling-standardised LBGs. As SLD has the potential to be severely impacted by data absence, correlation tests were carried out between SLD and the total number of

palaeolatitudinal bins without sampling (i.e. 0% SSC) for the aforementioned pair-wise combinations. Specifically, these tests determine whether the skewness in palaeolatitudinal sampling and/or data absence increases the difference between simulated and respective sampled/sampling-standardised LBGs, and hence their detectability.

4.3 Results

4.3.1 Spatial sampling coverage

Analyses of fossil occurrence collections (in their palaeorotated coordinates) from the PBDB indicate that Spatial Sampling Coverage (SSC; the percentage of sampled shallow marine cells) is heterogeneous through both time and space. Global SSC does not exceed 4% for any stage (max: 3.36% in the Albian), with a mean global SSC of 1.49% (± 0.74%, 1 standard deviation [1SD]) across all 56 geological stages (Table 4.1). SSC shows further heterogeneity spatially; whereas mean palaeolatitudinal SSC is 1.40% (± 1.48%, 1SD), that of 30–45°N is high, at 5.61% across all geological stages (Table 4.1). All other palaeolatitudinal bins have an average SSC lower than 3%, indicating unevenness in palaeolatitudinal sampling (Table 4.1). However, there is also temporal variability within palaeolatitudinal bins (Figure 4.7). For example, for palaeolatitudinal bin 30–45°N, the Barremian has a SSC of 2.78%, whereas the subsequent stage (Aptian) has a value of 10.40% (Figure 4.7). Analyses of the skewness in palaeolatitudinal SSC further highlights the unevenness between palaeolatitudinal bins, with a mean score of 1.41 (± 0.53, 1SD), suggesting the distribution of data is highly skewed, with the mean significantly higher than the median (Figure 4.8). Linear regression modelling shows a significant long-term shift in the skewness of palaeolatitudinal SSC ($R^2 = 0.349$, $P < 0.001$) from the Asselian to Piacenzian (Figure 4.8). In addition to the skewness of palaeolatitudinal SSC, results indicate that 30.21% of palaeolatitudinal bins lack any SSC.

Table 4.1. The mean and standard deviation (SD) of spatial sampling coverage (SSC) within palaeolatitudinal bins, for stratigraphic stages from Asselian to Piacenzian (298.9–2.58 Ma).

Maximum (°)	Minimum (°)	Hemisphere	Mean SSC (%)	SD SSC (%)
90	75	N	0.09	0.20
75	60	N	0.29	0.45
60	45	N	1.52	1.78
45	30	N	5.61	3.28
30	15	N	2.75	1.88
15	0	N	1.58	1.29
0	-15	S	1.83	2.06
-15	-30	S	0.82	1.19
-30	-45	S	1.07	1.70
-45	-60	S	0.62	1.10
-60	-75	S	0.44	0.79
-75	-90	S	0.18	0.58

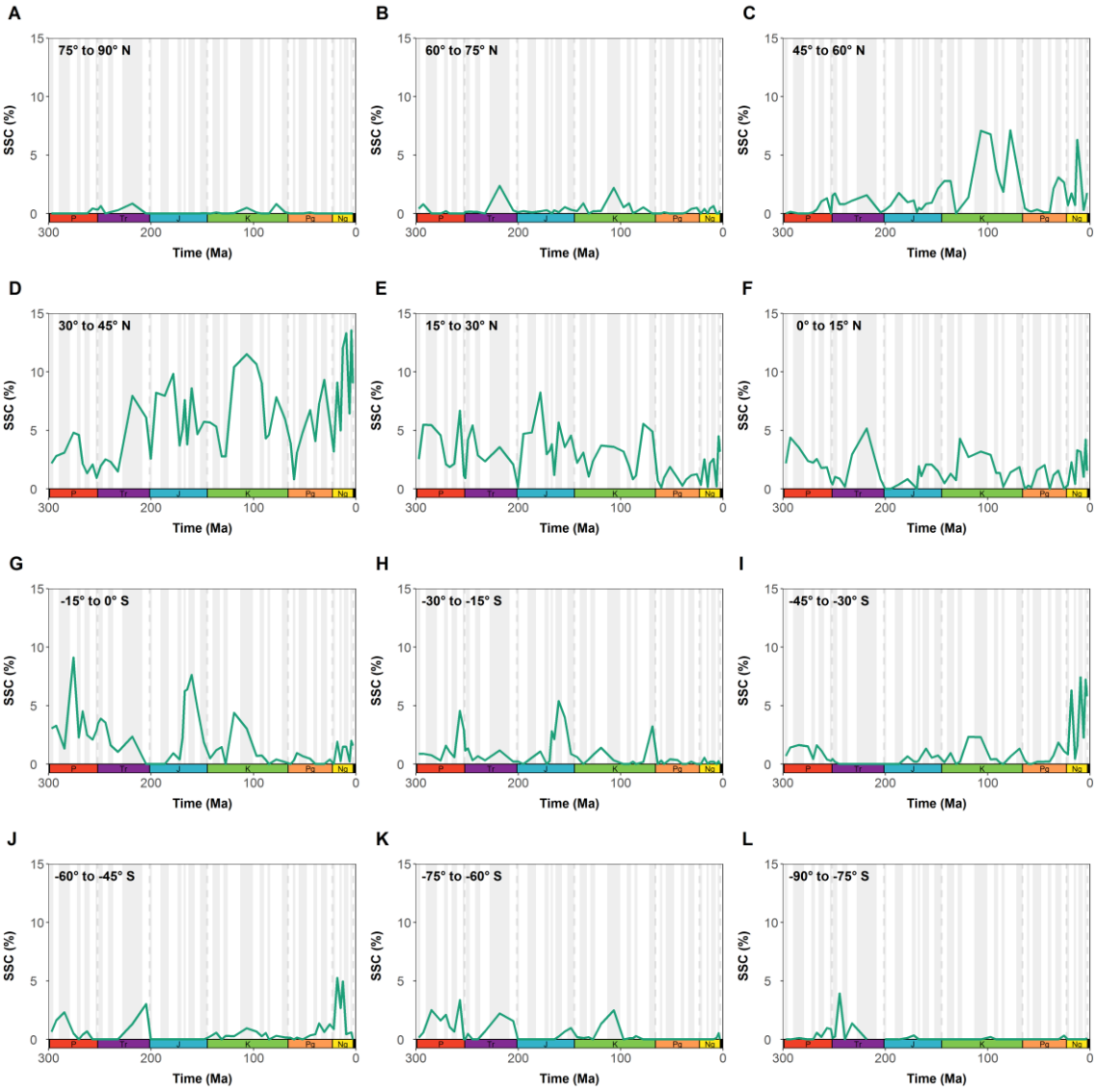


Figure 4.7. A palaeolatitudinal plot (15° bins) of spatial sampling coverage (SSC) for all stratigraphic stages from Asselian to Piacenzian. Text within plot indicates the respective palaeolatitudinal bin.

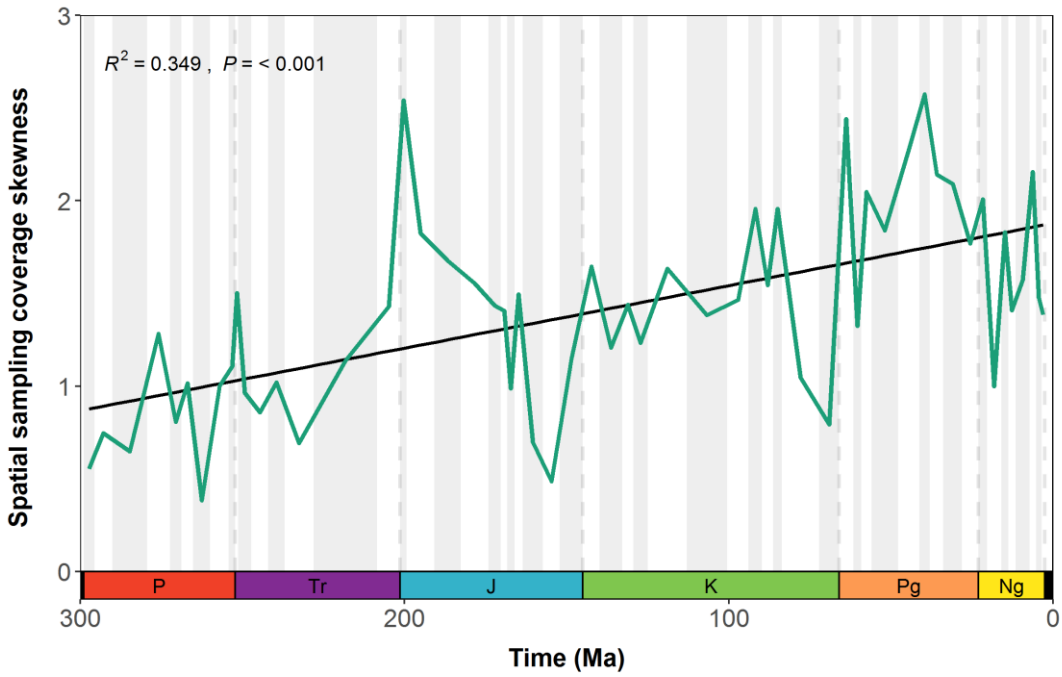


Figure 4.8. Palaeolatitudinal skewness of spatial sampling coverage from the Asselian to Piacenzian. Coefficient of determination (R^2) between time and skewness indicates a significant long-term increase in the skewness of palaeolatitudinal spatial sampling coverage.

Computation of the absolute palaeolatitudinal centroid of inferred shallow marine collections (collections within shallow marine masks) confirms a long-term shift in sampling from tropical palaeolatitudes in the late Permian–Middle Triassic, to temperate palaeolatitudes for most of the Jurassic, Cretaceous, and Paleogene (Figure 4.9). The mean of absolute palaeolatitudinal centroids is more equatorward (mean: 32.72°; 1SD: 6.67°) than that of the absolute latitudinal centroid of present-day coordinates (mean: 41.32°; 1SD: 5.56°), though still temperate.

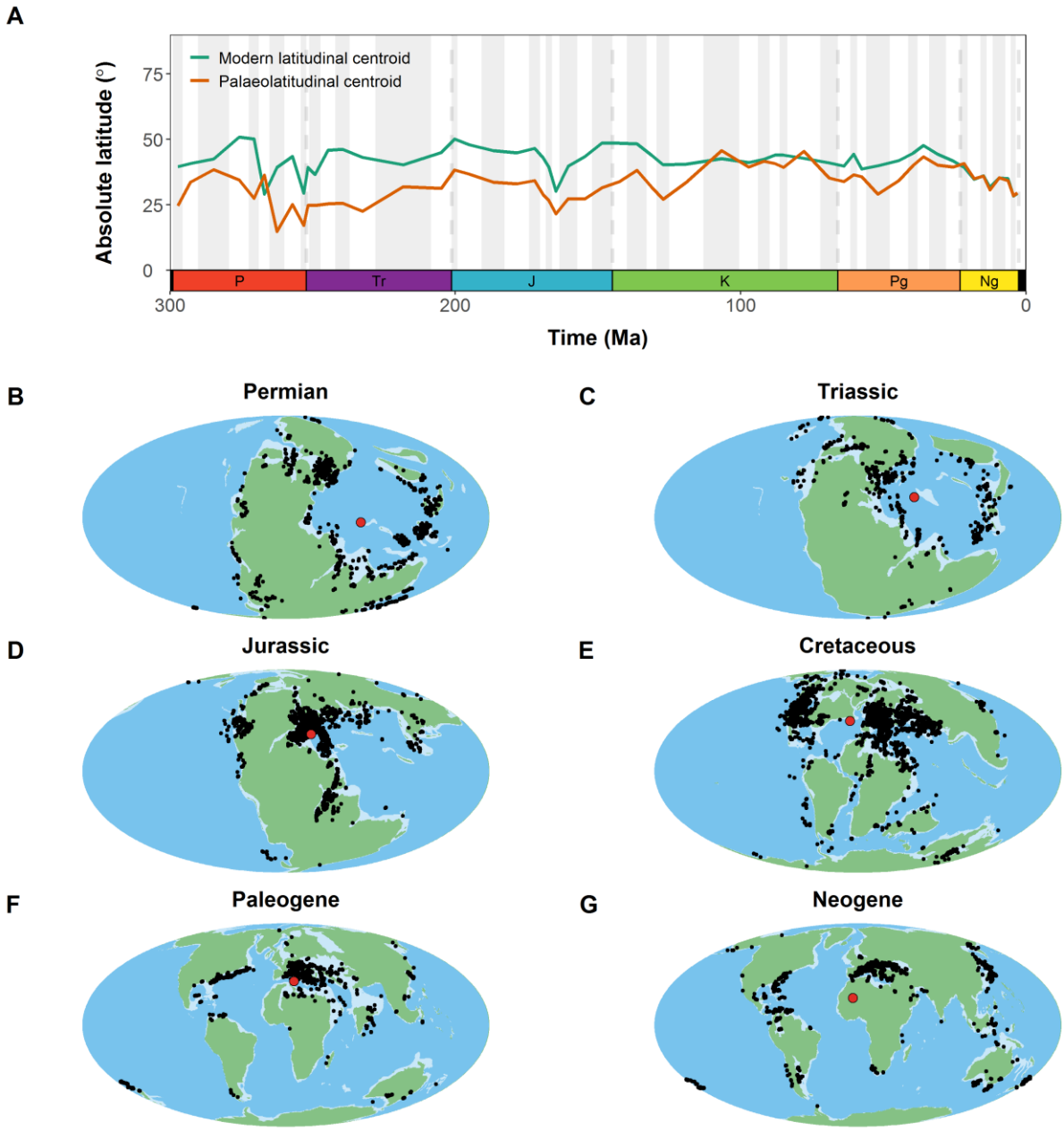


Figure 4.9. Palaeogeographic distribution of fossil collections housed in the Paleobiology Database. (A) Absolute latitudinal (green line) and palaeolatitudinal (orange line) centroids of inferred shallow marine collections, within their respective stratigraphic stages. (B–G) Global palaeogeographic reconstructions showing the distribution of inferred shallow marine collections (black circles) in the (B) Permian (298.9–251.9 Ma); (C) Triassic (251.9–201.3 Ma); (D) Jurassic (201.3–145 Ma); (E) Cretaceous (145–66 Ma); (F) Paleogene (66–23.03 Ma; and (G) Neogene (23.03–2.58 Ma). (B–G) Red circles indicate the palaeogeographic centroid of collections within their respective period. Palaeogeographic reconstructions are based on digital elevation models from Getech PLC.

4.3.2 Simulated latitudinal biodiversity gradients

Latitudinal biodiversity gradients (LBGs) were simulated for flat-, unimodal- and bimodal-types of gradient (Figure 4.10). However, as simulated LBGs are partially a function of shallow marine area, there is an expected natural variability in the shape of the gradient, emulating the species-area relationship. For example, a unimodal-type LBG for the Asselian (298.9–295.5 Ma) has a mean species richness of 469.94 at 0–15°N, and 213.11 at 30–45°N. Conversely, a unimodal-type LBG for the Albian (113–100.5 Ma), has a mean species richness of 598.49 at 0–15°N, and 300.42 at 30–45°N. This variability can be observed at broad-scale for all LBG-types within Figure 4.10 (individual stage-level plots are available in Appendix B).

Simulated flat-type LBGs, which are solely a product of available shallow marine area, demonstrate a long-term shift in the shape of the LBG. During the early Permian, simulated latitudinal richness peaked in temperate regions in both hemispheres, forming a bimodal-type LBG (Figure 4.10). However, by the Early Triassic relatively flat LBGs are simulated due to the increase in available shallow marine area in tropical regions. Further shifts in the shape of the simulated flat-type LBG occur across the Triassic/Jurassic boundary, with a single peak in richness at 30–45°N (Figure 4.10). During much of the Jurassic–Paleogene (201.3–23.03 Ma), species richness is concentrated in the Northern Hemisphere, particularly at tropical-temperate latitudes (15–45°N). However, during the early Miocene (23.03–15.97 Ma), the simulated flat-type LBGs become significantly flatter, and by the Messinian (7.25 Ma), steep unimodal-type LBGs are beginning to form (Figure 4.10). These shifts broadly reflect the relative steepness/shape of the simulated unimodal-type and bimodal-type LBGs in their respective stages (Figure 4.10; individual stage-level plots are available in Appendix B).

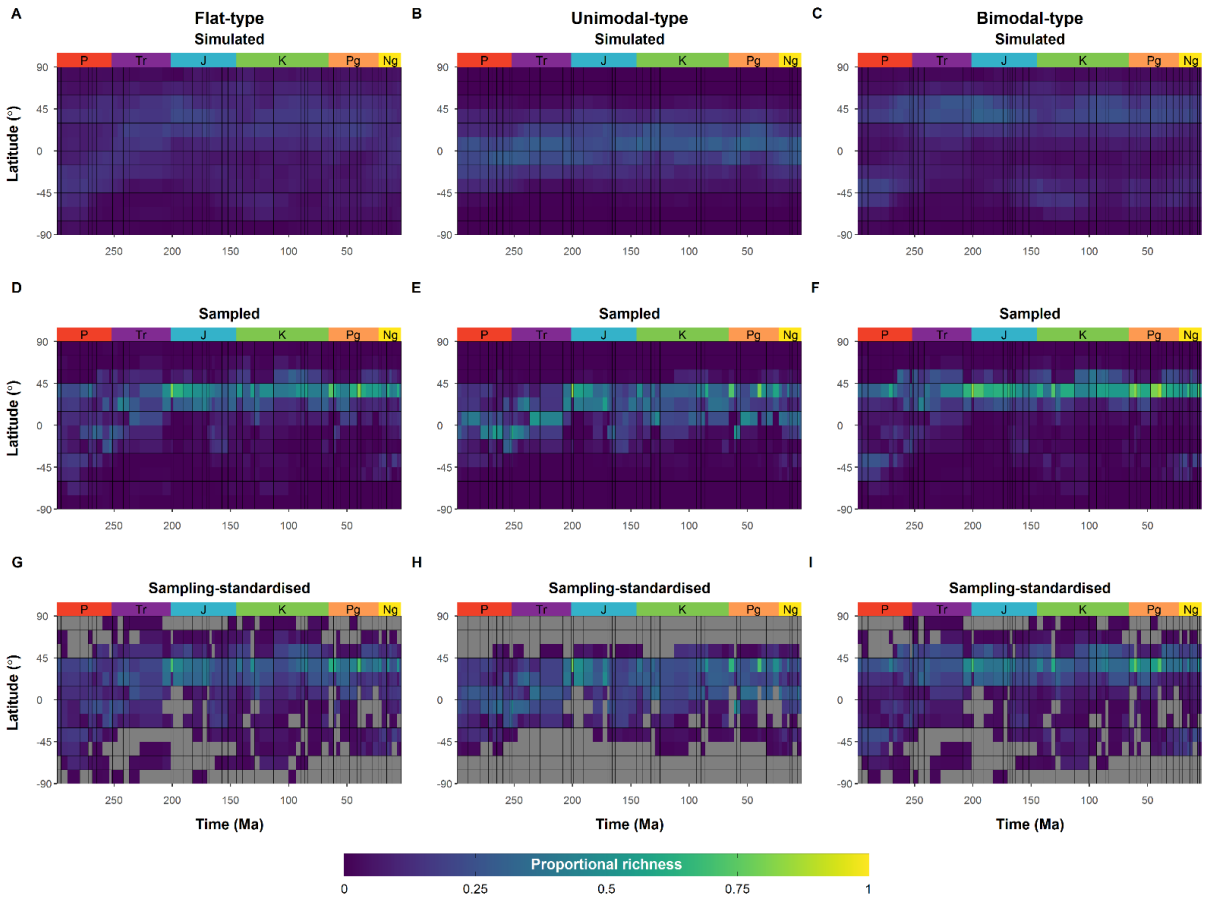


Figure 4.10. Heat maps of mean simulated (A–C), sampled (D–F), and sampling-standardised (classical rarefaction) (G–I) richness from the Asselian (298.9 Ma) to Piacenzian (2.58 Ma) at stage-level, and within 15° latitudinal bins. Latitudinal richness values within each stage (A–I) represent their proportional richness (latitudinal bin richness divided by total richness across latitudinal bins). Grey tiles (G–I) illustrate latitudinal bins with insufficient data to compute rarefied richness. For each type of latitudinal biodiversity gradient, simulated richness values (A–C) are based on the average bin value from the 100 replications. Sampled richness values (D–F) are based on the average bin value from the 100 sampled replications. Rarefied latitudinal richness estimates (G–I) are based on the mean of means of the 1,000 bootstrap replicates for each replication of latitudinal biodiversity gradient simulations (= 100).

4.3.3 Sampled latitudinal biodiversity gradients

The proportional latitudinal richness of all sampled LBGs is shown in Figure 4.10. Broad changes in the distribution of relative biodiversity between simulated LBGs and their sampled counterparts can be observed in Figure 4.11. Wilcoxon signed-rank test results indicate a statistically significant difference ($P < 0.05$) between simulated unimodal- and bimodal-type LBGs, indicating that these data are drawn from different populations. However, no statistically significant ($P = 0.379$) difference was found between sampled unimodal- and bimodal-type LBGs. Additionally, a statistically

significant difference ($P < 0.001$) was found between pair-wise combinations of simulated richness (within latitudinal bins), and respective sampled counterparts, for all LBG-types (flat, unimodal and bimodal). This suggests sampled LBGs are not representative of the 'true' simulated latitudinal distribution of biodiversity.

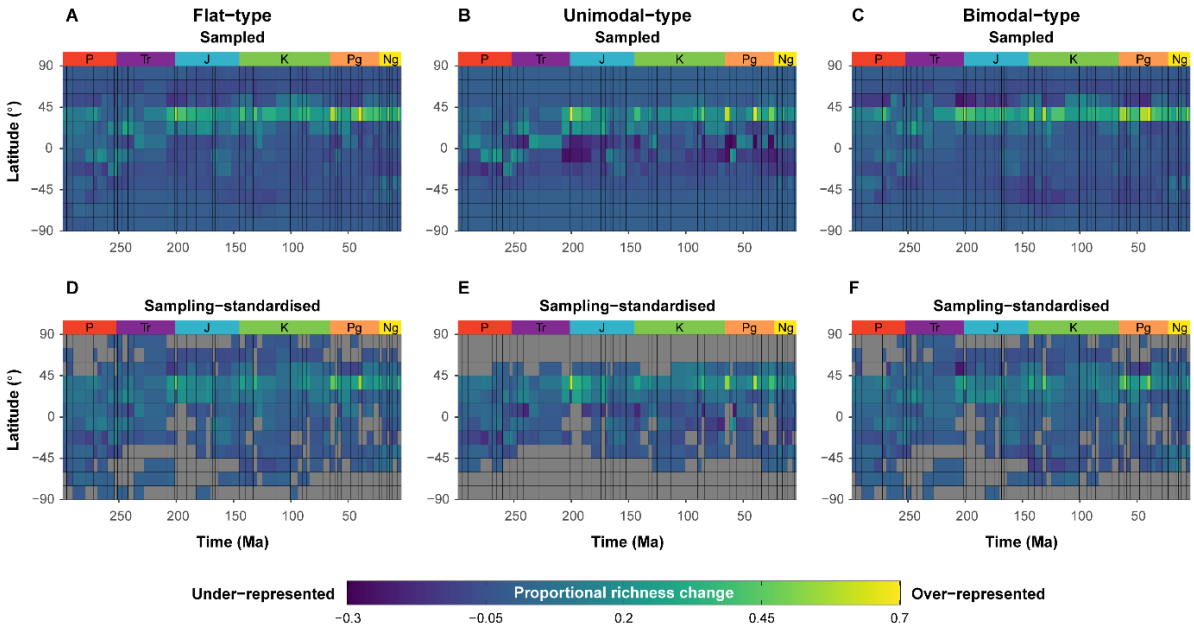


Figure 4.11. Heat maps of the change in proportional latitudinal richness between simulated and sampled/sampling-standardised latitudinal biodiversity gradients. Heat maps range from the Asselian (298.9 Ma) to Piacenzian (2.58 Ma) at stage level, and show data within 15° latitudinal bins. (A–C) Proportional richness change between mean simulated and sampled richness; (D–F) proportional richness change between mean simulated and sampling-standardised richness. For each type of latitudinal biodiversity gradient, simulated richness values were based on the mean bin value from the 100 simulation replications. Sampling-standardised latitudinal richness estimates (D–F) are based on the mean of means of the 1,000 bootstrap replicates for each replication of latitudinal biodiversity gradient simulations (= 100). Proportional latitudinal richness values were calculated by dividing each latitudinal bin by the total of all latitudinal bins within each stage. Richness change was calculated by subtracting proportional simulated latitudinal biodiversity gradients from sampled/sampling-standardised counterparts. Grey tiles illustrate latitudinal bins with insufficient data to compute sampling-standardised (classical rarefaction) richness estimates.

The sum of proportional latitudinal richness differences (SLD) between simulated unimodal- and bimodal-type LBGs remains fairly constant through time (Figure 4.12), with a mean difference of 0.993 (± 0.055, 1SD) along the entire time series. However, the mean difference is reduced to 0.833 (± 0.232, 1SD) for sampled unimodal- and bimodal-type LBGs, indicating increased similarity between curves after filtering by the spatial sampling window of fossil collections. Notably, the difference between unimodal- and bimodal-type LBGs is substantially lowered for numerous stages after

sampling (indicating increased similarity between LBGs); for example, the difference between Bartonian LBGs is reduced from 0.997 to 0.198 (Figure 4.12), and the resulting sampled LBGs appear virtually identical, regardless of the underlying simulated distribution of biodiversity (stage-level plots are available in Appendix B). This is particularly evident in the following stages: Hettangian–Pliensbachian, Santonian, Danian, Bartonian, and Chattian (Figure 4.12). Conversely, the SLD between sampled unimodal- and bimodal-type LBGs is comparatively high for most of the Permian and Triassic (Figure 4.12), with distinct LBGs recognisable for each simulated LBG type (Figure 4.10; stage-level plots are available in Appendix B).

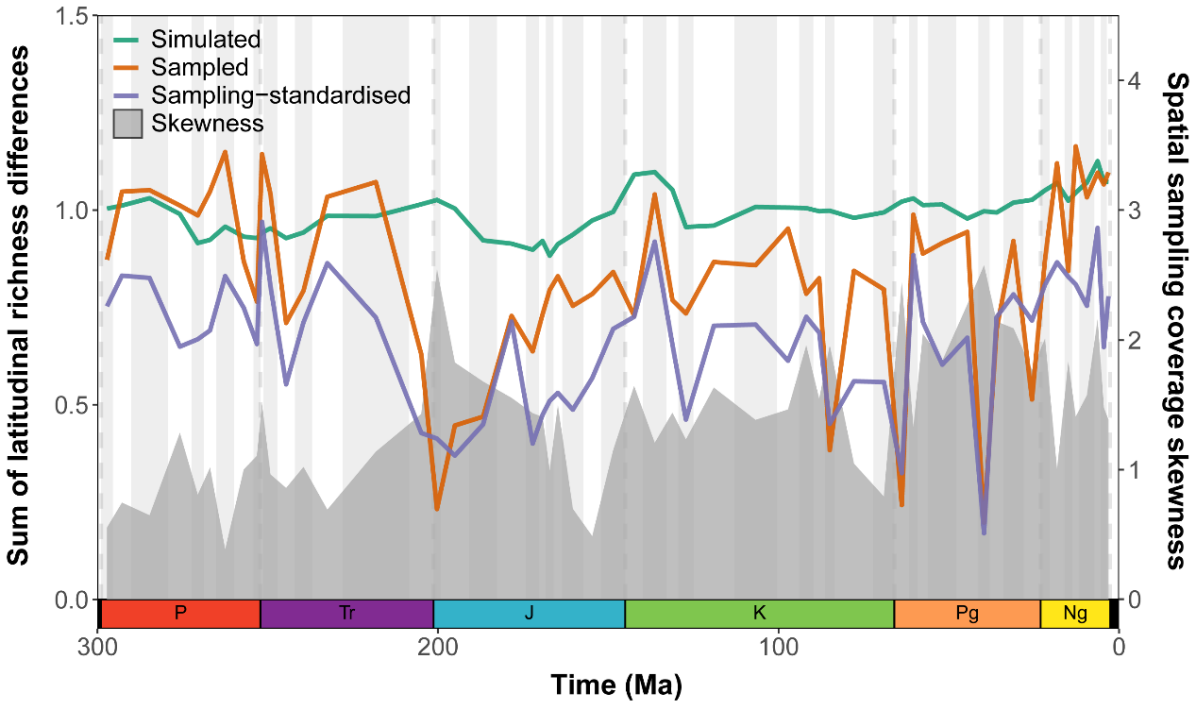


Figure 4.12. Sum of proportional latitudinal richness differences (Asselian to Piacenzian) between unimodal- and bimodal-type latitudinal biodiversity gradients. The green line indicates the sum of differences between proportional simulated unimodal- and bimodal-type latitudinal biodiversity gradients. This provides an expected difference between the two different types of latitudinal biodiversity gradient. The orange line indicates the sum of proportional mean latitudinal richness differences between sampled unimodal- and bimodal-type latitudinal biodiversity gradients. The purple line depicts the sum of proportional mean latitudinal richness differences between sampling-standardised unimodal- and bimodal-type latitudinal biodiversity gradients. The smaller the sum of latitudinal richness differences, the more similar the curves. Grey ribbon indicates the skewness of palaeolatitudinal spatial sampling coverage.

Sampled flat-type LBGs suggest that only 26/56 (~46%) stages would have their genuine peak in biodiversity recovered from their simulated counterparts (Figure 4.13), conforming to no apparent temporal trend. The SLD indicates a substantial difference between simulated and sampled flat-type LBGs, with a mean difference of 0.821 (± 0.199, 1SD) (Figure 4.14).

Sampled unimodal-type LBGs indicate a temporal shift in their detectability from their simulated counterparts. Genuine tropical peaks in biodiversity are frequently observed in their correct latitudinal bin for the Permian–Triassic (12/16 stages – 75%) and for the Neogene (6/8 stages – 75%) (Figure 4.13). However, in the Jurassic–Paleogene, only 6/32 stages (~19%) recover their genuine tropical peak in biodiversity. In addition, 50% of Jurassic–Paleogene stages would be observed as having temperate peaks in biodiversity (30–60°), contrasting with their genuine tropical peak (0–30°). The SLD indicates a mean difference of 0.684 (± 0.285, 1SD) between simulated and sampled unimodal-type LBGs (Figure 4.14). This is notably lower than the SLD observed in flat-type LBGs, due to no biodiversity being simulated or sampled at high latitudes in unimodal-type LBGs.

The detectability of bimodal-type LBGs is less affected by variation in geographic sampling through time: 42/56 (75%) of stages record temperate peaks in biodiversity within their correct latitudinal bin, and only 2/56 stages (~4%; Wuchiapingian and Anisian) would have their temperate peak observed as a tropical peak. Half (7/14) of these incorrectly observed latitudinal peaks are within the Permian (Figure 4.13). The SLD indicates a substantial difference between simulated and sampled bimodal-type LBGs, with a mean difference of 0.824 (± 0.209, 1SD) (Figure 4.14).

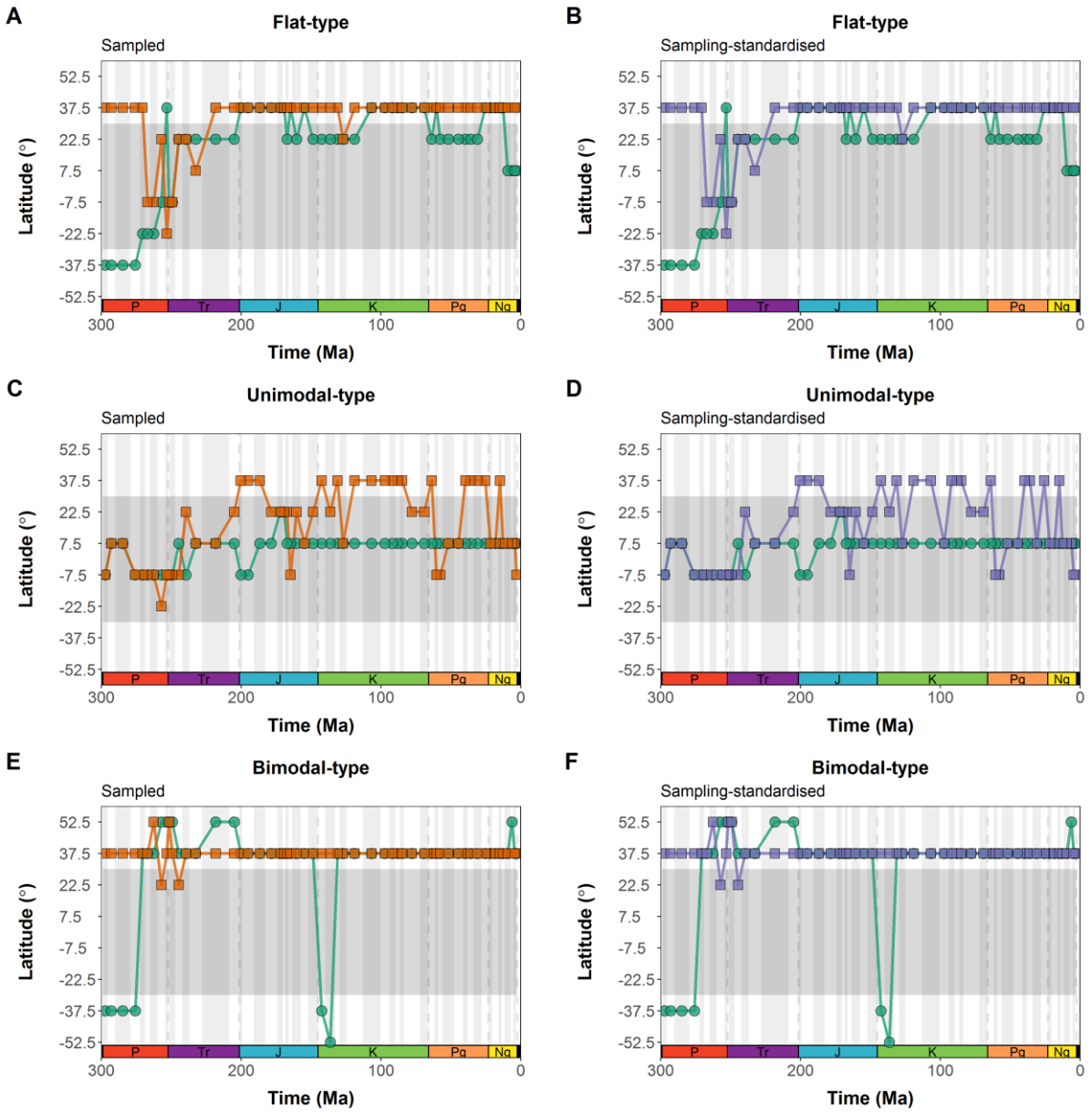


Figure 4.13. Asselian to Piacenzian (298.9–2.58 Ma) plot of the latitudinal bin with peak (maximum) diversity for simulated flat- (A; B), unimodal- (C; D) and bimodal-type (E; F) latitudinal biodiversity gradients. (A–F) Green points indicate the simulated known latitudinal bin with peak diversity; (A, C, E) orange squares depict the sampled peak diversity latitudinal bin; (B, D, F) purple squares indicate the sampling-standardised (classical rarefaction) peak diversity latitudinal bin. Dark-grey shading represents the extent of tropical latitudinal bins (30°S–30°N).

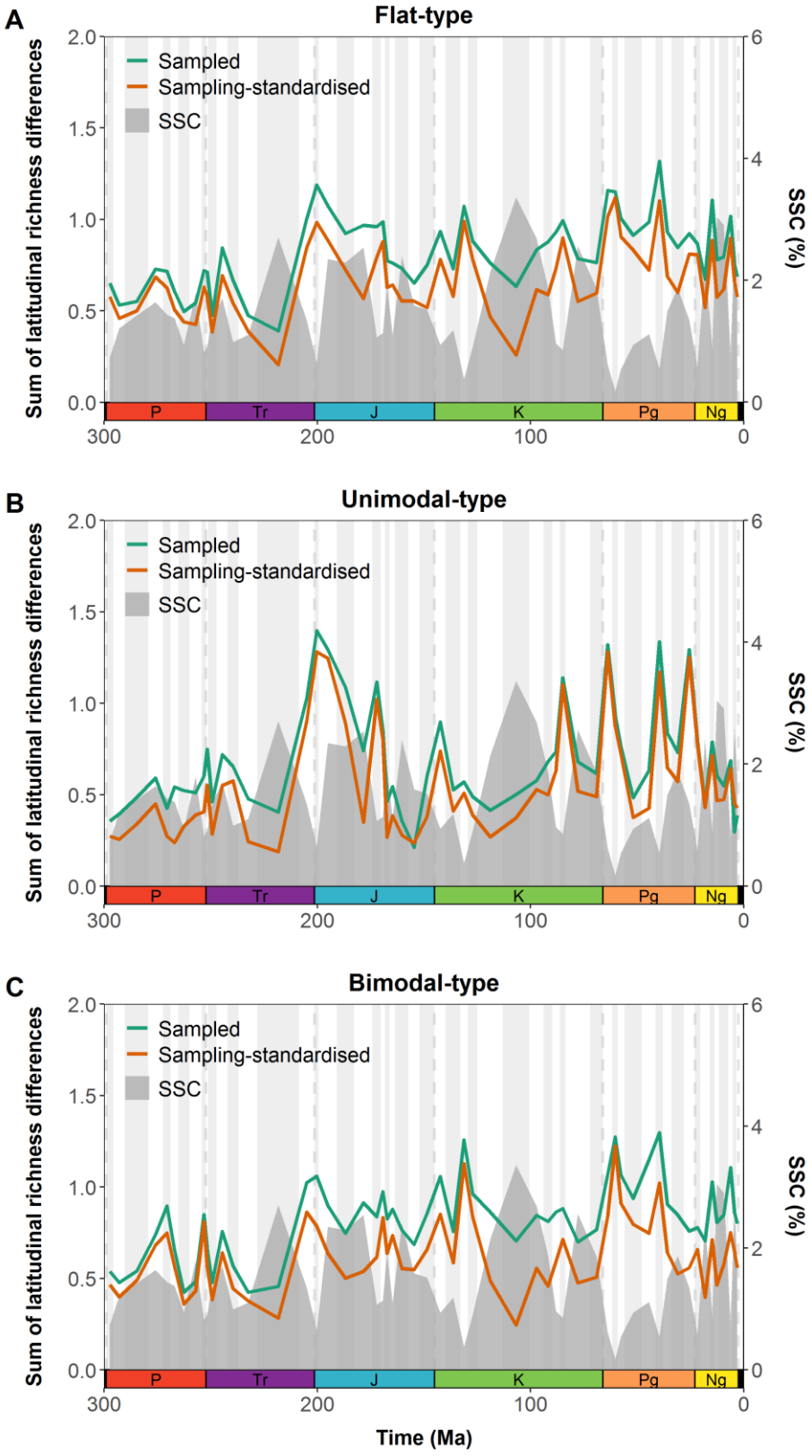


Figure 4.14. Sum of proportional latitudinal richness differences between simulated and sampled (green line), and simulated and sampling-standardised (orange line) latitudinal biodiversity gradients (A: flat-type, B: unimodal-type, C: bimodal-type). The smaller the difference, the more similar the curves. Grey ribbon on plots indicate the global spatial sampling coverage (SSC).

Linear modelling indicates a moderate to strong correlation between the SLD (simulated and sampled) and the skewness of palaeolatitudinal SSC for unimodal- ($r = 0.670$, $R^2 = 0.449$, $P < 0.001$) and bimodal-type LBGs ($r = 0.689$, $R^2 = 0.474$, $P < 0.001$) (Figure 4.15). Similar results are recovered for the relationship between the SLD (simulated and sampled) and the number of palaeolatitudinal bins without sampling, though unimodal-type LBGs ($r = 0.669$, $R^2 = 0.448$, $P < 0.001$) indicate a slightly stronger positive correlation than bimodal-type LBGs ($r = 0.544$, $R^2 = 0.295$, $P < 0.001$) (Figure 4.16).

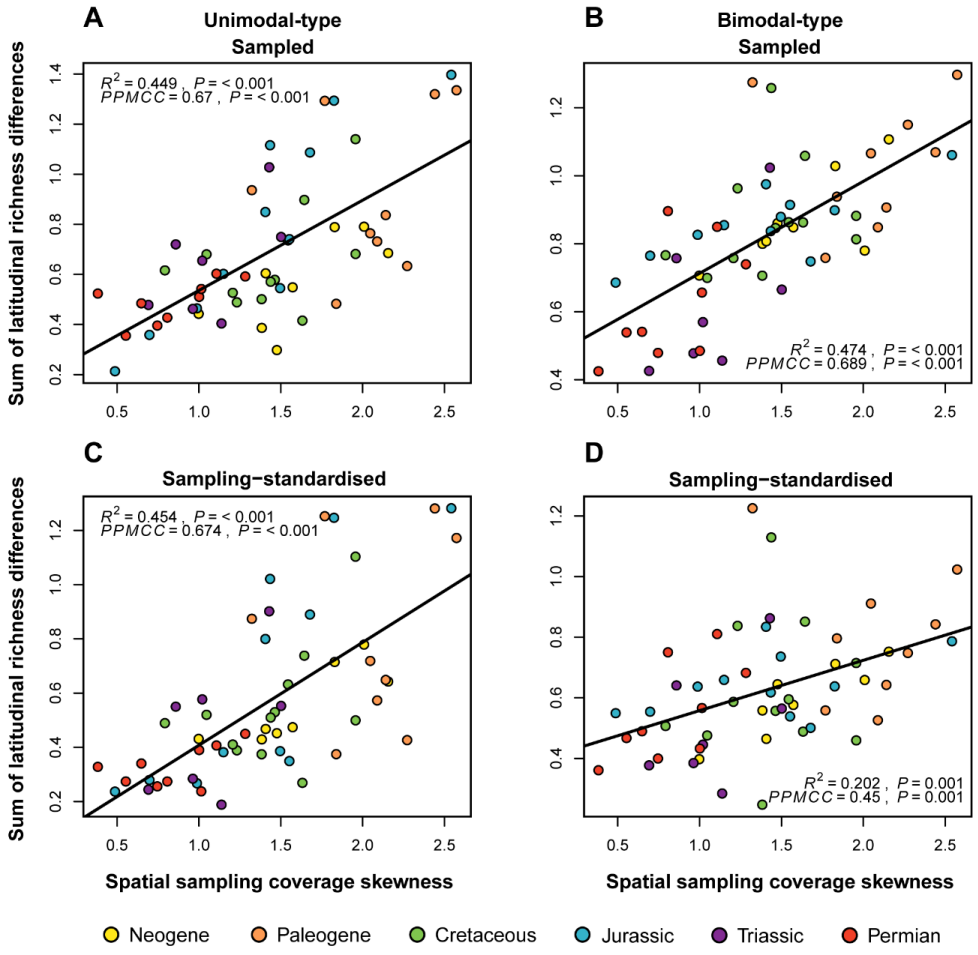


Figure 4.15. Relationship between the sum of proportional latitudinal richness differences and the skewness of palaeolatitudinal spatial sampling coverage. (A; B) Relationship between the sum of proportional latitudinal richness differences for simulated and sampled latitudinal richness, and palaeolatitudinal spatial sampling coverage skewness, for a unimodal- (A) and bimodal-type (B) latitudinal biodiversity gradient. (C; D) Relationship between the sum of proportional latitudinal richness differences for simulated and sampling-standardised (classical rarefaction) latitudinal richness, and palaeolatitudinal spatial sampling coverage skewness, for a unimodal- (C) and bimodal-type (D) latitudinal biodiversity gradient. The coefficient of determination (R^2) and the Pearson product-moment correlation coefficient (PPMCC) with associated P-values are depicted within each plot. Each point represents an individual stage, and is coloured by their respective geological period.

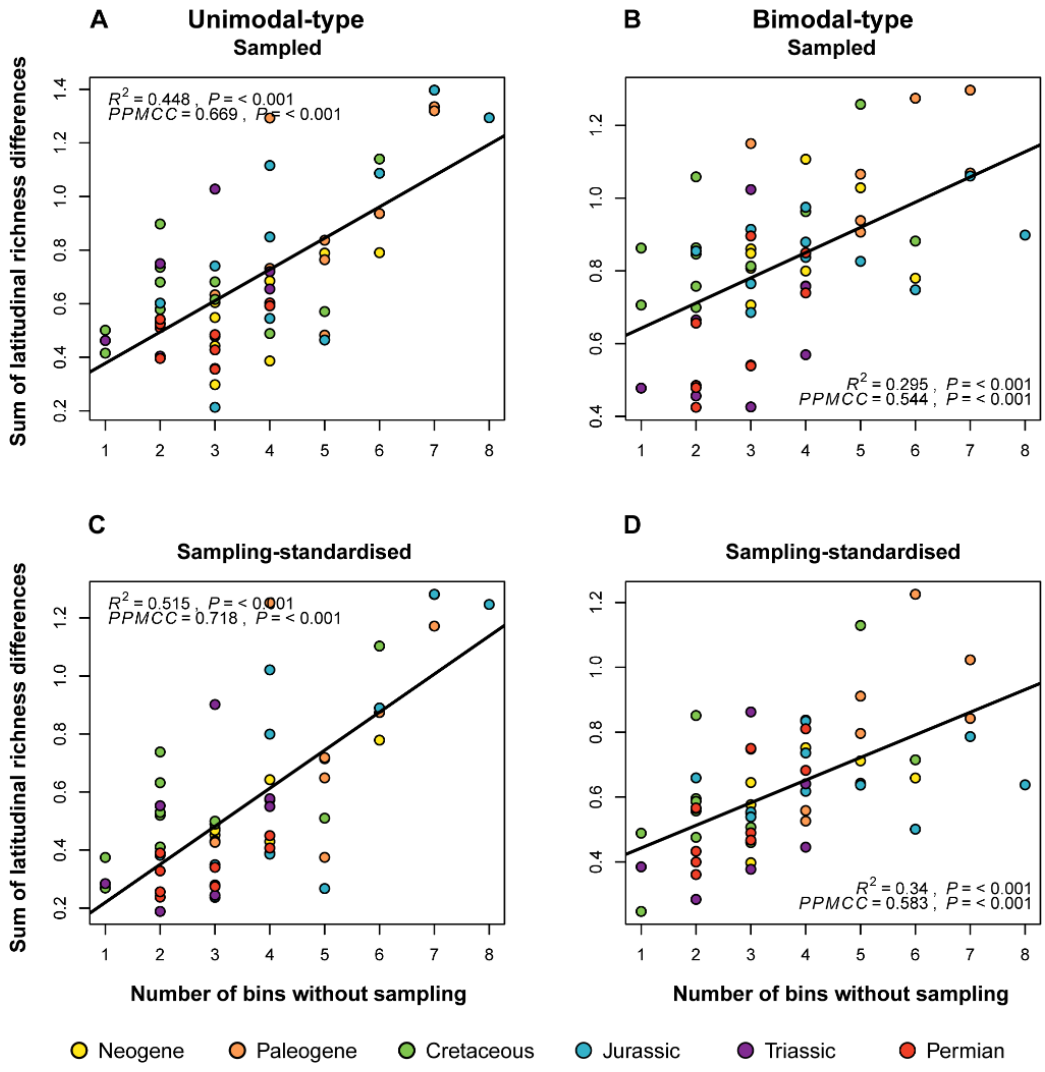


Figure 4.16. Relationship between the sum of proportional latitudinal richness differences and palaeolatitudinal data absence. (A; B) Relationship between the sum of proportional latitudinal richness differences for simulated and sampled latitudinal richness, and the number of palaeolatitudinal bins without any sampling, for a unimodal- (A) and bimodal-type (B) latitudinal biodiversity gradient. (C; D) Relationship between the sum of proportional latitudinal richness differences for simulated and sampling-standardised latitudinal richness, and the number of palaeolatitudinal bins without any sampling, for a unimodal-type (C) and bimodal-type (D) latitudinal biodiversity gradient. The coefficient of determination (R^2) and the Pearson product-moment correlation coefficient (PPMCC) with associated *P*-values are depicted within each plot. Each point represents an individual stage, and is coloured by their respective geological period.

Time series of slope estimates show a near-constant difference between simulated unimodal- and bimodal-type LBGs for both the Northern and Southern Hemisphere (Figure 4.17); unimodal LBGs show a negative slope in the Northern Hemisphere and positive slope in the Southern Hemisphere, whereas bimodal LBGs show no slope overall. However, after applying the spatial sampling window of fossil collections, slope

estimates of both unimodal and bimodal sampled LBGs show increased variability and significant overlap for Jurassic and Cretaceous stages in the Northern Hemisphere (Figure 4.17). Similar variability is also observed in the Southern Hemisphere (Figure 4.17), however only ~60% of stages could have slope estimates computed for unimodal-type LBGs, and 75% for bimodal-type LBGs due to poor sampling. Notably, after applying the spatial sampling window, the negative slope (decreasing richness with increasing latitude) of Northern Hemisphere simulated unimodal-type LBGs shifts to a positive slope (increasing richness with increasing latitude) in 8/56 stages (Figure 4.17). Furthermore, sampled unimodal- and bimodal-type LBGs frequently indicate significantly steeper gradients than their 'true' (simulated) gradients. Clear differences in slope estimates for Permian and Neogene stages are seen for Southern Hemisphere unimodal- and bimodal-type LBGs (Figure 4.17). However, the lack of continuous estimates between these time periods limits the observation of any long-term trends (Figure 4.17). Nevertheless, the slope estimate of sampled unimodal-type LBGs is significantly strengthened during the Permian compared to its simulated counterpart. Overall, variable spatial sampling strongly influences the observed angle and direction of slope estimates across the entire time series.

Global richness counts from the sampled flat-, unimodal- and bimodal-type LBGs express temporal differences in biodiversity through time, suggesting observed extinction and radiation patterns may be influenced by both underlying patterns of biodiversity and sampling (Figure 4.18). Coefficient of determination results suggest that global SSC explains a significantly larger proportion of the variance observed in global richness from sampled bimodal-type LBGs ($R^2 = 0.849$, $P < 0.001$), than unimodal-type LBGs ($R^2 = 0.527$, $P < 0.001$). However, global SSC explains the most variance in global richness from sampled flat-type LBGs ($R^2 = 0.884$, $P < 0.001$) (Figure 4.18).

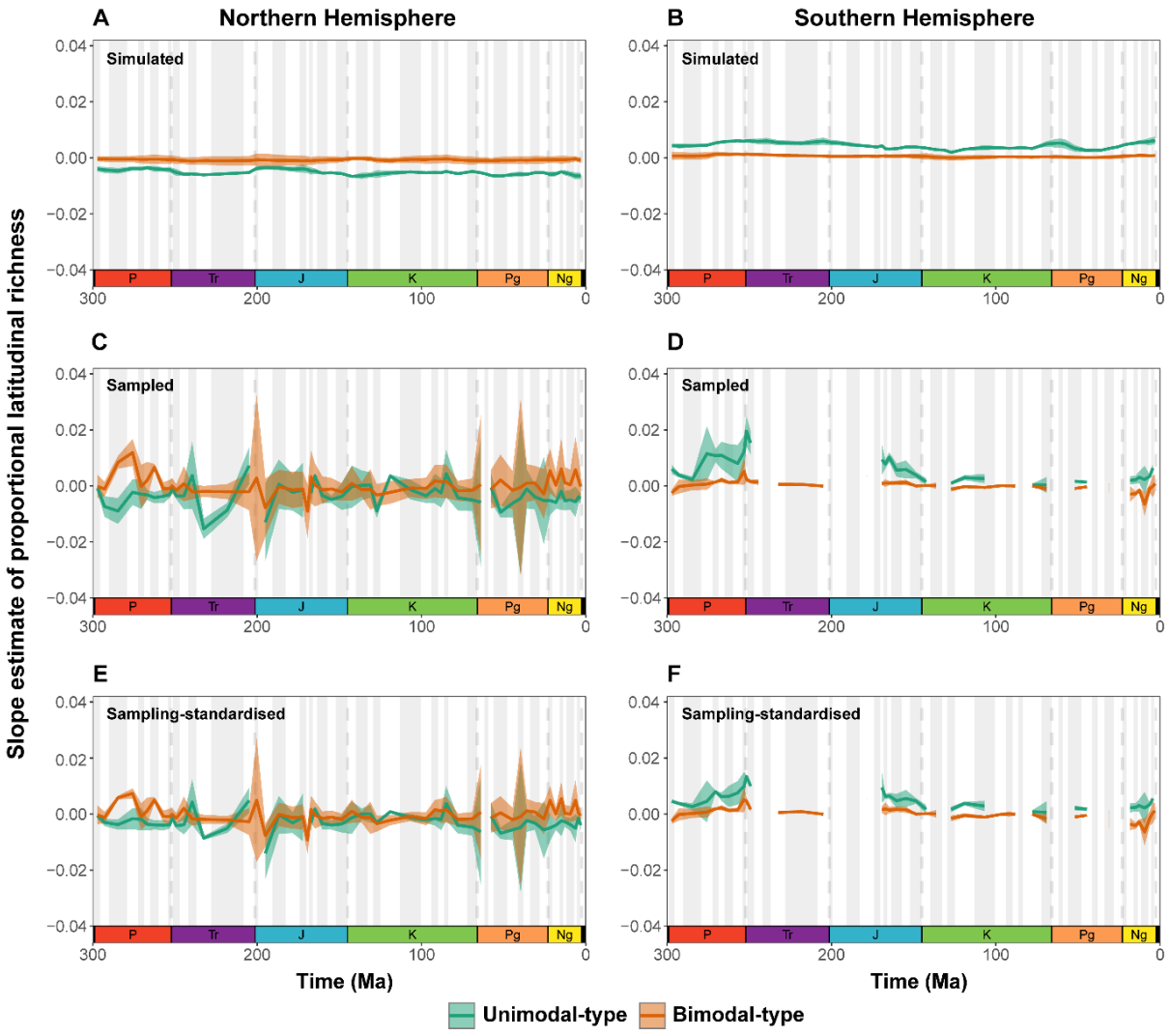


Figure 4.17. Slope estimates of simulated (A–B), sampled (C–D), and sampling-standardised (E–F) latitudinal biodiversity gradients. Slope estimates were generated by splitting latitudinal bins into Northern (A, C, E) and Southern Hemispheres (B, D, F), with proportional latitudinal richness regressed on the midpoint latitudes of latitudinal bins for each hemisphere (with a minimum threshold criterion of three latitudinal bins for slope estimation). Lines indicate the slope estimate, while coloured ribbons depict the standard error from slope estimation. Unimodal-type slope estimates are depicted in green, and bimodal-type slope estimates are shown in orange.

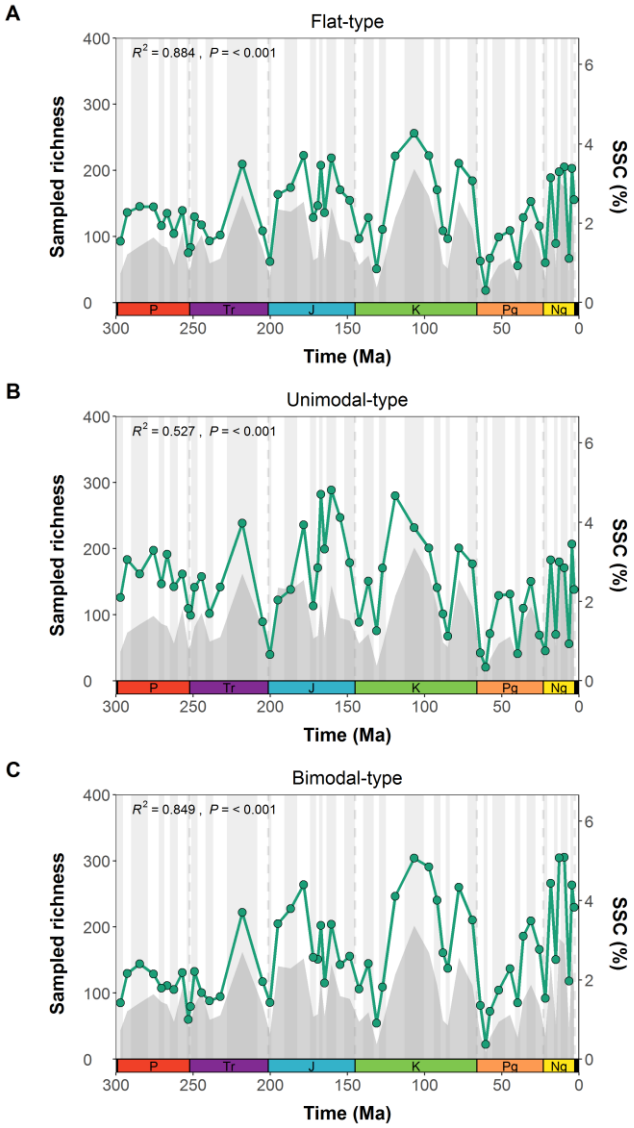


Figure 4.18. Global raw counts of sampled diversity from simulations of species' distributions and richness (= 1,000), conforming to a flat- (A), unimodal- (B), and bimodal-type (C) latitudinal biodiversity gradient. (A–C) Green points depict sampled richness at stage level based on the known sampling window (i.e. collections), while the grey ribbon illustrates the global spatial sampling coverage (SSC). Each stage, for each type of latitudinal biodiversity gradient, has a simulated richness of 1000 species, and any variation in the diversity curve is a result of the stage-level sampling window. The coefficient of determination (R^2) with associated *P*-values is depicted within each plot.

4.3.4 Sampling-standardisation latitudinal biodiversity gradients

Sampling-standardisation has a variable impact on the reconstruction of relative biodiversity patterns. Overall, sampling-standardisation slightly improves the detectability of genuine peaks (i.e. identifying the exact latitudinal bin) in latitudinal biodiversity for unimodal-type LBGs from 24/56 stages to 26/56 stages (Figure 4.13),

and for bimodal-type LBGs from 42/56 stages to 43/56 stages (Figure 4.13). However, there is no such improvement in the detectability of genuine peaks for flat-type LBGs (Figure 4.13). Overall, sampling-standardised LBGs frequently depict a 30–45°N peak in biodiversity for Jurassic–Paleogene stages, regardless of the simulated LBG-type.

The sum of proportional latitudinal richness differences (SLD) between simulated LBGs and sampling-standardised counterparts indicates an overall decrease in difference compared to their simulated and sampled counterparts (Figure 4.14). Wilcoxon signed-rank tests provide statistically significant ($P < 0.01$) support for this observation. Despite reducing the overall difference between simulated and sampled LBGs, Wilcoxon signed-rank test results indicate a statistically significant ($P < 0.05$) difference between simulated and sampling-standardised LBGs, similar to comparisons between simulated and sampled curves. Conversely, no statistically significant difference was found between sampling-standardised unimodal- and bimodal-type LBGs ($P = 0.325$) (Figure 4.12). Furthermore, sampling-standardisation tends to have a greater impact on reducing the relative latitudinal richness ratios between flat- and bimodal-type LBGs, than for unimodal-type LBGs (Figure 4.14).

Linear modelling indicates a moderate to strong correlation between the SLD (simulated and sampling-standardised) and the skewness of palaeolatitudinal SSC for unimodal- ($r = 0.674$, $R^2 = 0.454$, $P < 0.001$) and bimodal-type LBGs ($r = 0.450$, $R^2 = 0.202$, $P < 0.001$) (Figure 4.15). Similar results are observed for the relationship between the SLD (simulated and sampling-standardised) and the number of palaeolatitudinal bins without sampling, with unimodal-type LBGs ($r = 0.718$, $R^2 = 0.515$, $P < 0.001$) indicating a stronger relationship than bimodal-type LBGs ($r = 0.583$, $R^2 = 0.340$, $P < 0.001$) (Figure 4.16).

Time series of slope estimates for sampling-standardised LBGs largely reflect the results of sampled LBGs (Figure 4.17). Notable differences include the dampened variability in slope estimates, with the magnitude of slopes being more comparable to those of simulated gradients (Figure 4.17). However, 7/56 stages in the Northern Hemisphere still recovered a positive slope (increasing richness with increasing latitude)

for unimodal-type LBGs, instead of their 'true' negative slope (decreasing richness with increasing latitude) based on their simulated counterpart (Figure 4.17).

4.4 Discussion

This study's results show that distinguishing between different types of latitudinal biodiversity gradient (LBG) in deep time is often problematic due to limited spatial sampling. Spatiotemporal analyses indicate that observed LBGs are a poor representation of the underlying 'known' distribution of biodiversity, with significant differences between simulated LBGs and their sampled counterparts for all LBG-types (Wilcoxon signed-rank test, $P < 0.001$). This is further supported by additional stage level results; (1) sums of proportional latitudinal richness differences (SLD) show considerable variation between simulated and sampled LBGs (Figure 4.14); and (2) slope estimates of sampled LBGs (Figure 4.17) show significant differences in direction and magnitude compared to simulated slope estimates, after applying the geographic sampling window.

The same pattern of signal degradation following sampling is observed when comparing LBG types. Whilst the results indicate an expected significant difference between simulated unimodal- and bimodal-type LBGs (Wilcoxon signed-rank test, $P < 0.05$), no significant difference between (sampled) unimodal- and bimodal-type LBGs is found (Wilcoxon signed-rank test, $P = 0.379$) after applying the 'known' palaeogeographic sampling window. This finding is supported by results from the SLD between simulated unimodal- and bimodal-type LBGs, which indicate relatively sustained differences throughout the time period of study (Figure 4.12). Slope estimates echo these results; the near-continuous difference in slope angle between simulated unimodal- and bimodal-type LBGs is removed after applying the spatial sampling window (Figure 4.17). Consequently, despite different empirical distributions of biodiversity, relative biodiversity patterns might converge after sampling. As a result, differentiating between sampled unimodal- and bimodal-type LBGs is often not possible; for example, in only 50% of Jurassic–Paleogene stages can we accurately distinguish between

tropical and/or temperate peaks in diversity (Figure 4.13). This study's results corroborate previous work (Wall et al., 2009; Marcot et al., 2016; Close et al., 2017) in suggesting that deep time macroecological patterns can be strongly shaped by the available spatial sampling window, as opposed to the genuine distribution of biodiversity (Figure 4.10). Considering that the sampling regime applied here (all occurrences within a sampled cell are preserved and selected) is an impossible 'best-case' scenario for the fossil record, it is likely the impacts of variable spatial sampling are even more severe than reported here.

This study supports previous findings that demonstrate a temporal shift in palaeolatitudinal sampling from the Permian towards the present-day (Allison and Briggs, 1993; Ziegler et al., 2003; Vilhena and Smith, 2013). In general, this shift follows a poleward drift from tropical palaeolatitudes in the Permian and Triassic, to temperate palaeolatitudes in the Jurassic to Paleogene (Figure 4.9). A subsequent equatorward shift in sampling is initiated in the Neogene (Figure 4.9). Remarkably, this temporal shift in palaeolatitudinal sampling is well represented in unimodal-type LBG simulations (Figure 4.10). Genuine tropical peaks in diversity are observed in their correct latitudinal bin for 75% of Permian–Triassic and Neogene stages (Figure 4.13). However, in the Jurassic–Paleogene, a genuine latitudinal peak was only recovered in 6/32 stages (~19%). This is largely a result of the skewness in palaeolatitudinal spatial sampling coverage (SSC) (Figure 4.8) between 30–45°N during Jurassic–Paleogene stages, which leads to over-representation of relative biodiversity (Figure 4.11). This is further evident when comparing the SLD between unimodal- and bimodal-type LBGs, which tends to be significantly reduced when the skewness of palaeolatitudinal SSC is increased (Figure 4.12). Conversely, bimodal-type LBGs tend to have their genuine temperate peaks in biodiversity observed in their correct latitudinal bin (75% of stages) due to the agreement between simulated latitudinal richness and the spatial sampling window (Figure 4.7; Figure 4.10). Although this is largely related to the palaeo-location of the U.S.A., China, and Europe (i.e. regions of high sampling intensity) (Jackson and Johnson, 2001; Kidwell and Holland, 2002), the

presence of major epicontinental seas (e.g. Laurasian and Western Interior seaways) in the Northern Hemisphere during the Mesozoic enhanced the available area for marine faunas, contributing to the heterogeneous spatial distribution of marine fossils (Peters, 2005; Lagomarcino and Miller, 2012; Close et al., 2020b). This is supported by the simulated flat-type LBGs, which simulate high Mesozoic biodiversity in the Northern Hemisphere (Figure 4.10).

Sampling-standardisation has become a commonplace methodology in palaeontological studies for reducing the impact of fossil record bias upon diversity curves (Alroy, 2010b; Kiessling and Kocsis, 2015; Mannion et al., 2015; Benson et al., 2016; Nicholson et al., 2016; Cleary et al., 2018; Dunne et al., 2018; Allen et al., 2020; De Celis et al., 2020). This study's results indicate that whilst sampling-standardisation alleviates some issues of data quality, it is often confounded by spatial sampling variability. When broken down by LBG-type, simulation results show that sampling-standardisation tends to decrease the SLD between simulated and sampled LBGs, improving relative latitudinal richness ratios (Figure 4.14). This improvement is more prominent in bimodal-type LBGs than unimodal-type LBGs, with sampling-standardisation reducing the percentage of variance in the SLD explained by SSC skewness (Figure 4.15). This is a result of the close agreement between simulated bimodal-type LBGs and the spatial sampling window along the time series (Figure 4.7; Figure 4.10).

However, despite this improvement, sampling-standardisation generally decreases the SLDs between unimodal- and bimodal-type LBGs across the entire time series, therefore increasing similarity between LBG types (Figure 4.12). This is further supported by slope estimates, with sampling-standardised results failing to correct the artificial similarity between unimodal- and bimodal-type LBGs introduced by sampling, and instead narrowing the standard error associated with the slopes (Figure 4.17). This study's results also indicate only a slight improvement in the detectability of genuine peaks in latitudinal biodiversity after applying sampling-standardisation (Figure 4.13). However, this shortfall is not the result of the elected sampling-standardisation approach, but the available data. Numerous palaeolatitudinal bins

(~30%) in the study period have zero SSC, and hence zero species occurrences after applying the available spatial sampling window, which prevents the computation of rarefied biodiversity estimates. Due to this data absence, as well as preferential sampling between 30–45°N during the Mesozoic, sampling-standardised LBGs frequently identify a 30–45°N peak in biodiversity, regardless of the simulated LBG-type for Jurassic–Paleogene stages. It is possible that other sampling-standardisation approaches such as shareholder quorum subsampling (Alroy, 2010c) might perform better in estimating relative biodiversity patterns, when sufficient data are available (Alroy, 2010b). However, as a considerable percentage of the variance in the SLD for unimodal- (51.5%) and bimodal-type (34%) LBGs is due to data absence, which no sampling-standardisation approach can account for, it is unlikely to improve upon the detectability of genuine LBGs in deep time.

This study's results also permit the identification of particular time intervals that might be well or poorly suited for reconstructing LBGs in deep time. The reconstruction of different types of LBG appears to be particularly challenging for the Hettangian–Pliensbachian, Santonian, Danian, Bartonian, and Chattian (Figure 4.12; Figure 4.17). During these intervals, simulated unimodal- and bimodal-type LBGs are almost identical after applying the spatial sampling window (stage-level plots available in Appendix B). This limitation is driven by skewed palaeolatitudinal sampling towards the Northern Hemisphere (Figure 4.7; Figure 4.12). However, it should also be noted that when skewness in palaeolatitudinal sampling is low, the reconstruction of different types of LBG is possible, such as during the Permian and Early Triassic (Figure 4.8; Figure 4.12). Nevertheless, the impact of skewness in palaeolatitudinal sampling is likely negated at higher SSC due to latitudinal differences in species discovery curves.

Although these issues are mostly a concern for spatial studies, the temporal component of biodiversity is also strongly affected. Global biodiversity curves constructed from sampled LBGs support the hypothesis that palaeolatitudinal sampling bias impacts upon our understanding of phenomena such as extinction and radiation events (Allison

and Briggs, 1993) (Figure 4.18). As shown above, a large proportion of our understanding of the Mesozoic and Cenozoic fossil record is sourced from a single palaeolatitudinal band (30–45°) within the Northern Hemisphere (Allison and Briggs, 1993; Vilhena and Smith, 2013). If the LBG has varied through time, with shifts between temperate and tropical latitudinal peaks, this could add volatility to global biodiversity curves that have not accounted for palaeolatitudinal SSC (Close et al., 2017). If sampling remains focused on one palaeolatitudinal bin through time, an alternation in the LBG from a temperate to tropical peak could instead appear in the fossil record as a major extinction or radiation event (Allison and Briggs, 1993).

It should be noted that this study is not without limitations. Firstly, the simulations are simple, with biodiversity patterns only driven by the specified type of LBG, with the steepness of these gradients influenced by the available shallow marine area (cells), emulating the species-area-relationship. As such, they are not influenced by other factors that are likely crucial to the formation of the LBG, such as climate (Saupe et al., 2019c; Meseguer and Condamine, 2020). Although both abiotic and biotic drivers have been hypothesised to contribute to the formation of LBGs, here the principal focus is whether different relative latitudinal biodiversity patterns can be reconstructed after applying the 'known' sampling window, rather than reconstructing 'actual' biodiversity patterns in deep time. The results presented here might also be dependent upon the sampling protocol in which all occurrences were sampled (and hence biodiversity) within a cell providing it contains at least one collection. This simplified approach ignores the relationship between the number of samples (i.e. collections) and observed richness (i.e. richness-sample accumulation curve). However, using a weighted approach based on the number of collections within cells to sample occurrences would only further support the trends reported here, due to the concentration of collections between 30–45°N for the majority of the time series. The results presented here might also be dependent upon the coarse spatial resolution (1° x 1°) of this study. This utilised resolution was principally constrained by the availability of computational power, with higher spatial resolutions requiring orders of magnitude more time to run simulations

which would have been unfeasible to complete the ~300 million-year time series. However, while analyses at finer spatial resolutions might produce different results, it is likely that they would not change the general trends observed in this study. Finally, this study is limited by design to the shallow marine realm. However, the impact of variable spatial sampling on estimates of terrestrial diversity is well documented (Marcot et al., 2016; Close et al., 2017, 2020a; Fraser, 2017). As the terrestrial fossil record is generally less complete and abundant than the marine fossil record (Kidwell and Holland, 2002), it is likely that reconstructing terrestrial LBGs is also challenging.

This study highlights the impact of spatial bias on our understanding of past biogeographic patterns, identifying the potential issues of applying sampling-standardisation methods without considering the heterogeneity of global sampling. Whilst results show the application of such methods is not meaningless, they do highlight key issues with current approaches for reconstructing macroecological patterns in deep time. Specifically, these methods cannot account for artefactual data absence, which is shown to lead to erroneous conclusions. The advent of large, community-accessible palaeontological databases has substantially improved the availability of presence/occurrence information. However, few publicly accessible records succeed in documenting and differentiating between sites that have been sampled with no fossil occurrences found (sampled absence), versus sites that have not been sampled and therefore do not record fossil occurrences (potentially false absences). Inferential methods commonly used in ecology, such as ecological niche and occupancy modelling might represent an alternative approach, although they remain in their infancy in palaeobiological studies (Liow, 2013; MacKenzie et al., 2017; Chiarenza et al., 2019; Jones et al., 2019). Whilst these methods cannot replace prospecting for fossil sites, or inform us directly about biodiversity, they allow us to infer what data we might be missing, and from where. Birth-death models (e.g. PyRate (Silvestro et al., 2014)) might provide an alternative approach to estimating speciation and extinction rates from fossil occurrence data, by accounting for preservational processes (Silvestro et al., 2014; Condamine et al., 2019; Meseguer and Condamine, 2020). However, only

additional sampling within relatively poorly sampled regions will provide empirical evidence on latitudinal biodiversity patterns. Overall, this study's results suggest caution when attempting to reconstruct LBGs in deep time using current occurrence-based methods due to the heterogeneity in spatial sampling.

4.5 Summary

Simulated LBGs suggest that the current distribution of sampled area of shallow marine fossils rarely allows for differentiation between types of latitudinal biodiversity gradient (LBG). A long-term poleward shift in the palaeolatitudinal sampling window is observed, which enables unimodal-type LBGs to be readily identified in the Permian and Triassic when palaeolatitudinal sampling was less skewed towards temperate palaeolatitudes. The reconstruction of unimodal gradients in most of the Jurassic, Cretaceous and Palaeogene is limited due to skewed sampling towards northern temperate regions. However, more equable palaeolatitudinal sampling in the Neogene permits the recovery of unimodal gradients during this time period. Sampling-standardisation aids reconstruction of relative biodiversity patterns when palaeolatitudinal spatial sampling coverage is not severely skewed. However, reconstruction of deep time LBGs is severely impacted by artefactual absences, with a third of palaeolatitudinal bins suffering from complete data absence that prevents computation of sampling-standardised biodiversity estimates. Consequently, previous studies might therefore have failed to recover the 'true' LBG-type due to the heterogeneous distribution of the available sedimentary record and incomplete sampling.

–This page is intentionally left blank–

5 The evolution of the latitudinal biodiversity gradient in zooxanthellate corals

Disclosure: Some of the content reported in this chapter is in review at *Nature Communications*. While the primary author wrote most of this text, contribution by the co-authors of this study are contained in this chapter, as well as the input received from the peer review process. The relevant text, revised below, is from: Jones, L. A., Mannion, P.D. Farnsworth, A., Lunt, D.J. (in review). Climate and palaeogeography shaped the evolutionary history of the latitudinal biodiversity gradient of corals. *Nature Communications*.

OVERVIEW

Most organisms today conform to a latitudinal biodiversity gradient, in which species richness declines from tropical to polar regions. This gradient is broadly recognised as unimodal (i.e. peaking towards the equator), though the specifics of this gradient differ between taxonomic groups. However, despite this pattern being near-ubiquitous today, fossil occurrence data suggest that the latitudinal biodiversity gradient has varied through time, with flattened or even bimodal gradients observed in the geological past. In fact, unimodal-type latitudinal biodiversity gradients appear to be restricted to the Palaeozoic, and the last 30 million years, when 'icehouse' climate regimes have persisted. However, most previous studies have failed to account for the variation in sampled palaeogeographic area, which strongly biases inferences about past biodiversity patterns due to the empirical scaling of species richness with area. Here, this shortfall is addressed by implementing a sampling-standardisation protocol that draws data from geographic areas of uniform size. Owing to their vast evolutionary history and sensitivity to climatic drivers (i.e. sea surface temperature), zooxanthellate corals are used here to test whether unimodal-type gradients are restricted to the last 30 million years, or were present at other intervals during their ~250 million-year history. Reconstructions of sampling-standardised coral biodiversity suggest that unimodal-type latitudinal biodiversity gradients likely persisted during the Middle Jurassic and earliest Cretaceous, which are intervals marked by geologically long-lived 'cold-snaps'. In addition, this study's findings broadly agree with previous work in suggesting that the modern latitudinal biodiversity gradient became significantly steeper only in the last 20 million years, following the onset of 'icehouse' conditions. Overall, these results confirm that strong unimodal-type LBGs might be a relatively rare phenomenon that are primarily restricted to icehouse climate regimes. However, challenges remain in disentangling whether observed trends reflect a true biological signal, or are an artefact of heterogeneous spatial sampling.

5.1 Introduction

One of the most recognisable macroecological patterns today is the latitudinal biodiversity gradient (LBG), in which species richness declines from tropical to polar regions (Rosenzweig, 1995; Willig et al., 2003; Hillebrand, 2004). Although this pattern is near-ubiquitous in the present day, fossil occurrence data suggests that the 'modern-type' (i.e. unimodal) LBG has not been a permanent feature of the biosphere, with various taxonomic groups exhibiting a flattened or even bimodal gradient in deep time (Markwick, 1998; Archibald et al., 2010; Rose et al., 2011; Mannion et al., 2012; Yasuhara et al., 2012; Powell et al., 2015; Marcot et al., 2016; Nicholson et al., 2016; Brocklehurst et al., 2017; Kröger, 2018; Allen et al., 2020; Song et al., 2020). In fact, tropical peaks and poleward declines in taxonomic richness appear to be largely restricted to intervals of the Palaeozoic, and the past 30 million years (myr), when cold icehouse climatic regimes have persisted (Jablonski et al., 2006; Powell, 2009; Archibald et al., 2010; Yasuhara et al., 2012; Mannion et al., 2014; Marcot et al., 2016; Fenton et al., 2016). However, the fossil record is spatiotemporally biased due to geological (e.g. variable stratigraphic completeness, erosional and burial processes) and anthropogenic (e.g. variable spatial sampling, collector interest and sampling effort) factors, which limit its potential in understanding past biodiversity patterns. Whilst recent latitudinal biodiversity studies have tended to correct for sampling intensity (e.g. Mannion et al., 2012; Nicholson et al., 2016; Allen et al., 2020), they do not address the spatiotemporal heterogeneity in sampled geographic area (Vilhena and Smith, 2013; Benson et al., 2016; Close et al., 2017, 2020b). As demonstrated in Chapter 4, the reconstruction of different types of LBGs can be particularly impacted by this bias. Varying spatial sampling can result in radically different sizes of the underlying taxon pool (Vilhena and Smith, 2013; Close et al., 2017). Critically, changes in the palaeogeographic sampled area has the potential to substantially bias any estimation of relative diversity patterns, even when using sampling-standardized richness estimators (Close et al., 2018, 2020a). Novel approaches, that account for this

variation in geographic sampling, are needed to provide fairer estimates of latitudinal biodiversity patterns.

Today, zooxanthellate corals have a steep unimodal-type LBG (Veron, 2000; Kiessling et al., 2012; Spano et al., 2016), with high diversity confined to tropical regions and absolute latitudinal limits of 45° either side of the equator (Kiessling et al., 2012; Muir et al., 2015). Though broadly 'unimodal', it should be noted that this gradient is also marked by a small trough in biodiversity at the equator (Kiessling et al., 2012). The ecological life strategy (i.e. photosymbiosis) of zooxanthellate corals restricts them (and prolific reef-building) to warm, shallow, and high insolation areas (Kleypas et al., 1999; Couce et al., 2012; Muir et al., 2015). Although several zooxanthellate coral species have expanded their ranges poleward in response to increasing sea surface temperatures (Precht and Aronson, 2004; Yamano et al., 2011; Baird et al., 2012), it has been proposed that there is a latitudinal limit to this extension due to the availability of solar radiation for photosynthesis (Muir et al., 2015). However, throughout their ~250 myr evolutionary history, many zooxanthellate corals have occupied latitudes higher than 45° (Kiessling and Kocsis, 2015), raising a fundamental question about the latitudinal distribution of zooxanthellate coral biodiversity in deep time.

The ecological life strategy and long geological history of zooxanthellate corals makes them ideal candidates for assessing the presence of different types of LBG in deep time. In this thesis chapter, the latitudinal biodiversity patterns of zooxanthellate corals are evaluated using fossil occurrence data from the Paleobiology Database. Specifically, this study tests whether unimodal-type gradients are restricted to the past 30 myr or were also present at other intervals during zooxanthellate corals' ~250 myr evolutionary history. In order to provide fairer estimates of relative latitudinal biodiversity patterns, a novel sampling-standardisation protocol that accounts for heterogeneous spatial sampling is implemented here.

5.2 Methods

5.2.1 Fossil occurrence data

Coral occurrences (= 'Scleractinia') from the Anisian (247.1 million years ago [Ma]) to Piacenzian (2.58 Ma) were downloaded from the Paleobiology Database (PBDB; www.paleobiodb.org) on the 13th March 2020, yielding 27,233 occurrences. To improve data quality, this dataset was filtered to exclude data not identified to genus level, as well as taxonomically unresolved genera, based on expert opinions in Corallosphere (http://www.corallosphere.org/). Analyses were centred on zooxanthellate corals (Z-corals), and therefore azooxanthellate and apozooxanthellate corals were removed from the dataset. Defining life strategy within the fossil record is challenging, as soft tissue is rarely preserved, and there is little empirical evidence of symbiotic mode. For these analyses, the inferred symbiotic states of Z-coral genera from previous work were followed (Kiessling and Kocsis, 2015), retaining only those with high levels of confidence. This designation of photosymbiotic mode for genera was based on three lines of evidence: morphological, geochemical, and uniformitarian. Based solely on morphology, 96% of extant corals would have their symbiotic mode correctly classified, and this approach is therefore likely to be robust when applied to fossil data (Kiessling and Kocsis, 2015). The final dataset contains 15,324 fossil occurrences, from 3,121 unique collections. To allow reconstruction of latitudinal biodiversity patterns in deep time, occurrences were rotated from their modern coordinates to their palaeo-position via GPlates (www.gplates.org) (Wright et al., 2013), based on their temporal range midpoint.

5.2.2 Binning protocol

Following previous studies (Alroy, 2010b; Mannion et al., 2015; Close et al., 2017, 2020a), approximately equal-length time bins (~10 myr) were used to temporally bin fossil occurrences, and account for variable bin duration (Table 5.1). This was achieved by grouping stratigraphic stages together to construct composite time bins. There is no significant relationship between time (bin midpoint) and the duration of the

composite bins used here ($R^2 = 0$, $P = 0.559$), indicating no temporal trend in bin length. In accordance with previous studies (e.g. Close et al., 2020a), fossil occurrences were assigned to a time bin if that bin contained over 50% of the geological time range associated with that occurrence (defined by the minimum and maximum age ranges stated in the PBDB).

Table 5.1. Composite time bins used in this study. Bin length is approximately 10 million years, with a mean duration of 10.35 myr (standard deviation: 3.51 myr). Listed abbreviations are used throughout the Chapter to refer to specific intervals of time. Time bins are based on data from the R package 'divDyn' (Kocsis et al., 2019).

Time bin	Abbreviation	Maximum age (Ma)	Minimum age (Ma)	Duration
Cenozoic 6	Cn6	11.6	2.58	9.02
Cenozoic 5	Cn5	23	11.6	11.4
Cenozoic 4	Cn4	33.9	23	10.9
Cenozoic 3	Cn3	40.4	33.9	6.5
Cenozoic 2	Cn2	55.8	40.4	15.4
Cenozoic 1	Cn1	65.5	55.8	9.7
Cretaceous 8	K8	70.6	65.5	5.1
Cretaceous 7	K7	83.5	70.6	12.9
Cretaceous 6	K6	93.5	83.5	10
Cretaceous 5	K5	99.6	93.5	6.1
Cretaceous 4	K4	112	99.6	12.4
Cretaceous 3	K3	125	112	13
Cretaceous 2	K2	136.4	125	11.4
Cretaceous 1	K1	145.5	136.4	9.1
Jurassic 6	Jr6	150.8	145.5	5.3
Jurassic 5	Jr5	164.7	150.8	13.9
Jurassic 4	Jr4	171.6	164.7	6.9
Jurassic 3	Jr3	183	171.6	11.4
Jurassic 2	Jr2	189.6	183	6.6
Jurassic 1	Jr1	199.6	189.6	10
Triassic 4	Tr4	216.5	199.6	16.9
Triassic 3	Tr3	228	216.5	11.5
Triassic 2	Tr2	245	228	17
Triassic 1	Tr1	251	245	6

Based on their palaeocoordinates, fossil occurrences were binned into 30° latitudinal bands (Table 5.2). This is a common binning protocol applied in deep time studies (e.g. Fitzgerald and Carlson, 2006; Mannion et al., 2012; Kröger, 2018; Close et al., 2020b), and approximates tropical (0–30°), temperate (30–60°), and high latitude/polar

regions (60–90°). Whilst latitudinal biodiversity studies focused on the present day tend to use smaller latitudinal bin sizes (e.g. ≤ 5° (Roy et al., 1998)), the paucity of the fossil record necessitates the use of larger bins when studying macroecological patterns in deep time. Nevertheless, the general latitudinal biodiversity patterns (tropical vs. temperate peaks) of present-day Z-corals are easily recognised when binned by broader latitudinal bands (Figure 5.1).

Table 5.2. Latitudinal binning protocol used in this study. Latitudinal bins approximate tropical, temperate, and high latitude/polar regions in each hemisphere.

Latitudinal bin	Maximum (°)	Midpoint (°)	Minimum (°)	Hemisphere
1	90	75	60	Northern
2	60	45	30	Northern
3	30	15	0	Northern
4	0	-15	-30	Southern
5	-30	-45	-60	Southern
6	-60	-75	-90	Southern

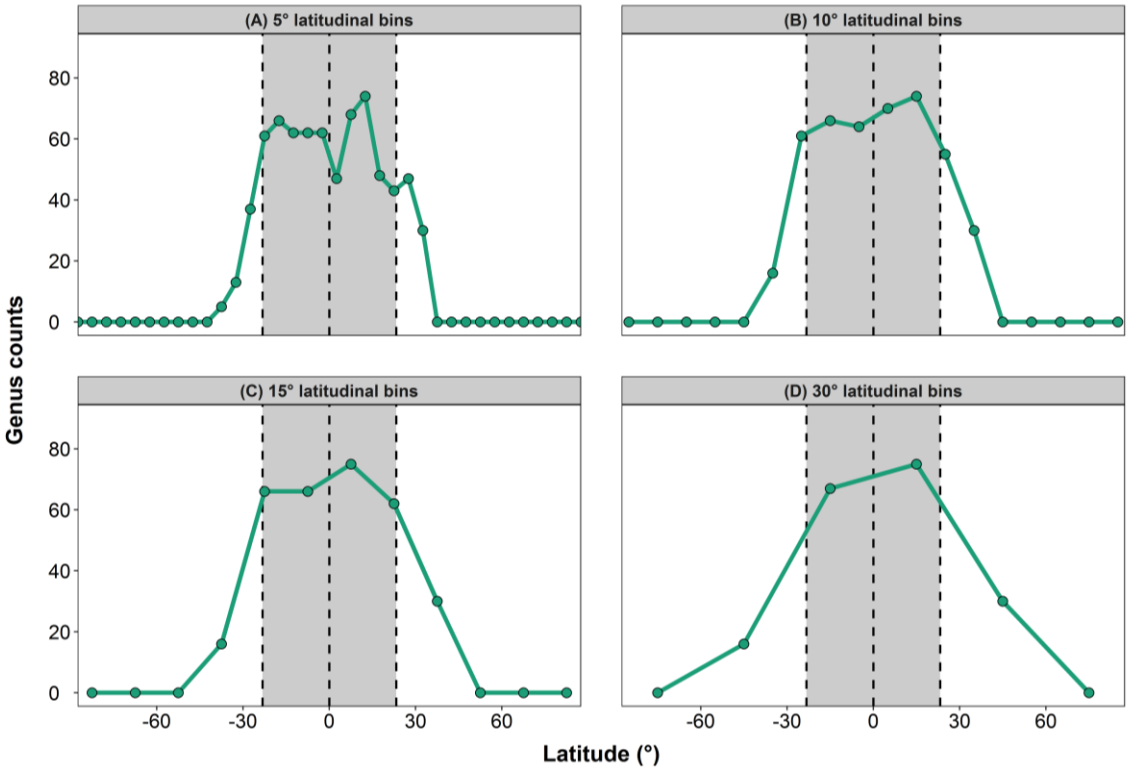


Figure 5.1. The present-day latitudinal biodiversity gradient of zooxanthellate corals at varying bin protocols. (A) 5° latitudinal bins; (B) 10° latitudinal bins; (C) 15° latitudinal bins; and (D) 30° latitudinal bins. Grey shaded area represents the extent of the tropics today. Dashed lines indicate the Equator, the Northern Tropic, and the Southern Tropic. Modern zooxanthellate coral data is as described in Chapter 3.

5.2.3 Latitudinal sampling and diversity

To assess the influence of sampling bias on face-value patterns drawn from the fossil record, raw counts of genera, collections, and formations were computed within their palaeolatitudinal bins. As diversity estimates might also be influenced by heterogeneities in spatial sampling, the number of occupied equal-area grid cells (250 km spacings) was calculated using the R package 'dggridR' ver. 0.1.12 (Barnes et al., 2017). In addition, to provide insight into the palaeogeographic spread of fossil sampling sites, the summed minimum-spanning tree length (MST; minimum length of segments that connect a set of points) (Gower and Ross, 1969) was computed between occupied grid cells, using the R package 'vegan' ver. 2.5-6 (Oksanen et al., 2019). The coefficient of determination (R^2) between genus counts and sampling proxies (collections, formations, occupied equal-area grid cells, and summed MST length) was also calculated to quantify the influence of variable sampling on face-value counts of genera.

Local richness (alpha diversity) was also estimated based on genus counts per collection (= assemblage). Using these data, a generalized additive model of the absolute palaeolatitudinal distribution of collections through time (weighted by genus richness) was generated to highlight the general latitudinal biodiversity trends across the entire time series.

5.2.4 Sampling-standardisation protocol

Palaeolatitudinal genus richness estimates were computed using coverage-based rarefaction (Chao and Jost, 2012), otherwise known as shareholder quorum subsampling (Alroy, 2010a). Coverage-based rarefaction (CR) provides an objective, frequency-dependent measure of diversity which is insensitive to variation in sampling (Chao and Jost, 2012). Specifically, CR utilises the theory of frequency-distribution coverage to make impartial estimates of biodiversity between temporal (or spatial) bins that might have been sampled with varying levels of intensity (Alroy, 2010a; Chao and Jost, 2012). This is achieved by standardising samples to equal levels of

biodiversity-sample completeness (= coverage). Coverage itself specifies the fraction of individuals from the underlying population that are represented by the sampled species. Good's u is the simplest and most frequently applied coverage estimator (Good, 1953), and is defined as one minus the number of singletons (a given taxonomic unit observed only once), divided by the total count of sampling units. Sampling is considered poor when there are many singletons, and good when there are few (Alroy, 2010a). CR has frequently been utilised in deep time studies to allow fair comparison between temporal and spatial bins (e.g. Alroy, 2010b; Mannion et al., 2015; Close et al., 2017, 2020a; Dunne et al., 2018; Dean et al., 2019). However, independently, CR does not correct for heterogeneity in spatial sampling, specifically the palaeogeographic area sampled. This is significant as species-area relationships are ubiquitous (MacArthur and Wilson, 1967; Connor and McCoy, 1979; Rosenzweig, 1995), and the taxon pools from which subsamples are drawn from are ultimately influenced by the size of the sampled palaeogeographic area (Close et al., 2017).

Fixed cell quota

To account for variability in sampled palaeogeographic area, CR is implemented with a grid cell rarefaction (GCR) procedure in this study (e.g. Close et al., 2020a). GCR randomly samples a fixed quota of occupied cells (cells containing fossil occurrences) to provide a spatially-standardised sampling pool from which to draw occurrences. Here, equal-area grid cells (250 km spacing) are used for GCR, with cell quotas of 4, 6, and 8 (GCR_4, GCR_6, and GCR_8) for each palaeolatitudinal band (1,000 subsampling trials). Equal-area grid cells (250 km spacings) were generated using the R package 'dggridR' ver. 0.1.12 (Barnes et al., 2017), and CR was implemented using the function estimateD() from the R package 'iNEXT' (Hsieh et al., 2016), rarefying by collections for each GCR subsampling trial. The sampling-standardisation procedure used here conducts CR via the equations of Chao & Jost (2012), and also provides extrapolated richness estimates based on the Chao1 estimator. Following recommendations in Hsieh et al. (2016), extrapolated richness estimates were limited to no more than twice the reference sample size in this study, as estimates exceeding this limit suggest a high

species-to-occurrence count ratio, indicating the focus bin is likely to be under-sampled. Reported values for palaeolatitudinal bins are the median value across subsampling trials, with 95% quantiles also provided.

Variable cell quota

As a higher level of sampling is likely to be more representative of the genuine latitudinal distribution of biodiversity, the number of occupied equal-area cells within each latitudinal band was calculated for each temporal bin. Using these data, a second set of richness estimates was generated for each temporal bin based on the minimum number of occupied equal-area cells across latitudinal bands. These analyses followed the same protocols outlined above ('Fixed cell quota'), except that a variable cell quota was used for each temporal bin (GCR_{min}; the minimum number of occupied cells across latitudinal bands). After initial data exploration, analyses were restricted to the two best sampled latitudinal bands to allow reconstruction of tropical and temperate biodiversity patterns at higher cell quotas: (1) 0–30°N; and (2) 30–60°N. Whilst this approach standardises sampled area between palaeolatitudinal bins, it is likely inappropriate for assessing latitudinal trends between temporal bins due to varying levels in spatial sampling patterns. However, maximising the number of occupied equal-area cells within temporal bins allows for higher confidence in observed latitudinal biodiversity patterns.

5.3 Results

5.3.1 Palaeolatitudinal sampling and biodiversity patterns

Palaeolatitudinal analyses highlight poor global fossil sampling coverage, with 2,587 collections reported for the Northern Hemisphere, and just 534 for its southern counterpart (Figure 5.2). Local richness estimates (alpha diversity) indicate that the distribution of latitudinal biodiversity has varied substantially along the studied time series (Figure 5.2). The generalized additive model of the absolute palaeolatitudinal position of collections (weighted by genus richness) with time suggest a low palaeolatitudinal distribution of biodiversity in the Middle Triassic, shifting to a more

poleward distribution by the end-Triassic (Figure 5.2). A subsequent long-term equatorward shift from the end-Triassic towards the Early Cretaceous is identified, followed by a poleward shift in the mid-Cretaceous, and eventual equatorward shift in the Late Cretaceous (Figure 5.2). The latitudinal distribution of biodiversity shifts poleward again during the mid-Paleogene, before a sharp equatorward shift towards the present day (Figure 5.2). Notably, the most poleward distribution obtained by Z-corals during their evolutionary history was at the end-Triassic, at a palaeolatitude of 61.24°N (Figure 5.2).

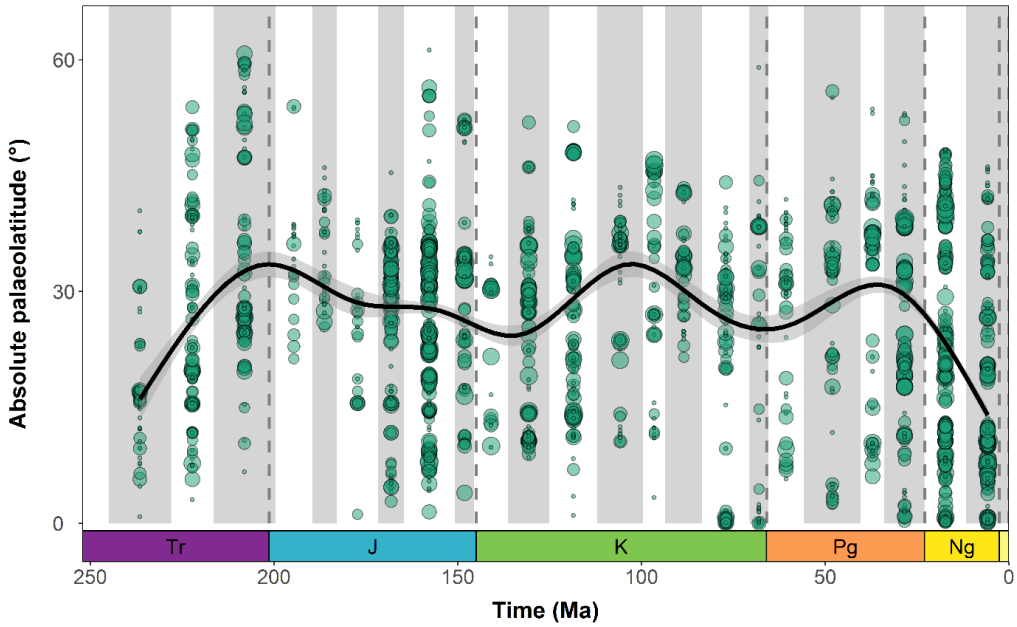


Figure 5.2. Absolute palaeolatitudinal distribution of fossil zooxanthellate coral bearing collections (Anisian to Piacenzian). The size of points is proportional to the logarithm of genus richness in each collection. Vertical grey/white shaded boxes illustrate each ~10 million-year time bin, whereas vertical dashed lines represent the start/end of a geological period. Generalized additive model smooth (black line), weighted by genus richness within collections, highlights the general trends across the time series. The black ribbon depicts the associated 95% confidence intervals of the generalized additive model.

Face-value counts of genera track proxies of sampling along the entire studied time series, with richness and sampling concentrated in Northern Hemisphere palaeolatitudinal bins (Figure 5.3–Figure 5.4). Linear regression analyses supports this observation with a high percentage of the variance in genus richness explained by sampling proxies (Figure 5.5): collections ($R^2 = 0.76$, $P < 0.001$); formations ($R^2 = 0.69$, $P < 0.001$); occupied equal-area grid cells ($R^2 = 0.77$, $P < 0.001$); and summed MST length ($R^2 = 0.39$, $P < 0.001$). Notably, there is a strong peak in the number of

collections during the Late Jurassic (Jr5), and towards the Recent in all palaeolatitudinal bins, with the exception of 30–60°S (Figure 5.3). The number of formations and occupied equal-area grid cells show similar temporal trends to collections (Figure 5.3). However, results from summed MST length show significant variability along the time series, and less agreement with genus counts than other sampling proxies (Figure 5.3–Figure 5.5). More specifically, summed MST length results suggest that the palaeogeographic spread of fossil sampling localities is heterogeneous through time and space (Figure 5.4). Palaeogeographic spread in sampling is particularly low during the Early Jurassic (J1–J2), and for K6 (early Late Cretaceous) for 0–30°N. However, the palaeogeographic spread in sampling is only notably low during the earliest Cretaceous (K1) for 30–60°N.

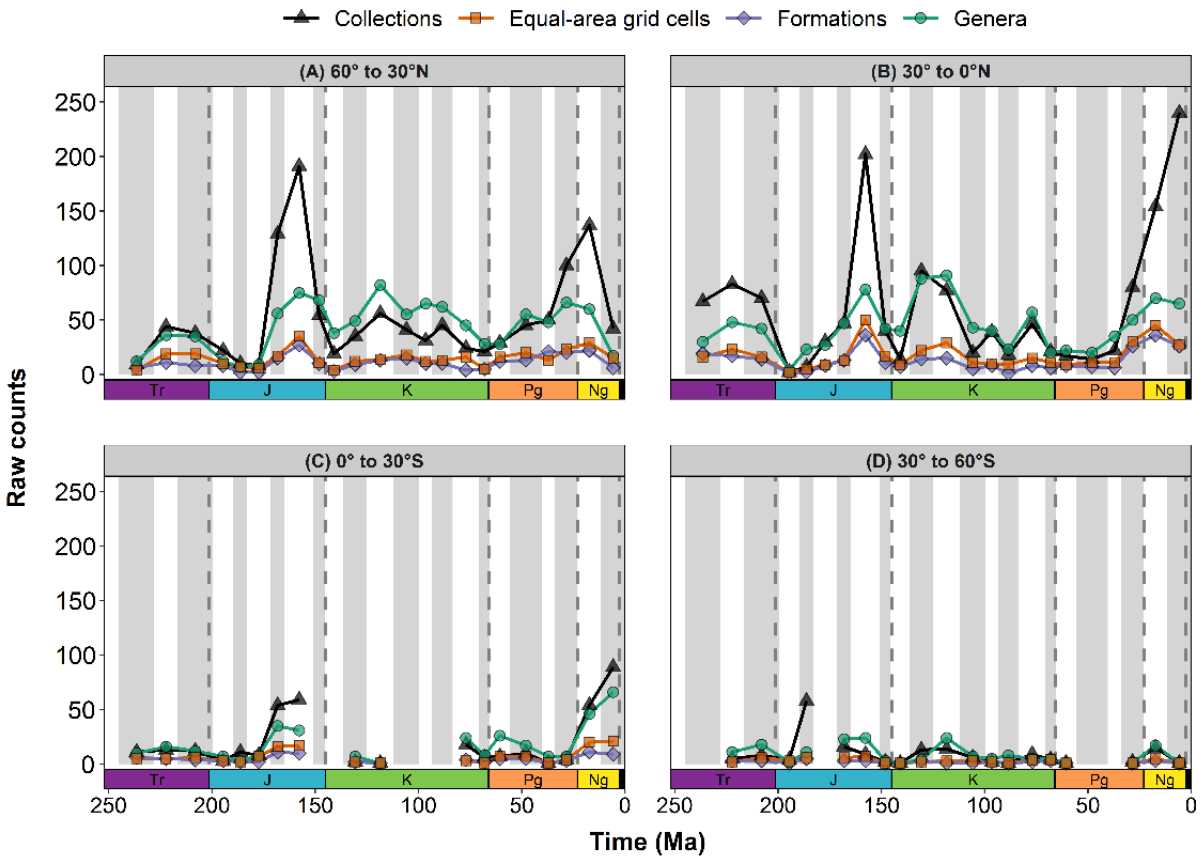


Figure 5.3. Raw counts of genera, collections, formations, and occupied equal-area grid cells (250 km spacings), within palaeolatitudinal and ~10 million-year time bins. (A) 30–60°N; (B) 0–30°N; (C) 0–30°S; and (D) 30–60°S. Palaeolatitudinal bins 60–90°N and 60–90°S are not depicted as virtually no data is available across the entire time series. For enhanced clarity, points with values of zero are not displayed within plots. Vertical grey/white shaded boxes illustrate each ~10 million-year time bin, whereas vertical dashed lines represent the start/end of a geological period.

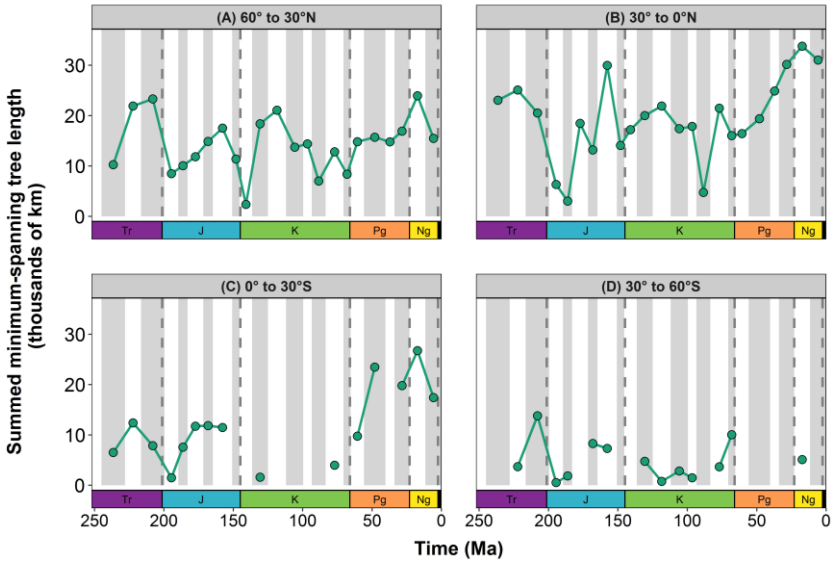


Figure 5.4. Summed minimum-spanning tree length between occupied equal-area grid cells (250 km spacings) within palaeolatitudinal, and ~10 million-year time bins. (A) 30–60°N; (B) 0–30°N; (C) 0–30°S; and (D) 30–60°S. Palaeolatitudinal bins 60–90°N and 60–90°S are not depicted as almost no data is available across the entire time series. For enhanced clarity, points with values of zero are not displayed within plots. Vertical grey/white shaded boxes illustrate each ~10 million-year time bin, whereas vertical dashed lines represent the start/end of a geological period.

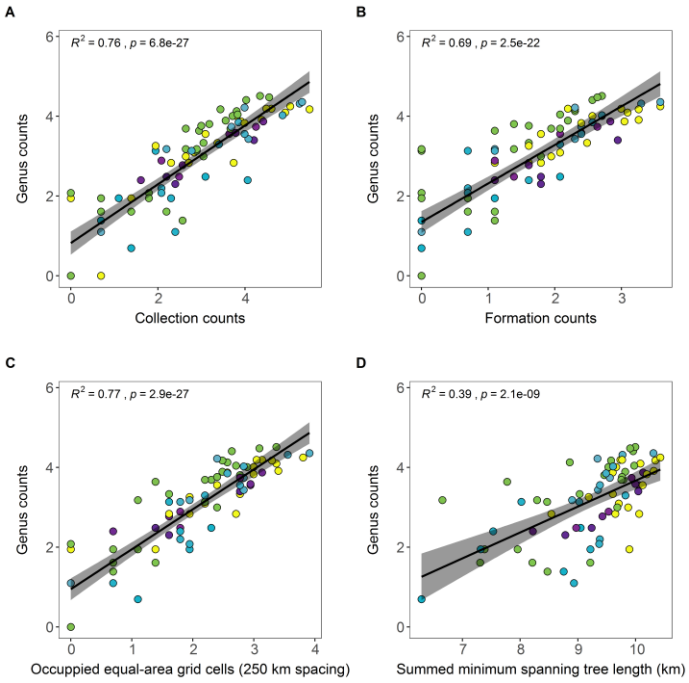


Figure 5.5. Relationship between uncorrected genus richness and sampling per palaeolatitudinal and temporal bin. (A) Relationship between genus counts and collection counts; (B) genus counts and formation counts; (C) genus counts and occupied equal-area grid cells (250 km spacings); and (D) genus counts and the summed minimum spanning tree length. Coefficient of determination (R^2) between variables is depicted in each plot, along with associated P-values. Black line depicts the line of regression from linear modelling, with the black ribbon indicating the 95% confidence interval. Colour of points is in accordance with the geological timescale of time bins: Triassic (purple); Jurassic (blue); Cretaceous (green); and Cenozoic (yellow).

Palaeolatitudinal face-value counts of genera tend to track sampling proxies along the entire studied time series (Figure 5.3 and Figure 5.5). As such, observed trends are discussed in brief here, under the proviso that raw counts are likely misleading and a function of heterogeneity in sampling regimes. The uncorrected fossil record indicates Z-corals maintained variable levels of tropical and temperate biodiversity throughout their evolutionary history, with instances of both tropical and temperate peaks in biodiversity identified along the time series (Figure 5.3). Across the Triassic/Jurassic boundary, generic diversity was reduced to near-zero in all palaeolatitudinal bins, though northern temperate palaeolatitudes (30–60°N) maintained relatively higher levels of biodiversity. Low Z-coral biodiversity was maintained in all palaeolatitudinal bins for most of the Early Jurassic, until richness increased during the Middle–Late Jurassic. However, a subsequent loss in generic diversity occurred across the Jurassic/Cretaceous boundary for all palaeolatitudinal bins (Figure 5.3). Nevertheless, the Early Cretaceous (K3) hosted the maximum generic diversity for both Northern Hemisphere temperate (30–60°N) and tropical (0–30°N) palaeolatitudinal bins across the entire time series. A subsequent long-term decline in genus richness occurred in these latitudinal bins towards the Cretaceous/Paleogene boundary, before increasing again towards the Recent. However, a prominent decline in Northern Hemisphere temperate (30–60°N) generic diversity is identified in the Neogene (Figure 5.3), while a concurrent increase in Southern Hemisphere tropical (0–30°S) diversity is observed towards the Recent (Figure 5.3).

5.3.2 Sampling-standardised richness estimates

Coverage-standardised richness estimates, implemented with GCR and a fixed cell quota ($GCR_{4–8}$), demonstrate the influence of variable spatial sampling on palaeolatitudinal trends in biodiversity (Figure 5.6). For example, under GCR_4, a minor decline in generic richness is observed across the Jurassic/Cretaceous boundary for both 0–30°N and 30–60°N (Figure 5.6). However, at higher cell quotas (GCR_6 and GCR_8), there is a prolific increase in Northern Hemisphere tropical (0–30°N) biodiversity across the boundary, while richness estimates could not be recovered for

its temperate (30–60°N) counterpart (Figure 5.6). Furthermore, after standardising for spatial sampling at higher cell quotas (GCR_6 and GCR_8), the earliest Cretaceous (K1) is recovered as the tropical peak in generic diversity across the entire time series, before declining towards the Late Cretaceous (Figure 5.6). Conversely, the K2 time bin maintains low generic richness at temperate latitudes (30–60°N), increasing towards the middle Cretaceous (K3–K5). Notably, under GCR_8, high diversity is maintained until the K7 time bin at 30–60°N (Figure 5.6). Conversely, under GCR_4 and GCR_6, estimated genus richness declines from the middle Cretaceous (K5) towards the end-Cretaceous.

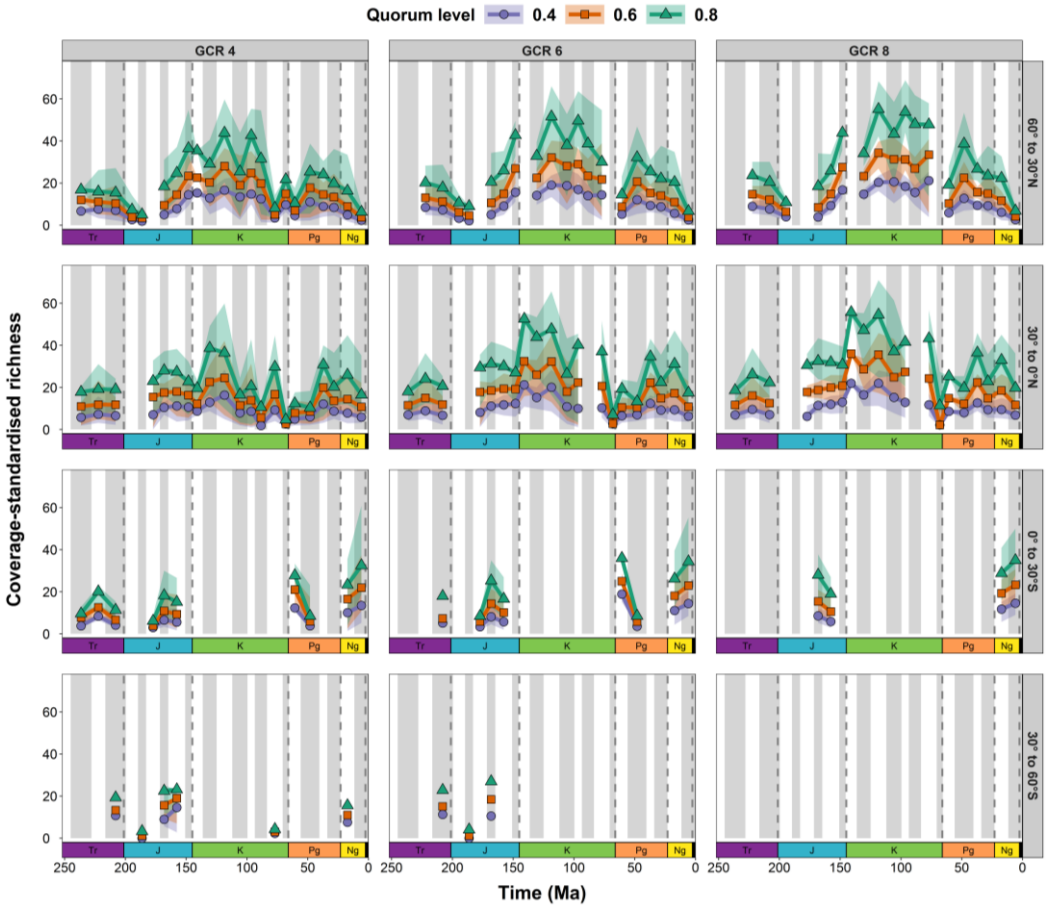


Figure 5.6. Coverage-standardised richness estimates implemented with a fixed grid cell rarefaction procedure (GCR). Estimates were computed within palaeolatitudinal and ~10 million-year time bins. Occupied equal-area grid cells (250 km spacings) were randomly sampled at a cell quota of 4 (left column), 6 (central column), and 8 (right column) for 1,000 subsampling GCR trials. Points indicate the median richness estimate across subsampling trials, and the ribbons depict the 95% quantile. Palaeolatitudinal bins (first row) 30–60°N; (second row) 0–30°N; (third row) 0–30°S; and (fourth row) 30–60°S are shown, but 60–90°N and 60–90°S are excluded as almost no data is available across the entire time series. Vertical grey/white shaded boxes illustrate each ~10 million-year time bin, whereas vertical dashed lines represent the start/end of a geological period.

Variable spatial sampling (number of occupied equal-area grid cells) prevents the computation of richness estimates for the majority of Southern Hemisphere latitudinal bins (Figure 5.6). However, richness estimates could also not be generated for some Northern Hemisphere latitudinal bins, such as 0–30°N during the Early Jurassic (J1–J2). This is due to only two occupied equal-area cells being sampled in temporal bin J1 for 0–30°N, and J2 exceeding the extrapolation limit of two times the reference sample. Nevertheless, some general palaeolatitudinal trends can be observed across the time series when focusing on 0–30°N and 30–60°N. From their origin in the Anisian (Middle Triassic), Z-corals appear to maintain similar levels of generic richness in both 0–30°N and 30–60°N latitudinal bins throughout the Triassic (Figure 5.6). Across the Triassic/Jurassic boundary, Z-coral diversity declines at temperate latitudes (30–60°N). However, the lack of estimates for 0–30°N prevents identification of any similar patterns in this latitudinal bin (Figure 5.6). During the Middle–Late Jurassic, generic richness was fairly stable within tropical latitudes (0–30°N), but prolifically increased at temperate latitudes (30–60°N) towards the Late Jurassic. Estimates could not be obtained at higher cell quotas, but GCR_4 suggests that temperate diversity declined across the Jurassic/Cretaceous boundary for temperate latitudes (30–60°N), with a similar decline at tropical latitudes (0–30°N) under GCR_4 (Figure 5.6). However, this is a product of the low cell quota, with a sharp increase in generic richness for tropical latitudes observed at higher cell quotas (GCR_6 and GCR_8). A subsequent long-term decline towards the Late Cretaceous occurs in tropical latitudes (0–30°N), whereas temperate richness (30–60°N) peaks in the middle Cretaceous, before also declining towards the latest Cretaceous (Figure 5.6). However, this long-term decline seems to extend towards the Recent at temperate latitudes (after a brief deviation in Cn2), whereas tropical generic richness rebounds after the Cretaceous/Paleogene boundary (Pg1), and maintains relatively constant levels of diversity towards the Recent (Figure 5.6).

Coverage-standardised richness estimates, implemented with GCR and a minimum cell quota (GCR_{min}), provide insight into the relative latitudinal biodiversity patterns

within temporal bins. However, they do not inherently provide a temporal perspective of shifts in latitudinal biodiversity patterns due to varying levels of spatial sampling between temporal bins. Nevertheless, results from GCR_{min} largely echo those from fixed cell quotas ($GCR_{4–8}$), though several differences are noteworthy. For example, after standardising by the minimum number of occupied cells, richness estimates are obtainable for the earliest Jurassic (J1) in both tropical (0–30°N) and temperate (30–60°N) latitudinal bins (Figure 5.7). These diversity estimates suggest that generic richness was low in both latitudinal bins, with the tropics (0–30°N) slightly more diverse. Although GCR_{min} allows the attainment of richness estimates for some bins previously lacking estimates (low number of occupied equal-area grid cells), it also results in some bins not being represented (e.g. K4 in 0–30°N) due to extrapolated estimates exceeding two times the reference sample (Figure 5.7). This suggests a high species-to-occurrence count ratio for these bins, and that they are likely under-sampled.

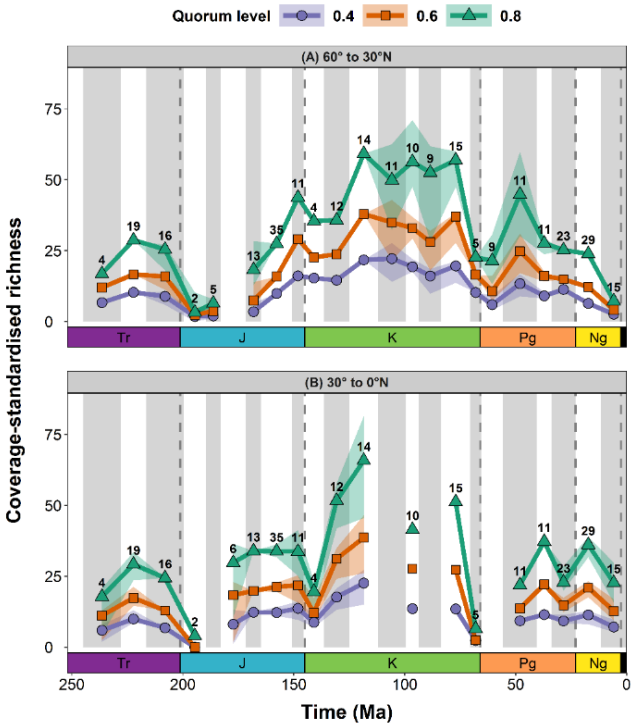


Figure 5.7. Coverage-standardised richness estimates implemented with a minimum grid cell rarefaction procedure (GCR_{min}). Estimates were computed within palaeolatitudinal and ~10 million-year time bins. Occupied equal-area grid cells (250 km spacings) were randomly sampled at the minimum cell quota for 1,000 trials, with coverage-standardised richness estimates computed for each. Points indicate the median value across estimates, and the ribbon depicts the 95% quantile. Numbers within plots indicate the GCR_{min} cell quota for respective time bins. Vertical shaded boxes illustrate each ~10 million-year time bin, whereas black dashed lines represent the start/end of a geological period.

Direct comparison of uncorrected tropical (0–30°N) and temperate (30–60°N) diversity in the Northern Hemisphere (best sampled bins) indicate prominent tropical peaks in generic richness are restricted to the Neogene (Cn6), and the Early Cretaceous (K2) (Figure 5.8). After standardising for spatial sampling heterogeneity, these general trends are supported, though an earlier onset of the present-day LBG is identified (Cn5–Cn6) (Figure 5.8). A prominent increase in tropical diversity (0–30°N) in the earliest Cretaceous is also observed (K1). However, the lack of available estimates for the temperate bin (30–60°N), prevents direct comparison (Figure 5.8). Furthermore, the Middle Jurassic (Jr4) latitudinal gradient is also marked by a tropical peak in diversity, declining poleward. However, for most of the time series, the latitudinal biodiversity gradient of Z-corals is either relatively flat (e.g. end-Triassic; Tr3–Tr4) or characterised by temperate peaks in diversity (e.g. Jr6).

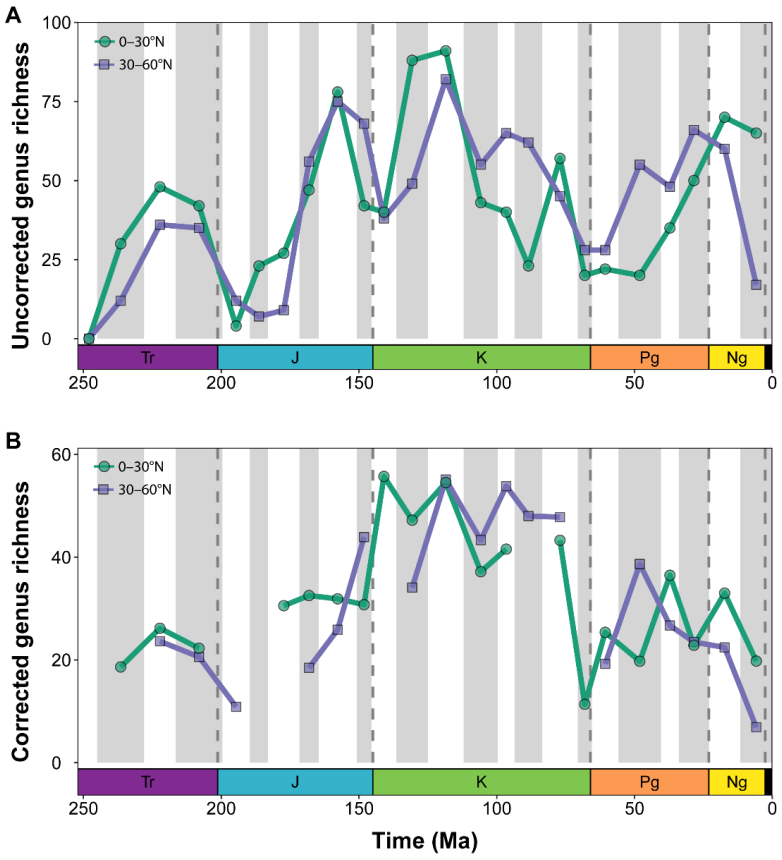


Figure 5.8. Comparison plot of (A) uncorrected and (B) corrected tropical (0–30°N) and temperate (30–60°N) diversity. Estimates were computed within palaeolatitudinal and ~10 million-year time bins. (A) Points indicate the raw counts of genus richness; (B) points indicate sampling-standardised richness estimates (GCR_8; quorum level = 0.8). Vertical shaded boxes illustrate each ~10 million-year time bin, whereas black dashed lines represent the start/end of a geological period

Linear regression analyses indicate a largely decoupled relationship between genus richness estimates (GCR_4 and quorum level 0.6) and sampling proxies after implementing the sampling-standardisation protocol of this study (Figure 5.9): collections ($R^2 = 0.076$, $P = 0.035$); formations ($R^2 = 0.17$, $P = 0.0013$); occupied equal-area grid cells ($R^2 = 0.085$, $P = 0.025$); and MST ($R^2 = 0.14$, $P = 0.0039$). Coefficient of determination (R^2) values minorly vary between richness estimates based on different GCR cell quotas and quorum levels. However, the same overall trends are observed.

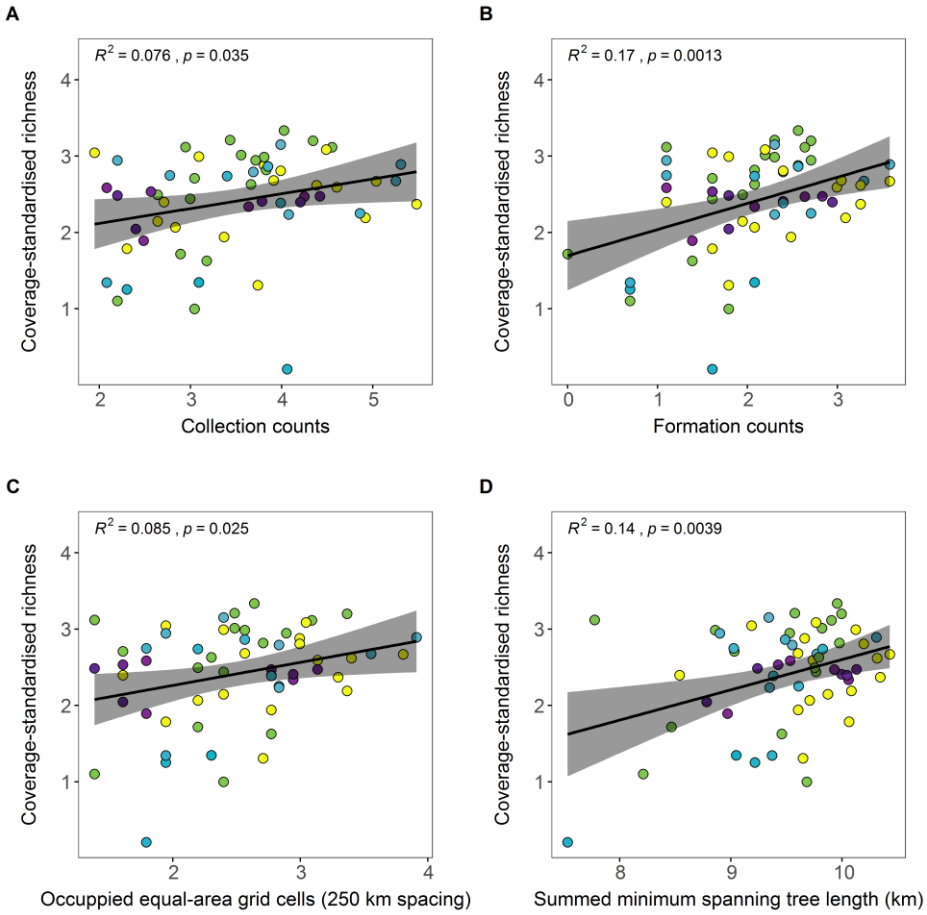


Figure 5.9. Relationship between sampling and coverage-standardised genus richness estimates (quorum level = 0.6), implemented with a grid cell (250 km spacings) rarefaction (GCR) procedure (cell quota = 4) per palaeolatitudinal and temporal bin. (A) Relationship between genus richness estimates and collection counts; (B) genus richness estimates and formation counts; (C) genus richness estimates and occupied equal-area grid cells (250 km spacings); and (D) genus richness estimates and the summed minimum spanning tree length. Coefficient of determination (R^2) between variables is depicted in each plot, along with associated P-values. Black line depicts the line of regression from linear modelling, with the black ribbon indicating the 95% confidence interval. Colour of points is in accordance with the geological timescale of time bins: Triassic (purple); Jurassic (blue); Cretaceous (green); and Cenozoic (yellow).

5.4 Discussion

The impact of sampling bias on the reconstruction of deep time biodiversity patterns has long been recognised as an issue (Alroy, 2010a; Mannion et al., 2012; Kiessling et al., 2012; Nicholson et al., 2016; Cleary et al., 2018; Close et al., 2018; Dunne et al., 2018; De Celis et al., 2020). To account for these biases, previous studies have tended to rarefy by sampling units (i.e. occurrences or collections) to provide fairer estimates of relative richness ratios (Raup, 1975; Kiessling et al., 2012; Alroy, 2014; Mannion et al., 2015; Cleary et al., 2018; Dunne et al., 2018). However, many previous studies have failed to account for the variability in sampled palaeogeographic area, which has the potential to strongly bias our understanding of deep time biodiversity trends via the empirical species-area relationship (although see recent work by Close et al., 2017, 2020a, 2020b). The results from the current study demonstrate that raw genus counts are heavily influenced by not only the number of collections and formations, but also the palaeogeographic spread of sampling (summed MST length) and sampled palaeogeographic area (Figure 5.5). In fact, the observed variation in sampled area (number of occupied equal-area cells) accounts for 77% of the variation in raw genus counts, while changes in the spread of sampling account for 39% of the variance in genus counts (Figure 5.5). This finding is in agreement with recent work focused on global biodiversity patterns within both the terrestrial and marine realm (Close et al., 2020a, 2020b). Over the entire time series, sampling regimes vary considerably with no apparent long-term trend identified. However, a clear peak in the number of collections, formations, and occupied equal-area cells is observed during the Late Jurassic (Jr5) and towards the Recent (Cn4–6). Similar prominent peaks are observed for the palaeogeographic spread of sampling (summed MST length) for 0–30°N, but are less apparent at 30–60°N (Figure 5.4).

Standardising richness estimates to a uniformly sampled palaeogeographic area demonstrates the impact of variable spatial sampling on observed temporal and spatial biodiversity patterns (Figure 5.6). For example, after standardising the sampled palaeogeographic area, the minor decline observed in tropical diversity (0–30°N) across

the Jurassic/Cretaceous boundary is computed as a major increase in relative diversity (Figure 5.8). However, this observation is limited to higher grid cell rarefaction (GCR) cell quotas (GCR_6 and GCR_8), with GCR_4 instead producing a tropical decline (0–30°N) across the Jurassic/Cretaceous boundary (Figure 5.6). This highlights the significance of differences in the richness-sample accumulation curve between bins, indicating richness estimates might be less reliable before reaching the asymptote of the curve. Nevertheless, after implementing coverage-based rarefaction with a GCR procedure, estimates of generic richness were largely decoupled from sampling proxies with all of them explaining less than 20% of the observed variance in diversity.

By contrast to the unimodal-type ('modern-type') latitudinal biodiversity gradient (LBG) observed in zooxanthellate corals (Z-corals) today, sampling-standardised richness estimates suggest that flat-type gradients and temperate peaks in diversity, were maintained for most of Z-corals' evolutionary history. The steep unimodal-type LBG observed today in zooxanthellate corals appears to only have originated during the Neogene (Cn5–Cn6), as a result of temperate (30–60°N) declines in biodiversity (Figure 5.6–Figure 5.8), as well as increases in Southern Hemisphere tropical diversity (0–30°S). This finding is supported by results from local richness estimates (Figure 5.2), and is in agreement with a number of previous studies in both the terrestrial and marine realm (Crame and Rosen, 2002; Rex et al., 2005; Alroy et al., 2008; Yasuhara et al., 2012; Marcot et al., 2016; Spano et al., 2016; Meseguer and Condamine, 2020; Close et al., 2020b). However, some studies have advocated for an earlier onset of this steepening, in the early Cenozoic (Fenton et al., 2016; Crame, 2020). A unimodal-type LBG also likely persisted during the first ~20 myr of the Cretaceous (K1–K2) (Figure 5.6 and Figure 5.8). However, the lack of temperate (30–60°N) richness estimates for the earliest Cretaceous (K1) prevents comparison with tropical bins. A second potential unimodal-type LBG occurs in the Middle Jurassic (Jr4) (Figure 5.6 and Figure 5.8). Whilst these intervals are not characterised by sustained 'icehouse' conditions, Middle Jurassic and earliest Cretaceous stages have previously been interpreted as intervals experiencing brief 'cold snaps' (Hallam et al., 1991; Gröcke et al., 2003; Royer, 2004),

with the Early Cretaceous occasionally referred to as a 'cool greenhouse' (Hay and Floegel, 2012). Previous studies have also found ammonites were most diverse around 20–30°N throughout the Jurassic and Early Cretaceous (Cecca et al., 2005), while brachiopods were marked by a temperate decline in diversity across the Jurassic/Cretaceous boundary (Powell, 2009; Powell et al., 2015).

Unimodal-type ('modern-type') latitudinal biodiversity gradients, with tropical peaks in diversity, have been suggested to form under cold icehouse climate regimes, whereas temperate peaks in diversity or flattened gradients are restricted to warmer greenhouse climate phases (Mannion et al., 2014). It has also been proposed that non-unimodal-type LBGs might also form during interglacials (e.g. Kiessling et al., 2012; Yasuhara et al., 2012; Mannion et al., 2014). However, the work presented in Chapter 3 suggests that previously observed tropical declines during interglacials might be a result of data absence. Nevertheless, the results presented in this study support the proposal that unimodal-type LBGs primarily form under icehouse climate regimes, whereas greenhouse climate phases are characterised by different gradients. However, based on sampling-standardised richness estimates for the Middle Jurassic and Early Cretaceous, this study's results suggest that geologically long-lived 'cold-snaps' might also result in unimodal-type LBGs. Nevertheless, recent work has suggested a somewhat contrarian view, and suggested environmental stability, not climate per se, may be one of the biggest drivers of unimodal-type LBGs (Song et al., 2020). Despite this, difficulty remains in establishing whether the temporal duration of interglacial/glacial cycles is sufficient to not only allow for the spatial reorganisation of diversity, but also to preserve such novel patterns through the accumulation of fossil material.

Whilst this study aims to provide fairer estimates of past Z-coral biodiversity patterns by correcting for spatial sampling biases, this is complicated by the interdependent nature of Earth System processes (Hannisdal and Peters, 2011; Close et al., 2017). Observed relationships between raw genus counts and sampling proxies (formations, collections, occupied equal-area cells, and summed MST length) might be the result of

bias in sampling regimes, with observed biodiversity trends driven purely by uneven spatial sampling. However, the observed relationships between raw genus counts and sampling proxies might also be due to 'common cause', in which Earth System processes (e.g. sea level change) determine the sampling opportunities available within a region (Peters, 2005; Butler et al., 2010; Hannisdal and Peters, 2011; Dunhill et al., 2014). In particular, the palaeogeographic spread of fossil occurrences, as well as the area occupied might be a genuine biological signal. As such, standardisation of spatial sampling could plausibly result in the removal of vital information for understanding past biodiversity patterns. Given the paucity of fossil data, and the intrinsic incompleteness of the fossil record, sole dependence on subsampling approaches to provide understanding of past biodiversity patterns is likely limited.

5.5 Summary

The results presented in this chapter suggest that the latitudinal biodiversity gradient of zooxanthellate corals was relatively flat, or characterised by temperate peaks in biodiversity, for most of their evolutionary history. Nevertheless, unimodal-type latitudinal biodiversity gradients are observed during 'cold-snap' intervals during the Middle Jurassic and Early Cretaceous. This study's findings agree with previous work that suggest the latitudinal biodiversity gradient became significantly steeper only in the last 20 million years, following the onset of 'icehouse' conditions. These results demonstrate that despite major changes in the Earth's climate over the past 250 million years, strong unimodal-type LBGs might be a relatively rare phenomenon that are primarily restricted to icehouse climate regimes. The sampling-standardisation protocol implemented in this study provides richness estimates decoupled from sampling biases. However, as is often the case with palaeobiological studies, determining conclusively whether observed trends reflect a true biological signal, or are the result of heterogeneous spatial sampling, is difficult. In the specific context of sampled palaeogeographic area, deciphering whether spatial and temporal variability in sampled area reflects varying levels of sampling effort, or just broader areas colonised by a specific taxon remains a significant challenge to palaeobiologists.

–This page is intentionally left blank–

6 Modelling the latitudinal distribution of reef habitat

Disclosure: Some of the content reported in this chapter is in review at *Nature Communications*. While the primary author wrote most of this text, contribution by the co-authors of this study are contained in this chapter, as well as the input received from the peer review process. The relevant text, revised below, is from: Jones, L. A., Mannion, P.D. Farnsworth, A., Lunt, D.J. (in review). Climate and palaeogeography shaped the evolutionary history of the latitudinal biodiversity gradient of corals. *Nature Communications*.

OVERVIEW

Warm-water coral reefs support the world's greatest biodiversity of marine organisms. The spatial distribution of these 'rainforests of the sea' explains the latitudinal and longitudinal biodiversity gradients observed in many reef-associated groups. Today, warm-water corals are limited to tropical and sub-tropical latitudes, restricted to approximately 30–35° either side of the equator. However, the geological record suggests these high biodiversity habitats had less tropically skewed distributions in the past, and maintained more poleward distributions. Consequently, the latitudinal distribution of reef-associated organisms likely tracked any shifts in their available habitat. Whilst the observed poleward extension in the past distribution of coral reefs is irrefutable, geographic sampling bias might be responsible for the underrepresentation of these habitats–and their associated biodiversity–within tropical latitudes. Here, ecological niche modelling and Earth System Modelling is combined to estimate the potential geographic distribution of warm-water coral reefs over the last ~250 million years. Using models of suitable habitat area through time, inference is made about the potential palaeolatitudinal distribution of biodiversity through time on the basis of the ubiquitous scaling of species richness with area. Model projections suggest that suitable habitat area was only strongly skewed towards tropical palaeolatitudes during the Early Cretaceous, and the last 30 million years. These results suggest that steep unimodal-type latitudinal biodiversity gradients were likely restricted to these time intervals. A temperate peak and tropical decline in reef-associated organisms might have been present during the Early Jurassic based on the palaeolatitudinal distribution of estimated suitable habitat area. However, the palaeolatitudinal gradient of suitable area was relatively flat throughout much of the last ~250 million years, suggesting that the palaeolatitudinal distribution of biodiversity might have been characterised by a similar gradient. Despite the relationship between estimated suitable habitat area and taxonomic richness being demonstrated for the modern, challenges remain in applying such approaches to deep time systems.

6.1 Introduction

Despite covering less than 0.1% of the world's oceans (Spalding and Grenfell, 1997), warm-water coral reefs are one of the most biologically diverse and economically valuable ecosystems on Earth (Moberg and Folke, 1999). In fact, tropical reefs support the world's greatest biodiversity of marine organisms (Roberts et al., 2002), with estimates of up to 35% of all described marine species depending on coral reefs (Reaka-Kudla, 2005; Knowlton et al., 2010). Today, these coral reefs are limited to tropical and subtropical latitudes (~34°N–32°S) (Johannes et al., 1983; Kleypas et al., 1999; Kiessling, 2001b), with the most poleward reef (33.48°N) found at Iki Island, off the southwest coast of Japan (Yamano et al., 2001). Reef growth is highly efficient in warmer tropical waters, but warm-water coral reefs become increasingly marginal at lower sea surface temperatures (and higher latitudes), with 16°C generally considered the minimum temperature extreme (Kleypas et al., 1999; Bellwood and Hughes, 2001). Consequently, many reef-associated groups, such as zooxanthellate corals and coral reef fishes, peak in diversity at tropical latitudes (Kiessling et al., 2012; Siqueira et al., 2016; Rabosky et al., 2018). However, a steep longitudinal biodiversity gradient also exists for many shallow-marine organisms today, with a global hotspot in biodiversity within the Indo-Australian Archipelago (Roberts et al., 2002; Briggs, 2007; Renema et al., 2008). Whilst climate appears to shape the latitudinal biodiversity gradient in reef-associated organisms today, the observed longitudinal biodiversity gradient is best explained by the distribution of shallow marine substrate (Briggs, 2007; Leprieur et al., 2016). This is important as climate and the distribution of shallow marine substrate has varied through geological time, yet both have the potential to shape biogeographic patterns. Similar to terrestrial organisms and land availability at tropical latitudes (e.g. Pellissier et al., 2017), if there is not sufficient suitable marine benthic substrate for marine taxa, the climatic conditions might be irrelevant for reef development. Therefore, univariate approaches are likely limited in their capacity to explain the evolution of global macroecological patterns, such as the latitudinal biodiversity gradient. It is the combination of multiple ecologically important variables that form

a 'Goldilocks Zone' for reef development, which in turn enable the accumulation of biodiversity within these habitats.

During periods of the Phanerozoic, coral reefs had less tropically dominated distributions, occupying palaeolatitudes as poleward as 46°N in the late Paleocene (Kiessling, 2001a). Given the dependence of many marine organisms on coral reef systems, shifts in the latitudinal distribution of reef habitat likely impacted upon the distribution of reef-associated organisms. In particular, variation in the distribution and size of reef habitat area might have shaped the latitudinal biodiversity gradient in deep time due to the ubiquitous scaling of species richness with area (MacArthur and Wilson, 1967; Connor and McCoy, 1979; Rosenzweig, 1995; Tittensor et al., 2010). Previous research has demonstrated a strong relationship between the biodiversity of reef fishes and corals with habitat availability for the present day (Bellwood and Hughes, 2001; Tittensor et al., 2010), and deep time studies have demonstrated the scaling of taxonomic richness with sampled area in the fossil record (Lagomarcino and Miller, 2012). However, inherent spatiotemporal biases in the sampling (e.g. variable geographic sampling) and preservation (e.g. erosion, burial and recycling of sedimentary packages) of fossil reef systems limits the evaluation of the palaeolatitudinal distribution of reef habitat in deep time (Kiessling, 2005).

Recent developments in Earth System Modelling are beginning to provide high-resolution spatially explicit climate and elevation data for the geological past (Markwick and Valdes, 2004; Farnsworth et al., 2019a, 2019b; Markwick, 2019; Haywood et al., 2019). When coupled with these data and (present day and fossil) occurrence datasets, ecological niche modelling (ENM) offers the opportunity to estimate the geographic distribution of a species (or habitat) through space and time. Significantly, these estimates of suitable habitat are less prone to the impacts of data absence, and can be used to test whether observed biodiversity patterns in deep time might be explained by variations in habitat size (e.g. Chiarenza et al., 2019). In this chapter, the potential distribution of warm-water coral reefs is estimated for the past ~250 million years (myr). To do so, an ENM was calibrated on the present-day

distribution of coral reefs and climate, and hindcast to stratigraphic stages from the Anisian (247.2 Ma) to the Piacenizan (2.58 Ma). Using these data, the palaeolatitudinal distribution of suitable habitat area was quantified to evaluate the potential for different types of latitudinal biodiversity gradients to form in deep time. The capacity of model projections to predict the distribution of observed fossil reef systems was also assessed, as well as the relationship between modern zooxanthellate corals diversity and estimated suitable habitat.

6.2 Methods

6.2.1 Occurrence data

Present day

The global distribution of warm-water coral reefs was downloaded from the United Nations Environment Programme (UNEP): World Conservation Monitoring Centre (http://www.data.unep-wcmc.org/datasets/1) on the 6th May 2020 (UNEP-WCMC et al., 2018). This dataset is currently the most comprehensive of its kind, and is compiled from multiple sources including the Millennium Coral Reef Mapping Project (~85% of the dataset), as well as the World Atlas of Coral Reefs (Spalding, 2001; IMaRS-USF and IRD, 2005; UNEP-WCMC et al., 2018). Notably, this dataset has been extensively validated by the UNEP World Conservation Monitoring Centre via field surveys and remote sensing (UNEP-WCMC et al., 2018). As the UNEP occurrence data is provided as shapefiles, it was converted to point occurrences in this study based on the reef geometry. This resulted in 46,453 point occurrences. Subsequently, these data were spatially subsampled at a resolution of 1° x 1°, resulting in the retention of 1,052 presence points. This did not affect the overall distribution of coral reefs, but prevented multiple records being excessively weighted during model calibration (Figure 6.1). The zooxanthellate coral dataset described in Chapter 3 was also used in this study to assess the relationship between predicted suitable habitat area and taxonomic richness (described further below).

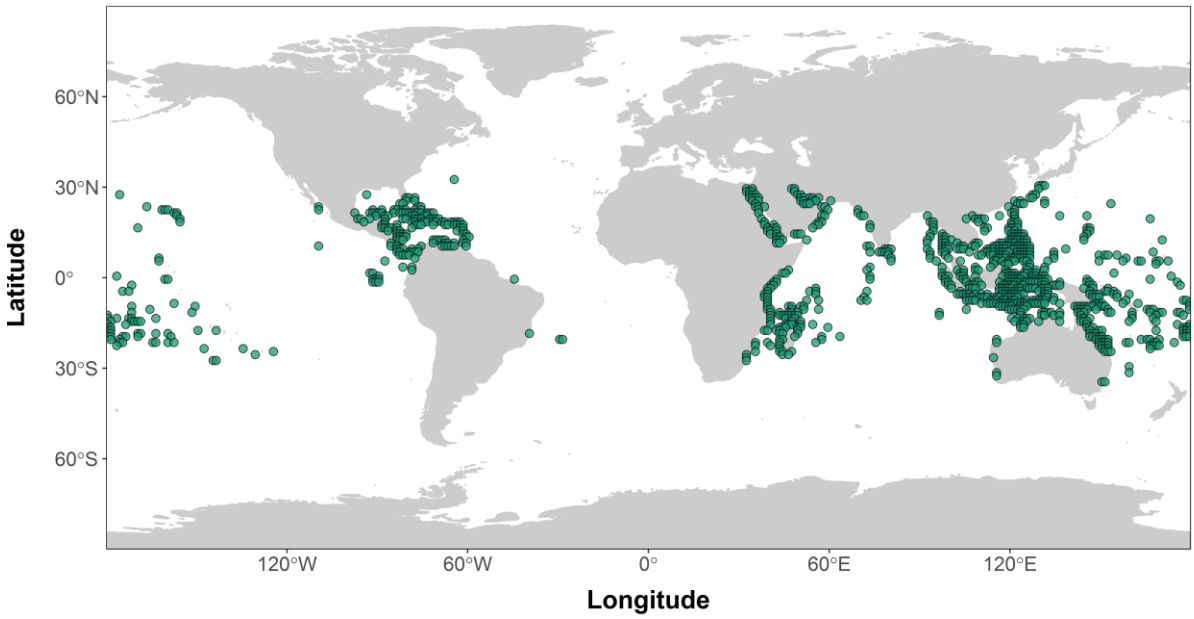


Figure 6.1. Global distribution of warm-water coral reefs during the present day. Distribution data is from the United Nations Environment Programme: World Conservation Monitoring Centre (https://www.data.unep-wcmc.org/datasets/1), and is spatially subsampled at a resolution of 1° x 1°. Data is projected in the coordinate reference system: World Geodetic System 1984 (WGS84).

Fossil

Fossil reef occurrence data were downloaded from the PaleoReef Database (accessible via: https://www.paleo-reefs.pal.uni-erlangen.de/) (Kiessling and Flügel, 2002) on the 6th May 2020. This database provides a range of data on fossil reef systems across the Phanerozoic, and currently contains geographical, geological and palaeontological information on more than 4,000 fossil reef sites. For this study, data on fossil coral reef systems from the Anisian (247.1 Ma) to Piacenzian (2.58 Ma) were extracted from the PaleoReef Database. Fossil reefs identified as cold-water coral reefs were removed from the dataset as these develop in fundamentally different environments to warm-water coral reefs. To increase data quality, fossil reef occurrence data not constrained to stratigraphic stage level were also removed from the dataset. Finally, to enable subsequent analyses, fossil reef occurrences were palaeorotated (based on modern coordinates) to their equivalent position in their binned stratigraphic stage. These rotations were achieved using the Getech PLC. plate model, following the methodologies of Markwick and Valdes (2004) and Markwick (2019). Significantly, this plate model is the basis for the palaeogeographic reconstructions used in palaeoclimate

and digital elevation modelling. The final dataset contains 375 occurrences across the Anisian–Piacenzian, though data quality is variable, with some stages and geographic areas containing no reported fossil coral reefs (Figure 6.2).

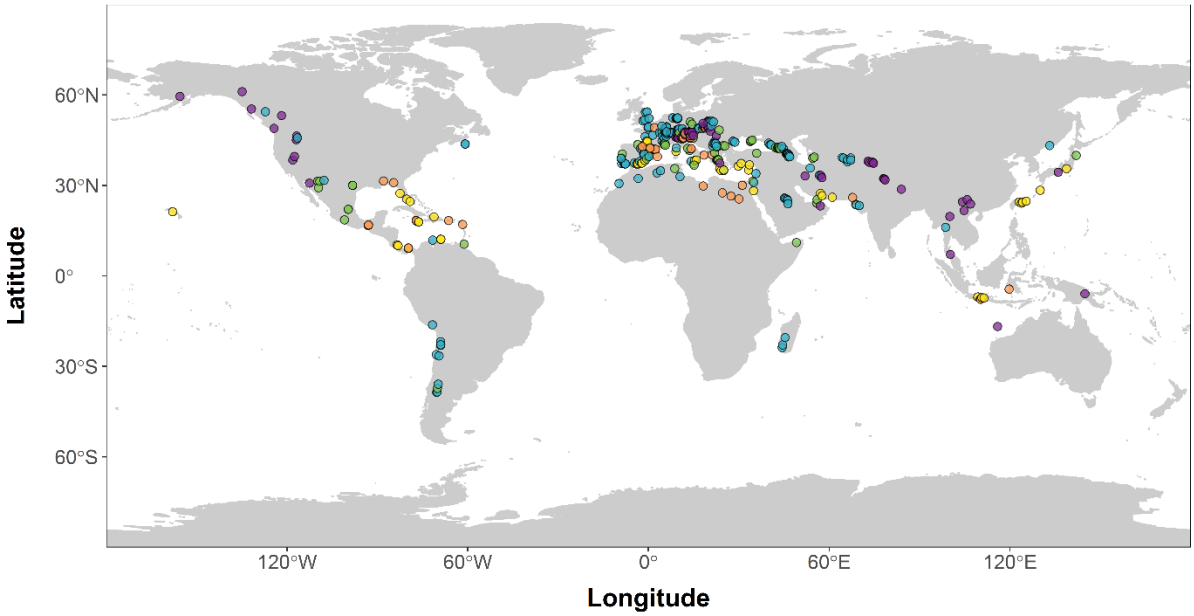


Figure 6.2. Global distribution of fossil (Anisian–Piacenzian) warm-water coral reefs occurrences used in this study. Distribution data is from the PaleoReef Database (https://www.paleo-reefs.pal.uni-erlangen.de/). Points represent the current geographic position of fossil reefs, and are coloured by their respective geological period of origin: Triassic (purple); Jurassic (blue); Cretaceous (green); Paleogene (orange); and Neogene (yellow). Note the concentration of reported reefs in European sites. Data is projected in the coordinate reference system: World Geodetic System 1984 (WGS84).

6.2.2 Environmental data

To estimate the potential distribution of warm-water coral reefs, four climate variables were used: August sea surface temperature (SST), February SST, August irradiance, and February irradiance. In general, these environmental variables are known to be limiting to the distribution of modern warm-water coral reefs (Kleypas et al., 1999; Veron, 2000; Couce et al., 2012), and can be viably determined for the geological past through palaeoclimatic modelling. Two monthly variables (August and February) of SST and irradiance were opted for as these represent seasonal hemispheric differences between the maximum and minimum annual values. Whilst additional variables, in particular aragonite saturation state (Kleypas et al., 1999), might be important for estimating distribution of warm-water coral reefs, not all variables can be viably

estimated for the geological past. Nevertheless, recent work has demonstrated that aragonite saturation state is of secondary significance when predicting the distribution of coral reefs (Couce et al., 2012), and several other studies have shown that geographic distributions can be reasonably approximated from a limited set of ecologically important variables (e.g. Kearney et al., 2010).

Climate variables for the present day (pre-industrial) and from the Anisian–Piacenzian, were derived from HadCM3BL-M2.1aE, a version of the HadCM3L atmosphere-ocean General Circulation Model (AOGCM) (Valdes et al., 2017). This particular AOGCM is equivalent to the heavily utilised HadCM3 model, but with a lower resolution ocean (Sheppard, 2003; IPCC, 2013; Saupe et al., 2014; Valdes et al., 2017). In addition, it has recently been used in a number of deep-time studies, including ecological modelling (Loptson et al., 2014; Marzocchi et al., 2015; Kennedy et al., 2015; Waterson et al., 2016; Chiarenza et al., 2019; Saupe et al., 2019a; Lyster et al., 2020). The HadCM3L has a horizontal resolution of 3.75° longitude x 2.5° latitude with a vertical resolution of 19 levels in the atmospheric component and 20 levels (5550 m depth) in the oceanic component (Valdes et al., 2017). Significantly, this version of HadCM3L utilises the Getech PLC digital elevation models (DEMs) as boundary conditions during simulations, providing spatially explicit data for when continent-configuration, topography and bathymetry were different from today. Palaeoclimate simulations were carried out for each geological stage between the Anisian and Piacenzian. For these simulations, the solar constant varies according to Gough (1981), and the CO_2 concentration is held constant from the Triassic to Eocene at 1,120 ppmv, decreasing to 560 ppmv during the Oligocene, 400 ppmv during the Miocene and early Pliocene, and finally 280 ppmv during the late Pliocene and pre-industrial. From the earliest Cretaceous to the Piacenzian, these simulations are identical to those described in Farnsworth et al. (2019a). Each simulation was run for 1,422 years. This is not long enough to reach full equilibrium, but it has been shown that the ocean circulation in the model does not substantially change after 1,422 years for the Cretaceous and Eocene simulations (Farnsworth et al., 2019b). Prior to the Cretaceous, only the

Kimmeridgian (Late Jurassic) simulation has been previously published (Armstrong et al., 2016). Further details on the HadCM3L climate model can be found in Valdes et al. (2017).

In this study, climate model data (pre-industrial and Anisian–Piacenzian) were downscaled to a horizontal resolution of 1° x 1° via bilinear interpolation. As warm-water coral reefs are restricted to the photic zone, a shallow-marine mask was used to clip all climate data. Shallow marine masks were generated for each time slice (pre-industrial and stratigraphic stages) based on bathymetric data from Getech's DEMs, which offer gridded representations of the Earth's topography and bathymetry. These DEMs are provided at a horizontal resolution of 0.1° x 0.1°, and have been used in a number of deep-time applications (e.g. Collins et al., 2018; Dean et al., 2019). To generate shallow marine masks, all DEMs were aggregated to a horizontal resolution of 1° x 1°, while preserving the minimum depth within each cell. This was done to prevent the loss of oceanic islands during the aggregation process. Subsequently, DEMs were clipped to retain only cells with a benthic substrate depth of 0–200 m. The extensive methods used to construct DEMs equivalent to those used in this study are described in Markwick and Valdes (2004), and Markwick (2019).

6.2.3 Ecological niche modelling algorithm

Ecological niche modelling (ENM) was implemented to estimate the global distribution of suitable habitats for warm-water coral reefs during the modern, and Anisian–Piacenizan stratigraphic stages. ENMs were generated using MaxEnt ver. 3.4.1 (Phillips et al., 2006, 2017), via the R package 'bimod2' ver. 3.3-7 (Thuiller et al., 2016). Specifically, this algorithm compares environmental combinations associated with known occurrences and randomly generated geographic points from the background extent (= 'background points') to create habitat suitability maps (Phillips et al., 2006). MaxEnt is a maximum entropy algorithm that has been shown to perform particularly well in previous studies utilising the fossil record (Saupe et al., 2014, 2019a; Waterson et al., 2016; Chiarenza et al., 2019; Jones et al., 2019). The ENM in this

study was calibrated using present-day coral reef occurrences and environmental conditions. The model was subsequently spatially projected ('hindcast') onto stage-level environmental conditions. To generate the ENM, 100 subsample replicates were used, with 20% of occurrences (randomly seeded) reserved for model testing. Multivariate environmental similarity surface (MESS) analyses (Elith et al., 2010) were used to identify and 'clamp' areas of novel environmental conditions across model projections. Mean ENM projections were converted to binary suitability maps (presence/absence) using two conventional threshold methods: 'MaxSSS' (maximising the sum of sensitivity [true positive rate] and specificity [false positive rate]) and 'Least Training Presence' (LTP), with the former often considered best practise for presence-only models (Liu et al., 2013, 2016). The use of these two different binary thresholds provides the opportunity to assess the sensitivity of the results to threshold selection.

6.2.4 Model verification

The ENM was validated using two conventional metrics: the area under the curve (AUC) statistic, determined from the receiver operating characteristics analyses (ROC) (Swets, 1988), and the true skill statistic (TSS) (Allouche et al., 2006). These statistical measures are based on the confusion matrix, where observed presence and absence/background data are compared to model predictions (Allouche et al., 2006). In general, evaluation criteria for AUC values have been interpreted as good (0.90–1.00), moderate (0.7–<0.9), and poor (0.5–<0.7), whereas a score of less than 0.5 is worse than one would expect from a random model (Franklin, 2010). Evaluation scores for TSS range from -1 to 1, where a score of 1 demonstrates perfect model performance, while less than 0 is considered worse than a random model (Allouche et al., 2006).

The capacity of discrete model projections to correctly predict fossil coral reef localities was also evaluated for each stage (i.e. intersecting Anisian fossil reef occurrences with the Anisian projection, etc.). To determine whether hindcast projections of suitable habitat were better at predicting the distribution of warm-water coral reefs than random, 1,000 sets of random points were generated for each stage, with each set equal

to the number of fossil coral reefs within the respective stage. From these sets, the mean percentage of 'accurately' predicted random points (i.e. points falling with suitable areas) was calculated. Subsequently, two-sample Wilcoxon rank-sum tests were carried out to determine whether the percentage of accurately predicted fossil reef localities across stages was significantly greater than those of randomly generated points ($a = 0.05$).

6.2.5 Post-modelling analyses

The relationship between predicted coral reef habitat and zooxanthellate coral biodiversity was evaluated by generating species and genus-area curves. To do so, suitable cells within the modern projection were randomly sampled from one to the total number of suitable cells, increasing at intervals of one cell. For each sample of cells, the species and genus richness of modern zooxanthellate coral occurrences intersecting with the sampled cells was computed, as well as the geographic area of the sampled cells. Species/genus-area curves were calculated with 100 replications, and the mean value is reported, along with the 95% confidence intervals. In addition, coefficient of determination tests (R^2) were performed to test the relationship between estimated suitable area and taxonomic (species and genus) richness within 5°, 10°, 15°, and 30° palaeolatitudinal bins.

To quantify temporal shifts (Anisian–Piacenzian) in the palaeolatitudinal distribution of suitable habitats, the centroid of suitable area was determined from the binary projections using the gCentroid() function from the R package 'rgeos' ver. 0.5-12 (Bivand and Rundel, 2019). To prevent hemispheric differences influencing the centroid, Northern and Southern hemispheres were calculated separately. In addition to centroid computation, the areal extent of suitable habitat was calculated within 30° palaeolatitudinal bins along the entire time series (Table 5.2). This is a common binning protocol applied in deep time studies (e.g. Fitzgerald and Carlson, 2006; Mannion et al., 2012; Kröger, 2018; Close et al., 2020b), and approximates tropical (0–30°), temperate (30–60°), and high latitude/polar regions (60–90°). Significantly, it also

allows comparison with the work presented in Chapter 5 and offers an opportunity to assess whether general palaeolatitudinal trends in zooxanthellate coral biodiversity might be a result of available reef habitat. However, it should be noted that the analyses in this chapter focus on stratigraphic stage-level bins (dictated by the available palaeoclimate and DEM data), whereas the work presented in Chapter 5 utilised near-equal-length time bins (~10 myr). Nevertheless, general trends along the time series are still comparable.

Table 6.1. Palaeolatitudinal binning protocol used in this study. Palaeolatitudinal bins approximate tropical, temperate, and high latitude/polar regions in each hemisphere.

Palaeolatitudinal bin	Maximum (°)	Midpoint (°)	Minimum (°)	Hemisphere
1	90	75	60	Northern
2	60	45	30	Northern
3	30	15	0	Northern
4	0	-15	-30	Southern
5	-30	-45	-60	Southern
6	-60	-75	-90	Southern

6.3 Results

6.3.1 Model verification

The modern-trained ecological niche model (ENM) performed exceptionally well, with high mean AUC (0.914 ± 0.006) and TSS (0.758 ± 0.014) scores, demonstrating a high discriminatory capacity. The ability of binary model projections to accurately predict fossil reef occurrences within stages ranged from 0% to 100% for both binary thresholds (LTP and MaxSSS) (Figure 6.3 and Table 6.2). For stages with a predictive performance of 0% (Aquitanian, Chattian, Selandian, and Sinemurian), occurrences were outside the bounds of the shallow marine mask, with the exception of the Tortonian for the MaxSSS binary prediction (Table 6.2). However, under the LTP threshold, 82.4% of reef occurrences were accurately predicted for the Tortonian, highlighting the significance of threshold selection. This difference in predictive capacity is to be expected as the very nature of the MaxSSS threshold aims to maximise the sum of sensitivity and specificity (reducing the geographic extent of estimated

suitable area). Nevertheless, over the entire time series, 221/375 (~59%) of fossil reefs were accurately predicted under the LTP binary threshold, whereas only 192/375 (~51%) occurrences were accurately predicted under the MaxSSS threshold. However, 100 (~27%) of the occurrences the model projections failed to predict are outside the bounds of the shallow marine mask, while an additional 20 (~5%) reside in areas of novel environmental conditions outside the training range of the ENM (discussed in detail within a later section). This accounts for the majority of the observed false negatives from model predictions. The impact of model clamping (keeping projections within the training range of the ENM) on the predictive accuracy of model projections is particularly apparent between the Bathonian and Valanginian (Middle Jurassic–Early Cretaceous). Whilst these clamped projections demonstrate a predictive accuracy of 25–69.6%, their non-clamped counterparts have an accuracy of 50–91.1% (Figure 6.3; Appendix C: Figure C.1).

The ability to predict fossil reef occurrences was independent of the geographic extent of estimated suitable area in this study. The predictive performance of model projections for randomly generated occurrences show only 3.9% to 7.8% of occurrences would be 'accurately' predicted for the LTP projections, and 2.3% to 5.2% for the MaxSSS projections. Two-sample Wilcoxon rank-sum tests further support this observation, indicating that model projections performed better than random for both binary thresholds ($n = 41$, $P < 0.001$). In addition, results from model verification exercises do not reflect any long-term temporal trends in predictive accuracy (i.e. model projections closer to the present day do not tend to be more capable of predicting the presence of fossil coral reefs than those in deep time). This suggests that model projections are generally as reliable for older stages, as they are for more recent stages.

Table 6.2. The predictive performance of model projections in identifying observed fossil coral reef occurrences, and those randomly generated. Results are shown as percentages for the two binary thresholds used in this study: (1) LTP (least training presence); and (2) MaxSSS (maximising the sum of sensitivity and specificity). Reported values for the random predictive performance is the mean percentage of predictive accuracy from 1,000 sets of n points, where n is the number of observed occurrences for each stage. Analyses could not be conducted for the Messinian, Serravallian, Langhian, and Toarcian as no reefs were present in the dataset for these stages.

Stage	Max Ma	Min Ma	# of points	LTP (%)		MaxSSS (%)	
				Observed	Random	Observed	Random
Piacenzian	3.60	2.59	13	53.85	3.91	38.46	2.30
Zanclean	5.33	3.60	6	66.67	4.07	33.33	2.48
Messinian	7.25	5.33	0	-	-	-	-
Tortonian	11.62	7.25	17	82.35	4.81	0.00	2.91
Serravallian	13.82	11.62	0	-	-	-	-
Langhian	15.97	13.82	0	-	-	-	-
Burdigalian	20.44	15.97	10	40.00	4.96	30.00	3.46
Aquitanian	23.03	20.44	1	0.00	5.30	0.00	4.40
Chattian	28.10	23.03	3	0.00	4.80	0.00	2.90
Rupelian	33.90	28.10	8	87.50	5.15	87.50	2.70
Priabonian	38.00	33.90	10	60.00	6.00	60.00	3.79
Bartonian	41.30	38.00	3	100.00	5.80	100.00	3.97
Lutetian	47.80	41.30	5	80.00	6.38	80.00	4.96
Ypresian	56.00	47.80	6	50.00	5.78	50.00	3.63
Thanetian	59.20	56.00	4	50.00	5.70	50.00	3.55
Selandian	61.60	59.20	1	0.00	7.80	0.00	3.70
Danian	66.00	61.60	7	57.14	5.97	57.14	4.04
Maastrichtian	72.10	66.00	6	50.00	7.45	50.00	4.57
Campanian	83.60	72.10	7	100.00	7.29	100.00	4.87
Santonian	86.30	83.60	2	100.00	6.25	100.00	4.15
Coniacian	89.80	86.30	1	100.00	6.40	100.00	4.60
Turonian	93.90	89.80	1	100.00	8.60	100.00	5.20
Cenomanian	100.50	93.90	3	33.33	6.53	33.33	4.50
Albian	113.00	100.50	9	44.44	6.81	44.44	4.38
Aptian	125.00	113.00	8	75.00	5.76	75.00	3.78
Barremian	129.40	125.00	9	100.00	5.58	100.00	3.56
Hauterivian	132.90	129.40	10	70.00	5.16	60.00	2.98
Valanginian	139.80	132.90	2	50.00	4.50	50.00	3.30
Berriasian	145.00	139.80	4	25.00	4.00	25.00	2.63
Tithonian	152.10	145.00	25	36.00	5.00	36.00	3.22
Kimmeridgian	157.30	152.10	33	30.30	4.75	30.30	3.68
Oxfordian	163.50	157.30	56	69.64	4.57	64.29	3.20
Callovian	166.10	163.50	6	33.33	4.38	33.33	3.05
Bathonian	168.30	166.10	6	33.33	4.23	33.33	3.25
Bajocian	170.30	168.30	17	88.24	4.26	82.35	2.97
Aalenian	174.10	170.30	2	100.00	5.00	100.00	3.75
Toarcian	182.70	174.10	0	-	-	-	-
Pliensbachian	190.80	182.70	1	100.00	5.70	100.00	4.20
Sinemurian	199.30	190.80	2	0.00	5.75	0.00	4.40
Hettangian	201.30	199.30	2	50.00	4.05	50.00	3.35
Rhaetian	208.50	201.30	20	80.00	4.34	65.00	2.92
Norian	228.00	208.50	28	57.14	4.03	50.00	2.96
Carnian	237.00	228.00	9	44.44	5.23	44.44	3.38
Ladinian	242.00	237.00	8	25.00	4.53	25.00	3.19
Anisian	247.20	242.00	4	25.00	5.08	25.00	3.58

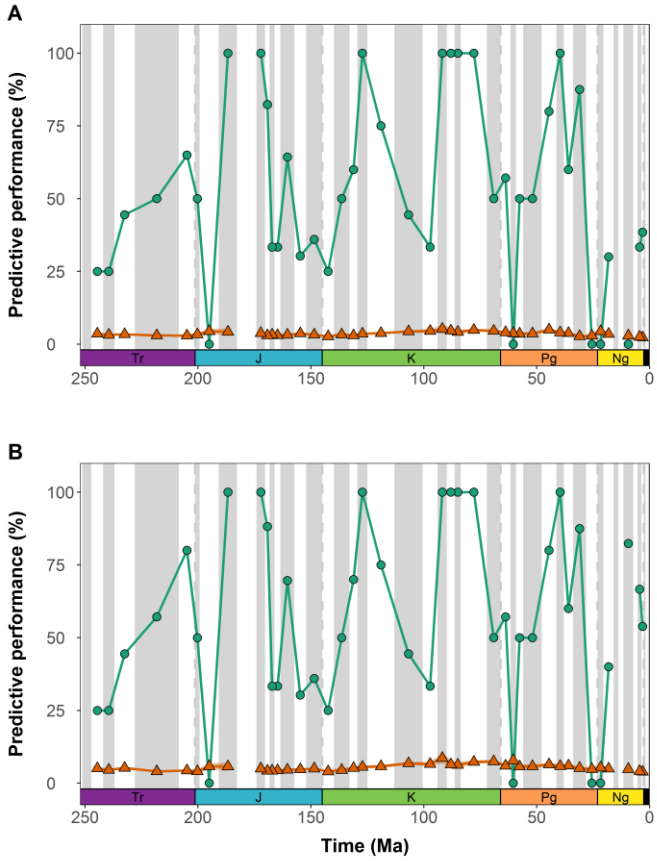


Figure 6.3. Predictive performance of model projections for binary thresholds (A) MaxSSS (maximising sensitivity and specificity); and (B) LTP (least training presence). Predictive success of fossil reef occurrences (percentage of fossil reef occurrences predicted to be suitable) is indicated by the green points; predictive success from random point generation is indicated by the orange triangles, along with the 95% confidence intervals. Vertical grey box shading illustrates stratigraphic stage, whereas vertical dashed lines indicate the start/end of a period.

6.3.2 Model predictions

Taxonomic richness-area relationship

Species and genus-area curves demonstrate a scaling of zooxanthellate coral biodiversity with estimated suitable area (Figure 6.4). Both species and genus-area curves follow near-identical trajectories regardless of the binary prediction (Figure 6.4). However, due to the broader areal extent of estimated suitable habitat under the LTP threshold, notably higher species richness is observed at the full extent of estimated suitable area. This observation is less pronounced in genus-area curves, which reach asymptote at smaller areal extents of suitable habitat, as to be expected. Analyses of the latitudinal relationship between suitable area and zooxanthellate coral biodiversity suggests a high proportion of the variance in taxonomic richness is explained by

estimated suitable area ($R^2 = 0.682–0.985$, $P < 0.01$) (Figure 6.5–Figure 6.8). Broadly, coefficient of determination values tend to be greater for the LTP binary projection, larger latitudinal bin sizes, and genus counts (Figure 6.5–Figure 6.8). Nevertheless, regardless of the linear model, latitudinal estimated suitable area explains 68.2–98.5% of the variance observed in latitudinal species richness (Figure 6.5–Figure 6.6). Similarly, 80.6–98.4% of the variance in latitudinal genus richness is explained by estimated suitable area (Figure 6.7–Figure 6.8).

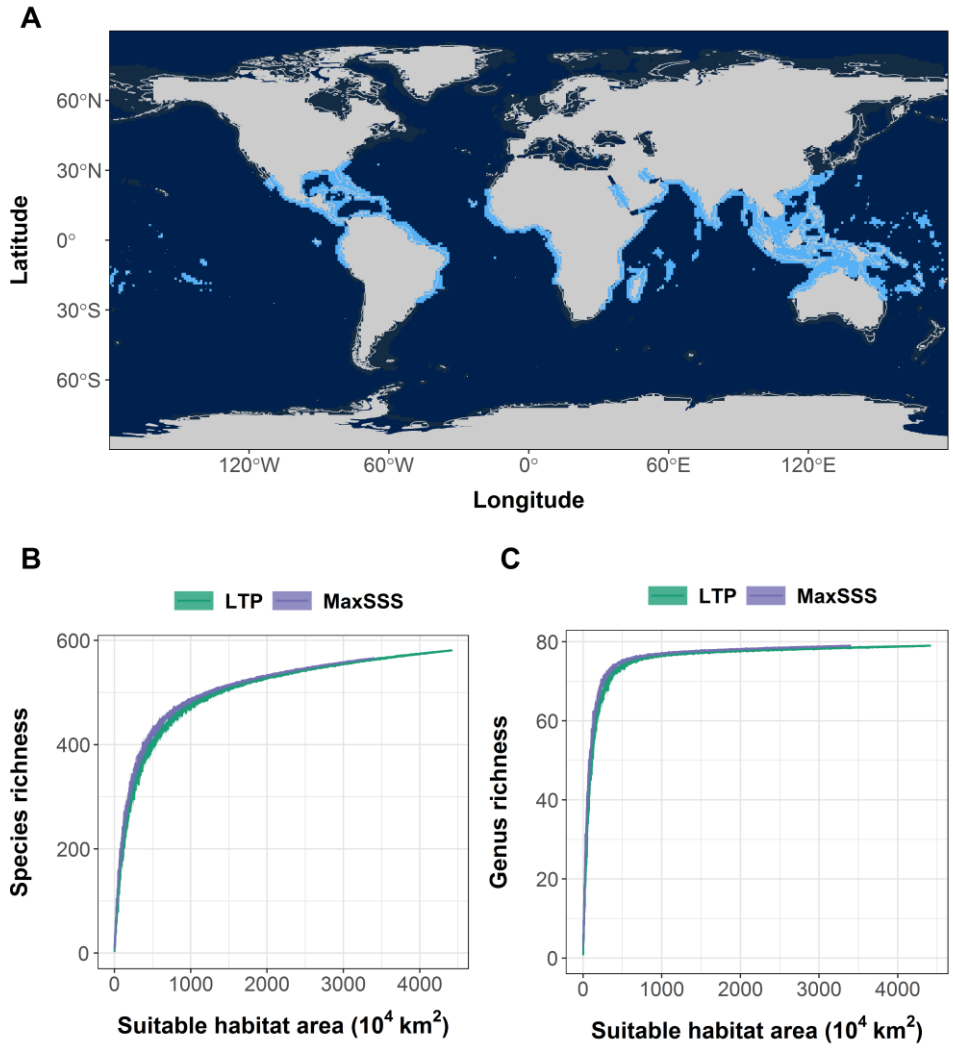


Figure 6.4. Binary habitat suitability map and species/genus-richness-area curves. (A) Binary habitat suitability map of the modern using the MaxSSS (maximising the sum of specificity and sensitivity) binary threshold. Suitable cells are depicted in light blue. (B–C) Species- and genus-area curves for modern zooxanthellate corals and estimated suitable habitat area for coral reefs derived from binary (MaxSSS and LTP [least training presence]) suitability maps of the modern. Data from the MaxSSS suitability map is depicted in purple, while LTP is shown in green. Zooxanthellate coral data is based on the dataset described in Chapter 3. Map data is projected in the coordinate reference system: World Geodetic System 1984 (WGS84).

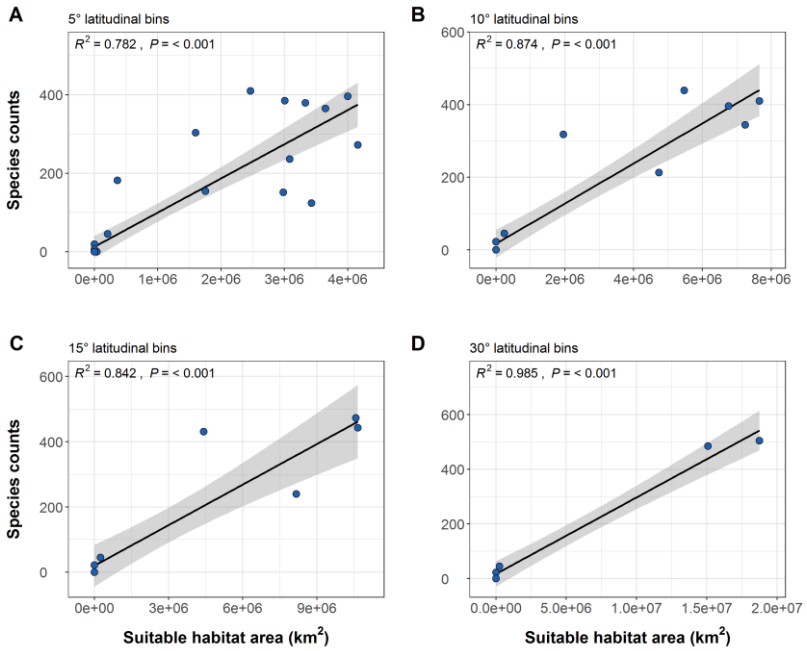


Figure 6.5. Relationship between estimated suitable habitat area and zooxanthellate coral species richness within variable latitudinal bin sizes. Estimated suitable habitat area is derived from the binary (MaxSSS) suitability map of the modern. Species count data is based on the zooxanthellate coral dataset described in Chapter 3. Latitudinal bin sizes are as follows: (A) 5°; (B) 10°; (C) 15°; and (D) 30°. The coefficient of determination (R^2) between latitudinal suitable area and species counts is displayed within each plot, along with associated *P*-values.

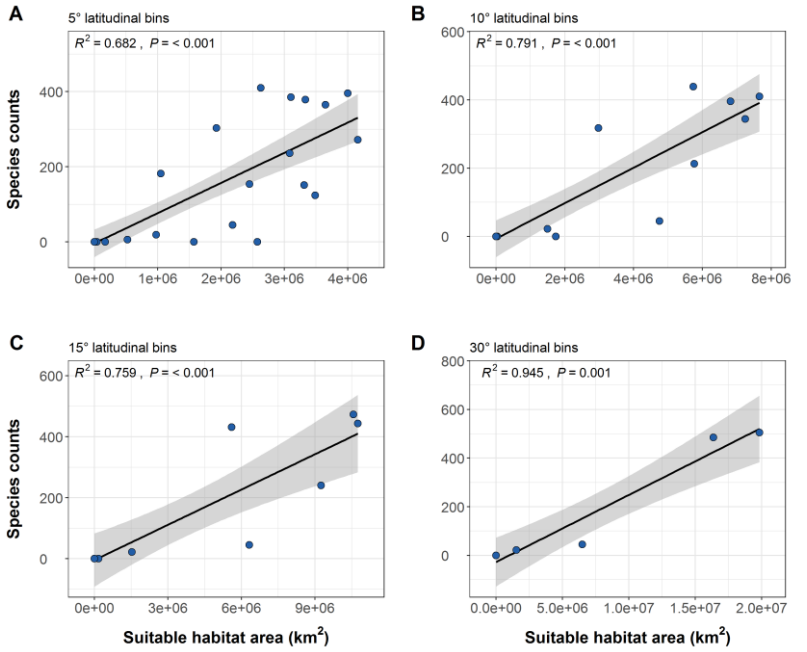


Figure 6.6. Relationship between estimated suitable habitat area and zooxanthellate coral species richness within variable latitudinal bin sizes. Estimated suitable habitat area is derived from the binary (LTP) suitability map of the modern. Species count data is based on the zooxanthellate coral dataset described in Chapter 3. Latitudinal bin sizes are as follows: (A) 5°; (B) 10°; (C) 15°; and (D) 30°. The coefficient of determination (R^2) between latitudinal suitable area and species counts is displayed within each plot, along with associated *P*-values.

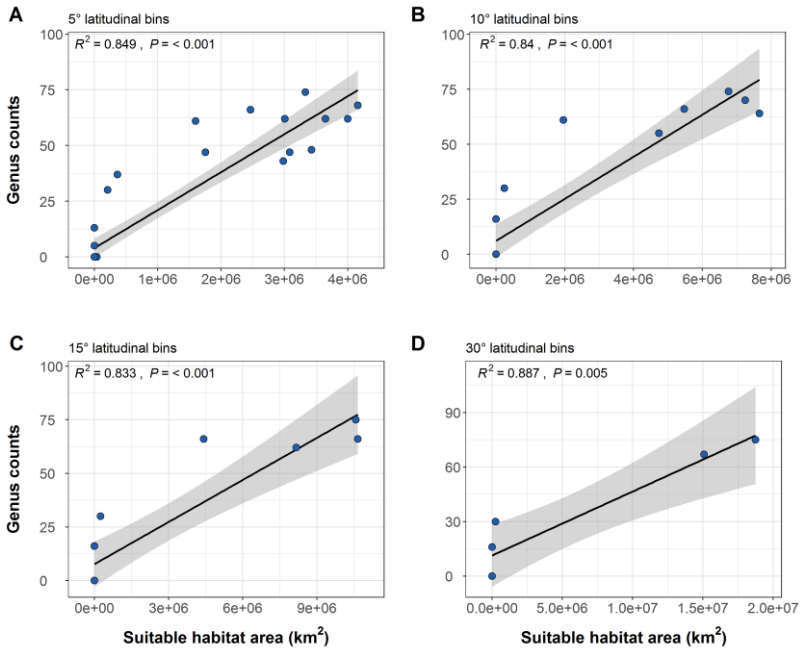


Figure 6.7. Relationship between estimated suitable habitat area and zooxanthellate coral genus richness within variable latitudinal bin sizes. Estimated suitable habitat area is derived from the binary (MaxSSS) suitability map of the modern. Genus count data is based on the zooxanthellate coral dataset described in Chapter 3. Latitudinal bin sizes are as follows: (A) 5°; (B) 10°; (C) 15°; and (D) 30°. The coefficient of determination (R^2) between latitudinal suitable area and genus counts is displayed within each plot, along with associated P-values.

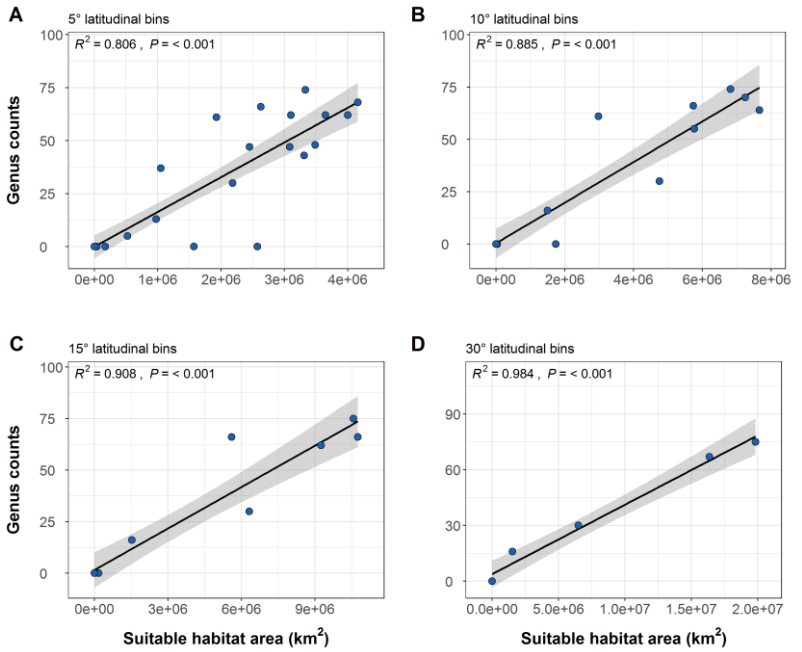


Figure 6.8. Relationship between estimated suitable habitat area and zooxanthellate coral genus richness within variable latitudinal bin sizes. Estimated suitable habitat area is derived from the binary (LTP) suitability map of the modern. Genus count data is based on the zooxanthellate coral dataset described in Chapter 3. Latitudinal bin sizes are as follows: (A) 5°; (B) 10°; (C) 15°; and (D) 30°. The coefficient of determination (R^2) between latitudinal suitable area and genus counts is displayed within each plot, along with associated P-values.

Palaeolatitudinal distribution of suitable habitat area

Palaeolatitudinal analyses suggest that the areal extent of suitable habitats was variable throughout the Mesozoic and Cenozoic. High palaeolatitudes (60–90°) north and south of the equator indicate almost no suitable area across the entire time series (Figure 6.9). However, a small amount of suitable area is predicted for 60–90°N in some intervals of the Triassic, Jurassic and Paleogene, while similar levels of suitable area are predicted for the Early Cretaceous at 60–90°S (Figure 6.9). Across the entire time series, estimated suitable habitat area is primarily concentrated in Northern Hemisphere tropical (0–30°N) and temperate (30–60°N) bins. Furthermore, whilst the amount of estimated suitable habitat area is similar between binary thresholds in tropical palaeolatitudinal bins (0–30°N and 0–30°S), LTP consistently estimates a significantly larger sum of suitable area for temperate palaeolatitudes than MaxSSS (30–60°N and 30–60°S). For the Triassic, tropical palaeolatitudes north and south of the equator have a larger areal extent of suitable habitat than temperate palaeolatitudes (Figure 6.9). However, a large increase in Northern Hemisphere suitable habitat area (30–60°N) is observed across the Triassic/Jurassic boundary. A subsequent long-term decline in temperate (30–60°N) suitable area is observed from the Early Jurassic to the Early Cretaceous, with a sharp decline across the Jurassic/Cretaceous boundary, reaching a minimum during the Valanginian (Figure 6.9). Conversely, a long-term increase in tropical (0–30°N) suitable area is estimated from the Early Jurassic to the Early Cretaceous, with a sharp increase in the earliest Cretaceous (Berriasian–Valanginian) (Figure 6.9). The areal extent of suitable habitat for the tropics (0–30°N) is then maintained throughout the Cretaceous. For northern temperate palaeolatitudes (30–60°N), estimated suitable habitat area increases from the Valanginian towards the end-Cretaceous. However, whilst the LTP binary threshold suggests similar areal extents of suitable habitat between northern tropical and temperate palaeolatitudes (0–30°N and 30–60°N) in the Late Cretaceous, MaxSSS suggests temperate suitable area was considerably smaller in areal extent than the tropics (Figure 6.9). Similar differences between the amount of estimated suitable area

can be observed for Southern Hemisphere temperate palaeolatitudes (30–60°S). A long-term decline in estimated suitable habitat area is observed from the end-Cretaceous towards the Recent for northern temperate palaeolatitudes (30–60°N), with a sharp decline towards the end-Paleogene. By contrast, tropical suitable habitat area (0–30°N) tends to decline throughout the Paleogene, plateauing in the Neogene (Figure 6.9). Notably, estimated suitable habitat area for the Southern Hemisphere (0–30°S) increases significantly from the mid-Paleogene towards the Recent.

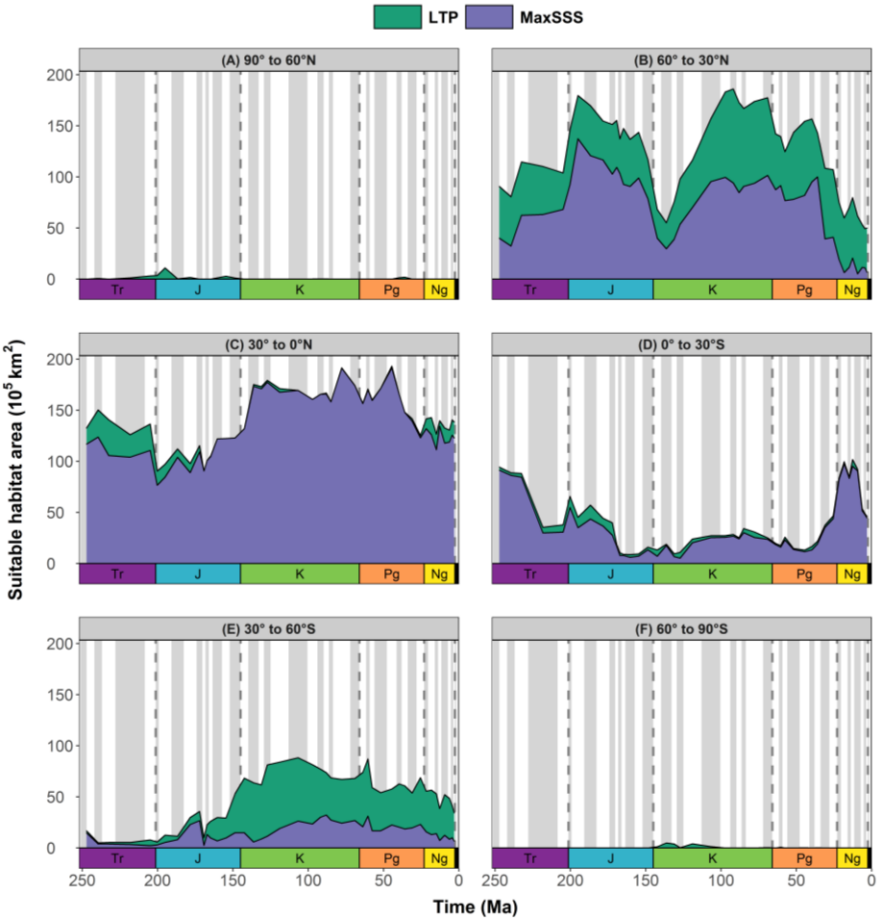


Figure 6.9. Palaeolatitudinal plots of estimated suitable habitat area (Anisian to Piacenzian) for warm-water coral reefs under binary thresholds LTP (least training presence) and MaxSSS (maximising the sum of sensitivity and specificity). Palaeolatitudinal bins: (A) 90–60°N; (B) 60–30°N; (C) 30–0°N; (D) 0–30°S; (E) 30–60°S; and (F) 60–90°S. Vertical grey box shading illustrates stratigraphic stages, whereas vertical dashed lines indicate the start/end of a period.

Temporal shifts in the centroid (centre of mass) of suitable habitats echo results from palaeolatitudinal analyses. The Northern Hemisphere shows a long-term equatorward shift in suitable habitats from the Sinemurian (LTP: 38.58°; MaxSSS: 34.09°) to the Piacenzian (LTP: 22.17°; MaxSSS: 15.85°) for both binary thresholds (Figure 6.10).

The Southern Hemisphere centroid expresses more volatility, with an absolute maximum palaeolatitude of 47.82° in the Hauterivian for binary threshold LTP (Figure 6.10). A prominent poleward shift in the Northern Hemisphere centroid is observed from the Rhaetian to Sinemurian (LTP: 6.41°; MaxSSS: 6.28°), whereas a pronounced equatorward shift is observed from the Tithonian to Valanginian (LTP: 7.73°; MaxSSS: 5.46°). In addition, large equatorial shifts in the Northern (LTP: 10.94°; MaxSSS: 13.37°) and Southern Hemisphere (LTP: 13.60 °; MaxSSS: 10.02°) centroids are observed from the Priabonian to the Recent for both binary thresholds (Figure 6.10). Whereas the Northern Hemisphere centroids show similar trends regardless of binary threshold, notable differences are observed for the Southern Hemisphere, particularly during the Cretaceous (Figure 6.10). For example, the palaeolatitudinal centroid shows a poleward shift from the Berriasian to the Valanginian for binary threshold LTP, whereas an equatorward shift is observed for binary threshold MaxSSS.

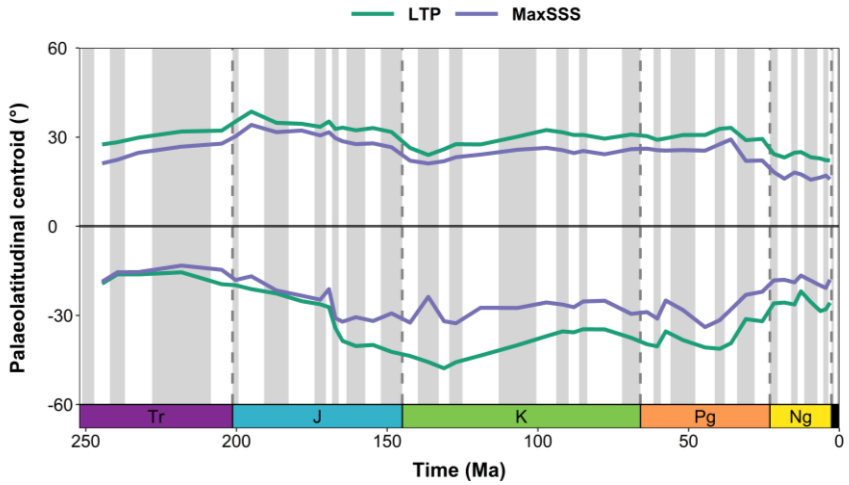


Figure 6.10. Palaeolatitudinal shifts in the centroid (centre of mass) of suitable habitat area from the Anisian to Piacenzian for warm-water coral reefs. The centroid was computed from suitability maps for each stratigraphic stage under binary thresholds: (1) LTP (least training presence); and (2) MaxSSS (maximising the sum of sensitivity and specificity). Each hemisphere was calculated separately, with respective centroid data plotted above or below the black line depicting the equator. Vertical grey box shading illustrates stratigraphic stages, whereas vertical dashed lines indicate the start/end of a period.

6.3.3 Model clamping and MESS analyses

Model clamping resulted in 20 fossil coral reef occurrences not being accurately predicted due to intersecting areas of novel environmental conditions. Multivariate Environmental Similarity Surface (MESS) analyses (Elith et al., 2010) indicate this is

a result of warmer sea surface temperatures at those localities than those observed in the present-day climatic range. Novel environmental conditions seem to be principally due to warmer sea surface temperatures along the entire studied time series. As a result, model clamping primarily influences the amount of estimated suitable habitat area for tropical palaeolatitudes. Whilst this does not influence the overall trends aforementioned, the large increase in the amount of estimated suitable habitat area for 0–30°N during the earliest Cretaceous (Berriasian–Valanginian) has a seemingly earlier onset, and peaks in the Oxfordian (Appendix C: Figure C.1). Furthermore, a larger areal extent of suitable habitat is predicted for the Southern Hemisphere along the entire time series (Appendix C: Figure C.1).

6.4 Discussion

Models of suitable conditions for warm-water coral reefs suggest that the palaeolatitudinal distribution of suitable area became increasingly skewed towards the tropics from the late Eocene (Priabonian; ~37 Ma) to the Recent (Figure 6.9–Figure 6.10). This was driven by: (1) declines in suitable area at northern temperate palaeolatitudes (30–60°N) due the onset of 'icehouse' climatic conditions (see also Fenton et al., 2016), which resulted in temperate decreases in sea surface temperature (Appendix C: Figure C.2–Figure C.3); and (2) increases in shallow marine area at southern tropical palaeolatitudes (0–30°S) due to the equatorward shift of the Australian Plate, and eventual convergence of the Eurasian, Australian, and Philippine plates (Appendix C: Figure C.4). This resulted in an increase in shallow marine environments in the tropics, which likely enabled the formation of the modern Indo-Australian Archipelago diversity hotspot (e.g. Renema et al., 2008; Leprieur et al., 2016). These findings are supported by analyses of the palaeolatitudinal centroid of suitable area, which suggest an equatorward shift of ~11–13° from the Priabonian to the Recent in the Northern Hemisphere, and a 10–14° equatorward shift in the Southern Hemisphere (Figure 6.10). On the basis of estimated suitable habitat area, warm-water coral reefs had a less tropically skewed distribution for most of the Mesozoic and the early Cenozoic (Figure 6.9–Figure 6.10). However, the Early

Cretaceous is one major exception to this, with the areal extent of suitable habitat particularly low at northern temperate palaeolatitudes (30–60°N) during the Valanginian, resulting in a tropically dominated distribution of suitable area (Figure 6.9). Interestingly, a major temperate (30–60°N) peak in suitable habitat area is observed for the Sinemurian (Early Jurassic), along with a large poleward shift in suitable habitat area from the Rhaetian to Sinemurian (LTP: 6.41°; MaxSSS: 6.28°). Palaeolatitudinal analyses also suggest suitable habitable area was largely skewed towards the Northern Hemisphere for the majority of the Mesozoic and Cenozoic (Figure 6.9). This is important as previous work has frequently advocated that there is a major global sampling bias towards the Northern Hemisphere (e.g. Kiessling, 2005; Close et al., 2020b). Whilst this is certainly accurate, the fact that suitable habitat area is skewed towards the Northern Hemisphere also suggests that greater sampling opportunities might be available in the Northern Hemisphere for reef-associated organisms.

Model verification exercises indicate that the modern-calibrated ENM has a high discriminatory capacity, with high mean AUC (0.914 ± 0.006) and TSS (0.758 ± 0.014) scores. However, the predictive performance of stage-level model projections (hindcasts) was variable between stages, with 0% to 100% of fossil reef occurrences accurately predicted (Figure 6.3 and Table 6.2). Averaged over the entire time series, only ~50–60% of fossil reef occurrences were accurately predicted, depending on the binary threshold (LTP: 221/375; MaxSSS: 192/375). Nevertheless, this is principally a result of a large number of occurrences (100/375) being outside the bounds of the shallow marine mask, suggesting that reefs were capable of residing at deeper depths in the geological past, or there are inaccuracies in the palaeo-rotation of fossil reefs or bathymetric reconstructions. An additional number of fossil reef occurrences (20/375) were not accurately predicted by model projections due to residing in novel environmental conditions, which were excluded from model projections due to the use of model clamping. These novel environmental conditions were principally the result of warmer sea surface temperatures than is observed in the present-day climatic range.

Again, this suggests coral reefs may have either resided in warmer sea surface temperatures than observed today, or the aforementioned inaccuracies. Nevertheless, two-sample Wilcoxon rank-sum tests indicate that model projections were more capable of accurately predicting fossil reef occurrences than would be expected at random for both binary thresholds ($n = 41$, $P < 0.001$). More specifically, the predictive capacity of model projections was not predicated on broad geographic estimates of suitable habitat, with only 2–8% of randomly generated points intersecting suitable habitats (Table 6.2).

Previous studies have constructed present-day species-area models using estimated suitable habitat area from ENMs to predict 'extinction debt' (i.e. loss of species in relation to loss of habitat) under future climate change scenarios (e.g. Thomas et al., 2004; Olivier et al., 2013). The use of such approaches has the potential to provide a null expectation of biodiversity patterns in deep time, though direct application is currently absent. In this study, linear models indicate a strong explanatory relationship ($R^2 = 0.682$–0.985, $P < 0.01$) between estimated suitable habitat area (for warm-water coral reefs) and zooxanthellate coral biodiversity (Figure 6.4–Figure 6.8). This association is observed for both species and genera at a global scale (Figure 6.4), and within latitudinal bins (Figure 6.5–Figure 6.8), suggesting a scaling of taxonomic richness with estimated suitable habitat area — i.e. the species (or genus) -area relationship (MacArthur and Wilson, 1967; Connor and McCoy, 1979; Rosenzweig, 1995; Lagomarcino and Miller, 2012). Whilst neither species- or genus-area-relationship models were explicitly generated for this study, several inferences can be made due to the ubiquitous scaling of species richness with area (Connor and McCoy, 1979; Rosenzweig, 1995). In particular, based on the palaeolatitudinal distribution of estimated suitable habitat area, steep unimodal-type latitudinal biodiversity gradients (LBGs) were likely restricted to the last ~30 myr, as well as the Early Cretaceous (Figure 6.9). This finding is in broad agreement with empirical data from the fossil record, which suggests zooxanthellate corals maintained unimodal-type LBGs during the Early Cretaceous and the last ~20 myr (Chapter 5). However, recent studies have

also found support for a unimodal-type LBG in the marine realm during the Middle Triassic (Song et al., 2020). Whilst estimates of suitable habitat area do not explicitly disagree with this finding, they do suggest that if a unimodal-type LBG persisted during the Middle Triassic, it was likely not as steep as the gradients reconstructed for the Early Cretaceous, or last 30 myr (Figure 6.9). Furthermore, the Sinemurian (Early Jurassic) might represent a temperate peak and equatorward decline in taxonomic richness (commonly referred to as a bimodal-type LBG) if the species-area relationship persists at these broad geographic scales in deep time (Figure 6.9). Nevertheless, the palaeolatitudinal distribution of estimated suitable habitat area suggests that flat-type (or relatively shallow unimodal/bimodal) LBGs likely persisted for most of the Mesozoic and early Cenozoic in reef-associated taxa.

Although models of the distribution of suitable area for coral reefs offer inference of the potential shape of the LBG in deep time, this study is not without limitations. First, the ecological model used in this study approximates the abiotic limits of warm-water coral reefs based on the climatic range observed today. As modern coral reefs reside at the upper thermal limit of the oceans, estimating their response to warmer sea surface temperatures is challenging. This limitation is evident by fossil coral reef occurrences (20/375) occupying areas of novel environmental conditions outside the calibration range of the ENM. Second, the spatial resolution (1° x 1°) of this study may also bias estimates of suitable habitat area (Seo et al., 2009). For example, it is possible that a suitable cell within the shallow marine mask contains only a small proportion of shallow benthic substrate (0–200 m), while another has a large proportion. In both instances, the same amount of suitable area would be calculated if the cells were at similar latitudes. Whilst this is a challenging issue to overcome, it is not limited to deep time studies: global neontological studies frequently use similar spatial resolutions due to limited environmental data availability (Couce et al., 2012, 2013; Freeman et al., 2013; Freeman, 2015). Furthermore, the use of finer spatial resolutions in deep time depends on the ability to estimate abiotic conditions at such resolutions. This is often challenging due to the incomplete nature of the geological

record, which prevents the validation of Earth System Models against environmental proxy data. Third, model projections of suitable habitat area are inevitably influenced by the availability of palaeoclimate data. Whilst it has become common for ENM studies to use a range of climate models to constrain model projections under future climate change scenarios (e.g. Zhang et al., 2015), no other General Circulation Model data covering the last ~250 myr is currently available. Fourth, it is possible that the species- and genus-area relationship observed for modern zooxanthellate corals is not directly applicable to zooxanthellate corals, or other reef-associated taxa in deep time. For example, several studies have advocated that habitat heterogeneity, rather than area itself, is the most important predictor of species richness (Boecklen, 1986; Báldi, 2008; Shen et al., 2009). Finally, the validity of estimated suitable habitat area to provide a null expectation of the distribution of biodiversity assumes that all suitable sites are accessible and occupied, which is often not the case due to dispersal limitations (e.g. restricted seaways, ocean circulation patterns, and distribution of the continents). Nevertheless, estimations of past suitable habitat offer the potential to disentangle whether observed biodiversity patterns in the fossil record are the result of abiotic drivers, sampling bias or some alternative mechanism (e.g. Chiarenza et al., 2019).

Despite the aforementioned limitations, few methods (if any) are without caveats, particularly when limited data is available. However, greater synthesis of results from multiple approaches offer the opportunity to make more robust conclusions about the evolution of spatial and temporal biodiversity patterns on Earth. Based on the estimates of suitable habitat presented here, it is clear that a unimodal-type latitudinal biodiversity gradient likely existed during the Early Cretaceous, and the last ~20–30 million years. This finding is in agreement with a previous analysis which used a fossil occurrence dataset of zooxanthellate corals (presented in Chapter 5). Future work should aim to test this study's findings further by using other reef-associated taxa (e.g. reef fishes), and alternative methods such as birth-death models (e.g. PyRate), which estimate the speciation and extinction rates (Silvestro et al., 2014; Meseguer and Condamine, 2020).

6.5 Summary

The results presented in this chapter suggest that the palaeolatitudinal distribution of suitable conditions for warm-water coral reefs was skewed towards the Northern Hemisphere for most of the last ~250 million years. This suggests that greater sampling opportunities might be available in the Northern Hemisphere for reef-associated organisms. Species- and genus-area curves demonstrate a strong relationship between modern zooxanthellate corals and estimated suitable habitat area. On the basis of this relationship, the latitudinal biodiversity gradient of reef-associated organisms likely became significantly steeper during the last 20–30 million years, forming the unimodal-type gradient observed today. This is a consequence of declines in suitable habitat area at northern temperate palaeolatitudes and increases at southern tropical palaeolatitudes. A second unimodal-type gradient likely persisted during the Early Cretaceous, due to a steep decline in the amount of suitable habitat area from the tropics to poles. Both of these findings are supported by previous work, including that presented in this thesis on zooxanthellate corals (Chapter 5). A temperate peak and tropical decline in reef-associated organisms may have been present during the Early Jurassic based on the palaeolatitudinal distribution of estimated suitable habitat area. However, aside from the aforementioned intervals, the latitudinal gradient of suitable area is fairly flat throughout the last ~250 million years, suggesting that the latitudinal biodiversity gradient might have also been relatively flat during this period. Whilst estimated suitable habitat area has the potential to provide a null expectation of the distribution of biodiversity, this may be too generalised due to the impacts of habitat heterogeneity, dispersal limitations and biotic interactions. Nevertheless, when coupled with empirical data from the fossil record, estimated suitable area offers the opportunity to disentangle whether observed biodiversity patterns are the result of abiotic drivers, or heterogeneous sampling regimes.

–This page is intentionally left blank–

7 Conclusions and future work

7.1 Key findings

This thesis employed a combination of statistical and modelling tools to quantitatively evaluate patterns in the distribution of marine biodiversity in deep time, including the presence and detectability of different types of latitudinal biodiversity gradient in deep time. Fossil occurrences have been used to reconstruct the distribution of biodiversity through space and time throughout the history of palaeobiology. However, the fossil record is inherently biased by taphonomic loss, variable stratigraphic completeness and collector bias (Raup, 1972; Sheehan, 1977; Jackson and Johnson, 2001; Peters and Foote, 2001; Smith, 2001; Alroy et al., 2001; Kiessling, 2005). This impacts upon any major interpretation of spatial and temporal biodiversity patterns from the fossil archive, including the latitudinal biodiversity gradient. As demonstrated in this thesis, the issue of data absence and heterogeneous spatial sampling may particularly skew our understanding of life in the past. Nevertheless, the use of novel subsampling approaches and inferential methods can yield a greater understanding of macroecological patterns in deep time. The key findings of this thesis follow.

In Chapter 3, ecological niche modelling was integrated with Earth system modelling and occurrence datasets (modern and fossil) to test a previously observed equatorial decline in zooxanthellate coral biodiversity during the Last Interglacial (125,000 years ago) (Kiessling et al., 2012). The findings of Chapter 3 suggest that the 'apparent' decline in equatorial biodiversity is likely an artefact of heterogeneous spatial sampling, with an underrepresentation of tropical latitudes. This conclusion is based on: (1) observed sampling regimes, with equatorial and tropical latitudes underrepresented; and (2) estimates of habitat suitability, which suggest equatorial and tropical latitudes were at least as suitable as today. Despite refuting the previously observed equatorial decline, results from ecological niche modelling do agree with the apparent poleward range expansion, with suitable habitats predicted at more poleward latitudes than observed today. Whilst focused on the 'apparent' equatorial decline, this study also demonstrated the value of coupling modern and fossil data to improve model predictions under projected global warming, as well as the geological past. The use of

fossil data in ecological niche modelling is becoming increasingly used to address a range of palaeobiological questions (e.g. Waterson et al., 2016; Chiarenza et al., 2019; Saupe et al., 2019a), including its value in 'Conservation Palaeobiology' (e.g. Lima-Ribeiro et al., 2017). With increasing availability of palaeoclimate model data, the use of ecological niche models will become a common tool in the palaeobiologists' toolkit. However, consensus on best practises when using ecological niche modelling in deep time is still lacking.

In Chapter 4, the detectability of different types of latitudinal biodiversity gradients from the fossil record was evaluated. To achieve this, a simulation framework was implemented using reconstructions of the Earth's palaeogeography and palaeobathymetry (based on Getech's digital elevation models). For these simulations, three different types of latitudinal biodiversity gradient were generated for the past ~300 million years (Permian–Neogene) for shallow marine environments (0–200 m depth): (1) a gradient with no specified peak in biodiversity (flat-type); (2) a tropical peak in biodiversity with a sharp decline towards the poles (unimodal-type, or 'modern-type'); and (3) temperate peaks in biodiversity that decline towards the poles and equator (bimodal-type). Subsequently, simulated latitudinal biodiversity gradients were sampled by the known spatial sampling window (based on fossil collections) to test whether the true gradient could be reconstructed. Results from this study suggest that the current distribution of sampled palaeogeographic area rarely allows for the differentiation between types of latitudinal biodiversity gradient. A long-term poleward shift in the palaeolatitudinal sampling window is observed, which enables unimodal-type latitudinal biodiversity gradient to be readily identified in the Permian and Triassic when palaeolatitudinal sampling was less skewed towards temperate palaeolatitudes. However, the reconstruction of unimodal gradients in most of the Jurassic, Cretaceous and Palaeogene is limited due to skewed sampling towards northern temperate regions. More equable palaeolatitudinal sampling in the Neogene permits the recovery of unimodal gradients during this time period. Yet, overall the reconstruction of deep time latitudinal biodiversity gradients is severely impacted by

the heterogeneous distribution of the available sedimentary record and incomplete sampling. This work supports recent studies that demonstrate spatial sampling patterns have a major impact on estimates of past biodiversity (Close et al., 2017, 2020a, 2020b), highlighting the need to account for variability in sampled geographic area, as a result of the ubiquitous scaling of species richness with area (MacArthur and Wilson, 1967; Connor and McCoy, 1979; Rosenzweig, 1995; Whittaker and Fernández-Palacios, 2007).

In Chapter 5, palaeolatitudinal trends in zooxanthellate coral biodiversity were assessed using a novel sampling-standardisation protocol—which accounts for heterogeneity in spatial sampling—to provide fairer estimates of biodiversity trends. Specifically, this study tested whether unimodal-type gradients are restricted to the past 30 million years when 'icehouse' climate regimes persisted (see Mannion et al., 2014), or were also present at other intervals during zooxanthellate corals' ~250 million year evolutionary history. The findings of this work suggest unimodal-type latitudinal biodiversity gradients were present during 'cold-snap' intervals during the Middle Jurassic and Early Cretaceous (Hallam et al., 1991; Gröcke et al., 2003; Royer et al., 2004; Grabowski et al., 2013). In addition, it appears that the modern latitudinal biodiversity gradient became significantly steeper only in the last 20 million years, following the onset of 'icehouse' conditions. This finding is in broad agreement with aspects of many previous studies (e.g. Crame and Rosen, 2002; Rex et al., 2005; Alroy et al., 2008; Yasuhara et al., 2012; Marcot et al., 2016; Spano et al., 2016; Meseguer and Condamine, 2020). Despite major changes in the Earth's climate over the past 250 million years, steep unimodal-type latitudinal biodiversity gradient might be a relatively rare phenomenon that are primarily restricted to icehouse climate regimes or sustained 'cold-snaps'. However, challenges remain in deciphering whether observed trends reflect a true biological signal, or are the result of heterogeneous spatial sampling. Specifically, this study did not determine conclusively whether spatial and temporal variability in sampled area reflects varying levels of sampling effort, or just broader areas colonised by a specific taxon.

Chapter 6 is an extension of the work presented in Chapter 5. In this chapter, the palaeolatitudinal distribution of coral reef habitat was estimated to evaluate the potential for different types of latitudinal biodiversity gradients to form for reef-associated taxa in deep time. To do so, ecological niche modelling was integrated with Earth System modelling to estimate the distribution of warm-water coral reefs over the past ~250 million years. This study's findings suggest that suitable habitat area was skewed towards the Northern Hemisphere for most of the last ~250 million years, implying that greater sampling opportunities might be available in the Northern Hemisphere for this time period. On the basis of estimated suitable habitat area and the species-area relationship, the latitudinal biodiversity gradient of reef-associated organisms appears to have become significantly steeper during the last 20–30 million years, forming the unimodal-type gradient observed today. A second unimodal-type gradient likely persisted during the Early Cretaceous. This is due to a steep decline in the amount of suitable habitat area from the tropics to poles during this interval. These findings support results from Chapter 5, and suggest that the observed unimodal-type gradient during the Early Cretaceous and the last 20–30 million years is likely a genuine biological signal, which can be explained by the distribution of suitable habitat area. A temperate peak and tropical decline in reef-associated organisms might have also been present during the Early Jurassic. However, aside from the aforementioned intervals, the latitudinal gradient of suitable area was fairly flat throughout the last ~250 million years, suggesting that the latitudinal biodiversity gradient might have also been relatively flat during this period.

Overall, the findings of this thesis strongly suggest the need to account for spatial sampling heterogeneity when attempting to reconstruct macroecological patterns in deep time. Given the inherent incompleteness of the fossil record, inferential methods such as ecological niche modelling provide a valuable tool in assessing the authenticity of observed biodiversity patterns.

7.2 Future work

The work presented throughout this thesis has addressed several palaeobiological questions using largely novel methods in the field. However, as with any study there is a limit to its scope. In Chapter 4, the detectability of different types of latitudinal biodiversity gradient was evaluated for shallow marine environments. Whilst the findings of this study are likely applicable to terrestrial environments, explicit testing is required to identify which regions and/or time intervals may be most appropriate for reconstructing the latitudinal biodiversity gradient on land. In addition, the simulations used in Chapter 4 were intentionally simple. However, future work should aim to generate more realistic occurrence-data by incorporating estimates of past climate from General Circulation Models. Significantly, this will enable the generation of species constrained by abiotic variables such as temperature and precipitation. Simulation-based studies are being increasingly implemented to address macroevolutionary questions (Tomašových et al., 2015; Qiao et al., 2016; Saupe et al., 2019c). In particular, process-based simulations hold significant value in their ability to test the mechanisms that lead to the emergence of observed macroecological patterns (Qiao et al., 2016; Saupe et al., 2019b, 2019c). In a similar approach to palaeoclimatic modelling and proxy data, future work should aim to model the biosphere using processed-based simulations and validate it against the limited data available from the fossil record.

Recent studies have begun to advocate the use of regional analyses over global as the latter do not truly capture a global signal (e.g. Close et al., 2020a, 2020b). Whilst some regional scale studies have already focused on well-sampled areas to examine the latitudinal biodiversity gradient (e.g. Fraser et al., 2014; Marcot et al., 2016), most analyses tend to use coarse latitudinal bins when assessing the latitudinal biodiversity gradient in deep time (Mannion et al., 2012; Nicholson et al., 2016; Kröger, 2018; Allen et al., 2020; Song et al., 2020). Future work on the latitudinal biodiversity gradient should consider variability in regional sampling. This will enable a more in-depth synthesis of the controls on observed patterns, including variability in outcrop area

(e.g. Chiarenza et al., 2019). Studies should also aim to test the sensitivity of results to different latitudinal bin sizes and placement. Recent work has already demonstrated the sensitivity of observed biodiversity patterns to temporal binning protocol (Dean et al., 2020), but further work is need for geospatial analyses. In addition, estimates of local richness (= alpha diversity) are likely valuable in examining the latitudinal biodiversity gradient as they offer an auxiliary view without the potential influence of binning protocol. Therefore, their inclusion in spatial studies is recommended.

Palaeobiological studies are limited by the coarse spatial and temporal resolutions of available data, whether occurrence datasets, palaeoclimatic data, or palaeogeographic reconstructions. However, while future studies will surely have access to higher-resolution palaeoclimate datasets, researchers should remain cautious of the trade-offs between model resolution and their ability to capture genuine broad-scale patterns. Given the potential for an increased amount of error to be introduced at higher spatial resolutions due to discordance between models (e.g. palaeorotations and palaeoclimate simulations), the use of Earth System model data with fossil occurrence datasets may be best suited to coarse spatial resolutions (e.g. 1° x 1°). In addition, future studies should aim to use a unified system approach, in which the palaeorotations of fossil occurrence datasets, as well as the boundary conditions of palaeoclimate simulations, are underpinned by the same palaeogeographic reconstructions ensuring congruence between datasets.

Lastly, whilst the fossil record is inherently incomplete, the recent dependence on databases such as the Paleobiology Database in palaeobiological studies is potentially problematic. The data contained within these databases is usually limited to the published literature. Consequently, immense quantities of so-called 'dark data' from museum collections remain excluded from the majority of deep time biodiversity studies, including those presented in this thesis. One recent study attempted to quantify this issue, and demonstrated that nine institutions across California, Oregon, and Washington contained 23 times the number of unique fossil localities for Cenozoic marine invertebrates than are currently in the Paleobiology Database (Marshall et al.,

2018). Whilst this figure is surely variable between taxonomic groups and time intervals, such 'dark data' evidently has importance for the reconstruction of biodiversity trends in deep time. Therefore, a long-term aim of the field should be to incorporate these data by working closely with museum curators and aiding the digitization of this 'dark data'. Nevertheless, it should be highlighted that the Paleobiology Database has enabled a plethora of studies, improved accessibility to data, and allowed reproducibility of results, all of which are an asset to palaeobiology.

–This page is intentionally left blank–

References

Abel, O., 1912, Grundzüge der Palaeobiologie der Wirbeltiere: Stuttgart, E. Schweizerbartsche Verlagsbuchhandlung Nagele.

Allen, A.P., and Gillooly, J.F., 2006, Assessing latitudinal gradients in speciation rates and biodiversity at the global scale: Ecology Letters, v. 9, p. 947–954, doi:10.1111/j.1461-0248.2006.00946.x.

Allen, B.J., Wignall, P.B., Hill, D.J., Saupe, E.E., and Dunhill, A.M., 2020, The latitudinal diversity gradient of tetrapods across the Permo-Triassic mass extinction and recovery interval: Proceedings of the Royal Society B: Biological Sciences, v. 287, doi:10.1098/rspb.2020.1125.

Allison, P.A., 1988, Konservat-Lagerstätten: Cause and Classification: Paleobiology, v. 14, p. 331–344.

Allison, P.A., and Bottjer, D.J., 2010, Taphonomy: process and bias through time: Netherlands, Springer, v. 32.

Allison, P.A., and Briggs, D.E.G., 1993, Paleolatitudinal sampling bias, Phanerozoic species diversity, and the end-Permian extinction: Geology, v. 21, p. 65–68.

Allison, P.A., and Briggs, D.E. (Eds.), 1991, Taphonomy: Releasing the Data Locked in the Fossil Record: New York, U.S.A., Plenum Publishers, Topics in Geobiology, v. 9.

Allison, P.A., and Wells, M.R., 2006, Circulation in large ancient epicontinental seas: what was different and why? PALAIOS, v. 21, p. 513–515, doi:10.2110/palo.2006.S06.

Allouche, O., Tsoar, A., and Kadmon, R., 2006, Assessing the accuracy of species distribution models: prevalence, kappa and the true skill statistic (TSS): Journal of Applied Ecology, v. 43, p. 1223–1232, doi:10.1111/j.1365-2664.2006.01214.x.

Alroy, J., 2014, Accurate and precise estimates of origination and extinction rates: Paleobiology, v. 40, p. 374–397, doi:10.1666/13036.

Alroy, J., 1996, Constant extinction, constrained diversification, and uncoordinated stasis in North American mammals: Palaeogeography, Palaeoclimatology, Palaeoecology, v. 127, p. 285–311, doi:10.1016/S0031-0182(96)00100-9.

Alroy, J. et al., 2001, Effects of sampling standardization on estimates of Phanerozoic marine diversification: Proceedings of the National Academy of Sciences, v. 98, p. 6261–6266, doi:10.1073/pnas.111144698.

Alroy, J., 2010a, Fair sampling of taxonomic richness and unbiased estimation of origination and extinction rates: The Paleontological Society Papers, v. 16, p. 55–80.

Alroy, J., 2010b, Geographical, environmental and intrinsic biotic controls on Phanerozoic marine diversification: Palaeontology, v. 53, p. 1211–1235, doi:10.1111/j.1475-4983.2010.01011.x.

Alroy, J., 2000, New methods for quantifying macroevolutionary patterns and processes: Paleobiology, v. 26, p. 707–733, doi:10.1666/0094-8373(2000)026<0707:NMFQMP>2.0.CO;2.

Alroy, J. et al., 2008, Phanerozoic Trends in the Global Diversity of Marine Invertebrates: Science, v. 321, p. 97–100, doi:10.1126/science.1156963.

Alroy, J., 2010c, The Shifting Balance of Diversity Among Major Marine Animal Groups: Science, v. 329, p. 1191–1194, doi:10.1126/science.1189910.

Alt, H., and Godau, M., 1995, Computing the Fréchet distance between two polygonal curves: International Journal of Computational Geometry & Applications, v. 5, p. 75–91.

Archibald, S.B., Bossert, W.H., Greenwood, D.R., and Farrell, B.D., 2010, Seasonality, the latitudinal gradient of diversity, and Eocene insects: Paleobiology, v. 36, p. 374–398, doi:10.1666/09021.1.

Archibald, S.B., Greenwood, D.R., and Mathewes, R.W., 2013, Seasonality, montane beta diversity, and Eocene insects: Testing Janzen's dispersal hypothesis in an equable world: Palaeogeography, Palaeoclimatology, Palaeoecology, v. 371, p. 1–8, doi:10.1016/j.palaeo.2012.10.043.

Arita, H.T., and Vázquez-Domínguez, E., 2008, The tropics: cradle, museum or casino? A dynamic null model for latitudinal gradients of species diversity: Ecology Letters, v. 11, p. 653–663, doi:10.1111/j.1461-0248.2008.01197.x.

Arldt, T., 1919, Handbuch der Palaeogeographie: Leipzig: Gebrüder Borntraeger, 1647 p.

Armstrong, H.A., Wagner, T., Herringshaw, L.G., Farnsworth, A.J., Lunt, D.J., Harland, M., Imber, J., Loptson, C., and Atar, E.F.L., 2016, Hadley circulation and precipitation changes controlling black shale deposition in the Late Jurassic Boreal Seaway: Paleoceanography, v. 31, p. 1041–1053, doi:10.1002/2015PA002911.

Baird, A.H., Sommer, B., and Madin, J.S., 2012, Pole-ward range expansion of Acropora spp. along the east coast of Australia: Coral Reefs, v. 31, p. 1063–1063, doi:10.1007/s00338-012-0928-6.

Báldi, A., 2008, Habitat heterogeneity overrides the species–area relationship: Journal of Biogeography, v. 35, p. 675–681, doi:10.1111/j.1365-2699.2007.01825.x.

Barnes, R., Sahr, K., Evenden, G., Johnson, A., and Warmerdam, F., 2017, dggridR: discrete global grids for R: R package version 0.1.12, https://CRAN.R-project.org/package=dggridR.

Barnosky, A.D. et al., 2011, Has the Earth's sixth mass extinction already arrived? Nature, v. 471, p. 51–57, doi:10.1038/nature09678.

Barnosky, A.D. et al., 2017, Merging paleobiology with conservation biology to guide the future of terrestrial ecosystems: Science, v. 355, doi:10.1126/science.aah4787.

Behrensmeyer, A.K., and Kidwell, S.M., 1985, Taphonomy's Contributions to Paleobiology: Paleobiology, v. 11, p. 105–119.

Behrensmeyer, A.K., Kidwell, S.M., and Gastaldo, R.A., 2000, Taphonomy and Paleobiology: Paleobiology, v. 26, p. 103–147.

Bellard, C., Bertelsmeier, C., Leadley, P., Thuiller, W., and Courchamp, F., 2012, Impacts of climate change on the future of biodiversity: Ecology Letters, p. 365–377, doi:10.1111/j.1461-0248.2011.01736.x.

Bellwood, D.R., and Hughes, T.P., 2001, Regional-Scale Assembly Rules and Biodiversity of Coral Reefs: Science, v. 292, p. 1532–1535, doi:10.1126/science.1058635.

Benson, R.B.J., and Butler, R.J., 2011, Uncovering the diversification history of marine tetrapods: ecology influences the effect of geological sampling biases: Geological Society, London, Special Publications, v. 358, p. 191–208, doi:10.1144/SP358.13.

Benson, R.B., Butler, R.J., Alroy, J., Mannion, P.D., Carrano, M.T., and Lloyd, G.T., 2016, Near-stasis in the long-term diversification of Mesozoic tetrapods: PLoS biology, v. 14, p. 1–27, doi:10.1371/journal.pbio.1002359.

Benson, R.B.J., Butler, R.J., Lindgren, J., and Smith, A.S., 2010, Mesozoic marine tetrapod diversity: mass extinctions and temporal heterogeneity in geological megabiases affecting vertebrates: Proceedings of the Royal Society B: Biological Sciences, v. 277, p. 829–834, doi:10.1098/rspb.2009.1845.

Benson, R.B.J., and Mannion, P.D., 2011, Multi-variate models are essential for understanding vertebrate diversification in deep time: Biology Letters, v. 8, p. 127–130, doi:10.1098/rsbl.2011.0460.

Berkelmans, R., De'ath, G., Kininmonth, S., and Skirving, W.J., 2004, A comparison of the 1998 and 2002 coral bleaching events on the Great Barrier Reef: spatial correlation, patterns, and predictions: Coral Reefs, v. 23, p. 74–83, doi:10.1007/s00338-003-0353-y.

Bivand, R., and Rundel, C., 2019, rgeos: Interface to Geometry Engine - Open Source ('GEOS'). R package version 0.5-2.:

Boecklen, W.J., 1986, Effects of Habitat Heterogeneity on the Species-Area Relationships of Forest Birds: Journal of Biogeography, v. 13, p. 59–68, doi:10.2307/2844849.

Booth, T.H., Nix, H.A., Busby, J.R., and Hutchinson, M.F., 2014, bioclim: the first species distribution modelling package, its early applications and relevance to most current MaxEnt studies: Diversity and Distributions, v. 20, p. 1–9, doi:10.1111/ddi.12144.

Briggs, J.C., 2007, Marine Longitudinal Biodiversity: Causes and Conservation: Diversity and Distributions, v. 13, p. 544–555, doi:10.1111/j.1472-4642.2007.00362.x.

Briggs, D.E.G., 2003, The Role of Decay and Mineralization in the Preservation of Soft-Bodied Fossils: Annual Review of Earth and Planetary Sciences, v. 31, p. 275–301, doi:10.1146/annurev.earth.31.100901.144746.

Brocas, W.M., Felis, T., Gierz, P., Lohmann, G., Werner, M., Obert, J.C., Scholz, D., Kölling, M., and Scheffers, S.R., 2018, Last Interglacial Hydroclimate Seasonality Reconstructed From Tropical Atlantic Corals: Paleoceanography and Paleoclimatology, v. 33, p. 198–213, doi:10.1002/2017PA003216.

Brocas, W.M., Felis, T., Obert, J.C., Gierz, P., Lohmann, G., Scholz, D., Kölling, M., and Scheffers, S.R., 2016, Last interglacial temperature seasonality reconstructed from tropical Atlantic corals: Earth and Planetary Science Letters, v. 449, p. 418–429, doi:10.1016/j.epsl.2016.06.005.

Brocklehurst, N., 2015, A simulation-based examination of residual diversity estimates as a method of correcting for sampling bias: Palaeontologia Electronica, v. 18.3.7T, p. 1–15, doi:10.26879/584.

Brocklehurst, N., Day, M.O., Rubidge, B.S., and Fröbisch, J., 2017, Olson's extinction and the latitudinal biodiversity gradient of tetrapods in the Permian: Proceedings of the Royal Society B: Biological Sciences, v. 284, p. 1–8.

Bronn, H.G., 1848, Index palaeontologicus, oder, Übersicht der bis jetzt bekannten fossilen Organismen: Stuttgart, E. Schweitzerbart, v. 2, p. 1–994.

Brown, J.H., 2013, Why are there so many species in the tropics? Journal of Biogeography, v. 41, p. 8–22, doi:10.1111/jbi.12228.

Brusatte, S.L. et al., 2015, The extinction of the dinosaurs: Biological Reviews, v. 90, p. 628–642, doi:10.1111/brv.12128.

Bush, A.M., and Bambach, R.K., 2004, Did alpha diversity increase during the Phanerozoic? Lifting the veils of taphonomic, latitudinal, and environmental biases: The Journal of Geology, v. 112, p. 625–642.

Butler, R.J., Benson, R.B.J., Carrano, M.T., Mannion, P.D., and Upchurch, P., 2010, Sea level, dinosaur diversity and sampling biases: investigating the 'common cause' hypothesis in the terrestrial realm: Proceedings of the Royal Society B: Biological Sciences, v. 278, p. 1165–1170, doi:10.1098/rspb.2010.1754.

Cairns, S.D., 2007, Deep-Water Corals: An Overview with special reference to Diversity and Distribution of Deep-Water Scleractinian Corals: Bulletin of Marine Science, v. 81, p. 311–322.

Cairns, S.D., 1999, Species richness of recent Scleractinia: Atoll Research Bulletin, v. 459, p. 1–46, doi:10.5479/si.00775630.459.1.

Capron, E., Govin, A., Stone, E.J., Masson-Delmotte, V., Mulitza, S., Otto-Bliesner, B., Rasmussen, T.L., Sime, L.C., Waelbroeck, C., and Wolff, E.W., 2014, Temporal and spatial structure of multi-millennial temperature changes at high latitudes during the Last Interglacial: Quaternary Science Reviews, v. 103, p. 116–133, doi:10.1016/j.quascirev.2014.08.018.

Cecca, F., Martin Garin, B., Marchand, D., Lathuiliere, B., and Bartolini, A., 2005, Paleoclimatic control of biogeographic and sedimentary events in Tethyan and peri-Tethyan areas during the Oxfordian (Late Jurassic): Palaeogeography, Palaeoclimatology, Palaeoecology, v. 222, p. 10–32, doi:10.1016/j.palaeo.2005.03.009.

Cesar, H.S.J. (Ed.), 2000, Collected essays on the economics of coral reefs: Kalmar, Cordio, 243 p.

Chao, A., and Jost, L., 2012, Coverage-based rarefaction and extrapolation: standardizing samples by completeness rather than size: Ecology, v. 93, p. 2533–2547, doi:10.1890/11-1952.1.

Cherns, L., and Wright, V.P., 2000, Missing molluscs as evidence of large-scale, early skeletal aragonite dissolution in a Silurian sea: Geology, v. 28, p. 791–794.

Chiarenza, A.A., Mannion, P.D., Lunt, D.J., Farnsworth, A., Jones, L.A., Kelland, S.-J., and Allison, P.A., 2019, Ecological niche modelling does not support climatically-driven dinosaur diversity decline before the Cretaceous/Paleogene mass extinction: Nature Communications, v. 10, p. 1–14, doi:10.1038/s41467-019-08997-2.

Chown, S.L., and Gaston, K.J., 2000, Areas, cradles and museums: the latitudinal gradient in species richness: Trends in Ecology & Evolution, v. 15, p. 311–315, doi:10.1016/S0169-5347(00)01910-8.

Chown, S.L., Gaston, K.J., and Williams, P.H., 1998, Global patterns in species richness of pelagic seabirds: the Procellariiformes: Ecography, v. 21, p. 342–350, doi:10.1111/j.1600-0587.1998.tb00399.x.

Clark, P.U., and Huybers, P., 2009, Interglacial and future sea level: Nature, v. 462, p. 856–857, doi:10.1038/462856a.

Cleary, T.J., Benson, R.B.J., Evans, S.E., and Barrett, P.M., 2018, Lepidosaurian diversity in the Mesozoic–Palaeogene: the potential roles of sampling biases and environmental drivers: Royal Society Open Science, v. 5, p. 1–18, doi:10.1098/rsos.171830.

Cleary, T.J., Moon, B.C., Dunhill, A.M., and Benton, M.J., 2015, The fossil record of ichthyosaurs, completeness metrics and sampling biases: Palaeontology, v. 58, p. 521–536, doi:10.1111/pala.12158.

Close, R.A., Benson, R.B.J., Alroy, J., Carrano, M.T., Cleary, T.J., Dunne, E.M., Mannion, P.D., Uhen, M.D., and Butler, R.J., 2020a, The apparent exponential radiation of Phanerozoic land vertebrates is an artefact of spatial sampling biases: Proceedings of the Royal Society B: Biological Sciences, v. 287, p. 20200372, doi:10.1098/rspb.2020.0372.

Close, R.A., Benson, R.B.J., Saupe, E.E., Clapham, M.E., and Butler, R.J., 2020b, The spatial structure of Phanerozoic marine animal diversity: Science, v. 368, p. 420–424, doi:10.1126/science.aay8309.

Close, R.A., Benson, R.B., Upchurch, P., and Butler, R.J., 2017, Controlling for the species-area effect supports constrained long-term Mesozoic terrestrial vertebrate diversification: Nature communications, v. 8, p. 1–11, doi:10.1038/ncomms15381.

Close, R.A., Evers, S.W., Alroy, J., and Butler, R.J., 2018, How should we estimate diversity in the fossil record? Testing richness estimators using sampling-standardised discovery curves: Methods in Ecology and Evolution, v. 9, p. 1386–1400, doi:10.1111/2041-210X.12987.

Collins, D.S., Avdis, A., Allison, P.A., Johnson, H.D., Hill, J., and Piggott, M.D., 2018, Controls on tidal sedimentation and preservation: Insights from numerical tidal modelling in the Late Oligocene–Miocene South China Sea, Southeast Asia: Sedimentology, v. 65, p. 2468–2505, doi:10.1111/sed.12474.

Colwell, R.K., and Hurtt, G.C., 1994, Nonbiological gradients in species richness and a spurious Rapoport effect: American Naturalist, v. 144, p. 570–595, doi:10.1086/285695.

Colwell, Robert.K., and Lees, D.C., 2000, The mid-domain effect: geometric constraints on the geography of species richness: Trends in Ecology & Evolution, v. 15, p. 70–76, doi:10.1016/S0169-5347(99)01767-X.

Colwell, R.K., Rahbek, C., and Gotelli, N.J., 2004, The mid-domain effect and species richness patterns:what have we learned so far? The American Naturalist, v. 163, p. E1-23, doi:10.1086/382056.

Condamine, F.L., Romieu, J., and Guinot, G., 2019, Climate cooling and clade competition likely drove the decline of lamniform sharks: Proceedings of the National Academy of Sciences, v. 116, p. 20584–20590, doi:10.1073/pnas.1902693116.

Connor, E.F., and McCoy, E.D., 1979, The statistics and biology of the species-area relationship: The American Naturalist, v. 113, p. 791–833.

Cooper, G.A., 1958, The Science of Paleontology: Journal of Paleontology, v. 32, p. 1010–1018.

Cooper, R.A., Maxwell, P.A., Crampton, J.S., Beu, A.G., Jones, C.M., and Marshall, B.A., 2006, Completeness of the fossil record: Estimating losses due to small body size: Geology, v. 34, p. 241–246, doi:10.1130/G22206.1.

Cotgreave, P., and Harvey, P.H., 1994, Evenness of Abundance in Bird Communities: Journal of Animal Ecology, v. 63, p. 365–374, doi:10.2307/5554.

Couce, E., Ridgwell, A., and Hendy, E.J., 2012, Environmental controls on the global distribution of shallow-water coral reefs: Journal of Biogeography, v. 39, p. 1508–1523, doi:10.1111/j.1365-2699.2012.02706.x.

Couce, E., Ridgwell, A., and Hendy, E.J., 2013, Future habitat suitability for coral reef ecosystems under global warming and ocean acidification: Global Change Biology, v. 19, p. 3592–3606, doi:10.1111/gcb.12335.

Crame, J.A., 2020, Early Cenozoic evolution of the latitudinal diversity gradient: Earth-Science Reviews, v. 202, p. 1–10, doi:10.1016/j.earscirev.2020.103090.

Crame, J.A., 2001, Taxonomic diversity gradients through geological time: Diversity and Distributions, v. 7, p. 175–189, doi:10.1111/j.1472-4642.2001.00106.x.

Crame, J.A., and Rosen, B.R., 2002, Cenozoic palaeogeography and the rise of modern biodiversity patterns: Geological Society, London, Special Publications, v. 194, p. 153–168, doi:10.1144/GSL.SP.2002.194.01.12.

Dalbeck, P., Cusack, M., Dobson, P.S., Allison, N., Fallick, A.E., and Tudhope, A.W., 2011, Identification and composition of secondary meniscus calcite in fossil coral and the effect on predicted sea surface temperature: Chemical Geology, v. 280, p. 314–322, doi:10.1016/j.chemgeo.2010.11.018.

Darwin, C., 1859, On the Origin of Species by Means of Natural Selection, or Preservation of Favoured Races in the Struggle for Life: London, John Murray.

Davis, E.B., McGuire, J.L., and Orcutt, J.D., 2014, Ecological niche models of mammalian glacial refugia show consistent bias: Ecography, v. 37, p. 1133–1138, doi:10.1111/ecog.01294.

De Celis, A., Narváez, I., and Ortega, F., 2020, Spatiotemporal palaeodiversity patterns of modern crocodiles (Crocodyliformes: Eusuchia): Zoological Journal of the Linnean Society, v. 189, p. 635–656, doi:10.1093/zoolinnean/zlz038.

Dean, C.D., 2018, Untangling the web of life: reconstructing spatial patterns in the palaeoenvironment, palaeoecology and taphonomy of the Western Interior Seaway [Ph.D.]: Imperial College London, doi:10.25560/72866.

Dean, C.D., Allison, P.A., Hampson, G.J., and Hill, J., 2019, Aragonite bias exhibits systematic spatial variation in the Late Cretaceous Western Interior Seaway, North America: Paleobiology, v. 45, p. 571–597, doi:10.1017/pab.2019.33.

Dean, C.D., Chiarenza, A.A., and Maidment, S.C.R., 2020, Formation binning: a new method for increased temporal resolution in regional studies, applied to the Late Cretaceous dinosaur fossil record of North America: Palaeontology, doi:10.1111/pala.12492.

Dean, C.D., Mannion, P.D., and Butler, R.J., 2016, Preservational bias controls the fossil record of pterosaurs: Palaeontology, v. 59, p. 225–247, doi:10.1111/pala.12225.

Dietl, G.P., Kidwell, S.M., Brenner, M., Burney, D.A., Flessa, K.W., Jackson, S.T., and Koch, P.L., 2015, Conservation Paleobiology: Leveraging Knowledge of the Past to Inform Conservation and Restoration: Annual Review of Earth and Planetary Sciences, v. 43, p. 79–103, doi:10.1146/annurev-earth-040610-133349.

Dimitriadou, E., Hornik, K., Leisch, F., Meyer, D., and Weingessel, A., 2008, Misc functions of the Department of Statistics (e1071), TU Wien: R package, v. 1, p. 5–24.

Dirzo, R., and Raven, P.H., 2003, Global State of Biodiversity and Loss: Annual Review of Environment and Resources, v. 28, p. 137–167, doi:10.1146/annurev.energy.28.050302.105532.

Dirzo, R., Young, H.S., Galetti, M., Ceballos, G., Isaac, N.J.B., and Collen, B., 2014, Defaunation in the Anthropocene: Science, v. 345, p. 401–406, doi:10.1126/science.1251817.

Dunhill, A.M., Hannisdal, B., and Benton, M.J., 2014, Disentangling rock record bias and common-cause from redundancy in the British fossil record: Nature Communications, v. 5, p. 1–9, doi:10.1038/ncomms5818.

Dunhill, A.M., Hannisdal, B., Brocklehurst, N., and Benton, M.J., 2018, On formation-based sampling proxies and why they should not be used to correct the fossil record: Palaeontology, v. 61, p. 119–132, doi:10.1111/pala.12331.

Dunne, E.M., Close, R.A., Button, D.J., Brocklehurst, N., Cashmore, D.D., Lloyd, G.T., and Butler, R.J., 2018, Diversity change during the rise of tetrapods and the impact of the 'Carboniferous rainforest collapse': Proceedings of the Royal Society B: Biological Sciences, v. 285, p. 1–8, doi:10.1098/rspb.2017.2730.

Dutton, A., and Lambeck, K., 2012, Ice Volume and Sea Level During the Last Interglacial: Science, v. 337, p. 216–219, doi:10.1126/science.1205749.

Ebach, M.C., and Dowding, E.M., 2017, Theodor Arldt (1878–1960): Parochial Pauker and Pioneering Palaeobiogeographer: Zootaxa, v. 4319, p. 157–168, doi:10.11646/zootaxa.4319.1.8.

Edwards, P.N., 2011, History of climate modeling: WIREs Climate Change, v. 2, p. 128–139, doi:10.1002/wcc.95.

Efremov, I.A., 1940, Taphonomy: a new branch of paleontology: The Pan-American Geologist, v. 74, p. 81–93.

Elith, J., Kearney, M., and Phillips, S., 2010, The art of modelling range-shifting species: Methods in Ecology and Evolution, v. 1, p. 330–342, doi:10.1111/j.2041-210X.2010.00036.x.

Esty, W.W., 1986, The Efficiency of Good's Nonparametric Coverage Estimator: The Annals of Statistics, v. 14, p. 1257–1260, doi:10.1214/aos/1176350066.

Farnsworth, A. et al., 2019a, Past East Asian monsoon evolution controlled by paleogeography, not CO2: Science Advances, v. 5, p. 1–13, doi:10.1126/sciadv.aax1697.

Farnsworth, A., Lunt, D.J., O'Brien, C.L., Foster, G.L., Inglis, G.N., Markwick, P., Pancost, R.D., and Robinson, S.A., 2019b, Climate Sensitivity on Geological Timescales Controlled by Nonlinear Feedbacks and Ocean Circulation: Geophysical Research Letters, v. 46, p. 9880–9889, doi:10.1029/2019GL083574.

Fastovsky, D.E., Huang, Y., Hsu, J., Martin-McNaughton, J., Sheehan, P.M., and Weishampel, D.B., 2004, Shape of Mesozoic dinosaur richness: Geology, v. 32, p. 877–880, doi:10.1130/G20695.1.

Feeley, K.J., and Stroud, J.T., 2018, Where on Earth are the "tropics"? Frontiers of Biogeography, v. 10, doi:10.21425/F5FBG38649.

Fenton, I.S., Pearson, P.N., Dunkley Jones, T., Farnsworth, A., Lunt, D.J., Markwick, P., and Purvis, A., 2016, The impact of Cenozoic cooling on assemblage diversity in planktonic foraminifera: Philosophical Transactions of the Royal Society B: Biological Sciences, v. 371, p. 1–12, doi:10.1098/rstb.2015.0224.

Field, R. et al., 2009, Spatial species-richness gradients across scales: a meta-analysis: Journal of Biogeography, v. 36, p. 132–147, doi:10.1111/j.1365-2699.2008.01963.x.

Fieldsend, T.W., 2020, A Global-Scale Mid-Domain Effect Cannot Explain the Latitudinal Gradient in Species Richness: Acta Biotheoretica, v. 68, p. 271–274, doi:10.1007/s10441-019-09361-z.

Fine, P.V.A., 2015, Ecological and Evolutionary Drivers of Geographic Variation in Species Diversity: Annual Review of Ecology, Evolution, and Systematics, v. 46, p. 369–392, doi:10.1146/annurev-ecolsys-112414-054102.

Fitzgerald, P.C., and Carlson, S.J., 2006, Examining the latitudinal diversity gradient in Paleozoic terebratulide brachiopods: should singleton data be removed? Paleobiology, v. 32, p. 367–386, doi:10.1666/05029.1.

Flato, G. et al., 2013, Evaluation of Climate Models, *in* Stocker, T.F., Qin, D., Plattner, G.-K., Tignor, M., Allen, S.K., Boschung, J., Nauels, A., Xia, Y., Bex, V., and Midgley, P.M. eds., Climate Change 2013: The Physical Science Basis. Contribution of Working Group I to the Fifth Assessment Report of the Intergovernmental Panel on Climate Change, Cambridge, United Kingdom and New York, NY, USA, Cambridge University Press, p. 741–866, doi:10.1017/CBO9781107415324.020.

Foote, M., 1992, Rarefaction Analysis of Morphological and Taxonomic Diversity: Paleobiology, v. 18, p. 1–16.

Foote, M., 1994, Temporal Variation in Extinction Risk and Temporal Scaling of Extinction Metrics: Paleobiology, v. 20, p. 424–444.

Foote, M., Crampton, J.S., Beu, A.G., Marshall, B.A., Cooper, R.A., Maxwell, P.A., and Matcham, I., 2007, Rise and Fall of Species Occupancy in Cenozoic Fossil Mollusks: Science, v. 318, p. 1131–1134, doi:10.1126/science.1146303.

Foote, M., and Raup, D.M., 1996, Fossil preservation and the stratigraphic ranges of taxa: Paleobiology, v. 22, p. 121–140.

Franklin, J., 2010, Mapping Species Distributions: Spatial Inference and Prediction: Cambridge, United Kingdom, Cambridge University Press, doi:10.1017/CBO9780511810602.

Fraser, D., 2017, Can latitudinal richness gradients be measured in the terrestrial fossil record? Paleobiology, v. 43, p. 479–494, doi:10.1017/pab.2017.2.

Fraser, D., Hassall, C., Gorelick, R., and Rybczynski, N., 2014, Mean Annual Precipitation Explains Spatiotemporal Patterns of Cenozoic Mammal Beta Diversity and Latitudinal Diversity Gradients in North America: PLoS ONE, v. 9, p. 1–10, doi:10.1371/journal.pone.0106499.

Freeman, L.A., 2015, Robust Performance of Marginal Pacific Coral Reef Habitats in Future Climate Scenarios: PLOS ONE, v. 10, p. 1–16, doi:10.1371/journal.pone.0128875.

Freeman, L.A., Kleypas, J.A., and Miller, A.J., 2013, Coral Reef Habitat Response to Climate Change Scenarios: PLoS ONE, v. 8, p. 1–14, doi:10.1371/journal.pone.0082404.

Freiwald, A., Fossa, J.H., Grehan, A., Koslow, T., and Roberts, J.M., 2004, Cold-water coral reefs: out of sight-no longer out of mind: UNEP-WCMC.

Friedman, M., and Sallan, L.C., 2012, Five hundred million years of extinction and recovery: a phanerozoic survey of large-scale diversity patterns in fishes: Palaeontology, v. 55, p. 707–742, doi:10.1111/j.1475-4983.2012.01165.x.

Fu, D. et al., 2019, The Qingjiang biota—A Burgess Shale–type fossil Lagerstätte from the early Cambrian of South China: Science, v. 363, p. 1338–1342, doi:10.1126/science.aau8800.

García Molinos, J., Halpern, B.S., Schoeman, D.S., Brown, C.J., Kiessling, W., Moore, P.J., Pandolfi, J.M., Poloczanska, E.S., Richardson, A.J., and Burrows, M.T., 2016, Climate velocity and the future global redistribution of marine biodiversity: Nature Climate Change, v. 6, p. 83–88, doi:10.1038/nclimate2769.

Gaston, K.J., and Blackburn, T.M., 1996, The tropics as a museum of biological diversity: an analysis of the New World avifauna: Proceedings of the Royal Society of London. Series B: Biological Sciences, v. 263, p. 63–68, doi:10.1098/rspb.1996.0011.

Gates, W.L., 1976, The Numerical Simulation of Ice-Age Climate with a Global General Circulation Model: Journal of the Atmospheric Sciences, v. 33, p. 1844–1873, doi:10.1175/1520-0469(1976)033<1844:TNSOIA>2.0.CO;2.

Glynn, P.W., 1984, Widespread Coral Mortality and the 1982–83 El Niño Warming Event: Environmental Conservation, v. 11, p. 133–146, doi:10.1017/S0376892900013825.

Good, I.J., 1953, The Population Frequencies of Species and the Estimation of Population Parameters: Biometrika, v. 40, p. 237–264, doi:10.1093/biomet/40.3-4.237.

Gordon, C., Cooper, C., Senior, C.A., Banks, H., Gregory, J.M., Johns, T.C., Mitchell, J.F.B., and Wood, R.A., 2000, The simulation of SST, sea ice extents and ocean heat transports in a version of the Hadley Centre coupled model without flux adjustments: Climate Dynamics, v. 16, p. 147–168, doi:10.1007/s003820050010.

Gough, D.O., 1981, Solar interior structure and luminosity variations: Solar Physics, v. 74, p. 21–34, doi:10.1007/BF00151270.

Gower, J.C., and Ross, G.J.S., 1969, Minimum Spanning Trees and Single Linkage Cluster Analysis: Journal of the Royal Statistical Society. Series C (Applied Statistics), v. 18, p. 54–64, doi:10.2307/2346439.

Greenstein, B.J., and Pandolfi, J.M., 2008, Escaping the heat: range shifts of reef coral taxa in coastal Western Australia: Global Change Biology, v. 14, p. 513–528, doi:10.1111/j.1365-2486.2007.01506.x.

Gröcke, D.R., Price, G.D., Ruffell, A.H., Mutterlose, J., and Baraboshkin, E., 2003, Isotopic evidence for Late Jurassic–Early Cretaceous climate change: Palaeogeography, Palaeoclimatology, Palaeoecology, v. 202, p. 97–118, doi:10.1016/S0031-0182(03)00631-X.

Grupstra, C.G.B., Coma, R., Ribes, M., Leydet, K.P., Parkinson, J.E., McDonald, K., Catllà, M., Voolstra, C.R., Hellberg, M.E., and Coffroth, M.A., 2017, Evidence for coral range expansion accompanied by reduced diversity of Symbiodinium genotypes: Coral Reefs, v. 36, p. 981–985, doi:10.1007/s00338-017-1589-2.

Guinan, J., Brown, C., Dolan, M.F.J., and Grehan, A.J., 2009, Ecological niche modelling of the distribution of cold-water coral habitat using underwater remote sensing data: Ecological Informatics, v. 4, p. 83–92, doi:10.1016/j.ecoinf.2009.01.004.

Hair Jr, J.F., Hult, G.T.M., Ringle, C., and Sarstedt, M., 2016, A primer on partial least squares structural equation modeling (PLS-SEM): London, United Kingdom, Sage publications.

Hallam, A., Grose, J.A., and Ruffell, A.H., 1991, Palaeoclimatic significance of changes in clay mineralogy across the Jurassic-Cretaceous boundary in England and France: Palaeogeography, Palaeoclimatology, Palaeoecology, v. 81, p. 173–187, doi:10.1016/0031-0182(91)90146-I.

Hannisdal, B., and Peters, S.E., 2011, Phanerozoic Earth System Evolution and Marine Biodiversity: Science, v. 334, p. 1121–1124, doi:10.1126/science.1210695.

Hawkins, B.A., 2001, Ecology's oldest pattern? Trends in Ecology & Evolution, v. 16, p. 470, doi:10.1016/S0169-5347(01)02197-8.

Haywood, A.M. et al., 2019, What can Palaeoclimate Modelling do for you? Earth Systems and Environment, v. 3, p. 1–18, doi:10.1007/s41748-019-00093-1.

Heron, S.F., Maynard, J.A., van Hooidonk, R., and Eakin, C.M., 2016, Warming Trends and Bleaching Stress of the World's Coral Reefs 1985–2012: Scientific Reports, v. 6, p. 1–14, doi:10.1038/srep38402.

Hillebrand, H., 2004, On the generality of the latitudinal diversity gradient: The American Naturalist, v. 163, p. 192–211.

Hoegh-Guldberg, O., 2011, Coral reef ecosystems and anthropogenic climate change: Regional Environmental Change, v. 11, p. 215–227, doi:10.1007/s10113-010-0189-2.

Hoffman, J.S., Clark, P.U., Parnell, A.C., and He, F., 2017, Regional and global sea-surface temperatures during the last interglaciation: Science, v. 355, p. 276–279, doi:10.1126/science.aai8464.

Holland, S.M., 1995, The Stratigraphic Distribution of Fossils: Paleobiology, v. 21, p. 92–109.

Holloway, M.D., Sime, L.C., Singarayer, J.S., Tindall, J.C., and Valdes, P.J., 2016, Reconstructing paleosalinity from δ18O: Coupled model simulations of the Last Glacial Maximum, Last Interglacial and Late Holocene: Quaternary Science Reviews, v. 131, p. 350–364, doi:10.1016/j.quascirev.2015.07.007.

Hooidonk, R. van, Maynard, J.A., Manzello, D., and Planes, S., 2014, Opposite latitudinal gradients in projected ocean acidification and bleaching impacts on coral reefs: Global Change Biology, v. 20, p. 103–112, doi:10.1111/gcb.12394.

Hsieh, T.C., Ma, K.H., and Chao, A., 2016, iNEXT: an R package for rarefaction and extrapolation of species diversity (Hill numbers): Methods in Ecology and Evolution, v. 7, p. 1451–1456, doi:10.1111/2041-210X.12613.

Hughes, T.P. et al., 2017a, Coral reefs in the Anthropocene: Nature, v. 546, p. 82–90, doi:10.1038/nature22901.

Hughes, T.P. et al., 2017b, Global warming and recurrent mass bleaching of corals: Nature, v. 543, p. 373–377, doi:10.1038/nature21707.

Hughes, L., Cawsey, E.M., and Westoby, M., 1996, Geographic and Climatic Range Sizes of Australian Eucalypts and a Test of Rapoport's Rule: Global Ecology and Biogeography Letters, v. 5, p. 128–142, doi:10.2307/2997395.

Humboldt, A. von, 1808, Ansichten der Natur: Cotta, Tübingen.

Humboldt, A. von, and Bonpland, A., 1807, Essai sur la Géographie des Plantes; Accompagne d'un Tableau Physique des Régions Équinoxiales: Paris: Fr. Schoell, 155 p.

Hunt, T.S., 1873, The Paleogeography of the North-American Continent: Journal of the American Geographical Society of New York, v. 4, p. 416–431, doi:10.2307/196403.

Hutchinson, G.E., 1957, Population studies – Animal ecology and demography – Concluding remarks: Cold Spring Harbor Symposia on Quantitative Biology, v. 22, p. 415–427, doi:10.1101/SQB.1957.022.01.039.

IMaRS-USF, and IRD, 2005, Millennium Coral Reef Mapping Project: Cambridge, United Kingdom, UNEP World Conservation Monitoring Centre.

IPCC, 2013, Climate Change 2013: The Physical Science Basis. Contribution of Working Group I to the Fifth Assessment Report of the Intergovernmental Panel on Climate Change: Cambridge, United Kingdom and New York, NY, USA, Cambridge University Press, 1535 p., doi:10.1017/CBO9781107415324.

IPCC, 2014, Climate change 2014: synthesis report. Contribution of Working Groups I, II and III to the Fifth Assessment Report of the Intergovernmental Panel on Climate Change: Geneva, Switzerland, Intergovernmental Panel on Climate Change, 151 p.

Jablonski, D., 2008, Extinction and the spatial dynamics of biodiversity: Proceedings of the National Academy of Sciences, v. 105, p. 11528–11535, doi:10.1073/pnas.0801919105.

Jablonski, D., Belanger, C.L., Berke, S.K., Huang, S., Krug, A.Z., Roy, K., Tomasovych, A., and Valentine, J.W., 2013, Out of the tropics, but how? Fossils, bridge species, and thermal ranges in the dynamics of the marine latitudinal diversity gradient: Proceedings of the National Academy of Sciences, v. 110, p. 487–494, doi:10.1073/pnas.1308997110.

Jablonski, D., Huang, S., Roy, K., and Valentine, J.W., 2017, Shaping the latitudinal diversity gradient: new perspectives from a synthesis of paleobiology and biogeography: The American Naturalist, v. 189, p. 1–12.

Jablonski, D., Roy, K., and Valentine, J.W., 2006, Out of the tropics: evolutionary dynamics of the latitudinal diversity gradient: Science, v. 314, p. 102–106, doi:10.1126/science.1130880.

Jackson, J.B., and Johnson, K.G., 2001, Measuring past biodiversity: Science, v. 293, p. 2401–2404.

Jeffers, D., and Willis, K.J., 2014, Vegetation response to climate change during the Last Interglacial–Last Glacial transition in the southern Bekaa Valley, Lebanon: Palynology, v. 38, p. 195–206, doi:10.1080/01916122.2014.880958.

Jetz, W., and Fine, P.V.A., 2012, Global Gradients in Vertebrate Diversity Predicted by Historical Area-Productivity Dynamics and Contemporary Environment: PLoS Biology, v. 10, p. e1001292, doi:10.1371/journal.pbio.1001292.

Jiang, L.-Q., Feely, R.A., Carter, B.R., Greeley, D.J., Gledhill, D.K., and Arzayus, K.M., 2015, Climatological distribution of aragonite saturation state in the global oceans: Global Biogeochemical Cycles, v. 29, p. 1656–1673, doi:10.1002/2015GB005198.

Johannes, R., Wiebe, W., Crossland, C., Rimmer, D., and Smith, S., 1983, Latitudinal limits of coral reef growth: Marine Ecology Progress Series, v. 11, p. 105–111, doi:10.3354/meps011105.

Johnson, K.G., 2003, New data for old questions: Paleobiology, v. 29, p. 19–21.

Jones, L.A., Mannion, P.D., Farnsworth, A., Valdes, P.J., Kelland, S.-J., and Allison, P.A., 2019, Coupling of palaeontological and neontological reef coral data improves forecasts of biodiversity responses under global climatic change: Royal Society Open Science, v. 6, p. 1–13, doi:10.1098/rsos.182111.

Kearney, M.R., Wintle, B.A., and Porter, W.P., 2010, Correlative and mechanistic models of species distribution provide congruent forecasts under climate change: Conservation Letters, v. 3, p. 203–213, doi:10.1111/j.1755-263X.2010.00097.x.

Kennedy, A.T., Farnsworth, A., Lunt, D.J., Lear, C.H., and Markwick, P.J., 2015, Atmospheric and oceanic impacts of Antarctic glaciation across the Eocene-Oligocene transition: Philosophical Transactions. Series A, Mathematical, Physical, and Engineering Sciences, v. 373, p. 1–18, doi:10.1098/rsta.2014.0419.

Kidwell, S.M., 1986, Models for fossil concentrations: paleobiologic implications: Paleobiology, v. 12, p. 6–24, doi:10.1017/S0094837300002943.

Kidwell, S.M., 1997, Time-averaging in the marine fossil record: Overview of strategies and uncertainties: Geobios, v. 30, p. 977–995, doi:10.1016/S0016-6995(97)80219-7.

Kidwell, S.M., and Flessa, K.W., 1996, The Quality of the Fossil Record: Populations, Species, and Communities: Annual Review of Earth and Planetary Sciences, v. 24, p. 433–464, doi:10.1146/annurev.earth.24.1.433.

Kidwell, S.M., and Holland, S.M., 2002, The Quality of the Fossil Record: Implications for Evolutionary Analyses: Annual Review of Ecology and Systematics, v. 33, p. 561–588, doi:10.1146/annurev.ecolsys.33.030602.152151.

Kiessling, W., 2005, Habitat effects and sampling bias on Phanerozoic reef distribution: Facies, v. 51, p. 24–32, doi:10.1007/s10347-004-0044-3.

Kiessling, W., 2001a, Paleoclimatic significance of Phanerozoic reefs: Geology, v. 29, p. 751–754, doi:10.1130/0091-7613(2001)029<0751:PSOPR>2.0.CO;2.

Kiessling, W., 2001b, Phanerozoic Reef Trends Based on the Paleoreef Database, *in* Stanley, G.D. ed., The History and Sedimentology of Ancient Reef Systems, Boston, MA, Springer US, Topics in Geobiology, v. 17, p. 41–88, doi:10.1007/978-1-4615-1219-6_2.

Kiessling, W., and Flügel, E., 2002, Paleoreefs—A database on Phanerozoic reefs: SEPM Society for Sedimentary Geology, v. 72, doi:10.2110/pec.02.72.0077.

Kiessling, W., and Kocsis, Á.T., 2015, Biodiversity dynamics and environmental occupancy of fossil azooxanthellate and zooxanthellate scleractinian corals: Paleobiology, v. 41, p. 402–414, doi:10.1017/pab.2015.6.

Kiessling, W., Simpson, C., Beck, B., Mewis, H., and Pandolfi, J.M., 2012, Equatorial decline of reef corals during the last Pleistocene interglacial: Proceedings of the National Academy of Sciences, v. 109, p. 21378–21383, doi:10.1073/pnas.1214037110.

Kim, S.W. et al., 2019, Refugia under threat: Mass bleaching of coral assemblages in high-latitude eastern Australia: Global Change Biology, v. 25, p. 3918–3931, doi:10.1111/gcb.14772.

Kinlock, N.L., Prowant, L., Herstoff, E.M., Foley, C.M., Akin-Fajiye, M., Bender, N., Umarani, M., Ryu, H.Y., Şen, B., and Gurevitch, J., 2018, Explaining global variation in the latitudinal diversity gradient: Meta-analysis confirms known patterns and uncovers new ones: Global Ecology and Biogeography, v. 27, p. 125–141.

Kleypas, J.A., Mcmanus, J.W., and Meñez, L.A.B., 1999, Environmental Limits to Coral Reef Development: Where Do We Draw the Line? American Zoologist, v. 39, p. 146–159, doi:10.1093/icb/39.1.146.

Knowlton, N., 2001, Coral Reef Biodiversity—Habitat Size Matters: Science, v. 292, p. 1493–1495, doi:10.1126/science.1061690.

Knowlton, N., Brainard, R.E., Fisher, R., Moews, M., Plaisance, L., and Caley, M.J., 2010, Coral Reef Biodiversity, *in* McIntyre, A.D. ed., Life in the World's Oceans, Oxford, UK, Wiley-Blackwell, p. 65–78, doi:10.1002/9781444325508.ch4.

Kocsis, Á.T., Reddin, C.J., Alroy, J., and Kiessling, W., 2019, The R package divDyn for quantifying diversity dynamics using fossil sampling data: Methods in Ecology and Evolution, v. 10, p. 735–743, doi:10.1111/2041-210X.13161.

Kröger, B., 2018, Changes in the latitudinal diversity gradient during the Great Ordovician Biodiversification Event: Geology, v. 46, p. 127–130.

Krug, A.Z., Jablonski, D., Valentine, J.W., and Roy, K., 2009, Generation of Earth's First-Order Biodiversity Pattern: Astrobiology, v. 9, p. 113–124, doi:10.1089/ast.2008.0253.

Kunin, W.E., 1998, Extrapolating Species Abundance Across Spatial Scales: Science, v. 281, p. 1513–1515, doi:10.1126/science.281.5382.1513.

Lagomarcino, A.J., and Miller, A.I., 2012, The Relationship between Genus Richness and Geographic Area in Late Cretaceous Marine Biotas: Epicontinental Sea versus Open-Ocean-Facing Settings: PLOS ONE, v. 7, p. 1–9, doi:10.1371/journal.pone.0040472.

Lawrence, D.R., 1968, Taphonomy and Information Losses in Fossil Communities: GSA Bulletin, v. 79, p. 1315–1330.

Le Treut, H., Somerville, R., Cubasch, U., Ding, Y., Mauritzen, C., Mokssit, A., Peterson, T., and Prather, M., 2007, Historical Overview of Climate Change Science, *in* Solomon, S., Qin, D., Manning, M., Chen, Z., Marquis, M., Averyt, K.B., Tignor, M., and Miller, H.L. eds., Climate Change 2007: The Physical Science Basis. Contribution of Working Group I to the Fourth Assessment Report of the Intergovernmental Panel on Climate Change, Cambridge, United Kingdom, Cambridge University Press, v. 16.

Leprieur, F. et al., 2016, Plate tectonics drive tropical reef biodiversity dynamics: Nature Communications, v. 7, p. 1–8, doi:10.1038/ncomms11461.

Lewis, S.L., and Maslin, M.A., 2015, Defining the Anthropocene: Nature, v. 519, p. 171–180, doi:10.1038/nature14258.

Liaw, A., and Wiener, M., 2002, Classification and regression by randomForest: R News, v. 2, p. 18–22.

Lima-Ribeiro, M.S., Moreno, A.K.M., Terribile, L.C., Caten, C.T., Loyola, R., Rangel, T.F., and Diniz-Filho, J.A.F., 2017, Fossil record improves biodiversity risk assessment under future climate change scenarios: Diversity and Distributions, v. 23, p. 922–933, doi:10.1111/ddi.12575.

Liow, L.H., 2013, Simultaneous estimation of occupancy and detection probabilities: an illustration using Cincinnatian brachiopods: Paleobiology, v. 39, p. 193–213.

Liu, C., Newell, G., and White, M., 2016, On the selection of thresholds for predicting species occurrence with presence-only data: Ecology and Evolution, v. 6, p. 337–348, doi:10.1002/ece3.1878.

Liu, C., White, M., and Newell, G., 2013, Selecting thresholds for the prediction of species occurrence with presence-only data: Journal of Biogeography, v. 40, p. 778–789, doi:10.1111/jbi.12058.

Lloyd, G.T., 2012, A refined modelling approach to assess the influence of sampling on palaeobiodiversity curves: new support for declining Cretaceous dinosaur richness: Biology Letters, v. 8, p. 123–126, doi:10.1098/rsbl.2011.0210.

Lloyd, G.T., and Friedman, M., 2013, A survey of palaeontological sampling biases in fishes based on the Phanerozoic record of Great Britain: Palaeogeography, Palaeoclimatology, Palaeoecology, v. 372, p. 5–17, doi:10.1016/j.palaeo.2012.07.023.

Lloyd, G.T., Pearson, P.N., Young, J.R., and Smith, A.B., 2012, Sampling bias and the fossil record of planktonic foraminifera on land and in the deep sea: Paleobiology, v. 38, p. 569–584, doi:10.1666/11041.1.

Loptson, C.A., Lunt, D.J., and Francis, J.E., 2014, Investigating vegetation-climate feedbacks during the early Eocene: Climate of the Past, v. 10, p. 419–436.

Lyman, R.L., 1994, Vertebrate taphonomy: Cambridge, United Kingdom, Cambridge University Press.

Lyster, S.J., Whittaker, A.C., Allison, P.A., Lunt, D.J., and Farnsworth, A., 2020, Predicting sediment discharges and erosion rates in deep time—examples from the late Cretaceous North American continent: Basin Research, p. 1–27, doi:10.1111/bre.12442.

MacArthur, R.H., and Wilson, E.O., 1967, The Theory of Island Biogeography: Princeton, U.S.A., Princeton University Press.

MacKenzie, D.I., Nichols, J.D., Royle, J.A., Pollock, K.H., Bailey, L., and Hines, J.E., 2017, Occupancy estimation and modeling: inferring patterns and dynamics of species occurrence: London, United Kingdom, Academic Press.

Mannion, P.D., Benson, R.B.J., Carrano, M.T., Tennant, J.P., Judd, J., and Butler, R.J., 2015, Climate constrains the evolutionary history and biodiversity of crocodylians: Nature Communications, v. 6, p. 1–9, doi:10.1038/ncomms9438.

Mannion, P.D., Benson, R.B., Upchurch, P., Butler, R.J., Carrano, M.T., and Barrett, P.M., 2012, A temperate palaeodiversity peak in Mesozoic dinosaurs and evidence for Late Cretaceous geographical partitioning: Global Ecology and Biogeography, v. 21, p. 898–908.

Mannion, P.D., Chiarenza, A.A., Godoy, P.L., and Cheah, Y.N., 2019, Spatiotemporal sampling patterns in the 230 million year fossil record of terrestrial crocodylomorphs and their impact on diversity: Palaeontology, v. 62, p. 615–637, doi:10.1111/pala.12419.

Mannion, P.D., Upchurch, P., Benson, R.B.J., and Goswami, A., 2014, The latitudinal biodiversity gradient through deep time: Trends in Ecology & Evolution, v. 29, p. 42–50, doi:10.1016/j.tree.2013.09.012.

Marcot, J.D., Fox, D.L., and Niebuhr, S.R., 2016, Late Cenozoic onset of the latitudinal diversity gradient of North American mammals: Proceedings of the National Academy of Sciences, v. 113, p. 7189–7194.

Markwick, P.J., 1998, Crocodilian diversity in space and time: the role of climate in paleoecology and its implication for understanding K/T extinctions: Paleobiology, v. 24, p. 470–497, doi:10.1017/S009483730002011X.

Markwick, P.J., 2019, Palaeogeography in exploration: Geological Magazine, v. 156, p. 366–407.

Markwick, P.J., 2007, The palaeogeographic and palaeoclimatic significance of climate proxies for data-model comparisons, *in* Williams, M., Haywood, A.M., Gregory, F.J., and Schmidt, D.N. eds., Deep-Time Perspectives on Climate Change: Marrying the Signal from Computer Models and Biological Proxies, The Geological Society of London on behalf of The Micropalaeontological Society, p. 251–312, doi:10.1144/TMS002.13.

Markwick, P.J., and Valdes, P.J., 2004, Palaeo-digital elevation models for use as boundary conditions in coupled ocean–atmosphere GCM experiments: a Maastrichtian (late Cretaceous) example: Palaeogeography, Palaeoclimatology, Palaeoecology, v. 213, p. 37–63, doi:10.1016/j.palaeo.2004.06.015.

Marshall, C.R. et al., 2018, Quantifying the dark data in museum fossil collections as palaeontology undergoes a second digital revolution: Biology Letters, v. 14, p. 1–14, doi:10.1098/rsbl.2018.0431.

Martin, R.E., 1999, Taphonomy: a process approach: Cambridge, United Kingdom, Cambridge University Press, 526 p.

Marzocchi, A., Lunt, D.J., Flecker, R., Bradshaw, C.D., Farnsworth, A., and Hilgen, F.J., 2015, Orbital control on late Miocene climate and the North African monsoon: insight from an ensemble of sub-precessional simulations: Climate of the Past, v. 11, p. 1271–1295.

McCallum, M.L., 2015, Vertebrate biodiversity losses point to a sixth mass extinction: Biodiversity and Conservation, v. 24, p. 2497–2519, doi:10.1007/s10531-015-0940-6.

McCulloch, M.T., and Esat, T., 2000, The coral record of last interglacial sea levels and sea surface temperatures: Chemical Geology, v. 169, p. 107–129, doi:10.1016/S0009-2541(00)00260-6.

McKay, N.P., Overpeck, J.T., and Otto-Bliesner, B.L., 2011, The role of ocean thermal expansion in Last Interglacial sea level rise: Geophysical Research Letters, v. 38, doi:10.1029/2011GL048280.

McKenna, D.D., and Farrell, B.D., 2006, Tropical forests are both evolutionary cradles and museums of leaf beetle diversity: Proceedings of the National Academy of Sciences, v. 103, p. 10947–10951, doi:10.1073/pnas.0602712103.

Meseguer, A.S., and Condamine, F.L., 2020, Ancient tropical extinctions at high latitudes contributed to the latitudinal diversity gradient: Evolution, p. 1–22, doi:10.1111/evo.13967.

Miller, A.I., and Foote, M., 1996, Calibrating the Ordovician Radiation of marine life: implications for Phanerozoic diversity trends: Paleobiology, v. 22, p. 304–309, doi:10.1666/0094-8373-22.2.304.

Mittelbach, G.G. et al., 2007, Evolution and the latitudinal diversity gradient: speciation, extinction and biogeography: Ecology Letters, v. 10, p. 315–331, doi:10.1111/j.1461-0248.2007.01020.x.

Moberg, F., and Folke, C., 1999, Ecological goods and services of coral reef ecosystems: Ecological Economics, v. 29, p. 215–233, doi:10.1016/S0921-8009(99)00009-9.

Muhs, D.R., Simmons, K.R., and Steinke, B., 2002, Timing and warmth of the Last Interglacial period: new U-series evidence from Hawaii and Bermuda and a new fossil compilation for North America: Quaternary Science Reviews, v. 21, p. 1355–1383, doi:10.1016/S0277-3791(01)00114-7.

Muir, P.R., Wallace, C.C., Done, T., and Aguirre, J.D., 2015, Limited scope for latitudinal extension of reef corals: Science, v. 348, p. 1135–1138, doi:10.1126/science.1259911.

Newell, N.D., 1952, Periodicity in Invertebrate Evolution: Journal of Paleontology, v. 26, p. 371–385.

Nicholson, D.B., Holroyd, P.A., Valdes, P., and Barrett, P.M., 2016, Latitudinal diversity gradients in Mesozoic non-marine turtles: Royal Society open science, v. 3, p. 1–8.

Oksanen, J. et al., 2019, vegan: Community Ecology Package. R package version 2.5-6:

Olivier, P.I., Aarde, R.J. van, and Lombard, A.T., 2013, The use of habitat suitability models and species–area relationships to predict extinction debts in coastal forests, South Africa: Diversity and Distributions, v. 19, p. 1353–1365, doi:10.1111/ddi.12099.

O'Neill, B.C. et al., 2016, The Scenario Model Intercomparison Project (ScenarioMIP) for CMIP6: Geoscientific Model Development, v. 9, p. 3461–3482, doi:10.5194/gmd-9-3461-2016.

Pandolfi, J.M. et al., 2003, Global Trajectories of the Long-Term Decline of Coral Reef Ecosystems: Science, v. 301, p. 955–958, doi:10.1126/science.1085706.

Pellissier, L., Heine, C., Rosauer, D.F., and Albouy, C., 2017, Are global hotspots of endemic richness shaped by plate tectonics? Biological Journal of the Linnean Society, v. 123, p. 247–261.

Peters, S.E., 2005, Geologic constraints on the macroevolutionary history of marine animals: Proceedings of the National Academy of Sciences, v. 102, p. 12326–12331.

Peters, S.E., and Foote, M., 2001, Biodiversity in the Phanerozoic: a reinterpretation: Paleobiology, v. 27, p. 583–601.

Peterson, A.T., Papeş, M., and Soberón, J., 2008, Rethinking receiver operating characteristic analysis applications in ecological niche modeling: Ecological Modelling, v. 213, p. 63–72, doi:10.1016/j.ecolmodel.2007.11.008.

Peterson, A.T., Soberón, J., Pearson, R.G., Anderson, R.P., Martínez-Meyer, E., Nakamura, M., and Araújo, M.B., 2011, Ecological Niches and Geographic Distributions: Princeton, U.S.A., Princeton University Press, 329 p.

Phillips, J., 1860, Life on the earth its origin and succession: Cambridge, Macmillan, p. 1–252, doi:10.5962/bhl.title.22153.

Phillips, S.J., Anderson, R.P., Dudík, M., Schapire, R.E., and Blair, M.E., 2017, Opening the black box: an open-source release of Maxent: Ecography, v. 40, p. 887–893, doi:10.1111/ecog.03049.

Phillips, S.J., Anderson, R.P., and Schapire, R.E., 2006, Maximum entropy modeling of species geographic distributions: Ecological Modelling, v. 190, p. 231–259, doi:10.1016/j.ecolmodel.2005.03.026.

Plotnick, R.E., 2017, Recurrent hierarchical patterns and the fractal distribution of fossil localities: Geology, v. 45, p. 295–298, doi:10.1130/G38828.1.

Poloczanska, E.S. et al., 2013, Global imprint of climate change on marine life: Nature Climate Change, v. 3, p. 919–925, doi:10.1038/nclimate1958.

Poloczanska, E.S. et al., 2016, Responses of Marine Organisms to Climate Change across Oceans: Frontiers in Marine Science, v. 3, p. 1–21, doi:10.3389/fmars.2016.00062.

Powell, M.G., 2007, Latitudinal diversity gradients for brachiopod genera during late Palaeozoic time: links between climate, biogeography and evolutionary rates: Global Ecology and Biogeography, v. 16, p. 519–528, doi:10.1111/j.1466-8238.2007.00300.x.

Powell, M.G., 2009, The latitudinal diversity gradient of brachiopods over the past 530 million years: The Journal of Geology, v. 117, p. 585–594.

Powell, M.G., Beresford, V.P., and Colaianne, B.A., 2012, The latitudinal position of peak marine diversity in living and fossil biotas: Journal of Biogeography, v. 39, p. 1687–1694, doi:10.1111/j.1365-2699.2012.02719.x.

Powell, M.G., Moore, B.R., and Smith, T.J., 2015, Origination, extinction, invasion, and extirpation components of the brachiopod latitudinal biodiversity gradient through the Phanerozoic Eon: Paleobiology, v. 41, p. 330–341.

Precht, W.F., and Aronson, R.B., 2004, Climate flickers and range shifts of reef corals: Frontiers in Ecology and the Environment, v. 2, p. 307–314, doi:10.1890/1540-9295(2004)002[0307:CFARSO]2.0.CO;2.

Procheș, Ș., 2001, Back to the sea: secondary marine organisms from a biogeographical perspective: Biological Journal of the Linnean Society, v. 74, p. 197–203, doi:10.1006/bijl.2001.0565.

Qiao, H., Saupe, E.E., Soberón, J., Peterson, A.T., and Myers, C.E., 2016, Impacts of Niche Breadth and Dispersal Ability on Macroevolutionary Patterns: The American Naturalist, v. 188, p. 149–162, doi:10.1086/687201.

R Core Team, 2019, R: A Language and Environment for Statistical Computing (Version 3.6.2, R Foundation for Statistical Computing, Vienna, Austria, 2019):

Rabosky, D.L. et al., 2018, An inverse latitudinal gradient in speciation rate for marine fishes: Nature, v. 559, p. 392–395, doi:10.1038/s41586-018-0273-1.

Rapoport, E.H., 1975, Areografía: estrategias geográficas de las especies: Mexico City, Mexico, Fondo de Cultura Económica, 214 p.

Rapoport, E.H., 1982, Areography: geographical strategies of species: New York, Pergamon.

Rasmussen, C.M.Ø., Kröger, B., Nielsen, M.L., and Colmenar, J., 2019, Cascading trend of Early Paleozoic marine radiations paused by Late Ordovician extinctions: Proceedings of the National Academy of Sciences, v. 116, p. 7207–7213, doi:10.1073/pnas.1821123116.

Raup, D.M., 1976a, Species diversity in the Phanerozoic: a tabulation: Paleobiology, v. 2, p. 279–288.

Raup, D.M., 1976b, Species diversity in the Phanerozoic: an interpretation: Paleobiology, v. 2, p. 289–297.

Raup, D.M., 1972, Taxonomic diversity during the Phanerozoic: Science, v. 177, p. 1065–1071.

Raup, D.M., 1975, Taxonomic Diversity Estimation Using Rarefaction: Paleobiology, v. 1, p. 333–342.

Raup, D.M., and Sepkoski, J.J., 1982, Mass Extinctions in the Marine Fossil Record: Science, v. 215, p. 1501–1503, doi:10.1126/science.215.4539.1501.

Reaka-Kudla, M.L., 2005, Biodiversity of Caribbean coral reefs, *in* Miloslavich, P. and Klein, E. eds., Caribbean Marine Biodiversity, Pennsylvania, U.S.A., Des Tech Publishers, p. 259–276.

Reddin, C.J., Kocsis, Á.T., and Kiessling, W., 2019, Climate change and the latitudinal selectivity of ancient marine extinctions: Paleobiology, v. 45, p. 70–84, doi:10.1017/pab.2018.34.

Renema, W. et al., 2008, Hopping Hotspots: Global Shifts in Marine Biodiversity: Science, v. 321, p. 654–657, doi:10.1126/science.1155674.

Rex, M.A., Crame, J.A., Stuart, C.T., and Clarke, A., 2005, Large-Scale Biogeographic Patterns in Marine Mollusks: A Confluence of History and Productivity? Ecology, v. 86, p. 2288–2297, doi:10.1890/04-1056.

Riahi, K., Rao, S., Krey, V., Cho, C., Chirkov, V., Fischer, G., Kindermann, G., Nakicenovic, N., and Rafaj, P., 2011, RCP 8.5—A scenario of comparatively high greenhouse gas emissions: Climatic Change, v. 109, p. 33–57, doi:10.1007/s10584-011-0149-y.

Richter, R., 1928, Aktuopalaiontologie und Palaiobiologie, eine Abgrenzung: Senckenbergia, v. 10, p. 285–292.

Roberts, C.M. et al., 2002, Marine Biodiversity Hotspots and Conservation Priorities for Tropical Reefs: Science, v. 295, p. 1280–1284, doi:10.1126/science.1067728.

Rohde, K., 1992, Latitudinal Gradients in Species Diversity: The Search for the Primary Cause: Oikos, v. 65, p. 514–527, doi:10.2307/3545569.

Rolland, J., Condamine, F.L., Jiguet, F., and Morlon, H., 2014, Faster Speciation and Reduced Extinction in the Tropics Contribute to the Mammalian Latitudinal Diversity Gradient: PLoS Biology, v. 12, doi:10.1371/journal.pbio.1001775.

Rose, P.J., Fox, D.L., Marcot, J., and Badgley, C., 2011, Flat latitudinal gradient in Paleocene mammal richness suggests decoupling of climate and biodiversity: Geology, v. 39, p. 163–166, doi:10.1130/G31099.1.

Rosenzweig, M.L., 1995, Species Diversity in Space and Time: Cambridge, United Kingdom, Cambridge University Press, 462 p.

Roy, K., and Goldberg, E.E., 2007, Origination, Extinction, and Dispersal: Integrative Models for Understanding Present-Day Diversity Gradients.: The American Naturalist, v. 170, p. 15.

Roy, K., Jablonski, D., and Valentine, J.W., 1994, Eastern Pacific molluscan provinces and latitudinal diversity gradient: no evidence for "Rapoport's rule": Proceedings of the National Academy of Sciences, v. 91, p. 8871–8874, doi:10.1073/pnas.91.19.8871.

Roy, K., Jablonski, D., Valentine, J.W., and Rosenberg, G., 1998, Marine latitudinal diversity gradients: Tests of causal hypotheses: Proceedings of the National Academy of Sciences, v. 95, p. 3699–3702, doi:10.1073/pnas.95.7.3699.

Royer, D.L., 2004, CO2 as a primary driver of Phanerozoic climate: GSA TODAY, p. 7.

Ruddiman, W.F., 2013, The Anthropocene: Annual Review of Earth and Planetary Sciences, v. 41, p. 45–68, doi:10.1146/annurev-earth-050212-123944.

Rull, V., 2011, Neotropical biodiversity: timing and potential drivers: Trends in Ecology & Evolution, v. 26, p. 508–513, doi:10.1016/j.tree.2011.05.011.

Sanders, H.L., 1968, Marine Benthic Diversity: A Comparative Study: The American Naturalist, v. 102, p. 243–282.

Saupe, E.E., Farnsworth, A., Lunt, D.J., Sagoo, N., Pham, K.V., and Field, D.J., 2019a, Climatic shifts drove major contractions in avian latitudinal distributions throughout the Cenozoic:

Proceedings of the National Academy of Sciences, v. 116, p. 12895–12900, doi:10.1073/pnas.1903866116.

Saupe, E.E., Hendricks, J.R., Portell, R.W., Dowsett, H.J., Haywood, A., Hunter, S.J., and Lieberman, B.S., 2014, Macroevolutionary consequences of profound climate change on niche evolution in marine molluscs over the past three million years: Proceedings of the Royal Society B: Biological Sciences, v. 281, p. 1–9, doi:10.1098/rspb.2014.1995.

Saupe, E.E., Myers, C.E., Peterson, A.T., Soberón, J., Singarayer, J., Valdes, P., and Qiao, H., 2019b, Non-random latitudinal gradients in range size and niche breadth predicted by spatial patterns of climate: Global Ecology and Biogeography, v. 28, p. 928–942, doi:10.1111/geb.12904.

Saupe, E.E., Myers, C.E., Townsend Peterson, A., Soberón, J., Singarayer, J., Valdes, P., and Qiao, H., 2019c, Spatio-temporal climate change contributes to latitudinal diversity gradients: Nature Ecology & Evolution, v. 3, p. 1419–1429, doi:10.1038/s41559-019-0962-7.

Sciaini, M., Fritsch, M., Scherer, C., and Simpkins, C.E., 2018, NLMR and landscapetools: An integrated environment for simulating and modifying neutral landscape models in R: Methods in Ecology and Evolution, v. 9, p. 2240–2248.

Seilacher, A., 1970, Begriff und bedeutung der Fossil-Lagerstätten: Neues Jarhbuch für Geologie und Paläontologie Abhandlungen.

Seo, C., Thorne, J.H., Hannah, L., and Thuiller, W., 2009, Scale effects in species distribution models: implications for conservation planning under climate change: Biology Letters, v. 5, p. 39–43, doi:10.1098/rsbl.2008.0476.

Sepkoski, J.J., 1998, Rates of speciation in the fossil record: Philosophical Transactions of the Royal Society of London. Series B, Biological Sciences, v. 353, p. 315–326, doi:10.1098/rstb.1998.0212.

Sheehan, P.M., 1977, A reflection of labor by systematists? Paleobiology, v. 3, p. 325–328.

Shen, G., Yu, M., Hu, X.-S., Mi, X., Ren, H., Sun, I.-F., and Ma, K., 2009, Species–area relationships explained by the joint effects of dispersal limitation and habitat heterogeneity: Ecology, v. 90, p. 3033–3041, doi:10.1890/08-1646.1.

Sheppard, C.R.C., 2003, Predicted recurrences of mass coral mortality in the Indian Ocean: Nature, v. 425, p. 294–297, doi:10.1038/nature01987.

Signor, P.W., and Lipps, J.H., 1982, Sampling bias, gradual extinction patterns and catastrophes in the fossil record, *in* Geological Society of America Special Papers, Geological Society of America, v. 190, p. 291–296, doi:10.1130/SPE190-p291.

Silvestro, D., Salamin, N., and Schnitzler, J., 2014, PyRate: a new program to estimate speciation and extinction rates from incomplete fossil data: Methods in Ecology and Evolution, v. 5, p. 1126–1131, doi:10.1111/2041-210X.12263.

Singarayer, J.S., and Valdes, P.J., 2010, High-latitude climate sensitivity to ice-sheet forcing over the last 120kyr: Quaternary Science Reviews, v. 29, p. 43–55, doi:10.1016/j.quascirev.2009.10.011.

Siqueira, A.C., Oliveira-Santos, L.G.R., Cowman, P.F., and Floeter, S.R., 2016, Evolutionary processes underlying latitudinal differences in reef fish biodiversity: Global Ecology and Biogeography, v. 25, p. 1466–1476, doi:10.1111/geb.12506.

Smith, A.B., 2001, Large–scale heterogeneity of the fossil record: implications for Phanerozoic biodiversity studies: Philosophical Transactions of the Royal Society of London. Series B: Biological Sciences, v. 356, p. 351–367, doi:10.1098/rstb.2000.0768.

Smith, A.B., Lloyd, G.T., and McGowan, A.J., 2012, Phanerozoic marine diversity: rock record modelling provides an independent test of large-scale trends: Proceedings of the Royal Society B: Biological Sciences, v. 279, p. 4489–4495, doi:10.1098/rspb.2012.1793.

Smith, A.B., and McGowan, A.J., 2007, The Shape of the Phanerozoic Marine Palaeodiversity Curve: How Much Can Be Predicted from the Sedimentary Rock Record of Western Europe? Palaeontology, v. 50, p. 765–774, doi:10.1111/j.1475-4983.2007.00693.x.

Smith, A.B., and McGowan, A.J., 2011, The ties linking rock and fossil records and why they are important for palaeobiodiversity studies: Geological Society, London, Special Publications, v. 358, p. 1–7, doi:10.1144/SP358.1.

Soberón, J., and Nakamura, M., 2009, Niches and distributional areas: Concepts, methods, and assumptions: Proceedings of the National Academy of Sciences, v. 106, p. 19644–19650, doi:10.1073/pnas.0901637106.

Song, H., Huang, S., Jia, E., Dai, X., Wignall, P.B., and Dunhill, A.M., 2020, Flat latitudinal diversity gradient caused by the Permian–Triassic mass extinction: Proceedings of the National Academy of Sciences, p. 1–6, doi:10.1073/pnas.1918953117.

Soria-Carrasco, V., and Castresana, J., 2012, Diversification rates and the latitudinal gradient of diversity in mammals: Proceedings of the Royal Society B: Biological Sciences, v. 279, p. 4148–4155, doi:10.1098/rspb.2012.1393.

Soto-Centeno, J.A., and Steadman, D.W., 2015, Fossils reject climate change as the cause of extinction of Caribbean bats: Scientific Reports, v. 5, p. 1–7, doi:10.1038/srep07971.

Spalding, M.D., 2001, World Atlas of Coral Reefs: California, USA, The University of California Press, 436 p.

Spalding, M.D., and Brown, B.E., 2015, Warm-water coral reefs and climate change: Science, v. 350, p. 769–771, doi:10.1126/science.aad0349.

Spalding, M.D., and Grenfell, A.M., 1997, New estimates of global and regional coral reef areas: Coral Reefs, v. 16, p. 225–230, doi:10.1007/s003380050078.

Spalding, M., Spalding, M.D., Ravilious, C., and Green, E.P., 2001, World Atlas of Coral Reefs: California, USA, University of California Press, 456 p.

Spano, C.A., Hernández, C.E., and Rivadeneira, M.M., 2016, Evolutionary dispersal drives the latitudinal diversity gradient of stony corals: Ecography, v. 39, p. 836–843, doi:10.1111/ecog.01855.

Stanley, G.D., 2003, The evolution of modern corals and their early history: Earth-Science Reviews, v. 60, p. 195–225, doi:10.1016/S0012-8252(02)00104-6.

Starrfelt, J., and Liow, L.H., 2016, How many dinosaur species were there? Fossil bias and true richness estimated using a Poisson sampling model: Philosophical Transactions of the Royal Society B: Biological Sciences, v. 371, p. 1–10, doi:10.1098/rstb.2015.0219.

Stein, C.A., and Stein, S., 1992, A model for the global variation in oceanic depth and heat flow with lithospheric age: Nature, v. 359, p. 123–129, doi:10.1038/359123a0.

Stevens, G.C., 1989, The Latitudinal Gradient in Geographical Range: How so Many Species Coexist in the Tropics: The American Naturalist, v. 133, p. 240–256.

Stirling, C.H., Esat, T.M., Lambeck, K., and McCulloch, M.T., 1998, Timing and duration of the Last Interglacial: evidence for a restricted interval of widespread coral reef growth: Earth and Planetary Science Letters, v. 160, p. 745–762, doi:10.1016/S0012-821X(98)00125-3.

Stocker, T.F. et al., 2013, Technical Summary, *in* Stocker, T.F., Qin, D., Plattner, G.-K., Tignor, M., Allen, S.K., Boschung, J., Nauels, A., Xia, Y., Bex, V., and Midgley, P.M. eds., Climate Change 2013: The Physical Science Basis. Contribution of Working Group I to the Fifth Assessment Report of the Intergovernmental Panel on Climate Change, Cambridge, United Kingdom and New York, NY, USA, Cambridge University Press, p. 33–115, doi:10.1017/CBO9781107415324.005.

Stolarski, J., Kitahara, M.V., Miller, D.J., Cairns, S.D., Mazur, M., and Meibom, A., 2011, The ancient evolutionary origins of Scleractinia revealed by azooxanthellate corals: BMC Evolutionary Biology, v. 11, p. 1–11, doi:10.1186/1471-2148-11-316.

Stone, E.J., Lunt, D.J., Annan, J.D., and Hargreaves, J.C., 2013, Quantification of the Greenland ice sheet contribution to Last Interglacial sea level rise: Climate of the Past, v. 9, p. 621–639, doi:https://doi.org/10.5194/cp-9-621-2013.

Sunday, J.M., Bates, A.E., and Dulvy, N.K., 2012, Thermal tolerance and the global redistribution of animals: Nature Climate Change, v. 2, p. 686–690, doi:10.1038/nclimate1539.

Swets, J.A., 1988, Measuring the accuracy of diagnostic systems: Science, v. 240, p. 1285–1293, doi:10.1126/science.3287615.

Terborgh, J., 1973, On the Notion of Favorableness in Plant Ecology: The American Naturalist, v. 107, p. 481–501.

Thomas, C.D. et al., 2004, Extinction risk from climate change: Nature, v. 427, p. 145–148, doi:10.1038/nature02121.

Thomas, E., and Gooday, A.J., 1996, Cenozoic deep-sea benthic foraminifers: Tracers for changes in oceanic productivity? Geology, v. 24, p. 355–358, doi:10.1130/0091-7613(1996)024<0355:CDSBFT>2.3.CO;2.

Thomson, A.M. et al., 2011, RCP4.5: a pathway for stabilization of radiative forcing by 2100: Climatic Change, v. 109, p. 77–94, doi:10.1007/s10584-011-0151-4.

Thuiller, W., Georges, D., Engler, R., and Breiner, F., 2016, biomod2: Ensemble platform for species distribution modeling. R package version 3.3-7:

Thuiller, W., Lafourcade, B., Engler, R., and Araújo, M.B., 2009, BIOMOD – a platform for ensemble forecasting of species distributions: Ecography, v. 32, p. 369–373, doi:10.1111/j.1600-0587.2008.05742.x.

Tittensor, D.P., Mora, C., Jetz, W., Lotze, H.K., Ricard, D., Berghe, E.V., and Worm, B., 2010, Global patterns and predictors of marine biodiversity across taxa: Nature, v. 466, p. 1098–1101, doi:10.1038/nature09329.

Tomašových, A., Jablonski, D., Berke, S.K., Krug, A.Z., and Valentine, J.W., 2015, Nonlinear thermal gradients shape broad-scale patterns in geographic range size and can reverse Rapoport's rule: Global Ecology and Biogeography, v. 24, p. 157–167, doi:10.1111/geb.12242.

Turvey, S.T., and Saupe, E.E., 2019, Insights from the past: unique opportunity or foreign country? Philosophical Transactions of the Royal Society B: Biological Sciences, v. 374, p. 1–5, doi:10.1098/rstb.2019.0208.

Tyrberg, T., 2010, Avifaunal responses to warm climate: the message from Last Interglacial faunas. In Proceedings of the VII International Meeting of the Society of Avian Paleontology and Evolution, ed. W.E. Boles and T.H. Worthy: Records of the Australian Museum, doi:10.3853/j.0067-1975.62.2010.1543.

UNEP-WCMC, WorldFish Centre, WRI, and TNC, 2018, Global distribution of warm-water coral reefs, compiled from multiple sources including the Millennium Coral Reef Mapping Project: Cambridge, United Kingdom, UN Environment World Conservation Monitoring Centre, v. 4, http://data.unep-wcmc.org/datasets/1.

Upchurch, P., Mannion, P.D., Benson, R.B.J., Butler, R.J., and Carrano, M.T., 2011, Geological and anthropogenic controls on the sampling of the terrestrial fossil record: a case study from the Dinosauria: Geological Society, London, Special Publications, v. 358, p. 209–240, doi:10.1144/SP358.14.

Valdes, P.J. et al., 2017, The BRIDGE HadCM3 family of climate models:HadCM3@Bristol v1.0: Geoscientific Model Development, v. 10, p. 3715–3743, doi:10.5194/gmd-2017-16.

Valentine, J.W., Foin, T.C., and Peart, D., 1978, A provincial model of Phanerozoic marine diversity: Paleobiology, v. 4, p. 55–66, doi:10.1017/S0094837300005686.

Valentine, J.W., and Jablonski, D., 2015, A twofold role for global energy gradients in marine biodiversity trends: Journal of Biogeography, v. 42, p. 997–1005, doi:10.1111/jbi.12515.

Veeh, H.H., 1966, Th230/U238 and U234/U238 ages of Pleistocene high sea level stand: Journal of Geophysical Research (1896-1977), v. 71, p. 3379–3386, doi:10.1029/JZ071i014p03379.

Veron, J.E.N., 2000, Corals of the World: Townsville, Australia, Australian Institute of Marine Science.

Veron, J.E.N., Devantier, L.M., Turak, E., Green, A.L., Kininmonth, S., Stafford-Smith, M., and Peterson, N., 2009, Delineating the Coral Triangle: Galaxea, Journal of Coral Reef Studies, v. 11, p. 91–100, doi:10.3755/galaxea.11.91.

Vié, J.-C., Hilton-Taylor, C., Pollock, C., Ragle, J., Smart, J., Stuart, S.N., and Tong, R., 2009, Wildlife in a changing world–An analysis of the 2008 IUCN Red List of Threatened Species.: IUCN,.

Vilhena, D.A., and Smith, A.B., 2013, Spatial Bias in the Marine Fossil Record: PLoS ONE, v. 8, p. 1–7, doi:10.1371/journal.pone.0074470.

Waide, R.B., Willig, M.R., Steiner, C.F., Mittelbach, G., Gough, L., Dodson, S.I., Juday, G.P., and Parmenter, R., 1999, The Relationship Between Productivity and Species Richness:

Annual Review of Ecology and Systematics, v. 30, p. 257–300, doi:10.1146/annurev.ecolsys.30.1.257.

Wake, D.B., and Vredenburg, V.T., 2008, Are we in the midst of the sixth mass extinction? A view from the world of amphibians: Proceedings of the National Academy of Sciences, v. 105, p. 11466–11473, doi:10.1073/pnas.0801921105.

Wall, P.D., Ivany, L.C., and Wilkinson, B.H., 2009, Revisiting Raup: exploring the influence of outcrop area on diversity in light of modern sample-standardization techniques: Paleobiology, v. 35, p. 146–167.

Warren, R. et al., 2013, Quantifying the benefit of early climate change mitigation in avoiding biodiversity loss: Nature Climate Change, v. 3, p. 678–682, doi:10.1038/nclimate1887.

Wasmund, E., 1926, Biocoenose und Thanatocoenose: Biosoziologische Studie und Lebensgemeinschaften und Totengesellschaften: Archiv fur Hydrobiologie, v. 17, p. 1–116.

Waterson, A.M., Schmidt, D.N., Valdes, P.J., Holroyd, P.A., Nicholson, D.B., Farnsworth, A., and Barrett, P.M., 2016, Modelling the climatic niche of turtles: a deep-time perspective: Proceedings of the Royal Society B: Biological Sciences, v. 283, p. 1–9, doi:10.1098/rspb.2016.1408.

Weeks, L.G., 1947, Paleogeography of South America: American Association of Petroleum Geologists Bulletin, v. 31, p. 1194–1241.

Weigelt, J., 1927, Rezente Wirbeltierleichen und ihre paläobiologische Bedeutung: Leipzig, Verlag von Max Weg, 227 p.

Weir, J.T., and Schluter, D., 2007, The Latitudinal Gradient in Recent Speciation and Extinction Rates of Birds and Mammals: Science, v. 315, p. 1574–1576, doi:10.1126/science.1135590.

Whittaker, R.J., and Fernández-Palacios, J.M., 2007, Island biogeography: ecology, evolution, and conservation: Oxford, UK, Oxford University Press.

Wiens, J.J., 2007, Global Patterns of Diversification and Species Richness in Amphibians: The American Naturalist, v. 170, p. 21.

Wiens, J.A., Stralberg, D., Jongsomjit, D., Howell, C.A., and Snyder, M.A., 2009, Niches, models, and climate change: assessing the assumptions and uncertainties: Proceedings of the National Academy of Sciences of the United States of America, p. 19729–19736, doi:10.1073/pnas.0901639106.

Willig, M.R., Kaufman, D.M., and Stevens, R.D., 2003, Latitudinal gradients of biodiversity: pattern, process, scale, and synthesis: Annual review of ecology, evolution, and systematics, v. 34, p. 273–309.

Willig, M.R., and Lyons, S.K., 1998, An Analytical Model of Latitudinal Gradients of Species Richness with an Empirical Test for Marsupials and Bats in the New World: Oikos, v. 81, p. 93–98, doi:10.2307/3546471.

Willig, M.R., and Presley, S.J., 2018, Latitudinal Gradients of Biodiversity: Theory and Empirical Patterns, *in* Encyclopedia of the Anthropocene, Elsevier, p. 13–19, doi:10.1016/B978-0-12-809665-9.09809-8.

Wright, N., Zahirovic, S., Müller, R.D., and Seton, M., 2013, Towards community-driven paleogeographic reconstructions: integrating open-access paleogeographic and paleobiology data with plate tectonics: Biogeosciences, v. 10, p. 1529–1541, doi:10.5194/bg-10-1529-2013.

Yamano, H., Hori, K., Yamauchi, M., Yamagawa, O., and Ohmura, A., 2001, Highest-latitude coral reef at Iki Island, Japan: Coral Reefs, v. 20, p. 9–12, doi:10.1007/s003380100137.

Yamano, H., Sugihara, K., and Nomura, K., 2011, Rapid poleward range expansion of tropical reef corals in response to rising sea surface temperatures: Geophysical Research Letters, v. 38, doi:10.1029/2010GL046474.

Yasuhara, M., Hunt, G., Dowsett, H.J., Robinson, M.M., and Stoll, D.K., 2012, Latitudinal species diversity gradient of marine zooplankton for the last three million years: Ecology Letters, v. 15, p. 1174–1179, doi:10.1111/j.1461-0248.2012.01828.x.

Zhang, L., Liu, S., Sun, P., Wang, T., Wang, G., Zhang, X., and Wang, L., 2015, Consensus Forecasting of Species Distributions: The Effects of Niche Model Performance and Niche Properties: PLoS ONE, v. 10, p. 1–18, doi:10.1371/journal.pone.0120056.

Ziegler, P.A., 1999, Evolution of the Arctic-North Atlantic and the western Tethys – a visual presentation of a series of paleogeographic–paleotectonic maps: American Association of Petroleum Geologists Memoir, v. 43, p. 164–196.

Ziegler, P.A., 1982, Geological Atlas of Western and Central Europe: Amsterdam, Elsevier, 130 p.

Ziegler, P.A., 1990, Geological Atlas of Western and Central Europe: Shell Internationale Petroleum Maatschappi BV, v. 2, 239 p.

Ziegler, A., Eshel, G., Rees, P.M., Rothfus, T., Rowley, D., and Sunderlin, D., 2003, Tracing the tropics across land and sea: Permian to present: Lethaia, v. 36, p. 227–254, doi:10.1080/00241160310004657.

Ziegler, A.M., Scotese, C.R., and Barrett, S.F., 1983, Mesozoic and Cenozoic paleogeographic maps, *in* Brosche, P. and Sündermann, J. eds., Tidal Friction and the Earth's Rotation II, Berlin, Springer-Verlag, p. 240–252.

Ziegler, A.M., Scotese, C.R., McKerrow, W.S., Johnson, M.E., and Bambach, R.K., 1979, Paleozoic paleogeography: Annual Review of Earth and Planetary Sciences, v. 7, p. 473–502.

Zuber, S., 1934, Paleogeography of oil-bearing deposits in proto-Caspian countries: American Association of Petroleum Geologists Bulletin, v. 18, p. 777–785.

–This page is intentionally left blank–

Appendices

Appendix A

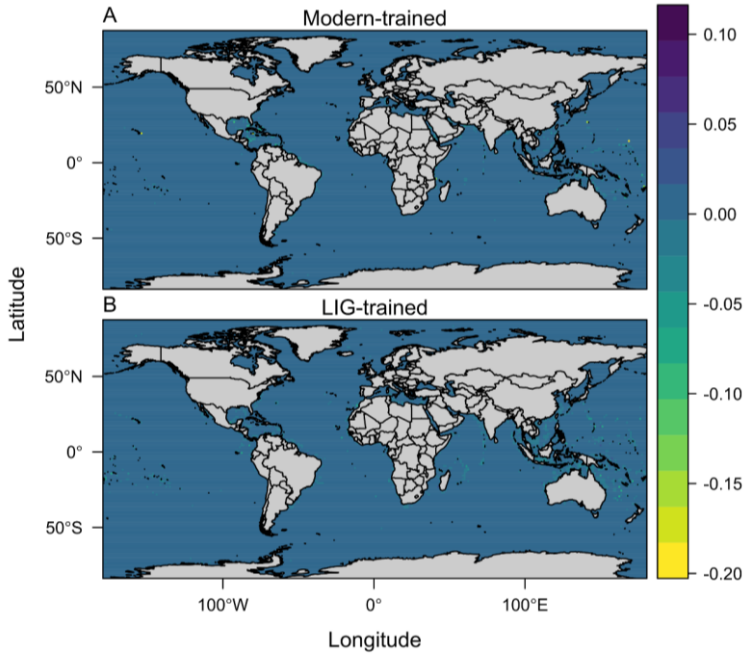


Figure A.1. Difference maps of estimated habitat suitability for the Last Interglacial (LIG). A) Modern-trained ecological niche modelling comparison of the LIG using the modern bathymetry and modern bathymetry + 10 m in LIG projections. B) LIG-trained ecological niche model comparison of the LIG using the modern bathymetry and modern bathymetry + 10 m for LIG training. Data is projected in the coordinate reference system: World Geodetic System 1984 (WGS84).

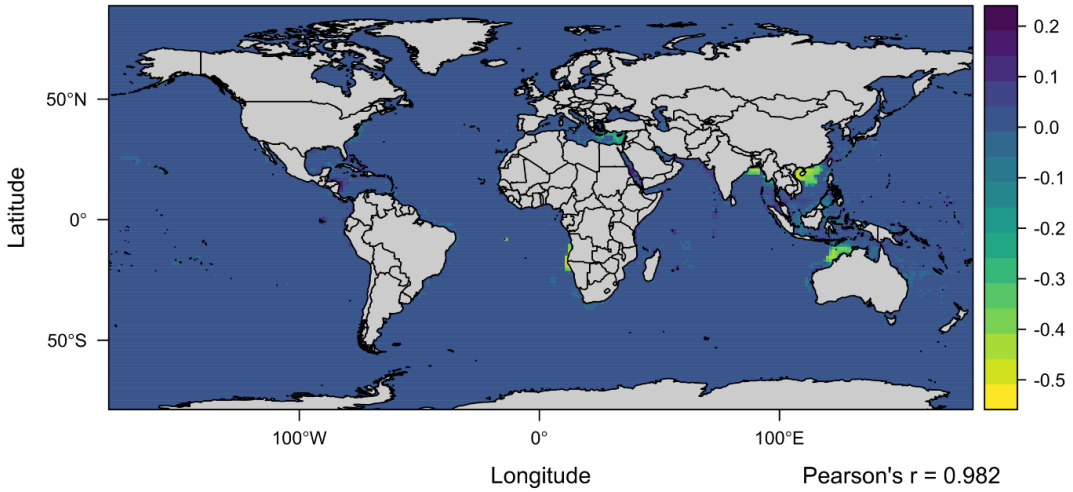


Figure A.2. Difference map of estimated habitat suitability for modern projections from the modern-trained ecological niche model with and without aragonite saturation state variable included. Pearson's correlation coefficient (Pearson's r) shows the correlation between the two projections. Data is projected in the coordinate reference system: World Geodetic System 1984 (WGS84).

Table A.1. Mean biomod2 variable importance test scores for modern-trained ecological niche model with aragonite saturation state variable included. These results display 1 - cor (Pearson correlation coefficient score) between predictions based on calibrated models, and predictions after one environmental variable is randomised. Higher values indicate higher importance in model calibration, whilst lower values indicate less importance.

Environmental variable	Mean variable contribution
Aragonite saturation state	0.14367
Bathymetry	0.81521
December–February irradiance	0.08713
June–August irradiance	0.13732
Annual salinity	0.05434
Annual sea surface temperature	0.43186

Table A.2. Mean biomod2 variable importance test scores for ecological niche models trained on both modern and Last Interglacial training datasets, for all modelling algorithms implemented. These results display 1 - cor (Pearson correlation coefficient score) between predictions based on calibrated models, and predictions after one environmental variable is randomised. Higher values indicate higher importance in model calibration, whilst lower values indicate less importance.

		Modelling algorithm		
	Environmental variable	MaxEnt	Bioclim	RandomForest
Modern	Bathymetry	0.86229	0.83352	0.79289
	December, January, February irradiance	0.01895	0.16982	0.08015
	June, July, August irradiance	0.08996	0.29486	0.09462
	Annual salinity	0.02147	0.1025	0.06003
	Annual sea surface temperature	0.53401	0.38374	0.44529

		Modelling algorithm		
	Environmental variable	MaxEnt	Bioclim	RandomForest
Last Interglacial	Bathymetry	0.84902	0.87536	0.67951
	December, January, February irradiance	0.03225	0.17303	0.22486
	June, July, August irradiance	0.06195	0.37765	0.20744
	Annual salinity	0.04829	0.23778	0.08172
	Annual sea surface temperature	0.56119	0.41206	0.47094

Appendix B

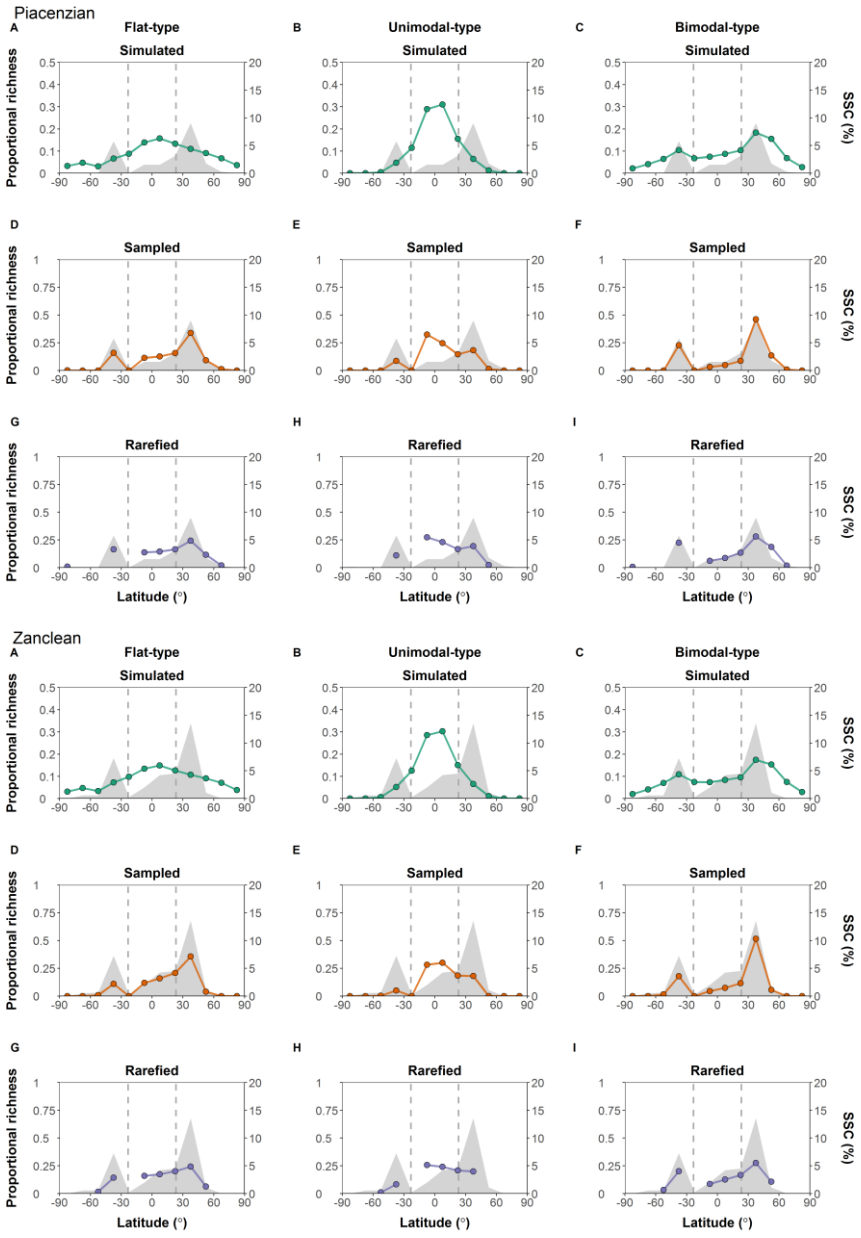
Table B.1. Kolmogorov-Smirnov two-sample test results from empirical range size frequency distributions and those simulated. Significant results ($P < 0.05$) are identified in bold font face and indicate statistically significant differences between groups.

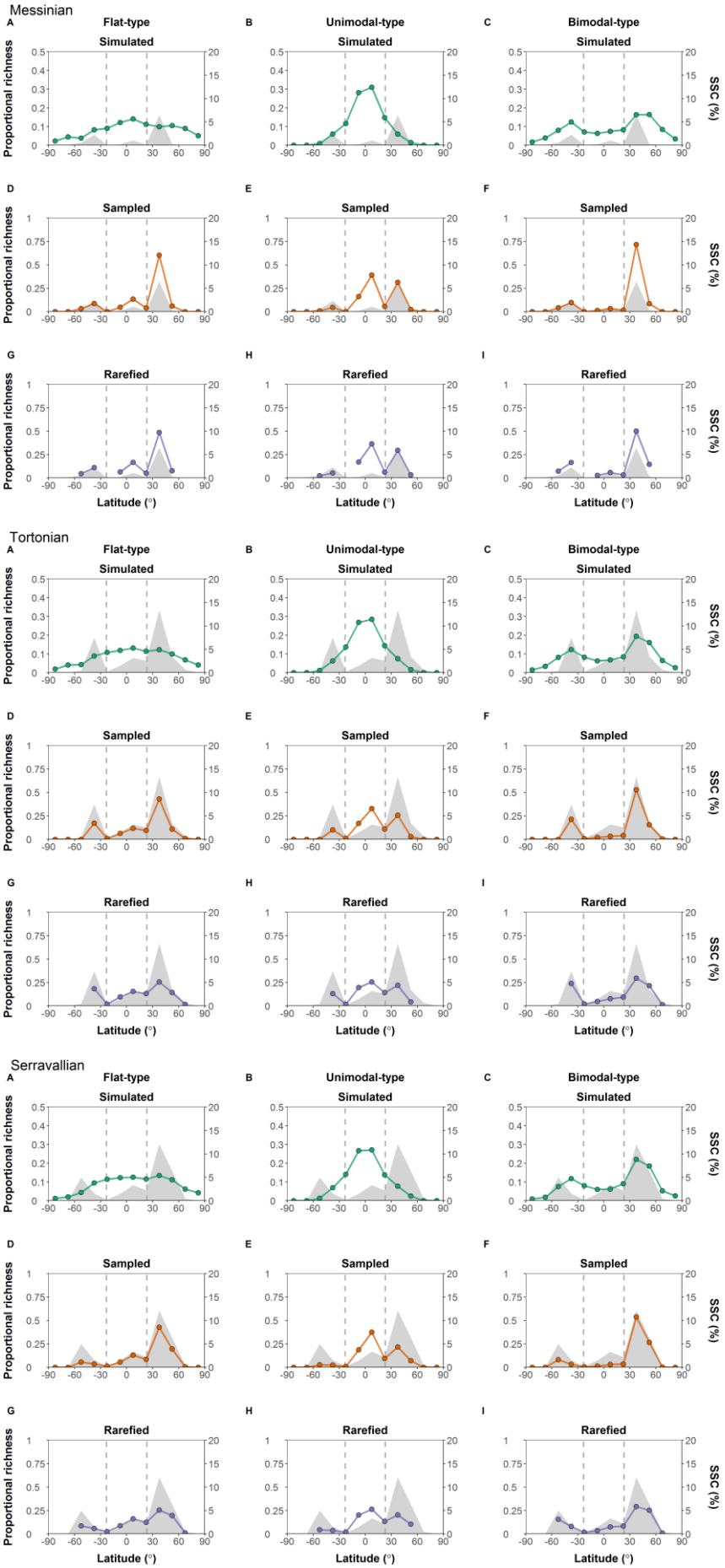
Comparison	Metric	D statistic	P
Simulated and Anthozoa	Latitude	0.338	0.485
Simulated and Anthozoa	Longitude	0.667	0.001
Simulated and Anthozoa	Great Circle distance	0.647	< 0.001
Simulated and Porifera	Latitude	0.194	0.972
Simulated and Porifera	Longitude	0.722	< 0.001
Simulated and Porifera	Great Circle distance	0.579	0.003
Simulated and Bivalvia	Latitude	0.338	0.485
Simulated and Bivalvia	Longitude	0.722	< 0.001
Simulated and Bivalvia	Great Circle distance	0.634	0.001
Simulated and Brachiopoda	Latitude	0.614	0.024
Simulated and Brachiopoda	Longitude	0.333	0.270
Simulated and Brachiopoda	Great Circle distance	0.424	0.061
Simulated and Echinoidea	Latitude	0.223	0.941
Simulated and Echinoidea	Longitude	0.389	0.131
Simulated and Echinoidea	Great Circle distance	0.321	0.256
Anthozoa and Bivalvia	Latitude	0.188	0.941
Anthozoa and Bivalvia	Longitude	0.167	0.964
Anthozoa and Bivalvia	Great Circle distance	0.202	0.796
Anthozoa and Brachiopoda	Latitude	0.616	0.007
Anthozoa and Brachiopoda	Longitude	0.889	< 0.001
Anthozoa and Brachiopoda	Great Circle distance	0.902	< 0.001
Anthozoa and Porifera	Latitude	0.210	0.862
Anthozoa and Porifera	Longitude	0.222	0.766
Anthozoa and Porifera	Great Circle distance	0.357	0.147
Anthozoa and Echinoidea	Latitude	0.375	0.265
Anthozoa and Echinoidea	Longitude	0.667	0.001
Anthozoa and Echinoidea	Great Circle distance	0.810	< 0.001
Bivalvia and Brachiopoda	Latitude	0.616	0.007
Bivalvia and Brachiopoda	Longitude	0.944	< 0.001
Bivalvia and Brachiopoda	Great Circle distance	0.950	< 0.001
Bivalvia and Porifera	Latitude	0.213	0.848
Bivalvia and Porifera	Longitude	0.222	0.766
Bivalvia and Porifera	Great Circle distance	0.300	0.329
Bivalvia and Echinoidea	Latitude	0.361	0.309
Bivalvia and Echinoidea	Longitude	0.667	0.001
Bivalvia and Echinoidea	Great Circle distance	0.714	< 0.001
Brachiopoda and Porifera	Latitude	0.550	0.019
Brachiopoda and Porifera	Longitude	0.944	< 0.001
Brachiopoda and Porifera	Great Circle distance	0.950	< 0.001
Brachiopoda and Echinoidea	Latitude	0.495	0.074
Brachiopoda and Echinoidea	Longitude	0.611	0.002
Brachiopoda and Echinoidea	Great Circle distance	0.602	0.001
Porifera and Echinoidea	Latitude	0.276	0.629
Porifera and Echinoidea	Longitude	0.722	< 0.001
Porifera and Echinoidea	Great Circle distance	0.619	0.001

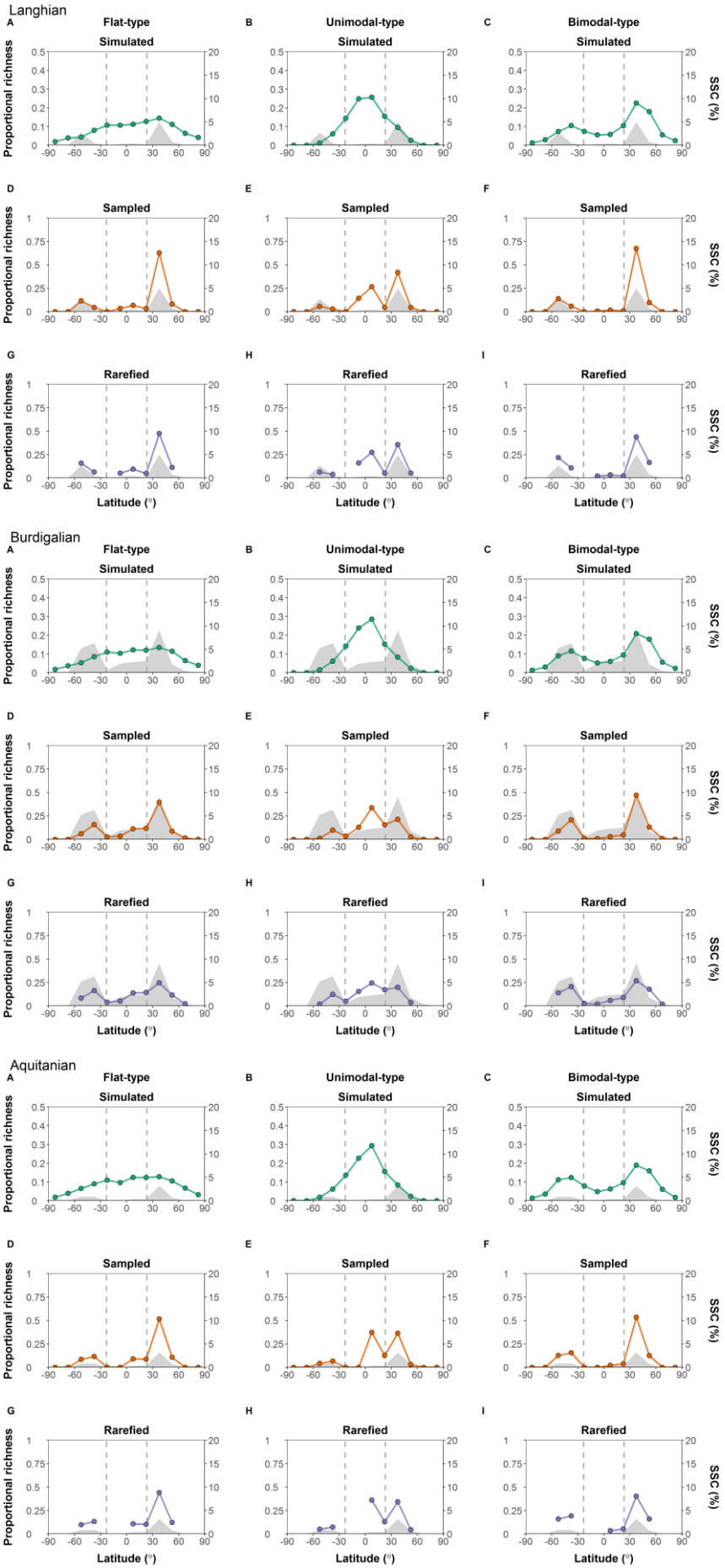
Table B.2. Kolmogorov-Smirnov two-sample test results from empirical occurrence frequency distributions and those simulated. Significant results ($P < 0.05$) are identified in bold font face and indicate statistically significant differences between groups.

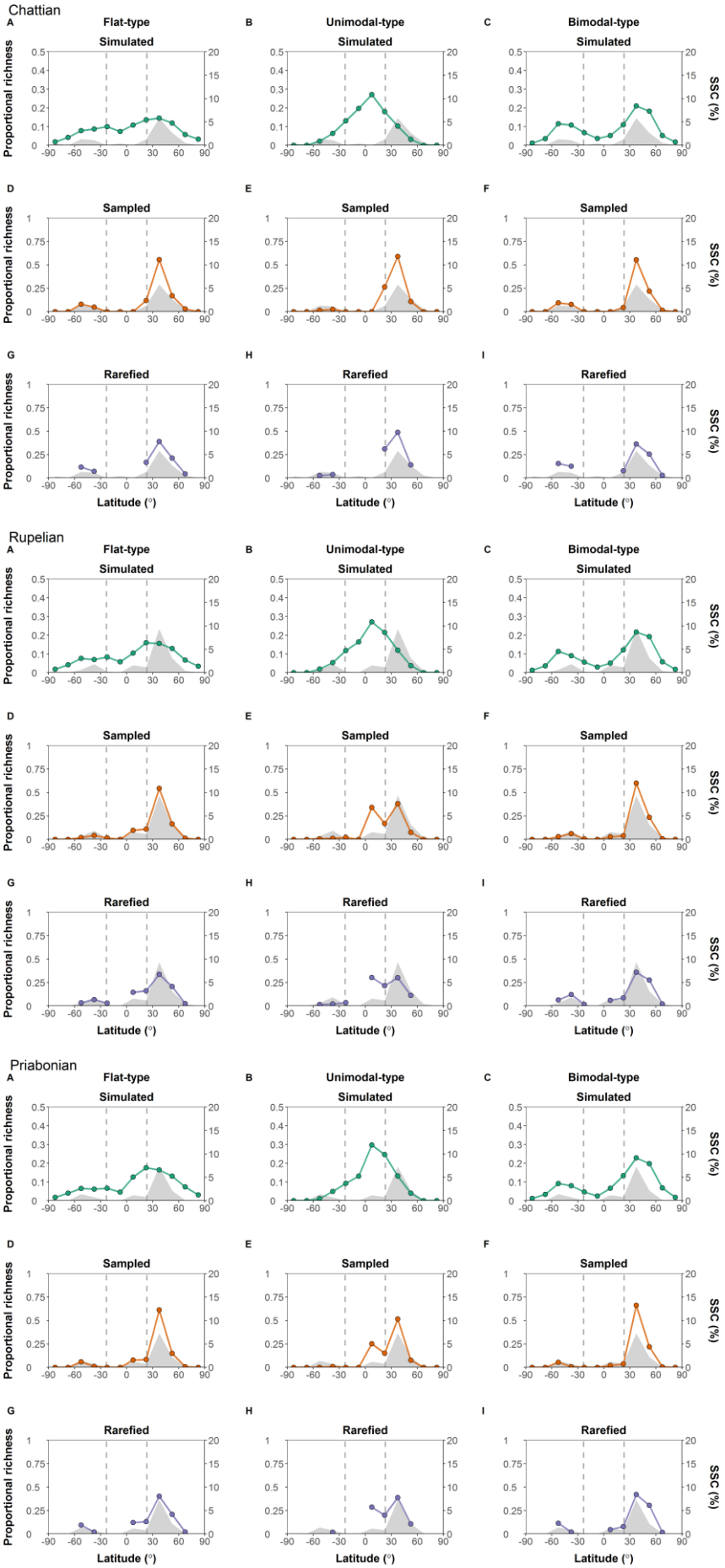
Comparison	D statistic	P
Simulated and Anthozoa	0.644	0.005
Simulated and Bivalvia	0.707	0.002
Simulated and Brachiopoda	0.313	0.523
Simulated and Porifera	0.553	0.025
Simulated and Echinoidea	0.615	0.010
Anthozoa and Bivalvia	0.188	0.941
Anthozoa and Brachiopoda	0.804	$<$ 0.001
Anthozoa and Porifera	0.438	0.094
Anthozoa and Echinoidea	0.546	0.020
Bivalvia and Brachiopoda	0.866	$<$ 0.001
Bivalvia and Porifera	0.438	0.094
Bivalvia and Echinoidea	0.671	0.002
Brachiopoda and Porifera	0.723	0.001
Brachiopoda and Echinoidea	0.719	0.001
Porifera and Echinoidea	0.279	0.582

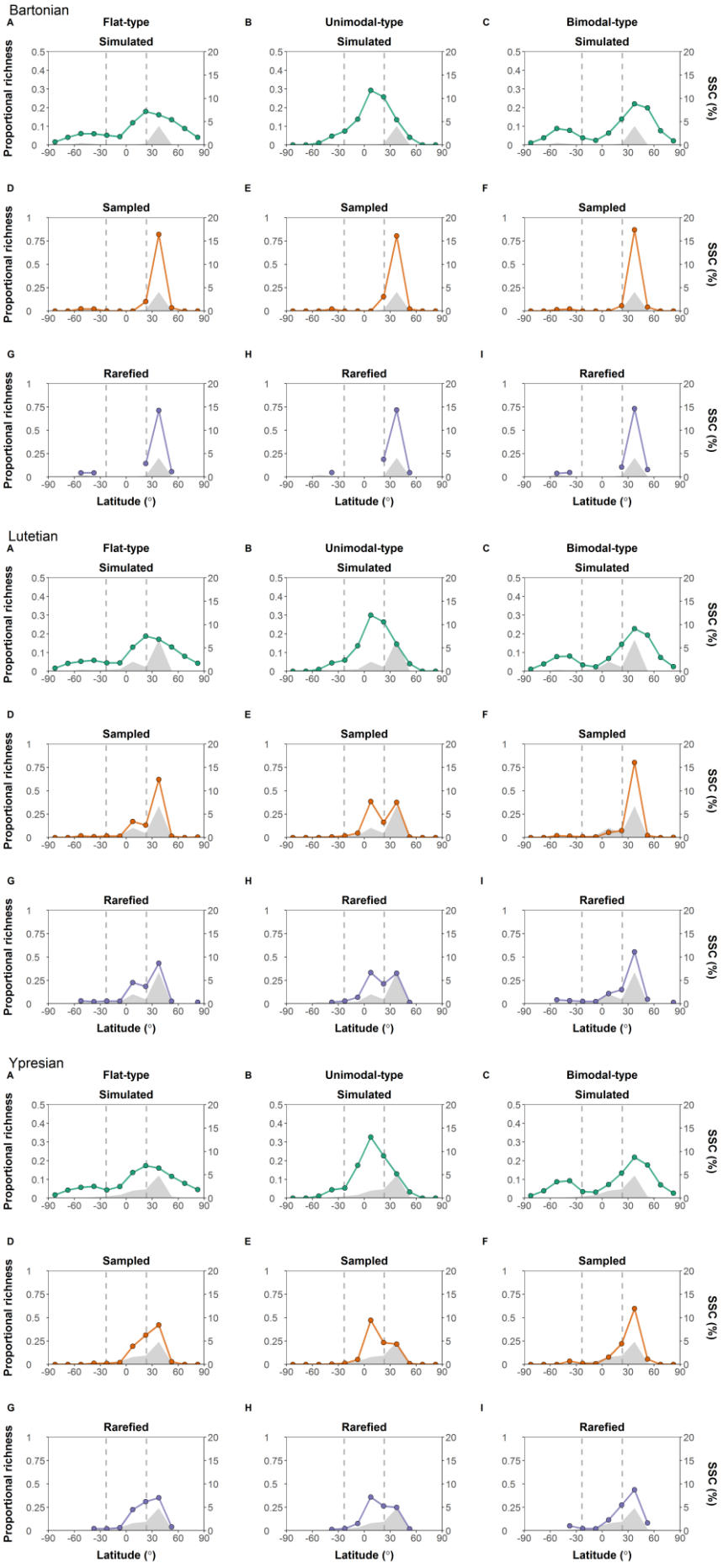
Figure B.1. Stage-level (Piacenzian–Asselian) latitudinal plots (15° bins) of simulated (A–C), sampled (D–F), and sampling-standardised (G–I) latitudinal biodiversity gradients for three different types of gradient (flat, unimodal and bimodal). Latitudinal proportional richness was calculated by dividing each latitudinal bin by the total of all latitudinal bins within each stage. For each type of latitudinal biodiversity gradient, simulated richness values were based on the mean bin value from the 100 simulation replications. Sampled gradients are the product of spatial sampling the simulated occurrences by the known geographic sampling window (based on fossil collections). Sampling-standardised latitudinal richness estimates (G–I) are based on the mean of means of the 1,000 bootstrap replicates for each replication of the sampled latitudinal biodiversity gradient simulations (= 100). Latitudinal proportional richness is depicted by the coloured points, while spatial sampling coverage (SSC) is shown by the grey shading. Dashed grey-lines depict the extent of the tropics today. The respective stage of each plot is described in the top-left corner of each plot.

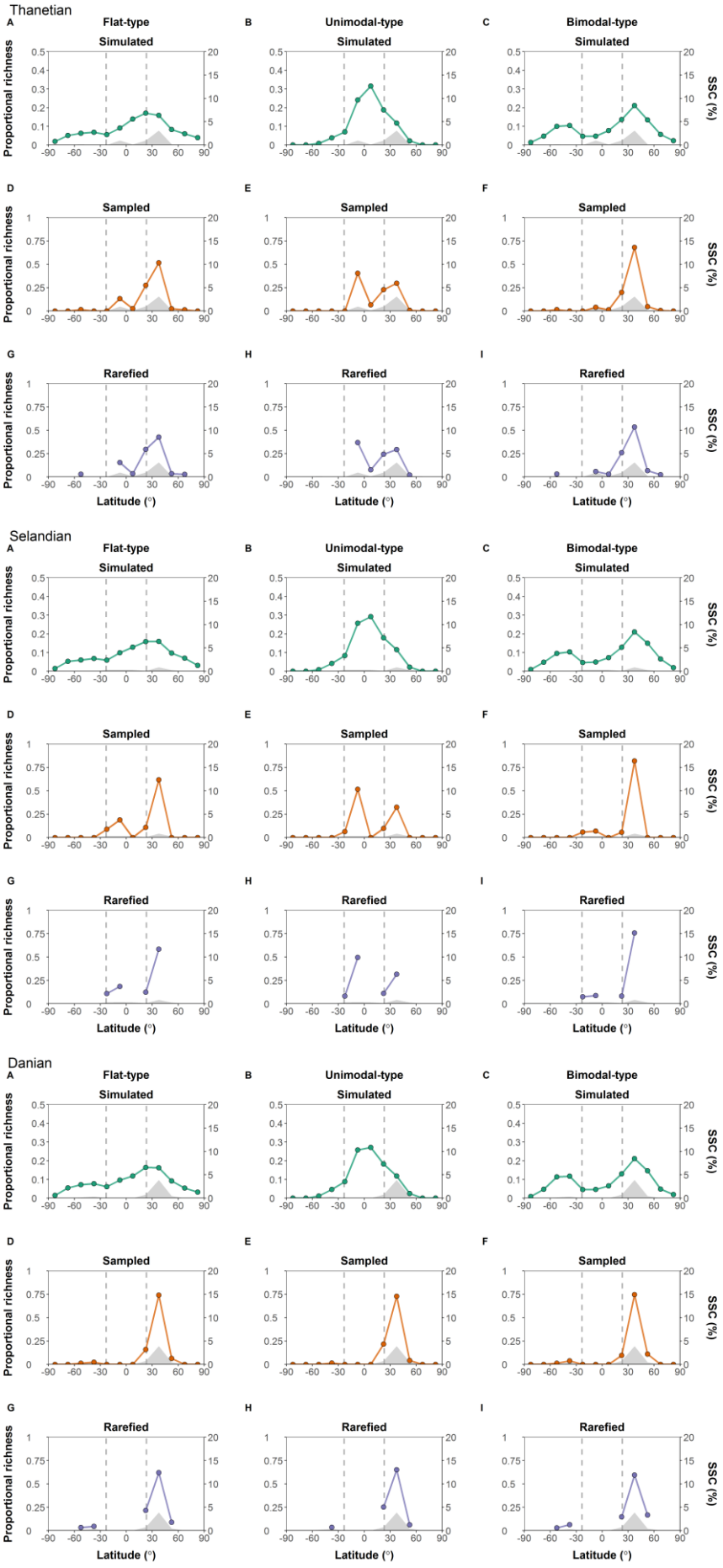


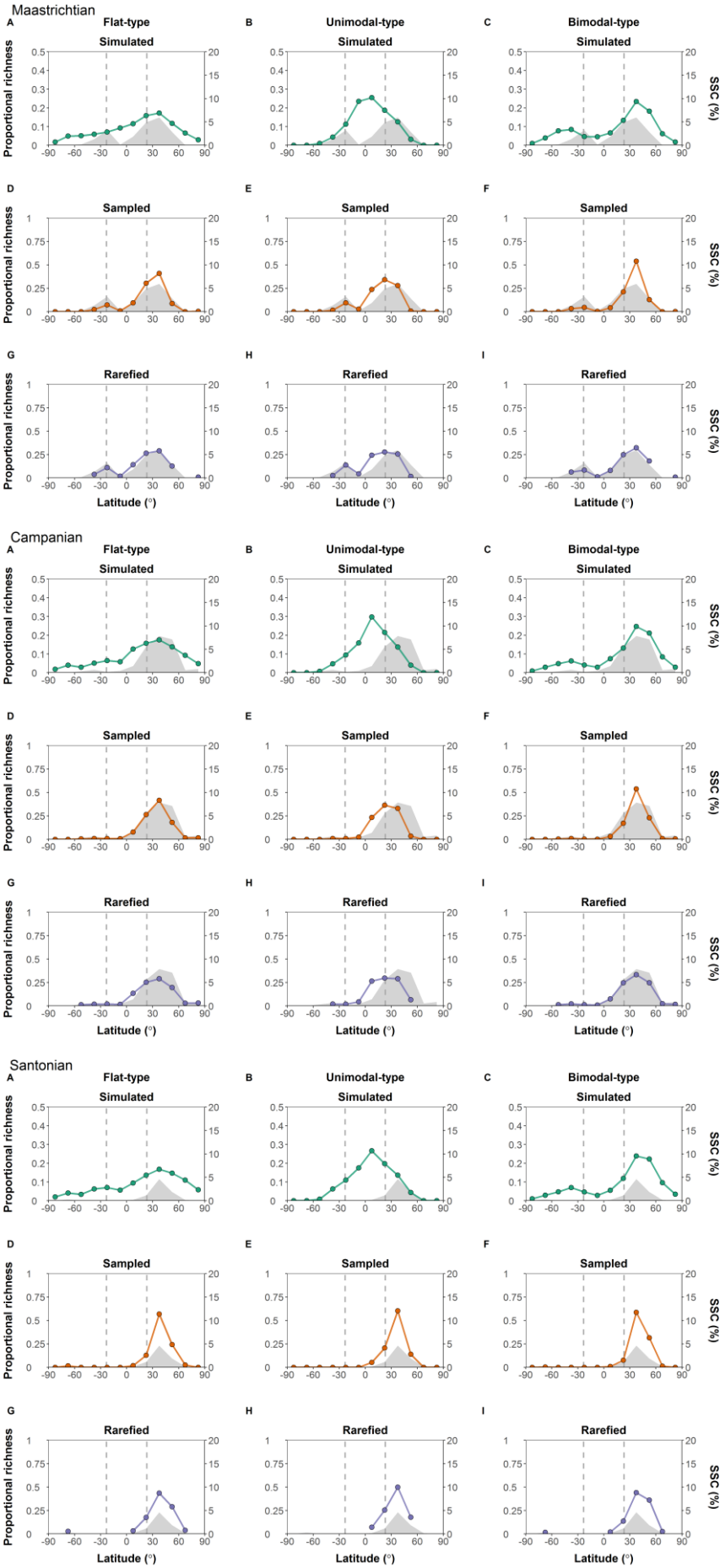

Messinian
A
Flat-type
Simulated
B
Unimodal-type
Simulated
C
Bimodal-type
Simulated
D
Sampled
E
Sampled
F
Sampled
G
Rarefied
H
Rarefied
I
Rarefied
Proportional richness
SSC (%)
Latitude (°)
Tortonian
A
Flat-type
Simulated
B
Unimodal-type
Simulated
C
Bimodal-type
Simulated
D
Sampled
E
Sampled
F
Sampled
G
Rarefied
H
Rarefied
I
Rarefied
Proportional richness
SSC (%)
Latitude (°)
Serravallian
A
Flat-type
Simulated
B
Unimodal-type
Simulated
C
Bimodal-type
Simulated
D
Sampled
E
Sampled
F
Sampled
G
Rarefied
H
Rarefied
I
Rarefied
Proportional richness
SSC (%)
Latitude (°)

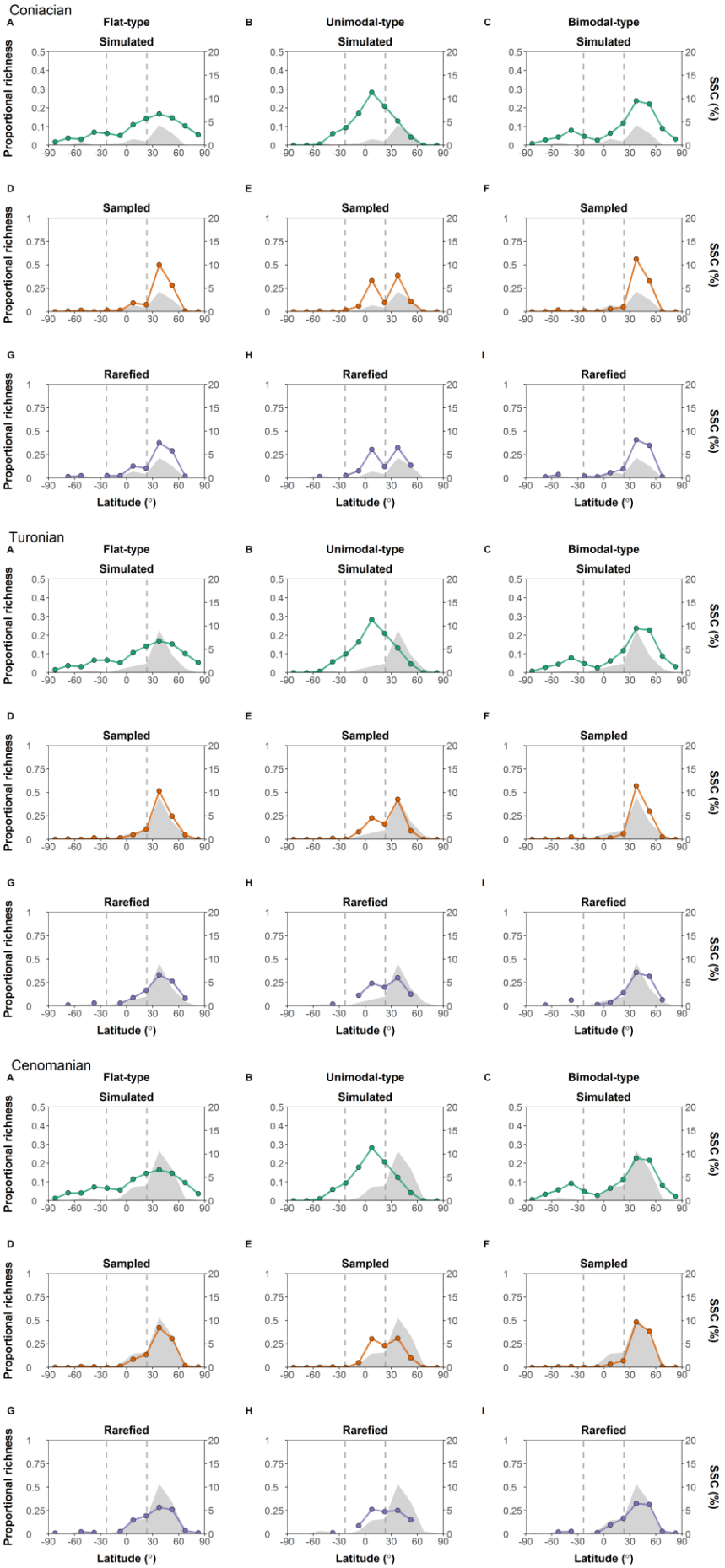

Langhian
A
Flat-type
Simulated
B
Unimodal-type
Simulated
C
Bimodal-type
Simulated
D
Sampled
E
Sampled
F
Sampled
G
Rarefied
H
Rarefied
I
Rarefied
Proportional richness
SSC (%)
Latitude (°)
Burdigalian
A
Flat-type
Simulated
B
Unimodal-type
Simulated
C
Bimodal-type
Simulated
D
Sampled
E
Sampled
F
Sampled
G
Rarefied
H
Rarefied
I
Rarefied
Proportional richness
SSC (%)
Latitude (°)
Aquitanian
A
Flat-type
Simulated
B
Unimodal-type
Simulated
C
Bimodal-type
Simulated
D
Sampled
E
Sampled
F
Sampled
G
Rarefied
H
Rarefied
I
Rarefied
Proportional richness
SSC (%)
Latitude (°)

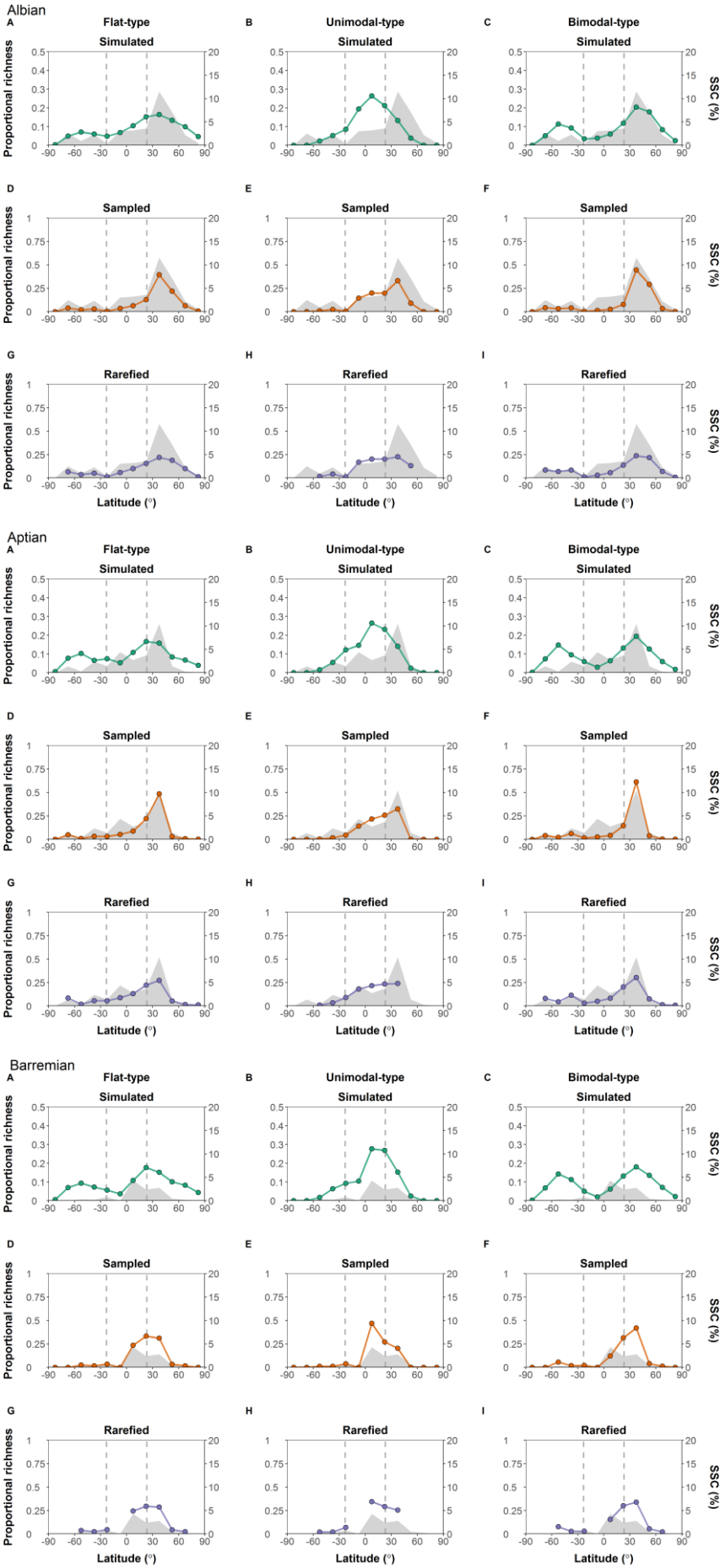

Chattian
A
Flat-type
Simulated
B
Unimodal-type
Simulated
C
Bimodal-type
Simulated
D
Sampled
E
Sampled
F
Sampled
G
Rarefied
H
Rarefied
I
Rarefied
Proportional richness
SSC (%)
Latitude (°)
Rupelian
A
Flat-type
Simulated
B
Unimodal-type
Simulated
C
Bimodal-type
Simulated
D
Sampled
E
Sampled
F
Sampled
G
Rarefied
H
Rarefied
I
Rarefied
Proportional richness
SSC (%)
Latitude (°)
Priabonian
A
Flat-type
Simulated
B
Unimodal-type
Simulated
C
Bimodal-type
Simulated
D
Sampled
E
Sampled
F
Sampled
G
Rarefied
H
Rarefied
I
Rarefied
Proportional richness
SSC (%)
Latitude (°)

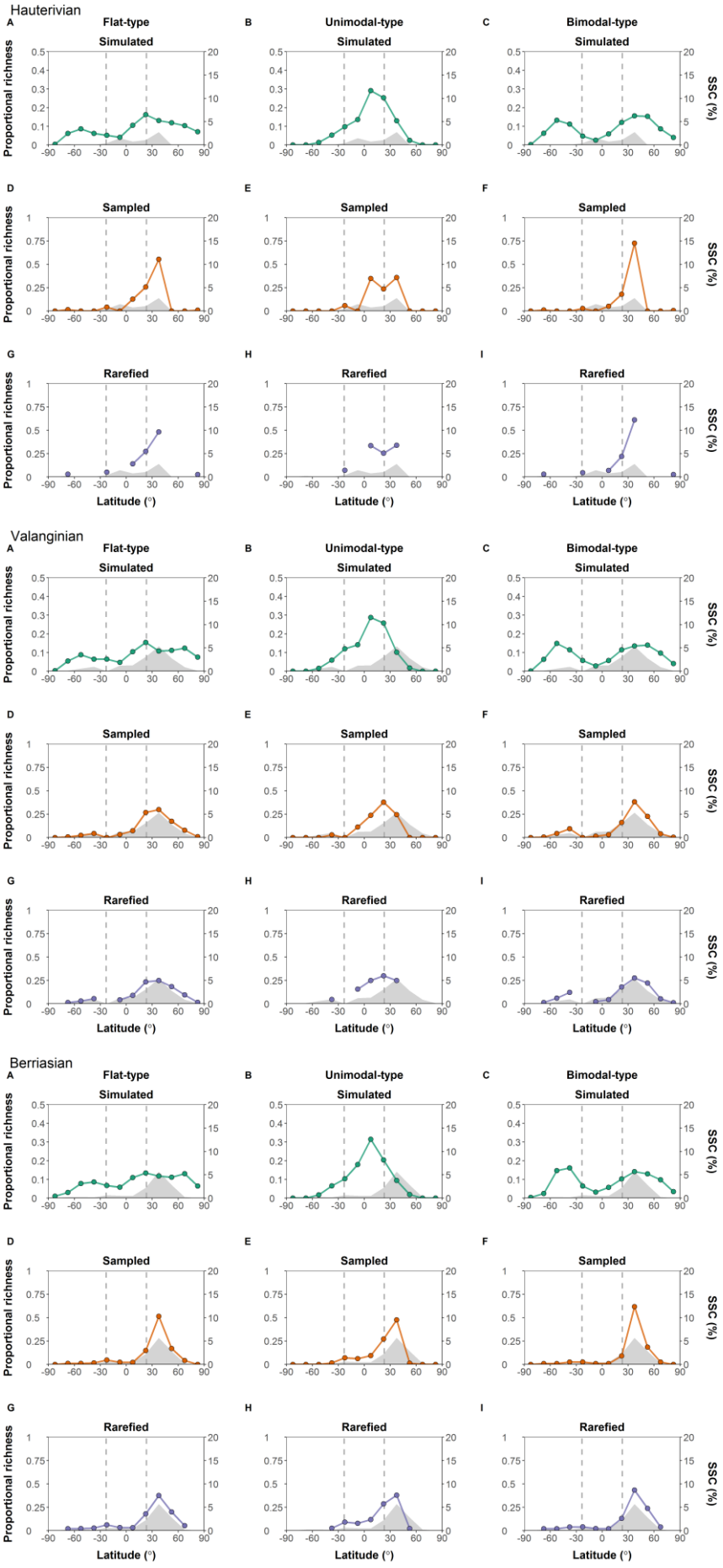

Bartonian
Lutetian
Ypresian
A
Flat-type
Simulated
B
Unimodal-type
Simulated
C
Bimodal-type
Simulated
D
Sampled
E
Sampled
F
Sampled
G
Rarefied
H
Rarefied
I
Rarefied
Proportional richness
SSC (%)
Latitude (°)

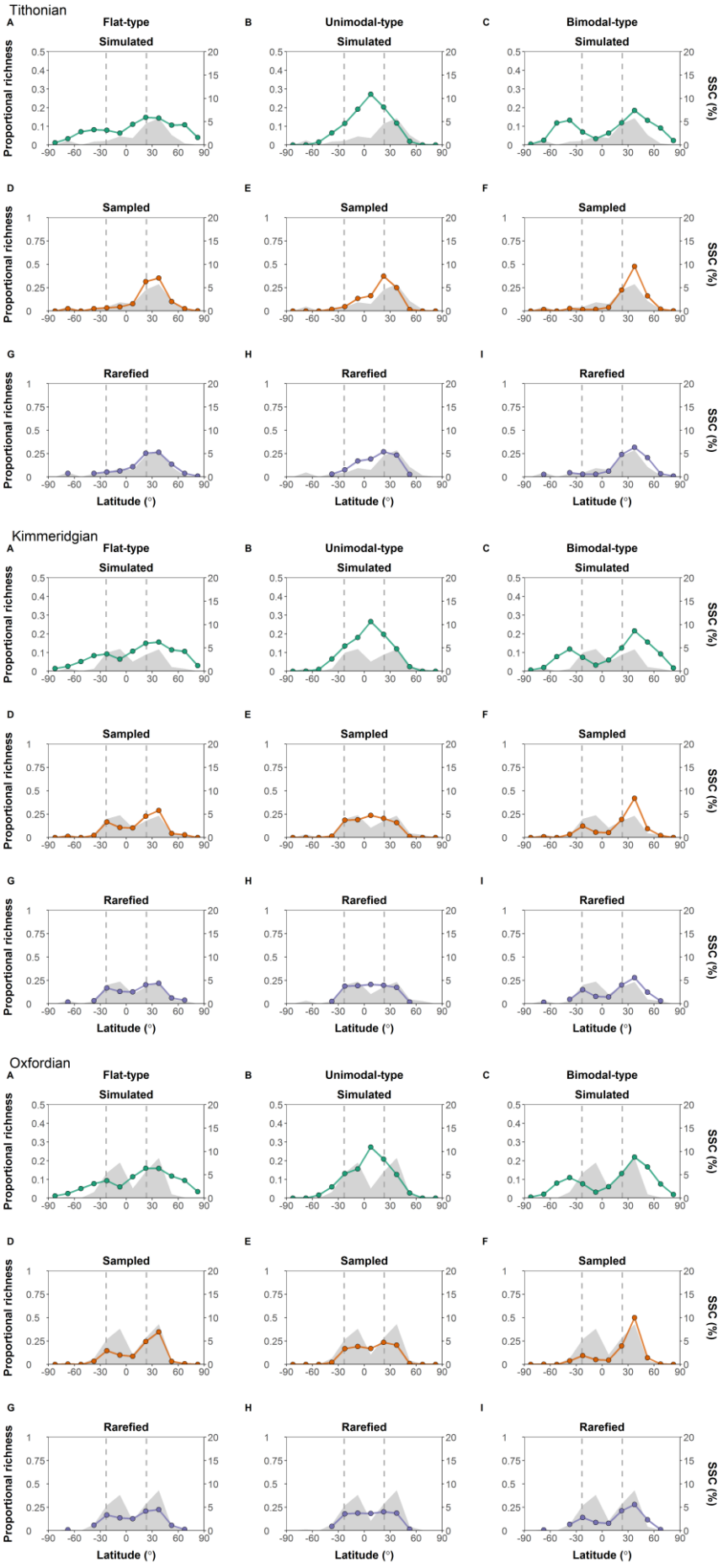

Thanetian
A
Flat-type
Simulated
B
Unimodal-type
Simulated
C
Bimodal-type
Simulated
D
Sampled
E
Sampled
F
Sampled
G
Rarefied
H
Rarefied
I
Rarefied
Proportional richness
SSC (%)
Latitude (°)
Selandian
A
Flat-type
Simulated
B
Unimodal-type
Simulated
C
Bimodal-type
Simulated
D
Sampled
E
Sampled
F
Sampled
G
Rarefied
H
Rarefied
I
Rarefied
Proportional richness
SSC (%)
Latitude (°)
Danian
A
Flat-type
Simulated
B
Unimodal-type
Simulated
C
Bimodal-type
Simulated
D
Sampled
E
Sampled
F
Sampled
G
Rarefied
H
Rarefied
I
Rarefied
Proportional richness
SSC (%)
Latitude (°)

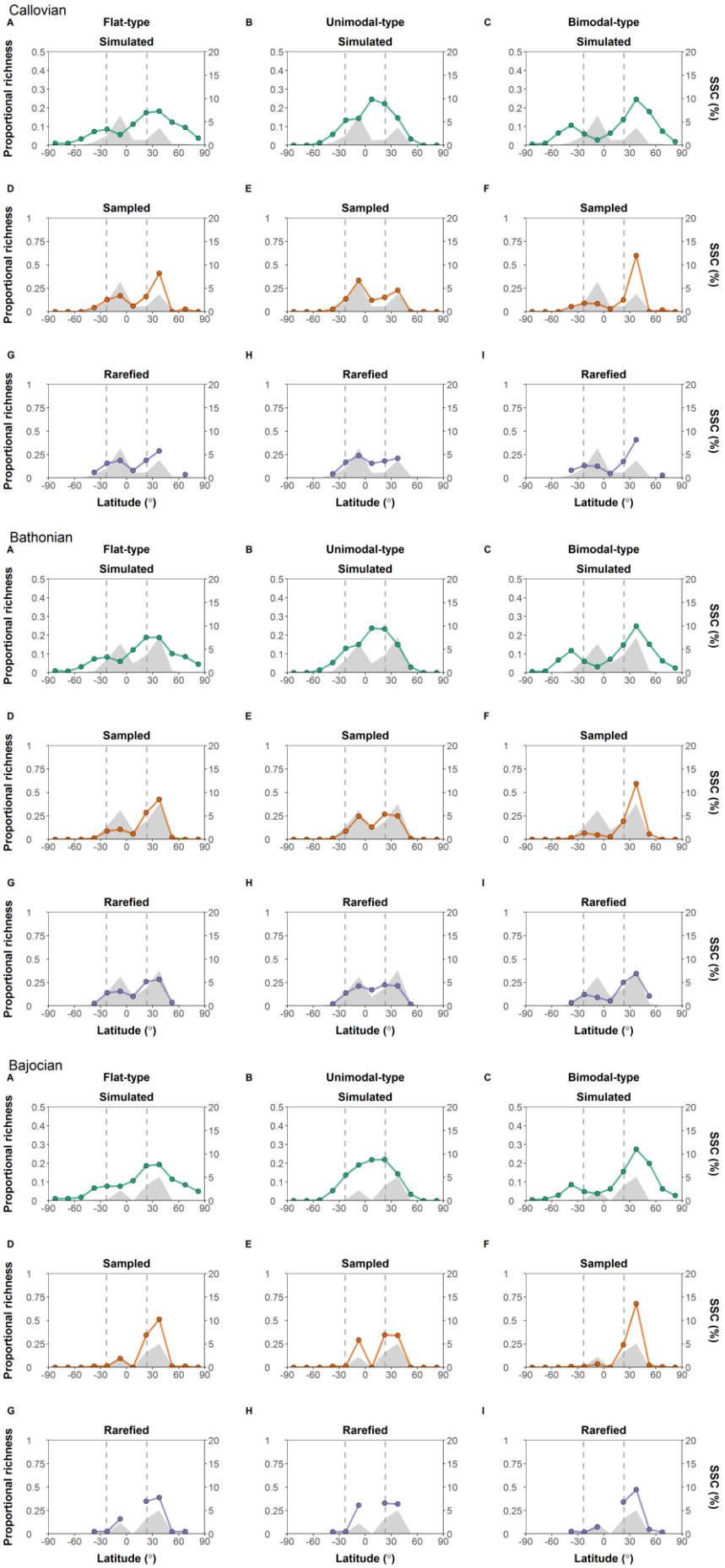

Maastrichtian
Campanian
Santonian
A
Flat-type
Simulated
B
Unimodal-type
Simulated
C
Bimodal-type
Simulated
D
Sampled
E
Sampled
F
Sampled
G
Rarefied
H
Rarefied
I
Rarefied
Proportional richness
SSC (%)
Latitude (°)

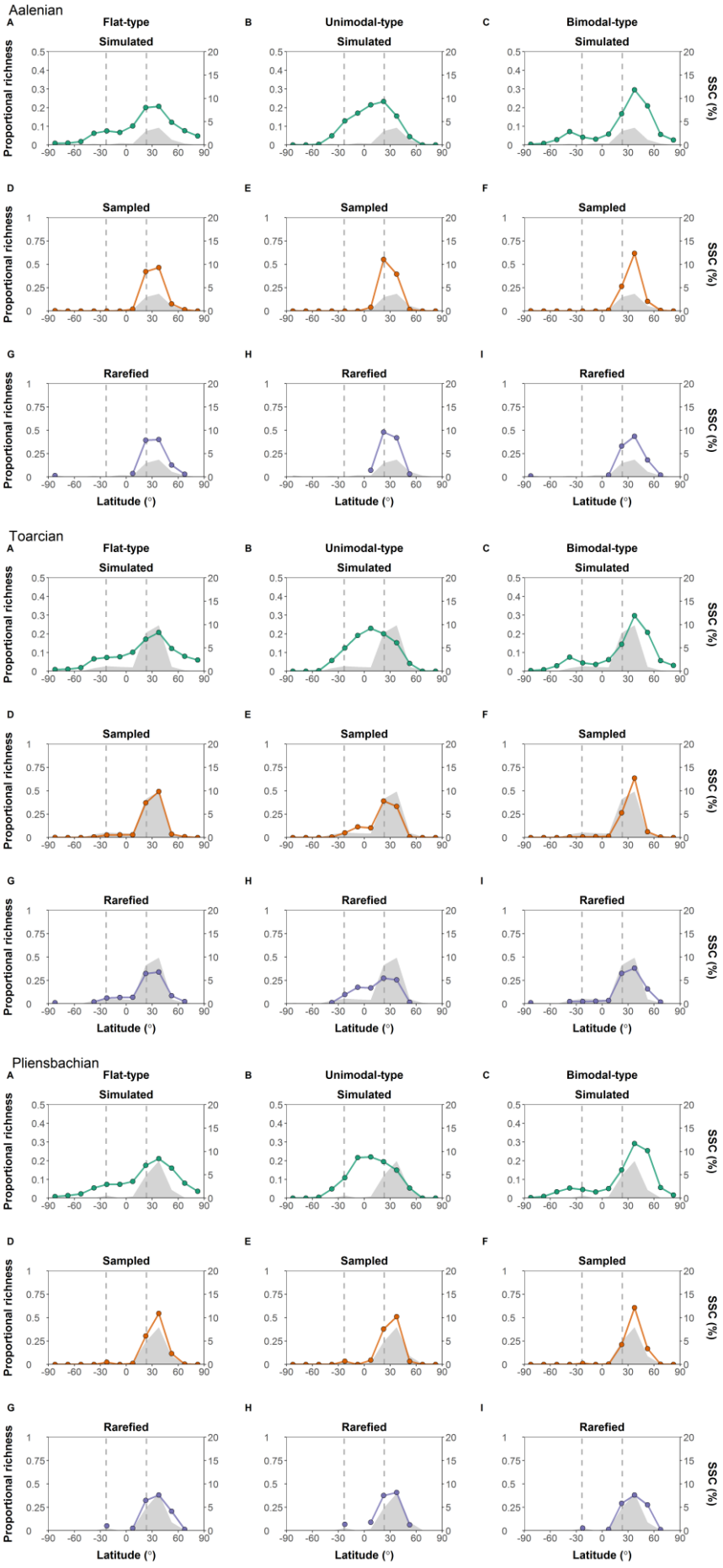

Coniacian
A
Flat-type
Simulated
B
Unimodal-type
Simulated
C
Bimodal-type
Simulated
D
Sampled
E
Sampled
F
Sampled
G
Rarefied
H
Rarefied
I
Rarefied
Proportional richness
SSC (%)
Latitude (°)
Turonian
A
Flat-type
Simulated
B
Unimodal-type
Simulated
C
Bimodal-type
Simulated
D
Sampled
E
Sampled
F
Sampled
G
Rarefied
H
Rarefied
I
Rarefied
Proportional richness
SSC (%)
Latitude (°)
Cenomanian
A
Flat-type
Simulated
B
Unimodal-type
Simulated
C
Bimodal-type
Simulated
D
Sampled
E
Sampled
F
Sampled
G
Rarefied
H
Rarefied
I
Rarefied
Proportional richness
SSC (%)
Latitude (°)

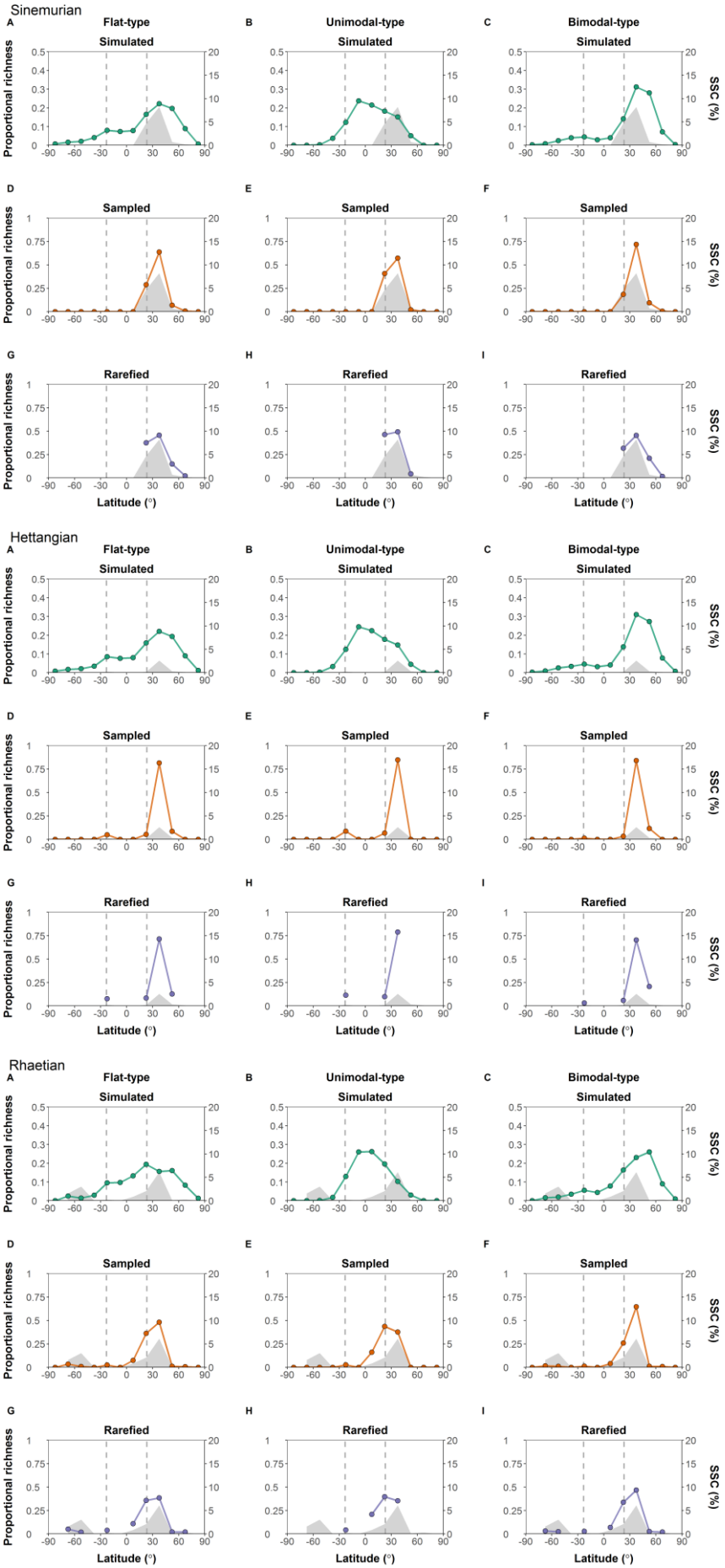

Albian
A
Flat-type
Simulated
B
Unimodal-type
Simulated
C
Bimodal-type
Simulated
D
Sampled
E
Sampled
F
Sampled
G
Rarefied
H
Rarefied
I
Rarefied
Proportional richness
SSC (%)
Latitude (°)
Aptian
A
Flat-type
Simulated
B
Unimodal-type
Simulated
C
Bimodal-type
Simulated
D
Sampled
E
Sampled
F
Sampled
G
Rarefied
H
Rarefied
I
Rarefied
Proportional richness
SSC (%)
Latitude (°)
Barremian
A
Flat-type
Simulated
B
Unimodal-type
Simulated
C
Bimodal-type
Simulated
D
Sampled
E
Sampled
F
Sampled
G
Rarefied
H
Rarefied
I
Rarefied
Proportional richness
SSC (%)
Latitude (°)

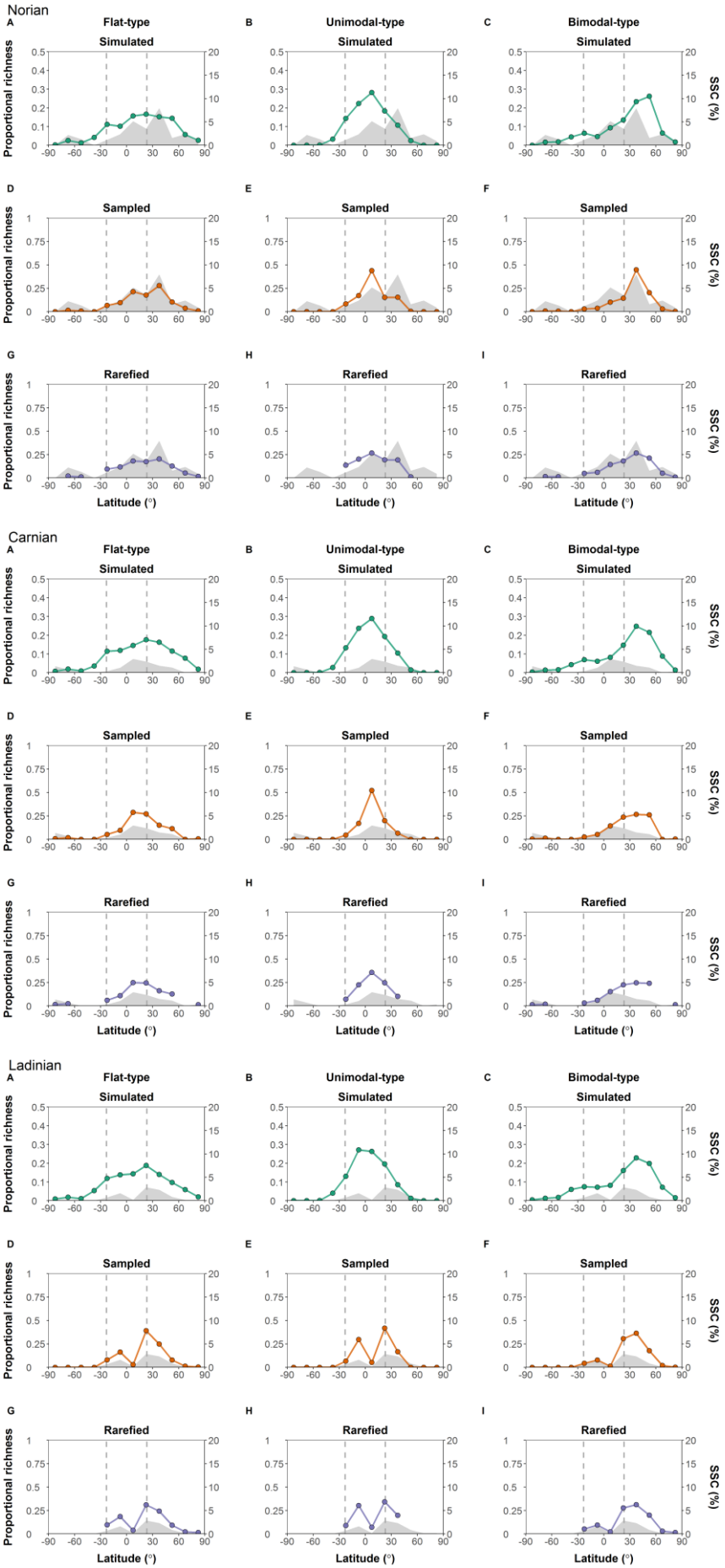

Hauterivian
A
Flat-type
Simulated
B
Unimodal-type
Simulated
C
Bimodal-type
Simulated
D
Sampled
E
Sampled
F
Sampled
G
Rarefied
H
Rarefied
I
Rarefied
Proportional richness
SSC (%)
Latitude (°)
Valanginian
A
Flat-type
Simulated
B
Unimodal-type
Simulated
C
Bimodal-type
Simulated
D
Sampled
E
Sampled
F
Sampled
G
Rarefied
H
Rarefied
I
Rarefied
Proportional richness
SSC (%)
Latitude (°)
Berriasian
A
Flat-type
Simulated
B
Unimodal-type
Simulated
C
Bimodal-type
Simulated
D
Sampled
E
Sampled
F
Sampled
G
Rarefied
H
Rarefied
I
Rarefied
Proportional richness
SSC (%)
Latitude (°)

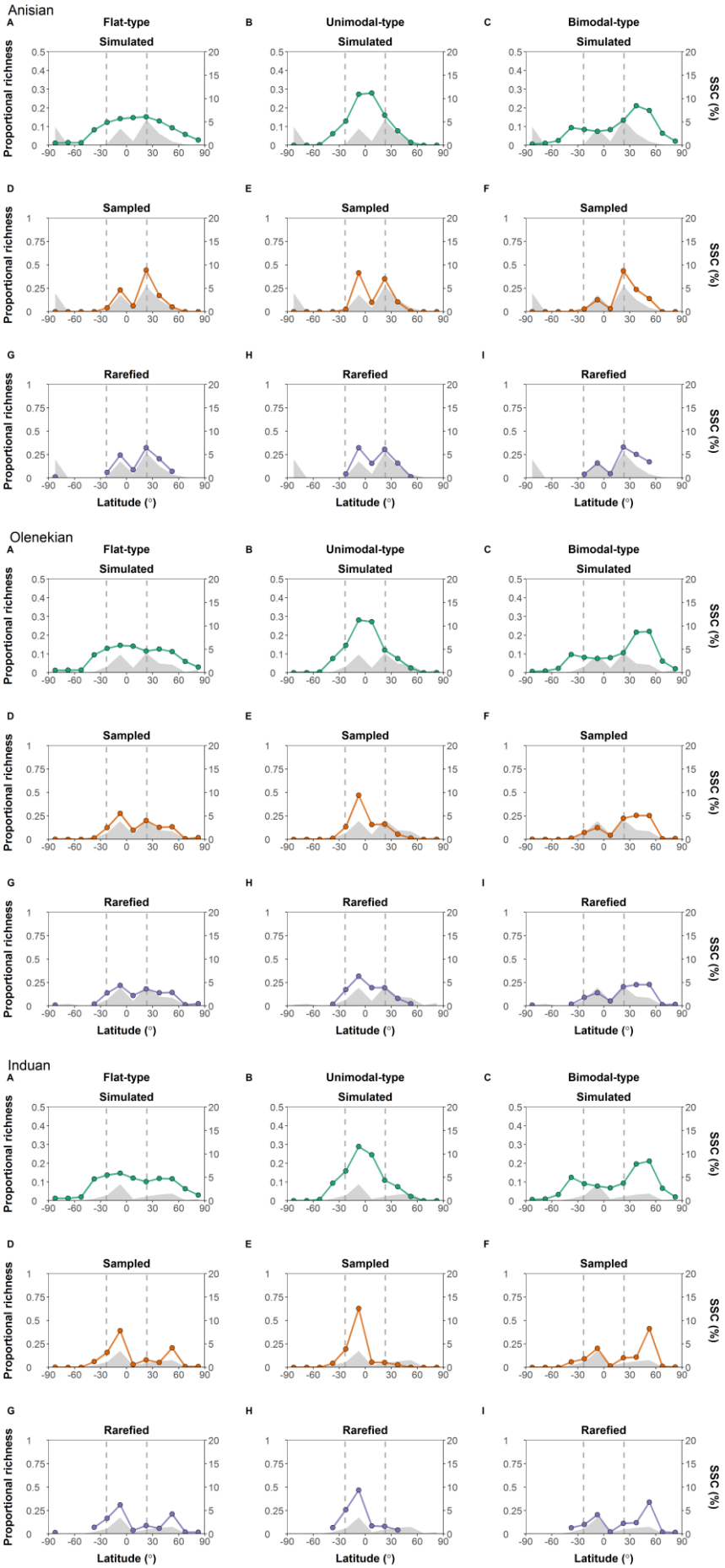

Tithonian
Kimmeridgian
Oxfordian
A
B
C
D
E
F
G
H
I
Flat-type
Unimodal-type
Bimodal-type
Simulated
Sampled
Rarefied
Proportional richness
SSC (%)
Latitude (°)

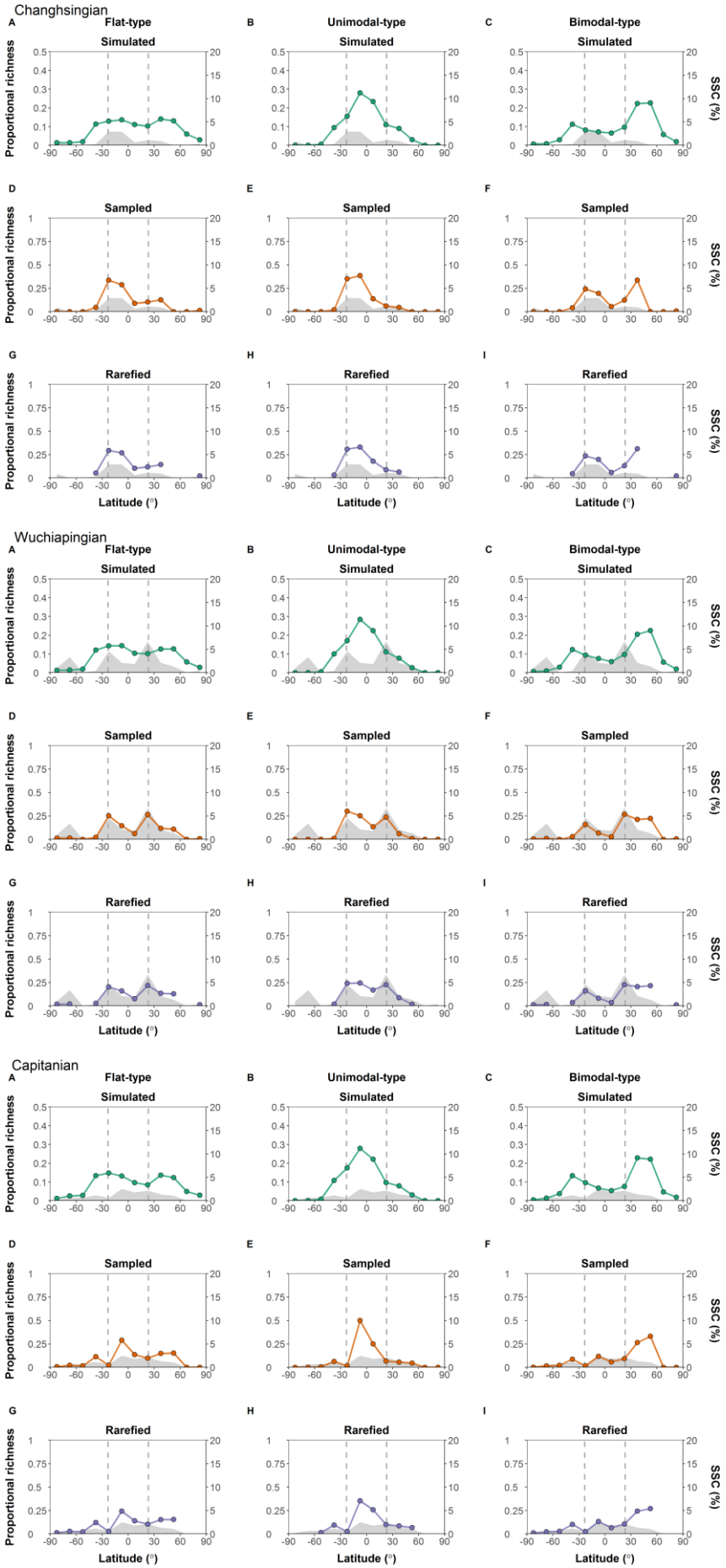

Callovian
A
Flat-type
Simulated
B
Unimodal-type
Simulated
C
Bimodal-type
Simulated
D
Sampled
E
Sampled
F
Sampled
G
Rarefied
H
Rarefied
I
Rarefied
Proportional richness
SSC (%)
Latitude (°)
Bathonian
A
Flat-type
Simulated
B
Unimodal-type
Simulated
C
Bimodal-type
Simulated
D
Sampled
E
Sampled
F
Sampled
G
Rarefied
H
Rarefied
I
Rarefied
Proportional richness
SSC (%)
Latitude (°)
Bajocian
A
Flat-type
Simulated
B
Unimodal-type
Simulated
C
Bimodal-type
Simulated
D
Sampled
E
Sampled
F
Sampled
G
Rarefied
H
Rarefied
I
Rarefied
Proportional richness
SSC (%)
Latitude (°)

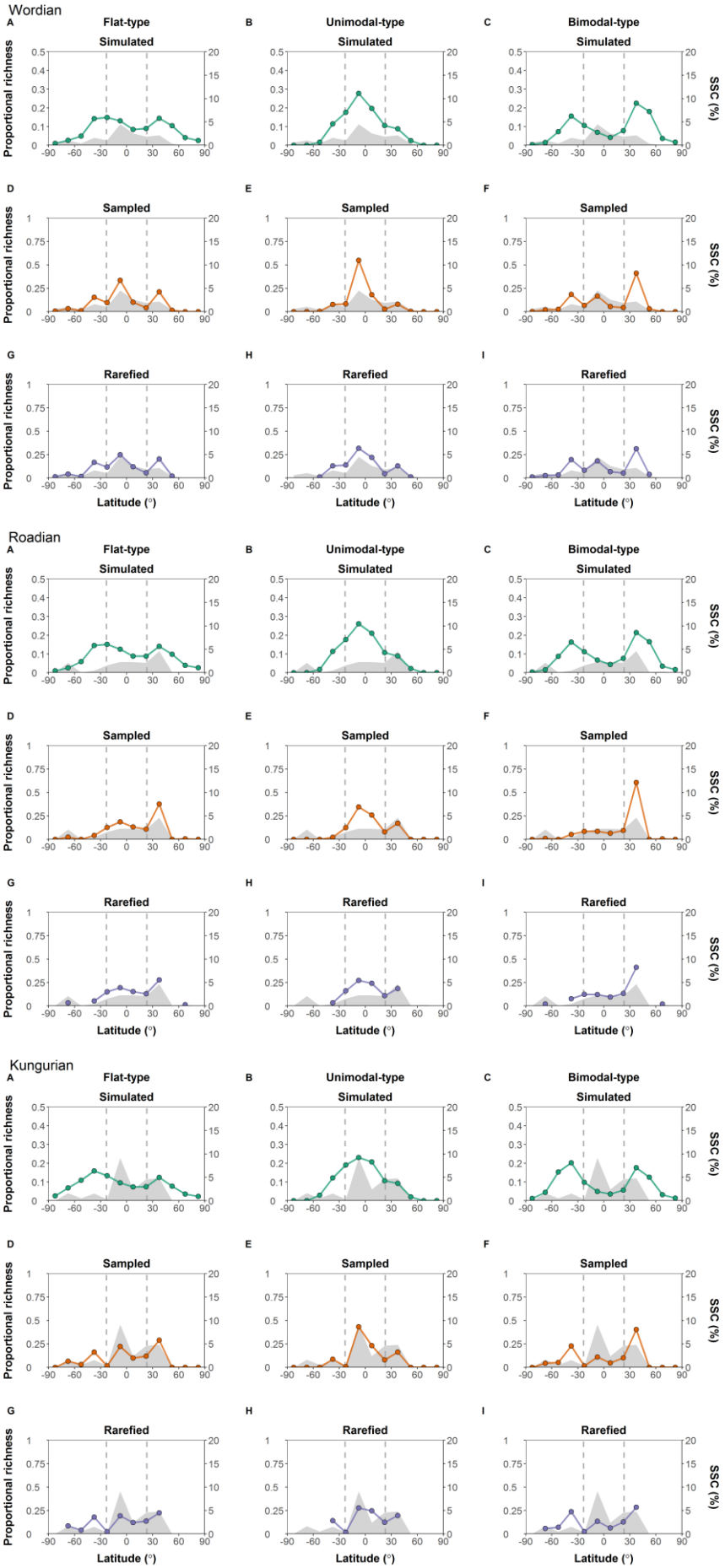

Aalenian
Toarcian
Pliensbachian
A
B
C
D
E
F
G
H
I
Flat-type
Unimodal-type
Bimodal-type
Simulated
Sampled
Rarefied
Proportional richness
SSC (%)
Latitude (°)

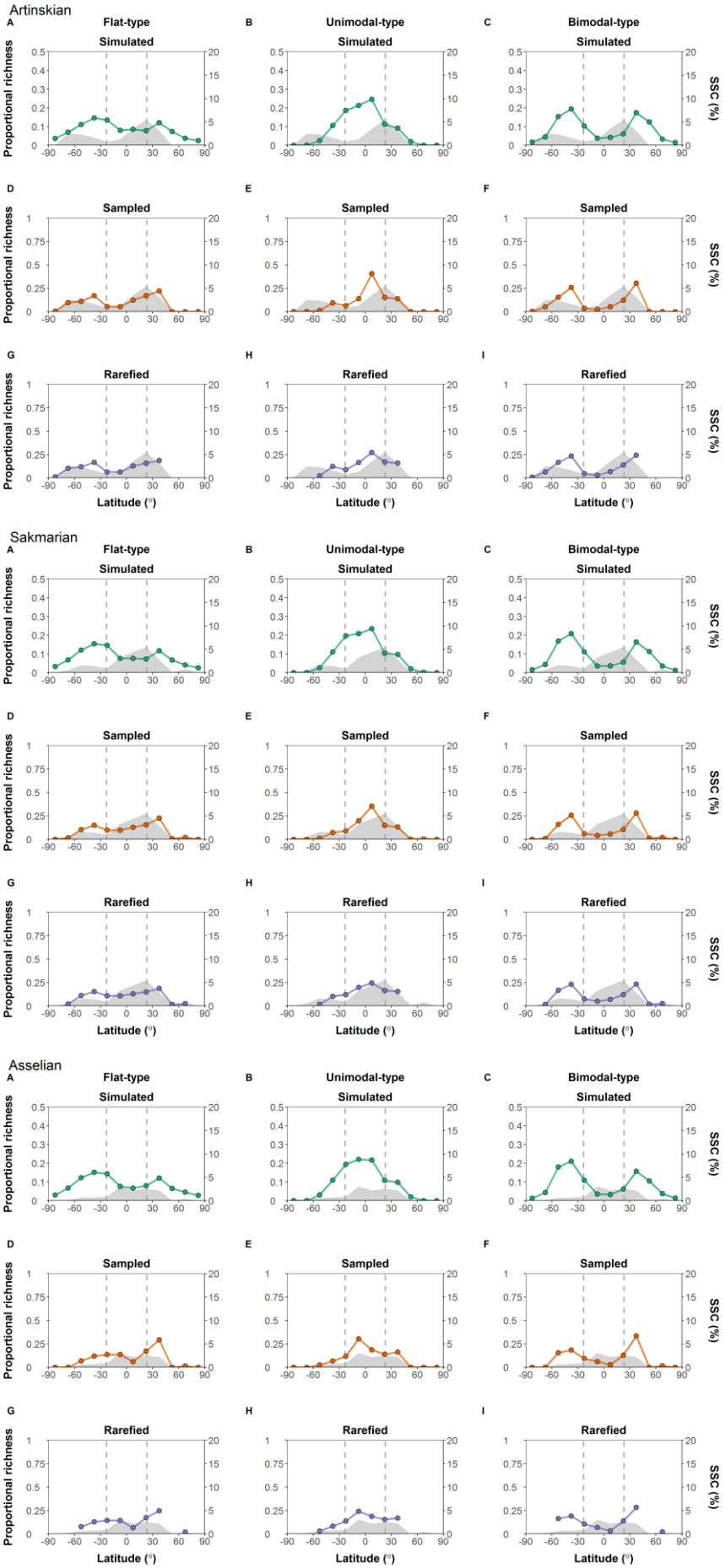

Sinemurian
Hettangian
Rhaetian
A
B
C
D
E
F
G
H
I
Flat-type
Unimodal-type
Bimodal-type
Simulated
Sampled
Rarefied
Proportional richness
SSC (%)
Latitude (°)


Norian
A
Flat-type
Simulated
B
Unimodal-type
Simulated
C
Bimodal-type
Simulated
D
Sampled
E
Sampled
F
Sampled
G
Rarefied
H
Rarefied
I
Rarefied
Proportional richness
SSC (%)
Latitude (°)
Carnian
Ladinian


Anisian
A
Flat-type
Simulated
B
Unimodal-type
Simulated
C
Bimodal-type
Simulated
D
Sampled
E
Sampled
F
Sampled
G
Rarefied
H
Rarefied
I
Rarefied
Proportional richness
SSC (%)
Latitude (°)
Olenekian
A
Flat-type
Simulated
B
Unimodal-type
Simulated
C
Bimodal-type
Simulated
D
Sampled
E
Sampled
F
Sampled
G
Rarefied
H
Rarefied
I
Rarefied
Proportional richness
SSC (%)
Latitude (°)
Induan
A
Flat-type
Simulated
B
Unimodal-type
Simulated
C
Bimodal-type
Simulated
D
Sampled
E
Sampled
F
Sampled
G
Rarefied
H
Rarefied
I
Rarefied
Proportional richness
SSC (%)
Latitude (°)


Changhsingian
Wuchiapingian
Capitanian
A
Flat-type
B
Unimodal-type
C
Bimodal-type
Simulated
D
E
F
Sampled
G
H
I
Rarefied
Proportional richness
SSC (%)
Latitude (°)


Wordian
A
Flat-type
Simulated
B
Unimodal-type
Simulated
C
Bimodal-type
Simulated
D
Sampled
E
Sampled
F
Sampled
G
Rarefied
H
Rarefied
I
Rarefied
Proportional richness
SSC (%)
Latitude (°)
Roadian
Kungurian


Artinskian
A
Flat-type
Simulated
B
Unimodal-type
Simulated
C
Bimodal-type
Simulated
D
Sampled
E
Sampled
F
Sampled
G
Rarefied
H
Rarefied
I
Rarefied
Proportional richness
SSC (%)
Latitude (°)
Sakmarian
A
Flat-type
Simulated
B
Unimodal-type
Simulated
C
Bimodal-type
Simulated
D
Sampled
E
Sampled
F
Sampled
G
Rarefied
H
Rarefied
I
Rarefied
Proportional richness
SSC (%)
Latitude (°)
Asselian
A
Flat-type
Simulated
B
Unimodal-type
Simulated
C
Bimodal-type
Simulated
D
Sampled
E
Sampled
F
Sampled
G
Rarefied
H
Rarefied
I
Rarefied
Proportional richness
SSC (%)
Latitude (°)

Appendix C

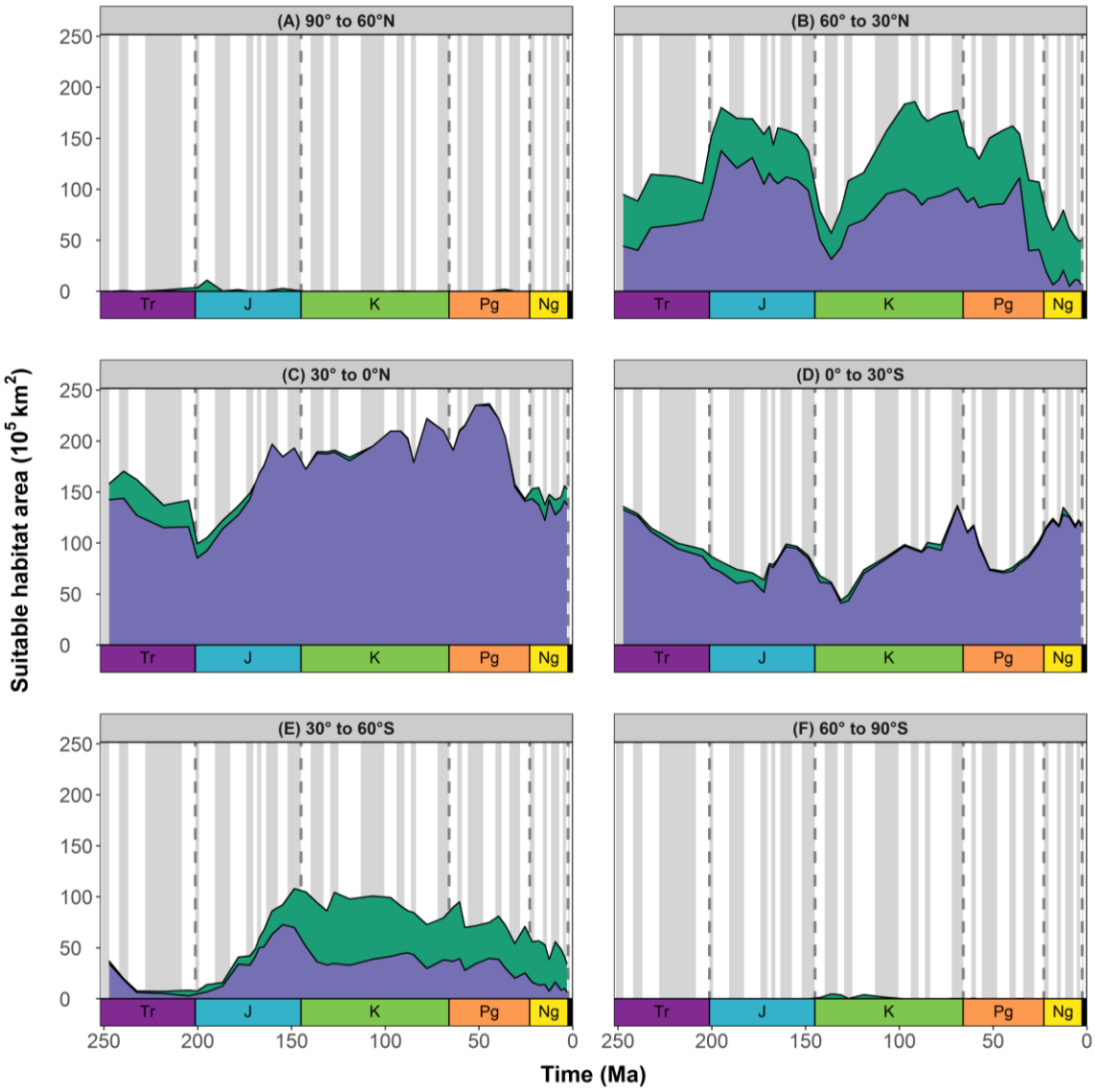


Figure C.1. Palaeolatitudinal plots of estimated unclamped suitable habitat area (Anisian to Piacenzian) for warm-water coral reefs under binary thresholds LTP (green; least training presence) and MaxSSS (purple; maximising the sum of sensitivity and specificity). Palaeolatitudinal bins: (A) 90–60°N; (B) 60–30°N; (C) 30–0°N; (D) 0–30°S; (E) 30–60°S; and (F) 60–90°S. Vertical grey box shading illustrates stratigraphic stages, whereas vertical dashed lines indicate the start/end of a period.

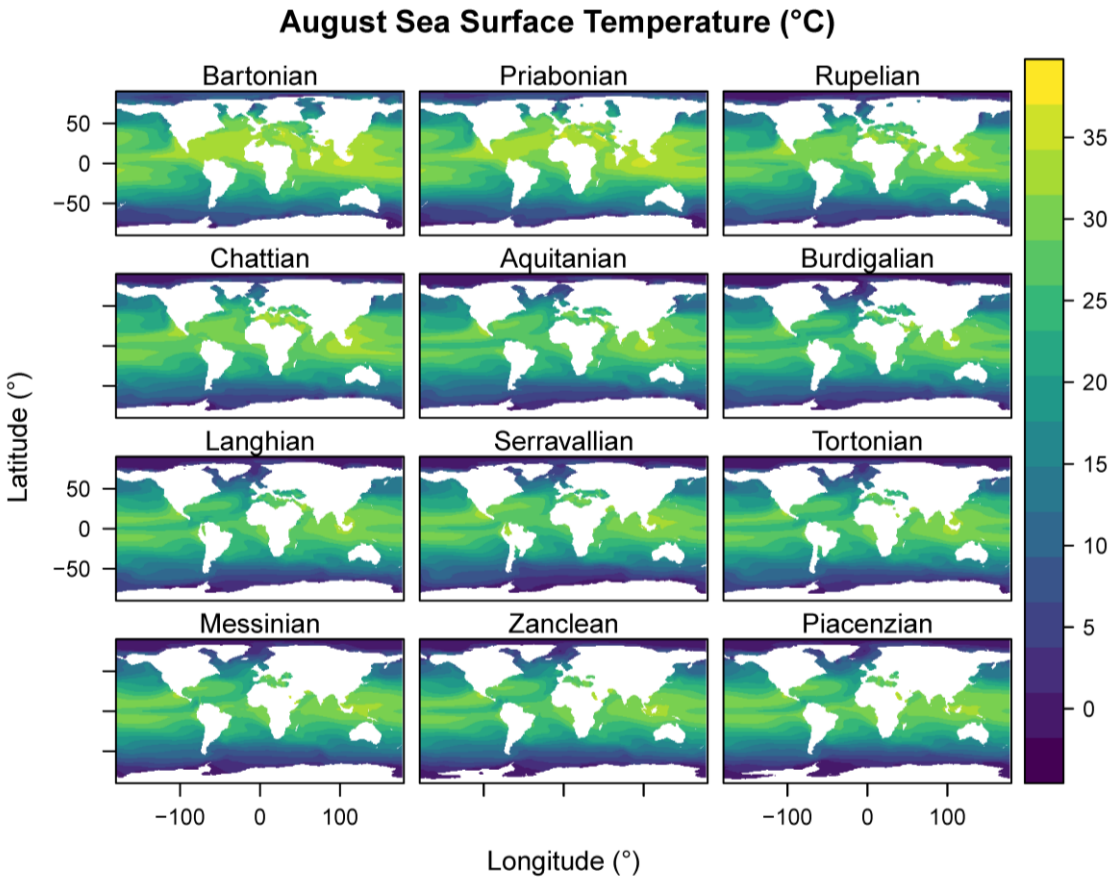


Figure C.2. Bartonian–Piacenzian mean stage-level August sea surface temperature (°C) from the HadCM3L. Note decline in sea surface temperature at temperate latitudes in the Northern Hemisphere.

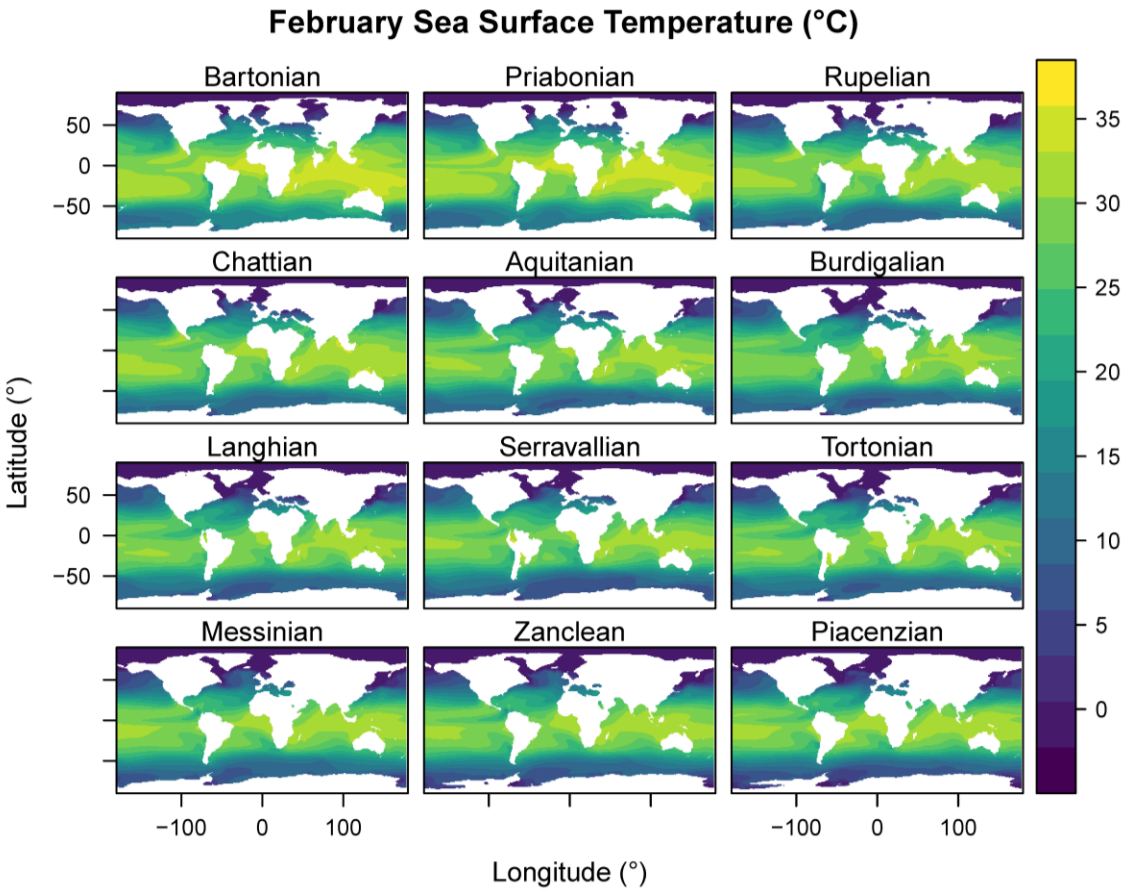


Figure C.3. Bartonian–Piacenzian mean stage-level February sea surface temperature (°C) from the HadCM3L. Note decline in sea surface temperature at temperate latitudes in the Northern Hemisphere.

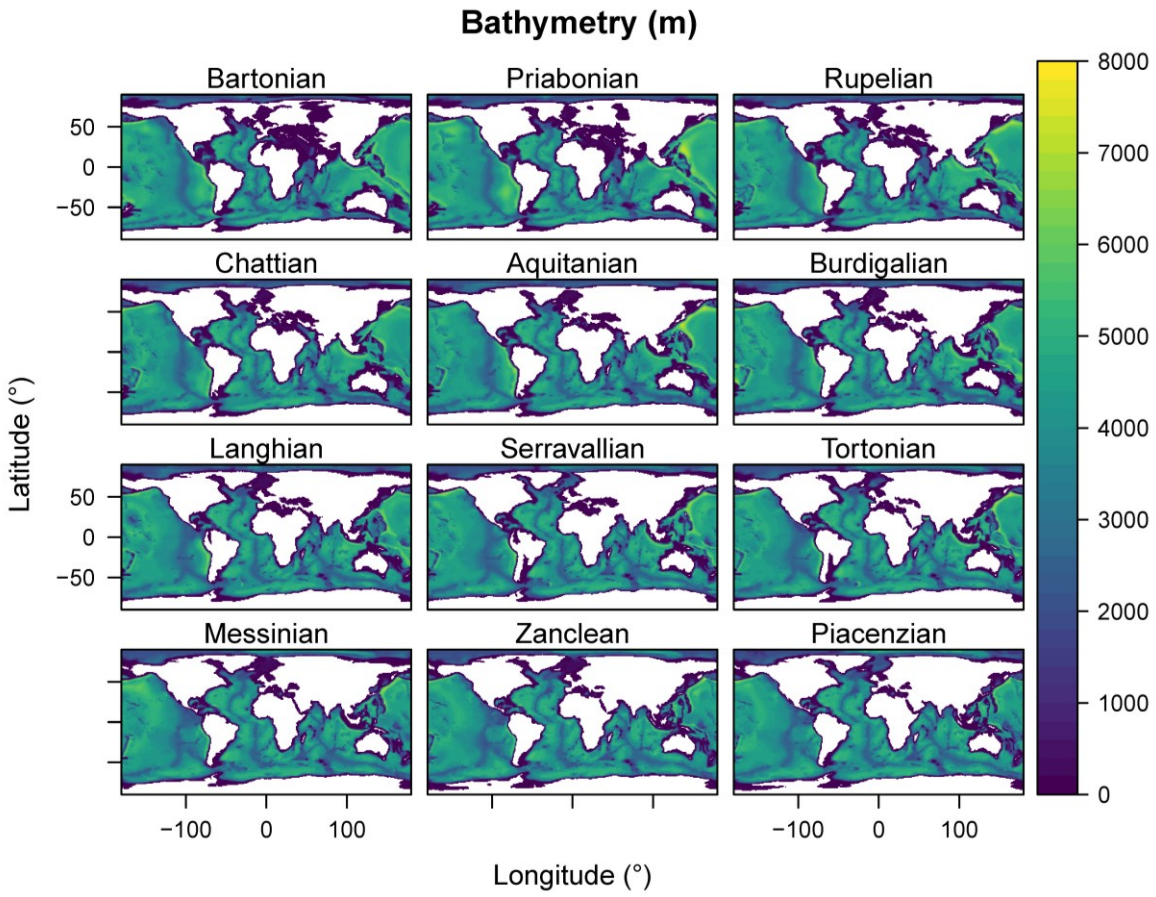


Figure C.4. Bartonian–Piacenzian palaeobathymetry reconstructions from the Getech PLC. digital elevation models. Note increase in shallow marine environment within the Indo-Australian Archipelago.